The synthesis, characterization and preliminary biological evaluation of triazole complexes of palladium

by

Annick van Niekerk

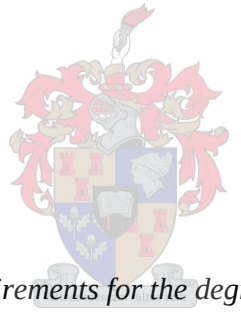

Thesis presented in fulfilment of the requirements for the degree of MSc in Chemistry in the Faculty of Natural Sciences at Stellenbosch University

Supervisor: Prof. S. F. Mapolie

March 2017

Declaration

By submitting this thesis electronically, I declare that the entirety of the work contained therein is my own original work, that I am the authorship owner thereof (unless to the extent explicitly otherwise stated) and that I have not previously in its entirety or in part submitted it for obtaining any qualification.

Signature:

Date: March 2017

Acknowledgements

I would like to thank my supervisor, Prof. Mapolie for his persistent support and unwavering interest in this project. You provided me with a project and a bursary when it was most needed and I truly appreciate the guidance you have given me over the past few years.

I also wish to thank the Organometallic research group and Dr P. Chellan for their helpful insights into my project, especially Dr A. Blanckenberg, whom has become a close friend and mentor.

My gratitude also goes to the Tbox lab under the supervision of Prof. S. Prince at the University of Cape Town, as well as Dr S. Kimani and Sandra Jordaan who performed the MTT assays.

I would also like to thank the staff at the Central Analytical Facility (CAF) especially Elsa Malherbe with the NMR unit for her never ending patience. My thanks also go to Trudy Jansen at the Department of Microbiology who supplied the *E. coli* cultures for the gel electrophoresis.

I wish to acknowledge the support provided by the technical staff of the Inorganic Chemistry building.

The financial assistance of the National Research Foundation (NRF) towards this research is hereby acknowledged. Opinions expressed and conclusions arrived at, are those of the author and are not necessarily to be attributed to the NRF.

And finally, I wish to thank my parents, Theo and Jo-Ann van Niekerk, and my sister, Daniella, for their continued support throughout my studies. You have endured much hardship in order to provide me with the opportunities you never had, and I will forever be in your debt.

Conference contributions

Poster presentation

Annick van Niekerk, Prof. S. F. Mapolie

Synthesis and characterization of palladium (II) complexes based on heterocyclic ligands derived from click chemistry for use as anti-cancer agents. SACI Inorg biennial conference at Grahamstown 2015.

Abstract

Palladium based anti-cancer agents have been identified as potential replacements for known platinum based chemotherapeutics. However, only a limited number of these compounds have managed to progress beyond the laboratory due to a lack of understanding surrounding their mode of action and structure activity relationships. Hence, the aim of this study was to synthesize a small library of *trans*-Pd(II)-1-substituted-4-phenyl-1,2,3-triazolyl and *N,N'*-bidentate Pd(II)-1-substituted-4-pyridyl-1,2,3-triazolyl complexes for evaluation against human breast cancer cell lines. The DNA interaction modes of the active compounds were investigated with DNA migration and DNA titration studies.

A number of known (**1a** – **3a**, **7a** – **9a**, **1b** – **3b**, **7b**, **9b**) and novel (**4a** – **6a**, **4b** – **6b**, **8b**) 1-substituted-4-phenyl-1,2,3-triazole and 1-substituted-4-pyridyl-1,2,3-triazole ligands were synthesized, in moderate to good yields. The N-bound substituents were varied in order to investigate the effects of sterics, electronics and hydrophilicity on the cytotoxicity of the resulting complexes. All ligands were characterized using FTIR, ^{1}H NMR and ^{13}C NMR spectroscopy, as well as ESI-MS spectrometry. Elemental analysis was also employed to confirm the purity of the compounds.

Complexation of **1a** – **9a** to Pd(II) yielded the *trans*-Pd(II)-phenyl-1,2,3-triazolyl complexes (**T1a** – **T9a**) in moderate to good yields. It was observed that these compounds dissociate in DMSO and an NMR study was conducted to confirm that ligand exchange indeed takes place. Complexation of ligands **1b** – **9b** to Pd(II) yielded the *N,N'*-bidentate-Pd(II)-pyridyl-1,2,3-triazolyl complexes (**N1b** – **N9b**) in moderate to good yields. Unlike the *trans*-Pd(II)-1-substituted-4-phenyl-1,2,3-triazolyl complexes, the *N,N'*-bidentate-Pd(II)-pyridyl-1,2,3-triazolyl complexes displayed no signs of ligand exchange in DMSO. Characterization of all complexes was carried out using FTIR, ^{1}H and ^{13}C NMR spectroscopy, ESI-MS and elemental analysis.

The kinetic solubility in a 2 % (V/V) DMSO/PBS solution of all complexes was determined using a turbidimetric assay. It was found that all complexes were moderately soluble with the exception of complexes **T2a**, **T7a**, **T9a** and **N1b**. The cytotoxicity of these complexes were thus evaluated as suspensions. Owing to the ligand dissociation observed for complexes **T1a** – **T9a**, the cytotoxicity observed for the treatment of cells with these complexes cannot be ascribed to the activity of the original complexes but rather to a mixture of species in solution.

The cytotoxicity of the complexes was evaluated employing a MTT Assay (3-(4,5-dimethylthiazol-2-yl)-2,5-diphenylterazolium bromide assay) against breast adenocarcinoma cell lines MCF-7 and MDA-MB-231. Complex **T8a** displayed moderate cytotoxicity against MCF-7 (IC_{50} = 40.69 (± 1.1) µM), while none of the other complexes displayed any anti-cancer activity at the complex concentrations tested.

Subsequently, evaluation of the ligands against MCF-7 showed that ligands **1a** – **4a** displayed moderate cytotoxicity while **7a** displayed anti-cancer activity (IC_{50} = 13.02 (± 1.2) µM) which is comparable to that of cisplatin. A structure-activity relationship in favour of the smaller N-bound substituents was established.

DNA migration and titration studies revealed that ligands **1a** – **4a** displayed moderate intercalative character. Complex **T8a** displayed covalent binding in the DNA migration study, similar to that observed for cisplatin. Ligand **7a** displayed weak intercalation based on the DNA migration study, but the DNA titration study revealed a potential multi-mode binding character.

The affinity of the ligands towards DNA did not correlate directly with the IC_{50} values obtained. This potentially indicates that the pharmacological target of the cytotoxic ligands is probably not DNA, and thus requires further investigation.

Opsomming

Kankerteenmiddels gebaseer op palladium is geïdentifiseer as moontlike plaasvervangers vir die bestaande platinum baseerde chemoterapeutiese middels. Tenspyte hiervan het slegs ‘n beperkte hoeveelheid palladium verbindings verder as die laboratorium gevorder, vermoedelik weens ‘n gebrek aan kennis rondom hul metode van aktiwiteit en struktuur-aktiwiteit verhoudings. Dus, die doel van hierdie studie was om ‘n reeks *trans*-Pd(II)-1-gesubstitueerde-4-feniel-1,2,3-triasoliel en *N,N’*-bidentate Pd(II)-1-gesubstitueerde-4-piridiel-1,2,3-triasoliel komplekse te evalueer as potensiële kankerteenmiddels, teen menslike borskanker sellyne. Die interaksie van die aktiewe verbindings met DNS is ook ondersoek deur middel van DNS migrasie en DNS titrasie studies.

A aantal bekende (**1a** – **3a**, **7a** – **9a**, **1b** – **3b**, **7b**, **9b**) en nuwe (**4a** – **6a**, **4b** – **6b**, **8b**) 1-gesubstitueerde-4-feniel-1,2,3-triasool and 1-gesubstitueerde-4-piridiel-1,2,3-triasool ligande was gesintetiseer, in matige tot goeie opbrengs. Die N-gebonde substituente is gevarieer om die effek van steriese hindernis, elektroniese interaksies en hidrofiliesiteit op die sitotoksisiteit van die komplekse te ondersoek. Al die ligande is gekarakteriseer deur van FTIR, ^{1}H KMR en ^{13}C KMR spektroskopie, asook ESI-MS spektrometrie gebruik te maak. Die suiwerheid van die verbindings is deur mikroanaliese bepaal.

Kompleksering van **1a** – **9a** aan ‘n Pd(II) sentrum, het die *trans*-Pd(II)-feniel-1,2,3-triasoliel komplekse (**T1a** – **T9a**) in matige to goeie opbrengs opgelewer. Daar is waargeneem dat hierdie komplekse in DMSO ligand uitruiling met die oplosmiddel ondergaan en ‘n KMR studie het bevestig dat liganduitruiling inderdaad wel in oplossing plaasvind. Kompleksering van ligande **1b** – **9b** aan ‘n Pd(II) sentrum, het die *N,N’*-bidentate-Pd(II)-piridiel-1,2,3-triasoliel komplekse (**N1b** – **N9b**) in matige tot goeie opbrengs opgelewer. Anders as in die geval van die *trans*-Pd(II)-feniel-1,2,3-triasoliel komplekse, toon die *N,N’*-bidentate-Pd(II)-piridiel-1,2,3-triasoliel komplekse geen tekens van liganduitruiling in DMSO nie. Alle komplekse is deur middel van FTIR, ^{1}H en ^{13}C KMR spektroskopie, ESI-MS spektrometrie en mikroanaliese gekarakteriseer.

Die kinetiese oplosbaarbeid van al die komplekse in ‘n 2 % DMSO/PBS oplossing is met ‘n turbidimetriese toets vasgestel. Al die komplekse is matig oplosbaar met die uitsluiting van komplekse **T2a**, **T7a**, **T9a** en **N1b**. Die sitotoksisiteit van hierdie komplekse is dus bepaal met suspensies. As gevolg van die liganduitruiling wat vir komplekse **T1a** – **T9a** waargeneem is, kan die sitotoksisiteit wat vir hierdie komplekse bepaal is, nie die aktiwiteit van die oorspronklike komplekse toegeskryf word nie, maar eerder aan ‘n mengsel van spesies teenwoordig in die oplossing.

Die sitotoksisiteit van die komplekse is ge-evalueer met ‘n MTT toets teen twee bors adenokarsinoom sellyne, MCF-7 en MDA-MB-231. Kompleks **T8a** het gematigde sitotoksisiteit teen MCF-7 (IK_{50} = 40.69 (± 1.1) µM) getoon, terwyl nie een van die ander komplekse enige antikanker aktiwiteit by die konsentrasies wat getoets is toon nie.

Daaropvolgende evaluasie van die ligande teen MCF-7 het aan die lig gebring dat ligande **1a** – **4a** gematigde sitotoksisiteit toon, terwyl ligand **7a** antikanker aktiwiteit (IK_{50} = 13.02 (± 1.2) µM) vergelykbaar aan dié van sisplatien toon. ‘n Struktuur-aktiwiteit verhouding ten gunste van die kleiner substituente is vasgestel.

DNS migrasie en titrasie studies het gewys dat ligande **1a** – **4a** gematigde interkalasie met DNS ondergaan. Kompleks **T8a** het kovalente binding aan DNS in die DNS migrasie studie getoon, soortgelyk aan dit gevind vir sisplatien. Ligand **7a** het swak interkalasie in die DNS migrasie studie getoon, maar die DNS titrasie studie het getoon dat **7a** moontlik ‘n veelvoudige binding karakter het.

Die affiniteit van die ligande teenoor DNS stem nie ooreen met die IK_{50} waardes wat in die MTT toets bepaal is nie. Dit dui moontlik aan dat DNS nie die farmakologiese teiken van die sitotoksiese ligande is nie, en dat verdere ondersoek benodig word.

Table of Contents

List of Figures

Chapter 1: A literature review on cancer treatments, the history of chemotherapy and anti-cancer palladium compounds

Chapter 2: Synthesis and Characterization of substituted-phenyl-1,2,3-triazole and substituted-pyridine-1,2,3-triazole ligands

Chapter 3: Synthesis and Characterization of *trans*- and *N,N'*-bidentate Pd(II) complexes

Chapter 4: Biological evaluation of *trans*- and *N,N'*-bidentate Pd(II) complexes

Chapter 5: Conclusions and Future Prospects

List of Schemes

List of Tables

List of Abbreviations

5-FU	Fluoropyrimidine-5-fluorouracil
µM	Micro molar
AACR	American Association for Cancer Research
ADMETox	Absorption, distribution, metabolism, excretion, toxicity
AIDS	Acquired Immune Deficiency Syndrome
ATR	Attenuated total reflectance
BSA	Bovine serum albumin
CCNSC	Cancer Chemotherapy National Service Center
CDK	Cyclin-dependent kinases
CMF	Cyclophosphamide, Methotrexate, 5-Fluorouracil
CML	Chronic Myelocytic Leukaemia
CNS	Central nervous system
CuAAC	Copper-catalyzed 1,3-dipolar Huisgen cycloaddition
DCM	Dichloromethane
dd	Doublet of doublets (NMR spectroscopy)
DIPEA	Diisopropylethylamine
DMEM	Dulbecco's Modified Eagle's Medium
DMF	Dimethyl formamide
DMSO	Dimethyl sulfoxide
DNA	Deoxynucleic acid
dppe	Bis(diphenylphosphino)ethane
dppf	Bis(diphenylphosphino)ferrocene
dt	Doublet of triplets (NMR spectroscopy)
ESI-MS	Electrospray Ionization Mass Spectrometry

Et_3N	Triethylamine
EtBr	Ethidium bromide
FDA	Food and Drug Administration
FTIR	Fourier Transform Infrared Spectroscopy
HSA	Human Serum Albumin
HOAc	Acetic Acid
IC_{50}	The concentration of an inhibitor that is required for 50 % growth inhibition of a cancer cell line *in vitro*
^{i}PrOH	Isopropanol
L-PAM	L-phenylanaline mustard
MeCN	Acetonitrile
MOMP	Methotrexate, Vincristine, Nitrogen-mustard, Predisone
MOPP	Nitrogen-mustard, Procarbazine, Vincristine, Prednisone
Mp	Melting point
MTT	3-(4,5-dimethylthiazol-2-yl)-2,5-diphenyltetrazolium bromide
Na_2EDTA	Di-sodium ethylenediamine tetraacetic acid
NCI	National Cancer Institute
NHC	N-heterocyclic carbene
NMR	Nuclear Magnetic Resonance
NSABP	National Surgical Adjuvant Breast Project
PBS	Phosphate buffered saline
PCP	Pneumocystis pneumonia
PE	Petroleum ether
PEPPSI	Pyridine enhanced precatalyst preparation stabilization and initiation
PTA	1,3,5-triaza-7-phosphadamantane
PVDF	Polyvinyl difluoride
q	Quartet (NMR spectroscopy)

qt	Quintet (NMR spectroscopy)
quat.	Quaternary
RPMI 1640	Roswell Park Memorial Institute cell growth medium
s	Singlet (NMR spectroscopy)
SVCP	Special Virus Cancer Program
t	Triplet (NMR spectroscopy)
^{t}BuOH	Tertiary butanol
td	Triplet of doublets
THF	Tetrahydrofuran
VAMP	Vincristine, Amethopterin, 6-Mercaptopurine, Predinisone

List of cell lines

A2780	Human ovarian cancer
A2780^{cisR}	Cisplatin resistant ovarian cancer
A2780^{ZD0473R}	Picoplatin resistant ovarian cancer
Bel17402	liver carcinoma
DU145	Hormone insensitive human prostate carcinoma
G361	Human melanoma (skin cancer)
HCT116	Human colon carcinoma
HeLa	Human cervical carcinoma
Hep-G2	Human liver carcinoma
HL60	Human promyelocytic leukaemia
HT29	Human Caucasian colorectal adenocarcinoma
HTC8	Ileocecal colorectal adenocarcinoma
Jurkat	T lymphocyte leukaemia
K562	Human chronic myelogenous leukaemia
KB	Epidermoid Human Carcinoma

L1210	Murine Leukaemia
L929	Cisplatin resistant murine fibriocarcinoma
LnCaP	Androgen-sensitive human prostate adenocarcinoma
MCF-7	Hormone sensitive breast adenocarcinoma
MDA-MB-231	Metastatic breast adenocarcinoma
MDA-MB-468	Metastatic breast adenocarcinoma
MKN28	Human gastric carcinoma (stomach cancer)
$MKN28^{R}$	Cisplatin resistant gastric carcinoma
MKN45	Human gastric carcinoma
$MKN45^{R}$	Cisplatin resistant gastric carcinoma
Neuro2a	Murine neuroblastoma
P388	Murine lymphoma
PC-3	Metastatic human prostate carcinoma
SKOV-3	Sloan-Kettering HER2 3+ ovarian cancer
SW403	Advanced human colon adenocarcinoma
SW620	Human Caucasian colon adenocarcinoma
U251	Human glioblastoma carcinoma (brain cancer)

Chapter 1: Cancer treatments, the history of chemotherapy and anti-cancer palladium compounds

Cancer is the second leading cause of death, after cardiovascular disease, worldwide with 5.5 % of all cancer related deaths in 2012 occurring in Sub-Saharan Africa.[1,2] It is estimated that cancer will become the leading cause of death within the next decade.[3] Currently, cancer related deaths account for 1 in 7 deaths worldwide.[4] Tumour growth is can be translated as a single cell's quest for immortality caused by a mutation in the DNA of the cell. This results in the obstruction of natural cell death pathways within the cell, resulting in uncontrolled proliferation. Ironically this quest would ultimately hasten the passing of the cell's host.[5]

1.1 The History of Cancer

It is a common misconception that cancer is a modern disease that is accelerated through the ever increasing pace of life. Although the incidence of cancer in the modern world seems higher than that compared to the early 20th century, one has to consider the technological and medical advances that have enabled us to identify cancer at much earlier stages than before. In truth, cancer is an ancient foe that has haunted mankind since ancient times.

The word 'cancer' has its roots in Ancient Greek. Hippocrates (460-370 BC) was the first to describe different tumours as *karkinos*, from the Greek for crab, presumably referring to the way in which tumours extend into the surrounding tissues. The Greek *karkinos* was later translated to the Latin *cancer* by Celsus, a Roman physician.[2,6]

The first documented case of cancer comes from the Edwin Smith Papyrus, dated 3000 BC,[6] which was copied from the writings of Imhotep, an ancient Egyptian healer. Under cure he wrote, "There is none."[5] Evidence of bone cancer was also found in the remains of Egyptian mummies, and breast cancer was described in their ancient writings from 1500 BC.[2]

During the 16th to 18th centuries the understanding of medicine advanced dramatically with Giovanni Morgagni of Padua (1761) performing the first autopsies and relating illness to pathological findings. This change in rhetoric can be regarded as the initial period of the field of oncology, the study of cancer, and other theories as to the causes of cancer, such as the humoral theory, the lymph theory and the chronic irritation theory, were laid to rest.[6]

The clinical treatment of cancer has changed and evolved over centuries and can thus be divided into three main branches: Surgery, Radiation and Chemotherapy. For the purposes of this thesis only chemotherapy will be discussed.

1.2 The history and development of chemotherapeutic agents

The German chemist, Paul Ehrlich, coined the term chemotherapy in the early 1900's with reference to the use of chemicals to treat disease. Due to his research and experimentation on animal models, the use of arsenic containing compounds for the treatment of syphilis was proven in rabbit models.[7]

Ehrlich's interests expanded into anti-cancer treatments as well, with his lab screening aniline dyes for their anti-tumour activities. This led to the first primitive alkylating drugs to be used in anti-cancer therapy.[2]

Surgery and radiotherapy dominated cancer treatment until the 1960's, mainly due to their immediate visual results, but by the end of the 1960's new studies had come to light that showed that the presence of micrometastases resulted in the recurrence of cancers treated with surgery and radiation.[8]

Prior to World War II (1939-1945), the most exciting achievement in the field of cancer chemotherapy was the introduction of hormonal therapy by Charles Huggins in 1939. His hormonal treatment of men with prostate cancer showed positive responses, and earned him a Nobel Prize (1966).[9]

WWII (1939-1945) launched a large number of research programmes aimed at drug discovery (antibiotics and antimalarial compounds) and nutritional research. Serendipitously some of this research led to the discovery of a large number of anti-cancer compounds.

During a German Luftwaffe air raid on 2 December 1943, sulfur mustard gas was spilled on American troops in the Bari Harbour, Italy. It was later observed that the bone marrow and lymph nodes of the men exposed were severely depleted. The promising results from the subsequent research done by Goodman and Gilman in 1943 (the work was only published in 1946 although completed in 1943 due to secrecy imposed on the researchers by the U.S. Office) resulted in the rapid synthesis and testing of various alkylating compounds. Thus nitrogen mustard, chlorambucil and cyclophosphamide came to be (Figure 1.1). Although this breakthrough was very exciting at the time, the remissions observed in patients turned out to be very brief and limited.[5,7,8]

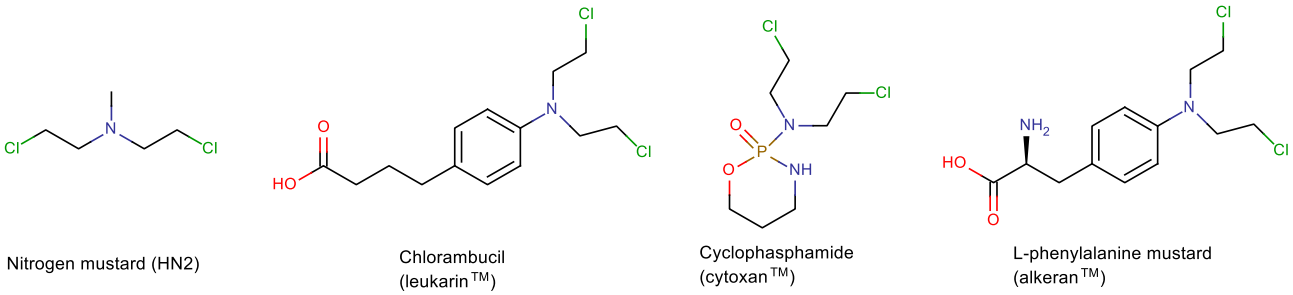

Figure 1.1: The alkylating agents based on nitrogen mustard.[7]

Cancer chemotherapy thus follows a strange logic, that every poison might be a potential cure in disguise.

The nutritional research programmes of that time discovered folic acid in green leafy vegetables and in 1937 folic acid was artificially synthesized for the first time. It was also discovered that a diet lacking in folic acid resulted in the same deficient bone marrow that was observed in the troops exposed to the mustard gas. This led a group of clinicians, Farber, Heinle and Welch, to believe that folic acid might have some anti-cancer properties. They tested their theory on children with leukaemia and unfortunately found that folic acid apparently accelerated cancer cell growth. Although this observation was later proven to be false, it led Farber in collaboration with Harriet Kilte to develop a series of folate antagonists that included aminopterin and amethopterin (now known as methotrexate). Farber tested these compounds in children with leukaemia in 1948 and the subjects showed complete remission. These compounds became the first of the anti-folates, an entire class of cancer chemotherapeutic drugs still used today (Figure 1.2).[5,7,9]

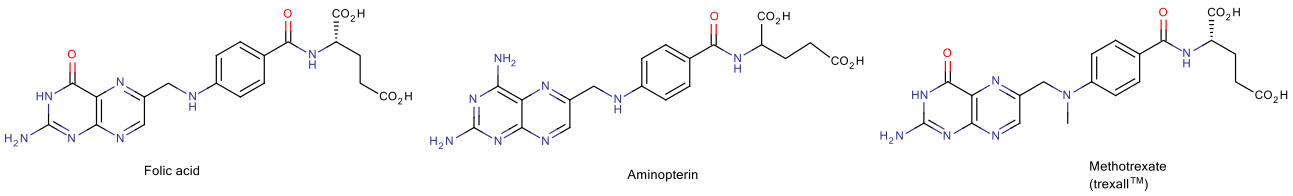

Figure 1.2: Anti-metabolites based on folic acid.[5,7]

The search for new antibiotics during the WWII period was based on the screening of various fermentation products. Along with the antibiotic activity of these compounds, the anti-tumour activity of certain agents was also investigated.[9] This yielded actinomycin D, an antibiotic with significant anti-tumour properties. Unfortunately, actinomycin D was so toxic that its antibacterial uses were severely limited, but cancer treatment was born from poison. Sydney Farber tested actinomycin D on various mouse cancers in 1954, and found that even a small dose could thwart leukaemias, lymphomas and breast cancers. He thus started a trial in 1955 to test this new drug in children with various cancers, including Wilms' tumour, a very rare kidney cancer. By the time Wilms' tumour is detected, it usually has already metastasized to the lungs, where it can only be treated with radiation

therapy and with only a small chance at success. The combination of actinomycin D and radiation proved to be highly effective against metastasized Wilms' tumours and thus ultimately 'cured' that specific form of cancer.[5] Actinomycin D was subsequently used for various paediatric cancers in the 1950s and 1960s.[7]

This was again the first drug of an entire class of anti-cancer antibiotics of which there is a large number still in use today (Figure 1.3).

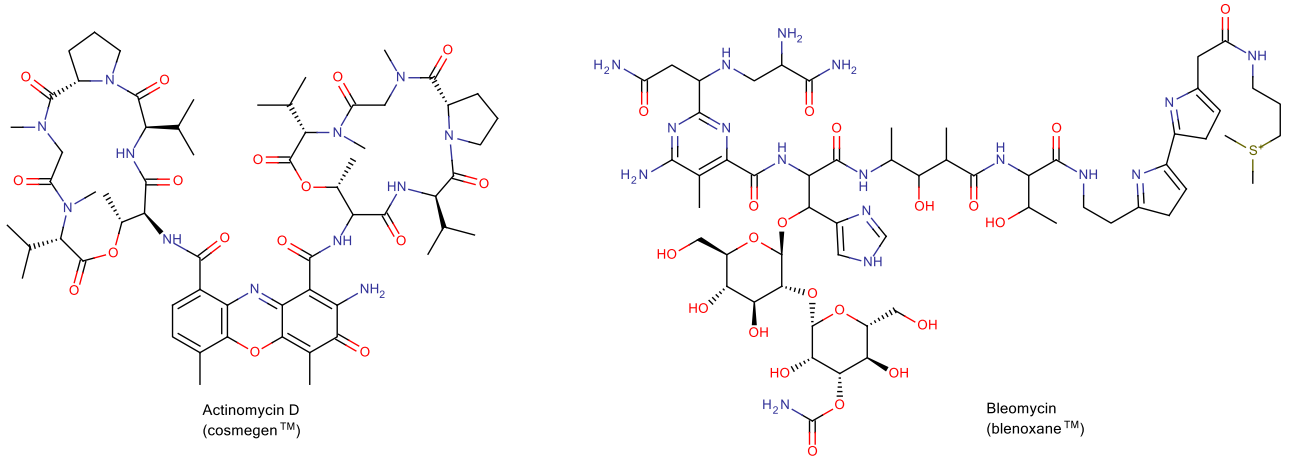

Figure 1.3: Anti-cancer antibiotics.[5]

Anti-metabolites arose from the research initiated by the activity observed for nitrogen mustard and methotrexate. The same year Farber showed the anti-cancer activity of methotrexate, Hitchings and Elion isolated an adenine metabolism inhibitor. From this observation they developed two drugs, 6-thioguanine and 6-mercaptopurine, that have been used in the treatment of leukaemia since 1951 (Figure 1.4). Thiopurines and their analogues have found wide spread use for the treatment of other diseases, including herpes viral infections and immunosuppressive agents for organ transplants. Their work earned them a Nobel Prize in 1988.[7]

Up until the mid-1950s most cancer chemotherapy was aimed at haematological cancers and not at solid tumours. It was not until Charles Heidelberger observed the increased use of uracil in rat hepatoma models that solid tumours became a chemotherapeutic target. By attaching a fluorine atom in the 5-position on the uracil base, he effectively 'attacked' the relevant biochemical pathway. His research yielded the first example of targeted therapy with the introduction of fluoropyrimidine 5-fluorouracil (5-FU), as shown in Figure 1.4. 5-FU showed activity against a wide range of solid tumours and remains to today the main drug used in the treatment of colorectal cancer.[5]

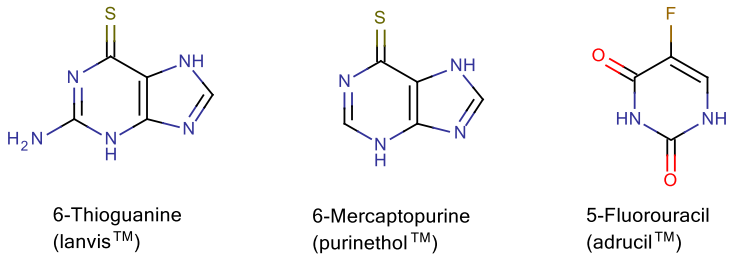

Figure 1.4: Anti-metabolites based on uracil[7].

The 1950s also yielded corticosteroids which produced brief remissions when used alone, but, in combination with some of the other drugs, prolonged remissions remarkably.[7]

Despite the existence of the National Cancer Institute (NCI) in the USA during WWII, very little progress was made at the time on the front of new chemotherapy drugs. This was due to the repurposing of resources marked for the NCI into the war effort. The NCI's contribution to the drug discovery programmes only became significant after the launch of the Cancer Chemotherapy National Service Center (CCNSC) in 1954. Between 1954 and 1964 the CCNSC tested nearly 215000 potential anti-cancer drugs and became responsible for nearly all the drugs used at that time for the treatment of cancer.[5,7,8]

One of the drugs tested by the CCNSC was a plant alkaloid ibenzmethyzin (renamed to procarbazine). The compound was isolated from *Vinca rosea* by the Eli Lilly Company in 1963 (Figure 1.5). Two different groups showed the spectacular activity of procarbazine against leukaemia and Hodgkin's lymphoma, Brunner and Young in 1967 and DeVita and colleagues in 1966 respectively.[5] The anti-cancer activity of these compounds were considered ground-breaking at the time due to the fact that they did not cause bone marrow depletion, as is observed for nitrogen mustard.[10] Along with procarbazine, a number of other alkaloids were isolated as well, including vincristine and vinblastine.[5]

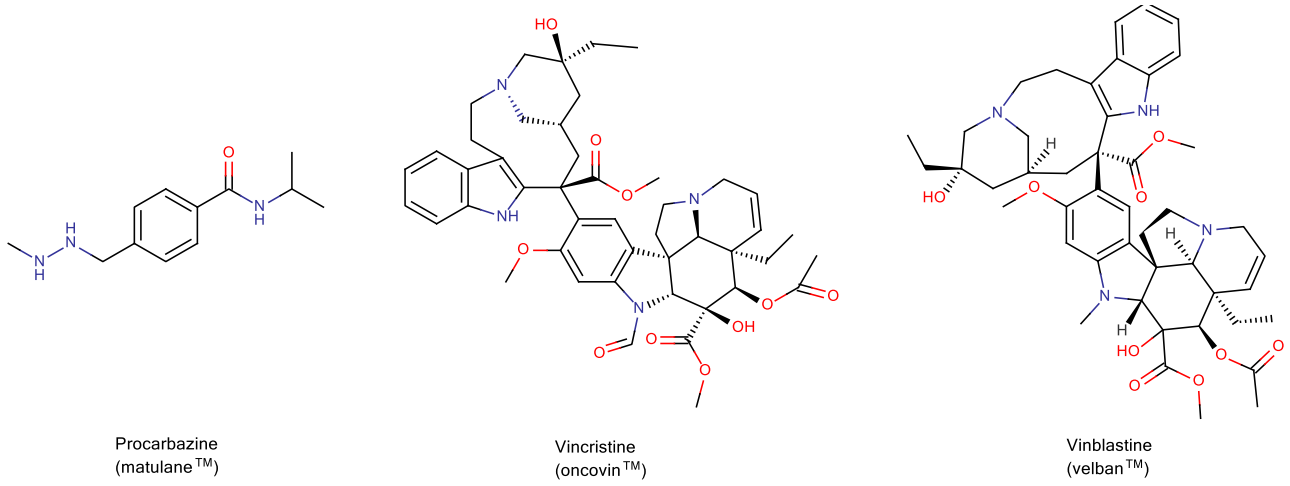

Figure 1.5: The plant alkaloids isolated from the *Vinca rosea* by the Eli Lily Company.[5]

All the drugs discovered up to that point were very useful, but ultimately inconsequential: they produced remissions, but the cancer would always return at some point. It thus became necessary to introduce combinational chemotherapy. Naturally this idea was met with severe scepticism, not only because it seemed to be a last desperate act, but also because it seemed unusually cruel to already vulnerable patients.[5,7]

Despite the severe objections, a group of chemotherapists, including Emil Frei and Emil Freireich, at the NCI launched the first combination chemotherapy study in 1962 called VAMP. VAMP included vincristine, amethopterin, 6-mercaptopurine and prednisone and was found to increase the childhood leukaemia remission rates to 60 %. Unfortunately the combined toxic effects of all four drugs were nearly unbearable and clinicians had to improvise palliative care with platelet transfusions and the aggressive use of antibiotics.[5,7]

VAMP was the first combinational therapy tested and became the standard of how we treat cancer today. Sadly, VAMP could not cross the blood-brain barrier and most of the children treated with VAMP returned with the leukaemia running rampant in their central nervous systems, ultimately dying due to an evolutionary mechanism that was supposed to protect them.[5,7]

In 1963 Tom Frei started looking into different combinations of known chemotherapeutic drugs, drugs that would complement each other in their activity. He also changed his focus from leukaemia, a haematological cancer, to Hodgkin's lymphoma, which would provide the perfect crossover to solid tumours. An added advantage of Hodgkin's lymphoma was that it progressed locally, from lymph node to lymph node, and did not tend to end up in the brain like leukaemia. The NCI chemotherapists had also reached a crossroads of sorts: if they could cure metastatic[a] Hodgkin's lymphoma with aggressive combinational chemotherapy, then they could unequivocally prove that cancer can be cured through chemical intervention.[5]

In 1964 DeVita, Zubrod, Frei and Freireich launched the MOMP (methotrexate, vincristine, nitrogen mustard and prednisone) trial on Hodgkin's lymphoma patients. Later that same year DeVita modified the trial slightly by substituting methotrexate with the more powerful procarbazine, and thus launched the MOPP trial for the patients with the more advanced lymphomas. Predictably, the highly toxic drug regimens had nearly devastated the patients' immune systems, leading to the first reported cases of PCP pneumonia, which would later be observed in AIDS sufferers.[5,8]

The results were, however, positive and nearly all the patients entered long, durable remissions, the MOPP trial being the most promising. The MOMP trial results were presented at the AACR (American Association for Cancer Research) meeting in 1965 and MOPP in 1967, both showing positive results. By the 1970s Hodgkin's lymphoma was generally considered 'curable' with the

[a] Metastatic refers to cancers that have progressed beyond the initial organ toward other areas of the body.

combination of radiation and chemotherapy.[7] The NCI chemotherapists had finally proven that chemotherapy can cure cancer.

The 1960s also yielded another important discovery in chemotherapy; the cytotoxic capabilities of *cis*-platinum (*cis*-dichlorodiaminoplatinum (II)). In 1965 Barnett Rosenberg investigated the biological effect of electricity on bacterial growth only to discover that the bacteria had stopped dividing entirely, but continued to grow into long filaments. At first this was thought to be due to the electrical current but it was later discovered that the platinum electrode had reacted with the growth medium to form a compound known as cis-platinum that was responsible for the static bacteria.[11,5,12] More information on *cis*-platinum, commercially known as cisplatin, and other organometallic compounds used for chemotherapy will be given in Section 1.3.2.

The 1970s heralded the age of adjuvant chemotherapy, where the drug would be used in addition to radiation and surgery even in early stage cancers. Naturally this was a point of much debate; should patients that have early stage cancers be exposed to potentially harmful drugs that they might not need? Although researchers began using adjuvant therapy on late stage breast cancer by the late 1960s, these programs were never studied within the confines of a clinical trial.[7]

The two programs in question include L-PAM (the single use of L-phenylalanine mustard) and CMF (cyclophosphamide, methotrexate and 5-fluorouracil). L-PAM was only tested in an adjuvant capacity by the National Surgical Adjuvant Breast Project (NSABP) under leadership of Bernard Fisher and resulted in an optimistic publication in 1975. The CMF study was tested in an adjuvant capacity by the NCI along with the Istituto Nazionale Tumori in Italy under guidance of Gianni Bonadonna. The CMF study also yielded positive results and was published in 1976. The positive results from both trials expanded the scope of adjuvant chemotherapy to many different tumours and cascaded throughout oncology as the next most promising field.[7,8]

In 1974 Lawrence Einhorn used the combination of cis-platinum, vinblastine and bleomycin to treat metastatic testicular cancer and subsequently increased the cure rate from 10 % to 60 %, as published in 1978.[7]

Today, adjuvant chemotherapy is indicated for a wide variety of cancers including breast, colorectal, pancreatic and cervical cancer.[8]

The 1970s also yielded the discovery of monoclonal antibodies that were only proven clinically useful in the 1990s. These antibodies do not work alone, but they do provide targeted chemotherapy when used in conjunction with chemotherapeutic agents and have thus become an integral part in combinational chemotherapy.[13]

Targeted chemotherapy has become the main focus of current research. This includes the search for compounds that would target specific cellular targets characteristic of a specific cancer. This

research finds its roots in the 1960s with the Special Virus Cancer Program (SVCP). Although the program did not meet its goals of identifying specific cancer causing viruses, it did however lead to the identification of oncogenes, suppressor oncogenes and new biological signalling pathways.[5]

This enabled the recent development of the Bcr-Abl tyrosine kinase inhibitor, imatinib (commercially known as Gleevec), for the treatment of chronic myelocytic leukaemia (CML). CML is unique in that it is caused by a single defective kinase whereas most cancers result from multiple kinase abnormalities. This has thus opened a new field of research into kinase inhibitors and the Food and Drug Administration (FDA) has recently approved a small number of kinase inhibitors for the treatment of cancers heretofore resistant to all other forms of chemotherapy.[7]

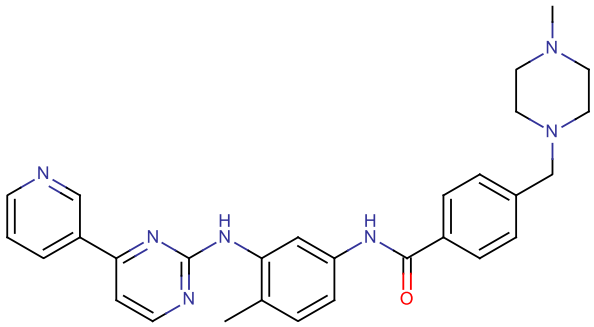

Imatinib
(gleevec™)

Figure 1.6: The first commercially available kinase inhibitor, imatinib[5].

Table 1.1 contains a summary of the different classes of chemotherapy drugs and their biological mechanisms.

1.3 Transition metal compounds in anti-cancer chemotherapy

Inorganic compounds were generally not considered suitable for anti-cancer chemotherapy since metals themselves were considered carcinogenic, thus the drug discovery focus prior to 1969 was mainly aimed at organic compounds. When Rosenberg and Van Camp demonstrated the potency of various platinum compounds in 1969, the drug discovery effort reorganised to incorporate more and more inorganic compounds.[12,14]

1.3.1 General screening of metal compounds

Prior to 1969 the interest in inorganic compounds and their salts was centred on the carcinogenicity of the compounds rather than their anti-cancer properties. A suspension of lead arsenate in benzene, known as Fowler's suspension, was the first metal-based remedy to undergo extensive clinical testing. Unfortunately, the extensive toxicological studies that are used in modern medicine were not

considered as acceptable protocol at the time and the true efficacy of the compound cannot be assessed by today's standards.[12]

Collier and Krause (1931) performed one of the most extensive early investigations into the anti-cancer activities of various metal salts.[15] No quantitative data were given but moderate activities of lead, chromium and manganese salts were described. Taylor and Carmichael (1953) tested several metal chlorides and nitrates but found that they were all generally ineffective. Geschickter and Reid (1947) tested oil soluble butylphthalate copper, nickel and cobalt complexes on humans.[12]

Table 1.1: A summary of the various classes of chemotherapeutic drugs with their biological mechanisms and drawbacks.

Type of anti-cancer agent	Examples	Biological mechanism	Drawbacks
Alkylating agents	Nitrogen mustard Chlorambucil Cyclophosphamide L-phenylalanine mustard	Formation of an ethyleneammonium intermediate that forms covalent bonds to DNA on purine bases to induce apoptosis[8].	Brief remissions. Quick onset resistance. Non-reversible mechanism[5].
Anti-folates	Aminopterin Methotrexate	Binds to folate dependent enzymes responsible for the synthesis of thymidylate and purines. Lack of those compounds induces apoptosis[8].	Severe bone-marrow toxicity. Quick onset resistance[5].
Anti-metabolites	6-thioguanine 6-mercaptopurine 5-fluorouracil	Targets uracil dependent biochemical pathways[8].	Severe toxicity. Brief remissions[8].
Anti-mitotics	Procarbazine Vincristine Vinblastine	Inhibits cell proliferation by preventing microtubule polymerization[8].	Not as cytotoxic and thus needs to be used in combinational therapy.
Metallic compounds[b]	Cisplatin Carboplatin Oxaliplatin	Formation of DNA-metal adducts leading to the formation of DNA crosslinks[16].	Severe neurotoxicity. Low water solubility. Emergence of platinum resistant cancers[17].
Monoclonal antibodies	Rituximab Transtuzumab	Disruption of the cancer cell signalling pathways[13].	Highly specific towards certain cancers resulting in highly expensive treatments[13]. Non-reproducible results[18].
Kinase inhibitors	Imatinib Gefitinib	Blocks kinase cascades linked to growth factor signalling pathways[2].	Emergence of resistance[19]. Narrow therapeutic indices[20].

[b] With the focus of platinum compounds.

They induced brief remissions in leukaemia patients lasting a mere 3 – 6 weeks and were required to increase the dosage 2 – 5 times before achieving a second remission.[12]

Balo and Bangu (1957) prepared various complexes with Krebs cycle metabolites and found that iron ascorbate enhanced the tumour growth in mouse models, cadmium ascorbate inhibited tumour growth but was highly toxic and that manganese malate was the perfect intermediate concerning toxicity. But none of these compounds exceeded the potency of the already known organic compounds.

The first known platinum and palladium compounds were tested by Krishner and colleagues in 1966. They tested various metals complexed to known anti-cancer compounds and identified five active compounds, three of which consisted of metals bound to 6-mercaptopurine (mp), an S-donor ligand. The palladium complex was $Na_2[Pd(mp)_2Cl_2]\cdot 5H_2O$ and the platinum complex was $Na_2[Pt(mp)_2Cl_4]\cdot 2H_2O$. The premise was that the ligand should bind so strongly to the metal so as not to dissociate within a biological environment.[12]

1.3.2 Platinum compounds

Most anti-cancer research regarding transition metals has been performed on platinum containing compounds due to their high efficacy observed by Rosenberg and Van Camp in 1965. Like many anti-cancer discoveries, the discovery of the anti-tumour activity of *cis*-platinum was purely coincidental as previously stated.[16] The image below contains the original photomicrographs of the effect cis-platinum has on bacterial growth.

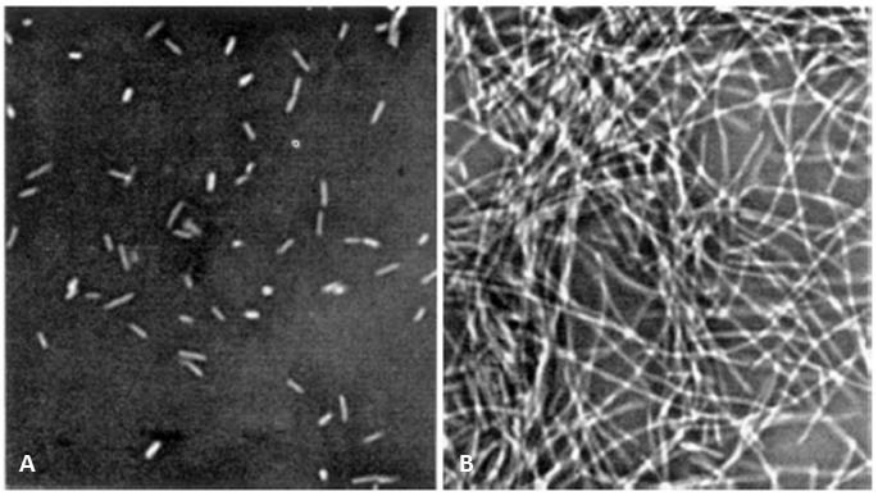

Figure 1.7: The original phase contrast photomicrographs of *E. coli* B x 600 published by Rosenberg et al.[21] in 1965.[21] A) *E. coli* grown normally in a chemically defined medium. B) Filamentous bacteria grown in the same medium with the incorporation of 10 ppm *cis*-platinum. Cell division is completely inhibited resulting in the formation of bacterial filaments.

Rosenberg and Van Camp went on to investigate the anti-tumour properties of various platinum complexes at length. Intuitively, they tested these compounds in mouse models and found that *cis*-

platinum completely inhibited the growth of Sarcoma-180.[16] They compared the cytotoxicity of both Pt(II) and Pt(IV) with amino ligands and ethylenediamine ligands and ultimately concluded that the original *cis*-[$Pt(NH_3)_2Cl_2$], commercially known today as cisplatin, was the most potent with a wide spectrum of activity.[12,16]

Within a year of Rosenberg and Van Camp's landmark study revealing the anti-cancer activity of cisplatin, additional reports of clinical trials conducted with the support of the NCI started to appear in literature. By 1973 it became clear that cisplatin was exceptionally useful in patients that were unresponsive to other chemotherapeutic agents.[16]

As previously mentioned, Woodman et al.[16] showed that cisplatin can be used in combination with other anti-cancer drugs resulting in increased anti-cancer activity. By mid-1974 Lawrence Einhorn's group treated metastatic testicular cancer with a combination of cisplatin, vinblastine and bleomycin and thus increased the cure rate of metastatic testicular cancer from 10% to 60% by the end of the trial in 1978.[7]

After the success achieved with cisplatin the research focus turned to analogues of *cis*-platinum in which both the neutral ligands and the charged ligands were investigated. An interesting observation of the chemistry of these compounds is the fact that the *trans*-isomer is usually inactive and mostly non-toxic when compared to *cis*-platinum. Thus the research focus remained on *cis*-platinum derivatives.[12]

The mechanism through which *cis*-platinum interacts with biological surroundings was investigated some time ago by Reishus and Martin (1961) and Cleare et al. (1978).[16] It is believed that the Cl-ligands dissociate from the Pt-centre and that water, or a ligand species, would coordinate in their place, thus resulting in the hydrated Pt-complex being the active species responsible for the anti-tumour activity observed.[12] The ligand exchange follows the sequential exchange as shown in Equation 1.1.[16]

$$cisPt(NH_3)_2Cl_2 \xrightarrow[H_2O]{} cis[Pt(NH_3)_2Cl(H_2O)]^+ + Cl^- \xrightarrow[H_2O]{} cisPt[(NH_3)_2(H_2O)_2]^{2+} + 2Cl^- \qquad (1.1)$$

The surprising cytotoxicity of cisplatin across a wide selection of cancers ignited a surge in the field of transition metal anti-cancer agents, thus resulting in various publications documenting the synthesis, application and biological interaction of platinum based anti-cancer compounds. Today there is a wide selection of cisplatin analogues commercially available, as shown in Figure 1.8.

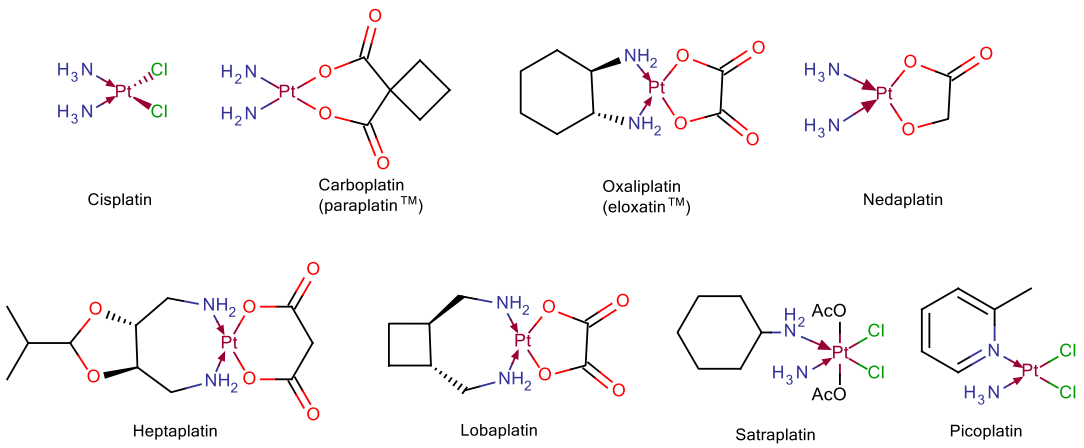

Figure 1.8: Cisplatin and various commercially available analogues[17].

Amid all the enthusiasm emanating from the discovery of cisplatin's anti-cancer activity, there was a single problem with regards to the use of modern platinum compounds: cisplatin is severely toxic to kidneys. Clinicians had to improvise methods to prevent patients from losing total kidney function. This included hydrating patients before, during and after chemotherapy and allowing slow infusion rates which circumvented the severity of the kidney damage.[16,22]

The global demand for platinum drugs has increased over the years, but there are some insurmountable side effects arising from the current platinum based drugs. Not only do these drugs lack specificity and are highly neurotoxic, but the increasing incidence of platinum resistant cancers has fuelled the search for alternative drugs.[22,17]

Various transition metals have been screened in the process to find alternatives to platinum, and palladium has been identified as a promising candidate due to its similar coordination chemistry. Subsequently, a large amount of research has been done on organopalladium compounds.[17]

1.3.3 Palladium compounds

A comprehensive review on transition metals in chemotherapy, published in 1974[12], stated that there was little to no hope for palladium (II) complexes since their animal testing yielded poor results when compared to that of platinum (II) complexes. The author speculated that this is due to the increased reactivity of the complexes *in vivo* and that these compounds would only be successful anti-tumour agents in the presence of strongly deactivating ligands.[12]

This was proven to be an erroneous assumption, since today there are many different palladium complexes that show significant anti-tumour activities. It has even been shown that some *trans* palladium (II) and palladium (IV) structures exhibit promising anti-cancer activity, thus disproving the initial generalization that a *cis* structure was crucial for anti-tumour activity.[14]

Various palladium salts similar to that of cisplatin have been investigated for their anti-cancer activities, but none have been as successful as their platinum analogues.[14] From the bulk of the research produced over the past five decades, it would appear that there are three distinct classes of Pd(II) anti-cancer compounds: *trans*-Pd(II) complexes, bidentate Pd(II) complexes and palladacycles. These will be discussed briefly below.

1.3.3.1 *Trans*-Palladium (II) complexes

Since the steric effects of a ligand could to a great extent govern the geometry around the metal centre, bulky monodentate ligands inevitably arrange themselves in *trans* positions around a d^8 palladium centre to result in a square planar geometry. It has been found that the *trans*-geometry around a palladium centre improves the cytotoxicity when compared to that of the *cis*-analogues, the opposite from what was observed for the platinum compounds.[17]

One of the first *trans*-Pd(II) complexes that showed notable anti-cancer potential was put forward by Tušek-Božić et al. in 1991[23] (Figure 1.9). This was based on complexes of the type *trans*-[Pd(2-dqmp)$_2$X$_2$] (2-dqmp = diethyl 2-quinolylmethylphosphonate and X = Cl or Br) and have evaluated against epidermoid human carcinoma (KB) and murine leukaemia (L1210). It was found that the bromide analogues displayed higher cytotoxic activity against both cell lines than the chloride analogues, possibly due to the increased solubility of the bromide analogues, but the compounds were still not as effective as cisplatin.[23] Although these results were not an improvement on the platinum analogues, this research provided the foundation for further investigations into the anti-tumoural activity of *trans*-Pd(II) complexes.

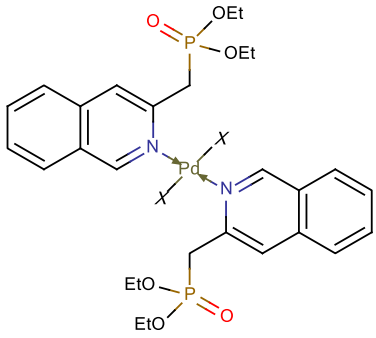

X = Cl (KB: IC_{50} = 64.9 µM, L1210: IC_{50} = 77.7 µM)
X = Br (KB: IC_{50} = 12.7 µM, L1210: IC_{50} = 2.76

Figure 1.9: One of the first *trans*-Pd (II) complexes that showed notable anti-cancer activity, *trans*-Pd(II) bis(quinonylmethyl-phosponate).[23]

Naturally-occurring ligands started to play a large role in drug discovery in the 1990s since the technological advancement of spectroscopy simplified structure elucidation. This resulted in the use of natural compounds as ligands, especially compounds that have already shown some biological activity such as the plant alkaloid harmine (7-methoxy-1-methyl-9H-pyrido[3,4-b]indole).[17]

Al-Allaf and Rashan[24] investigated the anti-cancer activity of *trans*-[Pd(harmine)(DMSO)Cl_2] against P388, L1210 and K562 and found that the complex showed superior activity when compared to cisplatin, carboplatin, 5-FU and the ligand itself.[24]

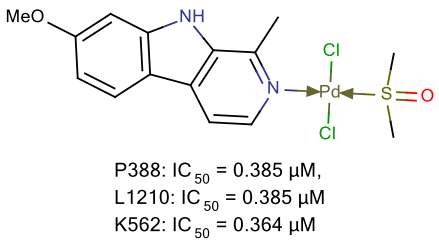

Figure 1.10: The *trans*-Pd(II) complex resulting from coordination to harmine and DMSO.[24]

In 2002 Abu-Surrah et al.[25] investigated the anti-cancer potential of an enantiomerically pure chiral *trans*-Pd (II) complex, *trans*-bis{endo-(1R)-1,7,7-trimethylbicyclo[2.2.1]-heptan-2-amino} palladium(II) dichloride. This compound performed worse than commercial platinum drugs with regards to the K562 and L929 cell lines but performed better than cisplatin and carboplatin in the HeLa cell line. The authors concluded that the compound had a higher non-specific toxicity than the platinum compounds which means that it would be a poor anti-cancer drug. It was however the first reported case of a chiral *trans*-Pd(II) complex.[25]

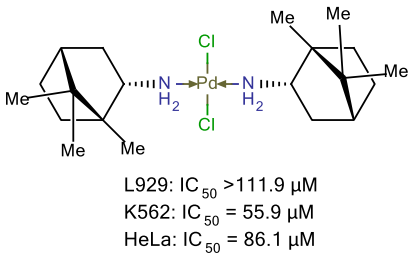

Figure 1.11: The structure of the first chiral *trans*-Pd(II) complex evaluated against various cell lines[25]**.**

In 2004 Gutiérrez and co-workers[26] synthesized another chiral *trans*-Pd(II) complex from an *α*-ketoimine, (S)-(-)-(1-phenylethylimino)benzyl-phenylketone, with the hope that the incorporation of various functional groups could help tailor the cytotoxic abilities of the subsequent drugs. The product unfortunately did not prove very promising since it also showed rather unselective cytotoxicity towards the PC-3, K562 and MCF-7 cancer cell lines, and resulted in higher IC_{50} values when compared to cisplatin.[26]

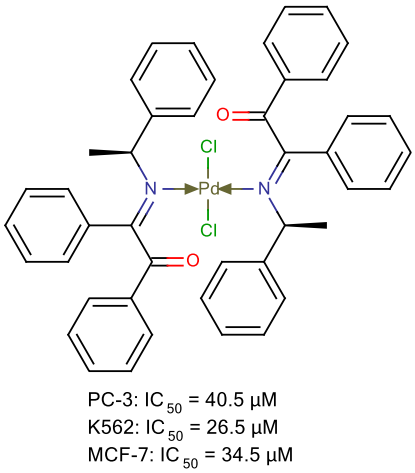

Figure 1.12: The chiral *α*-ketoimine *trans*-Pd(II) complex.[26]

To date, *trans*-Pd(II) complexes have always displayed lower cytotoxic ability when compared to known platinum drugs. The first true potential of *trans*-Pd(II) complexes only emerged in 2006 as demonstrated by Trávnícek and colleagues[27] Substituted benzylaminopurine compounds have shown some ability to inhibit cyclin-dependent kinases (CDK), kinases that play a regulatory role in the cell cycle. This research group thus complexed a number of these compounds to palladium in *cis*- and *trans*-conformations and evaluated them against a number of cell lines. The *trans*-palladium complexes resulted in improved anti-cancer activity as compared to the platinum analogues and commercial compounds. The *cis*-palladium analogues were also tested and performed weaker than the *trans*-compounds, as expected from previous research.[28,17,27]

Despite the many publications which conclude that *trans*-Pd analogues outperform the *cis*-Pd analogues, while the opposite is true for platinum compounds, there is, as yet, no definitive reason established for the difference in activity as related to the structure of the complexes. It has been speculated, but not proven, that the difference in activity is due to the way in which cisplatin interacts with DNA. The cytotoxicity of cisplatin is attributed to the formation of covalent bond between platinum and the N6 and N7 atoms of adjacent guanine base pairs on a single strand of DNA.[29,30] This mode of action relies on the *cis* structure of cisplatin. Since the mode of action of palladium complexes in general have not yet been established, the reason for the difference in activity between the *cis*-Pd and *trans*-Pd analogues is currently unknown, but preliminary indications are that the mode of action for these Pd-containing compounds differ from that of cisplatin.

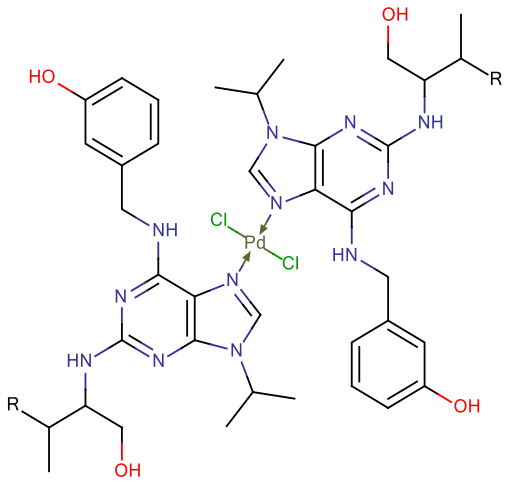

R = H (MCF-7: IC_{50} = 3 µM, K562: IC_{50} = 7 µM, G361: IC_{50} = 20 µM, HOS: IC_{50} = 12 µM)
R = Me (MCF-7: IC_{50} = 3 µM, K562: IC_{50} = 6 µM, G361: IC_{50} = 15 µM, HOS: IC_{50} = 15 µM)

Figure 1.13: The benzylaminopurine based *trans*-Pd(II) complexes that showed very promising anti-tumoural activity.[27]

A year later the same research group published the first *trans*-Pd(II) complex that showed selectivity, although the cytotoxicity of the complexes was not comparable to that of the commercial platinum compounds. The complex below showed selectivity towards malignant melanoma (G361) with an IC_{50} of 15 µM, as compared to that of cisplatin at 3 µM.[31]

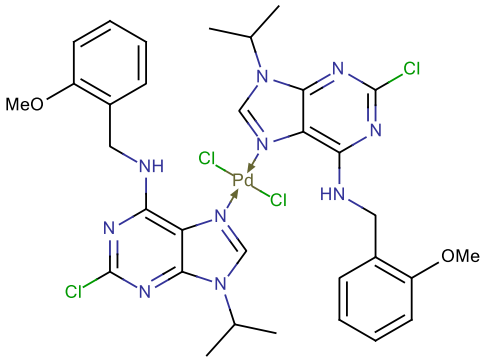

MCF-7: IC_{50} > 50 µM
K562: IC_{50} > 50 µM
G361: IC_{50} = 15 µM
HOS: IC_{50} > 50 µM

Figure 1.14: The structure of the first *trans*-Pd(II) complex that showed selectivity.[31]

Up until this point the ligands used for complexation to the palladium centres were chosen for three distinct reasons: 1) ligands that are important in biological systems, such as organophosphorus ligands,[23] 2) ligands that occur naturally, such as the harmine ligand,[24] and 3) ligands that have their own biological activity such as benzylaminopurine that is itself a kinase inhibitor.[27] Soon it became apparent that certain types of ligands enhance the cytotoxic activity of the compounds while others

diminish it and thus the research focus became more structure orientated, although no clear structure-activity relationships have been established.

In literature, one of the more prominent ligand moieties are planar aromatic compounds. The first *trans*-Pd(II) complexes to be tested against ovarian cancer had hydroxyl-substituted pyridine ligands.[32] The most effective compound among the three tested is shown below and performed better against cisplatin resistant ovarian cancer (A2780^{cisR}) and picoplatin resistant ovarian cancer (A2780^{ZD0473R}) than cisplatin itself.

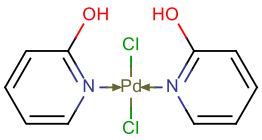

A2780: IC_{50} = 37 µM
A2780^{cisR}: IC_{50} = 5.6 µM
A2780^{ZD0473R}: IC_{50} = 3.1 µM

Figure 1.15: *trans*-Pd(2-hydroxypyridine)$_2$Cl$_2$, the first *trans*-Pd(II) complex to be evaluated against ovarian cancer.[32]

Building on this research Huq and co-workers[33] synthesized *trans*-Pd(II) complexes of the form *trans*-PdL_2Cl_2 where L = 2-methylpyridine, imidazole and 1,2-α-imidazopyridine, of which the last was also significantly active against the ovarian cancer cell lines A2780, A2780^{cisR}, A2780^{ZD0473R} and SKOV-3 (Sloan-Kettering HER2 3+ ovarian cancer). The most promising compound, *trans*-[Pd(1,2-α-imidazopyridine)$_2$Cl$_2$] was less active than cisplatin, but the IC_{50} values are comparable to that of cisplatin, especially against the cisplatin resistant cell lines.[33]

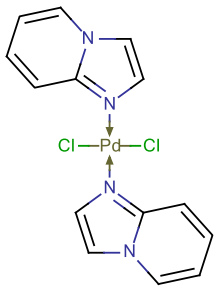

A2780: IC_{50} = 6.78 µM
A2780^{cisR}: IC_{50} = 7.95 µM
A2780^{ZD0473R}: IC_{50} = 6.03 µM
SKOV-3: IC_{50} = 4.36 µM

Figure 1.16: A *trans*-Pd(II) complex containing an imidazopyridine ligand that showed promising activity against ovarian cancer cell lines.[33]

Continuing along this line of inquiry, Mendía and colleagues[34] tested a series of PTA (1,3,5-triaza-7-phosphadamantane) palladium(II) thionate complexes and also compared their antiproliferative activity against ovarian cancer to that of the platinum(II) analogues. By doing this, the group kept the

concept of planarity with the thionate ligand but included a bulky phosphine ligand. This had a positive effect on the anti-cancer activity of the compound, by improving the IC_{50} values beyond that of cisplatin and better than those achieved by any of the other *trans*-Pd(II) complexes up to date.[34]

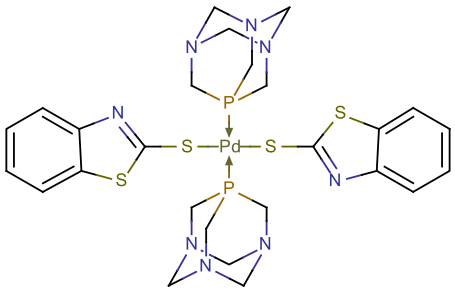

A2780: IC_{50} = 3.12 µM
A2780^{cisR} : IC_{50} = 1.62 µM

Figure 1.17: *Trans*-[Pd(benzothiazole-2-thionate)$_2$(PTA)$_2$] had shown to be highly effective against ovarian cancer.[34]

α-Keto-imines and α-diimines have also played an important role in the development of *trans*-Pd(II) complexes for anti-cancer purposes. This is due to the versatility regarding coordination and electronic effects that these compounds present.[35] In the article published by Gutiérrez an co-workers[35] a number of *cis* and *trans* unsymmetrical α-diimine Pd(II) complexes were evaluated against a wide selection of cancer cell lines. To their disappointment it was found that none of their compounds displayed significant anti-cancer activity relative to cisplatin, but there were varying IC_{50} values which could indicate a potential structure activity relationship.[35]

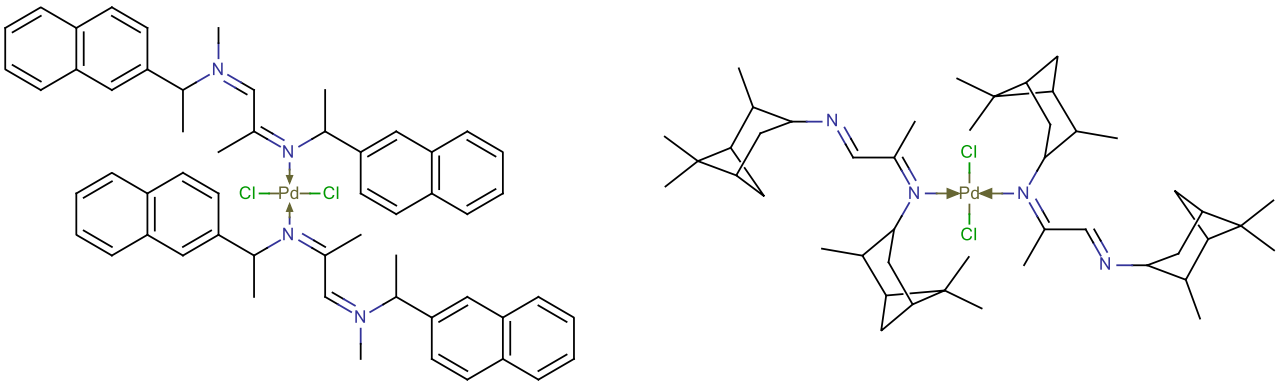

U251, PC-3, K562, HCT-15, MCF-7: IC_{50} = >100

Figure 1.18: Chiral Pd(II) complexes with α-diimine functionalities.[35]

The final functionality that has improved the anti-cancer activity of *trans*-Pd(II) complexes is N-heterocyclic carbenes (NHC).

In 2007 Panda and colleagues[36] explored the anti-cancer activities of palladium (II) N-heterocyclic carbene complexes, of which the complex that showed the most promise is shown in Figure 1.19.

They found that the NHC complexes displayed significantly higher anti-cancer activities when compared to cisplatin and that they induced natural cell death, apoptosis.

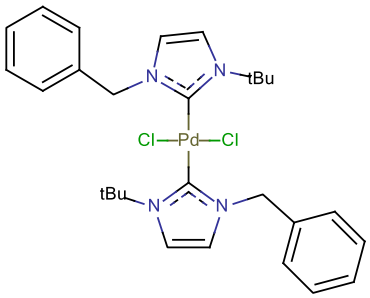

HeLa: IC_{50} = 4.0 µM
HCT 116: IC_{50} = 0.8 µM
MCF-7: IC_{50} = 1.0 µM

Figure 1.19: The Pd(II)-NHC complex that was first investigated in 2007. The complex showed remarkable anti-cancer activity when compared to that of cisplatin against the same cell lines.[36]

Building on this research, another group, Haque et al.[37], decided to expand on it in 2013 by changing the substituents on the N-heterocyclic carbenes in order to investigate less sterically hindered substituents. Unfortunately their compounds, as shown in Figure 1.20, were not as active as those developed by Panda and colleagues[36] and it is also clear that the structures of the carbenes have an unclear influence on the activity of the compounds.

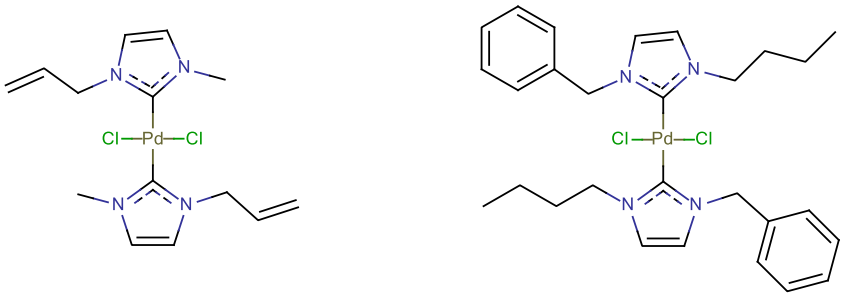

No anti-cancer activity detected

HCT 116: IC_{50} = 6.6 µM

Figure 1.20: The two NHC-carbene complexes investigated by Haque et al.[37]

In conclusion, *trans*-Pd(II) complexes have shown great promise in the field of anti-cancer activity with functionalities ranging from quinolones and α-diimines to pyridines and N-heterocyclic carbenes.

From the complexes reviewed, a number of conclusions can be drawn. Firstly, the inclusion of planar moieties increases the cytotoxicity of the complexes. This is possibly due to the intercalation of the planar ligands with DNA. Secondly, bulkier ligands appear to increase the cytotoxicity of the complexes, possibly due to the fact that they cause a greater distortion of the DNA. Finally, it has been observed that complexation of the Pd-centre to a bioactive ligand, increases the anti-cancer activity of the ligand.

Thus, it is clear that the ligand plays a very important role in the biological activity of the complex, but there is no definitive structure activity relationship that has become apparent yet. It is thus necessary to explore other ligand types in order to gather more information on these types of complexes.

1.3.3.2 *N,N*-bidentate Palladium (II) complexes

Trans-Pd(II) complexes have proven very useful but it remains necessary to explore the effect of the *cis*-isomers since the *cis*-Pt(II) complexes have proven so effective. As mentioned in the previous section, ligands surrounding Pd(II) centres prefer a *trans*-coordination due to steric constrains. Subsequently, multidentate ligands have enjoyed much attention due to their electronic and steric tailoring effects[17]. Naturally there are many different methods of chelation including *N,N'-* , *N,S-* , *S,S'-* , *N,P-* , and *P,P'*-coordinated compounds. For the purpose of this thesis, the focus will be on *N,N'*-bidentate ligands.[17]

The most explored ligand types are 2,2'-bipyridyls and 1,10-phenanthrolines, since they provide a strong sterically constrained planar systems that are entropically favoured, due to the chelate effect.[17]

One of the earliest *N,N'*-bidentate palladium(II) complexes were synthesized by Newkome et al.[38] in 1985, and although they did not investigate the cytotoxic capabilities of the compound, their research led to the investigation of *N,N'*-bidentate palladium(II) complexes as a class of cytotoxic drugs in their own right.

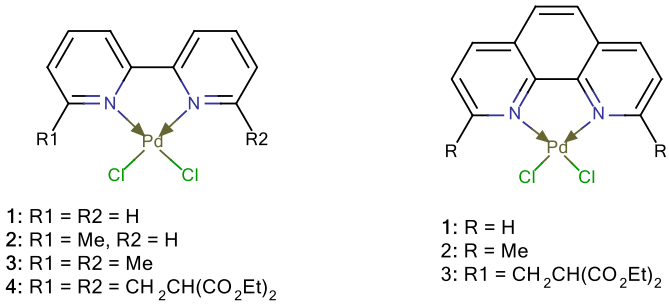

1: R1 = R2 = H
2: R1 = Me, R2 = H
3: R1 = R2 = Me
4: R1 = R2 = $CH_2CH(CO_2Et)_2$

1: R = H
2: R = Me
3: R1 = $CH_2CH(CO_2Et)_2$

Figure 1.21: The general structure of the first *N,N*-bidentate Pd(II) complexes.[38]

In 1991 Mansouri-Torshizi et al.[39] demonstrated that the inclusion of an oxygen leaving group somehow increases the anti-cancer activity of the complexes. Thus they studied the effects of incorporating selenite and tellurite into the Pd(II)-complexes on the anti-cancer activity of the compounds. The incorporation of the selenite greatly improved the anti-cancer activity of the complexes when compared to cisplatin.[39]

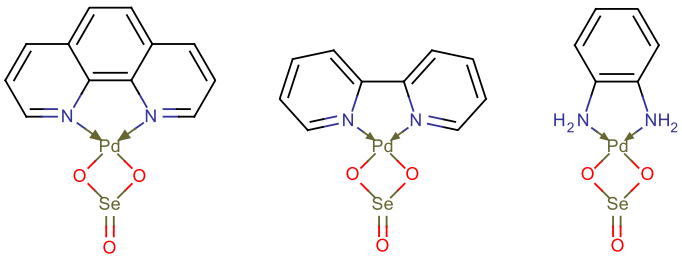

P388: IC_{50} = 3.0 µM for all three compounds

Figure 1.22: Examples of the first *N,N*-bidentate complexes that showed significant anti-cancer activity against the P388 cell line.[39]

Lin and colleagues[40] demonstrated in 1998 that the planarity of the ligand increased the level of intercalation of the complex into the structure of DNA. They demonstrated this with a number of tetradentate 1,10-phenanthroline complexes (Figure 1.23) and showed that an increase in the steric bulk of the ligand resulted in higher cytotoxic activity against leukaemia, L1210, and liver carcinoma, Bel17402.[40]

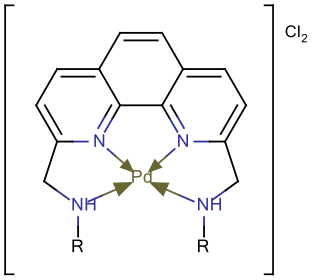

R = $CH_2CH_2CH_3$ (L210: IC_{50} = 10.62 µM, Bel7402: IC_{50} = 11.59 µM)
R = tBu (L1210: IC_{50} = 9.53 µM, Bel7402: IC_{50} = 10.26 µM)
R = cyclohexyl (L1210: IC_{50} = 8.20 µM, Bel7402: IC_{50} = 8.20 µM)

Figure 1.23: The general structure used by Lin and colleagues[40] to investigate the effect of steric substituents on the anti-cancer activity of the complex.

Building on the 2,2'-bipyridyl motif, Valentini et al.[41] used a bioactive ligand, 4,4'-dinonyl-2,2'-bipyridine, and a natural-occurring compound, curcumin , and complexed both to a Pd(II) centre. This resulted in a complex that showed higher IC_{50} values than pure curcumin, but induced a different cell death pathway in various different prostate cancer cell lines thus making the compound less toxic than the unbound curcumin.

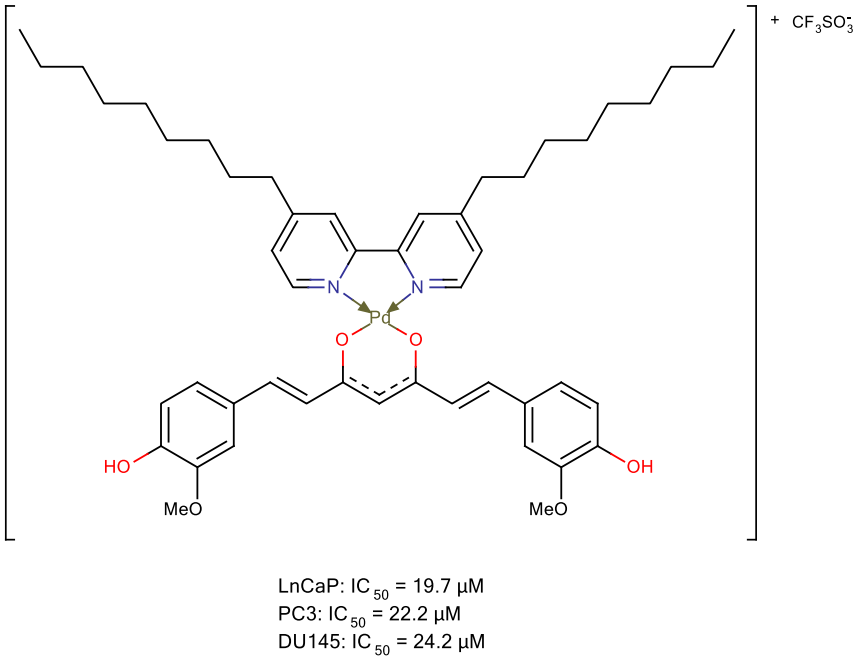

Figure 1.24: The structure of the complex resulting from the combination of curcumin and a bioactive 2,2'-bipyridyl ligand.[41]

Another interesting 2,2'-bipyridyl complex (Figure 1.25) arose from the investigation by Gao and co-workers[42] into the effects of the carbon chain length on the anti-cancer activity of the compounds. They found that an increase in the carbon chain length of the benzene-alkyl dicarboxlate ligand leads to an increase in the anti-cancer activity of the compounds, thus indicating that the flexibility of the compound plays an important role in the intercalation of the compound into the DNA structure. They investigated carbon chain lengths of 1 to 3 carbon atoms. The exact role of the aliphatic chain was, however, not determined by these researchers.[42]

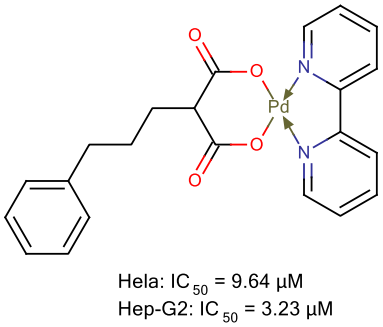

Figure 1.25: The structure of the most potent compound investigated by Gao and co-workers.[42]

Expanding upon the chelation of known biologically active compounds, Navarro-Ranninger and colleagues[43] proceeded to chelate spermine and putrescine to palladium salts in order to produce a number of polyamine complexes. The most promising of their compounds used 1,4-butane diamine as a ligand, as shown in Figure 1.26.

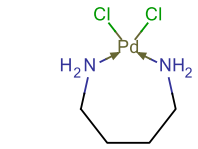

MCA-MB468: IC_{50} = 0.53 µM
HL60: IC_{50} = 0.43 µM

Figure 1.26: The spermine chelated Pd(II) complex.[43]

Moving away from the 2,2'-bipyridyl motive, Lin and co-workers[44] investigated a dimeric complex with Pd(II) centres stabilised by ethylenediamine bidentate ligands. They found a remarkably low IC_{50} value which prompted them to carry out further investigations in order to understand the way in which the electronics of the substituents influence the anti-cancer activity of the compound.[44]

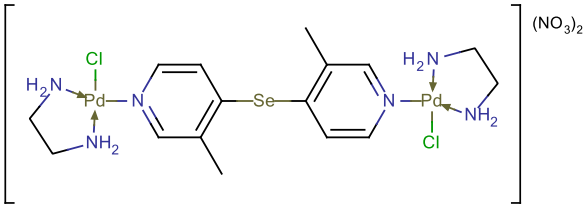

HCT8: IC_{50} = 11.8 µM

Figure 1.27: The dimeric complex that sparked the investigation into ethylenediamine type compounds.[44]

By simplifying the structure, they found that with an increase in the electron donating abilities of the pyridine substituents, a marked decrease in the anti-cancer activity of the complex is observed.[45] The most promising complex showed an IC_{50} similar to that of cisplatin against the human leukaemia cell line, HL60 (Figure 1.28).

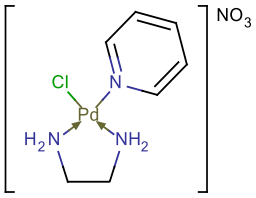

HL60: IC_{50} = 1.17 µM

Figure 1.28: One of the first ethylenediamine stabilized Pd(II) complexes to show significant anti-cancer activity.[45]

Mansouri-Torshizi et al.[46] synthesized an ethylenediamine stabilized quinolinato complex that showed significant anti-cancer activity against myelogenous leukaemia, K562, making it much more potent than any of the previous reported *N,N'*-bidentate complexes tested.

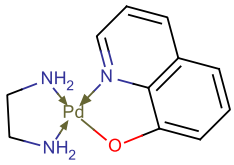

K562: IC_{50} = 0.08 µM

Figure 1.29: A highly potent *N,N*-bidentate system, ethylenediamine 8-hydroxyquinolinato.[46]

Mansouri-Torshizi et al.[47] then proceeded to take some inspiration from their first anti-cancer compounds (Figure 1.22) to produce and test a 1,10-phenanthroline dithiocarbamate Pd(II) complex. The complex was also evaluated against K562 and was found to be less potent than the quinoline based complex mentioned above. This amended the previous assumption that the planarity of the ligand was the main anti-cancer instigator.[47]

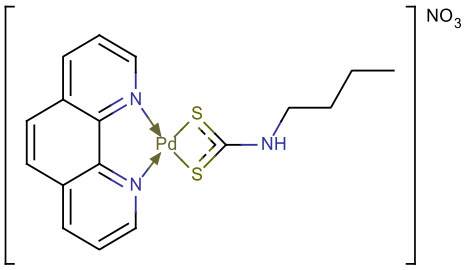

K562: IC_{50} = 10 µM

Figure 1.30: The 1,10-phenanthroline Pd(II) dithiocarbamate complex that showed significant anti-cancer activity.[47]

The quinoline motif appeared again a few years later in the form of an iminophosphorane derived from 8-aminoquinoline ligand. Casini and co-workers.[48] investigated a number of gold, palladium and platinum complexes with the ligand for both their anti-cancer activities and their luminescent properties. Figure 1.31 shows the *N,N'*-bidentate Pd(II) complex that displayed some anti-cancer activity. The study was unable to correlate the anti-cancer activity of the compound to the structure of the ligand, but it had become clear that although *N,N'*-bidentate ligands produce active anti-cancer complexes, they are not as active as the metallocycles of the same ligands.[48]

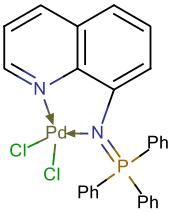

A2780: IC_{50} = 11.0 µM

Figure 1.31: The Pd(II) iminophosphorane that showed significant anti-cancer activity.[48]

More recently, with the advent of copper catalysed 'click' chemistry (see Chapter 2), the use of pyridyl-1,2,3-triazole chelating ligands has become of increasing importance in coordination chemistry. By combining the azide and alkyne moieties, the opportunity for rapid library expansion is created. Trivedi and colleagues[49] showed this with the incorporation of carbohydrate moieties into pyridyl-triazole *N,N'*-bidentate Pd(II) complexes. The use of carbohydrates in anti-cancer agents is well documented with compounds such as bleomycin (Figure 1.3), and thus helped the Pd(II) complexed compounds to show good anti-cancer activity.[49]

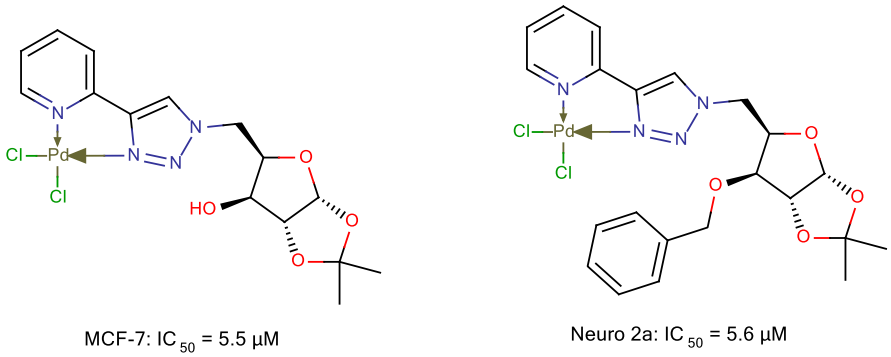

Figure 1.32: The first pyridyl-1,2,3-triazole Pd(II) complexes used as anti-cancer agents.[49]

In 2013 a separate group investigated the anti-cancer activity of similar compounds with imine functionalities rather than 1,2,3-triazoles. Katoaka and co-workers[50] investigated palladium and platinum glycoconjugated imines against cisplatin resistant gastric cancer cell lines (Figure 1.33). Although their compounds were not as active as oxaliplatin, the palladium compounds were more active than the platinum compounds and effectively overcame the cisplatin resistance.[50] Their work reiterated the importance of the Pd(II) centre stabilization.

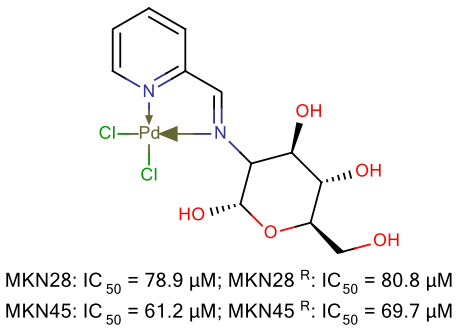

Figure 1.33: The glycoconjugated Pd(II) complexes with imine moieties tested against gastric cancer.[50]

From the review above two conclusions can be made regarding *N,N'*-bidentate Pd(II) complexes. The first is that there are small structural features that seem to play a specific role in the structure-activity relationships, but none that have been directly linked or proven consistently in various systems. The second is that the mode of Pd(II) stabilization greatly affects the anti-cancer activity of the compounds. This has also been the case with the *trans*-Pd(II) complexes discussed previously.

1.3.3.3 Palladacycles

It has been mentioned extensively that the stabilization of the Pd(II) centre plays a critical role in the anti-cancer activity of the compounds. Owing to this observation, it has been shown that Pd-C bonds are preferable to Pd-N bonds when it comes to anti-cancer activity, since the former withstand hydrolysis to a greater extent[51], although there are some exceptions to the rule. Additionally, it has also been shown that palladacycles are not only more stable, but also show a more selective cytotoxicity that is not the case for platinum compounds.[51]

Recently, a comprehensive review on the topic was published by Kapdi and Fairlamb.[17] For this reason, only a handful of significant compounds will be discussed here.

The first major publication in the field of anti-cancer palladacycles only came in 1993 by Higgins III et al.[52] in which they evaluated twelve palladacycles with various scaffolds against seven different cell lines. The compounds that showed the most activity are shown in Figure 1.34.

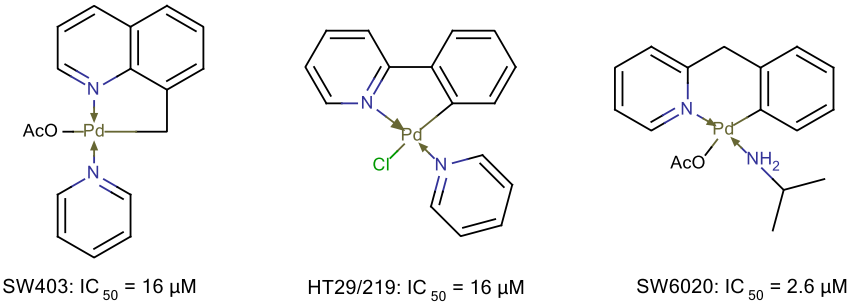

SW403: IC_{50} = 16 µM HT29/219: IC_{50} = 16 µM SW6020: IC_{50} = 2.6 µM

Figure 1.34: The compounds by Higgins et al.[52] that showed the most activity against the respective cell lines listed.

Ruiz et al.[53] synthesized similar compounds by substituting the pyridine coordination site with a substituted amine. In addition to the amine substitution they incorporated a model nucleobase, 1-methylcytosine, to make the compound more compatible with biological systems. The compound shown in Figure 1.35 displayed increased anti-cancer activity when compared to cisplatin under the same conditions.

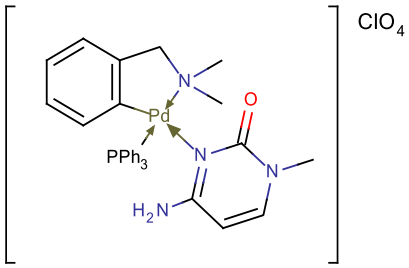

HL-60: IC_{50} = 3.0 µM

Figure 1.35: The palladacycle by Ruiz et al.[53] that showed the best anti-cancer activity.

The same C,N'-motif was reported previously by Travassos and colleagues[51] in which they employed bis(diphenylphosphino) ethane (dppe) as a ligand with various modes of action (Figure 1.36). The compounds shown in Figure 1.36 were not especially active, but have served as the basis for many projects since.

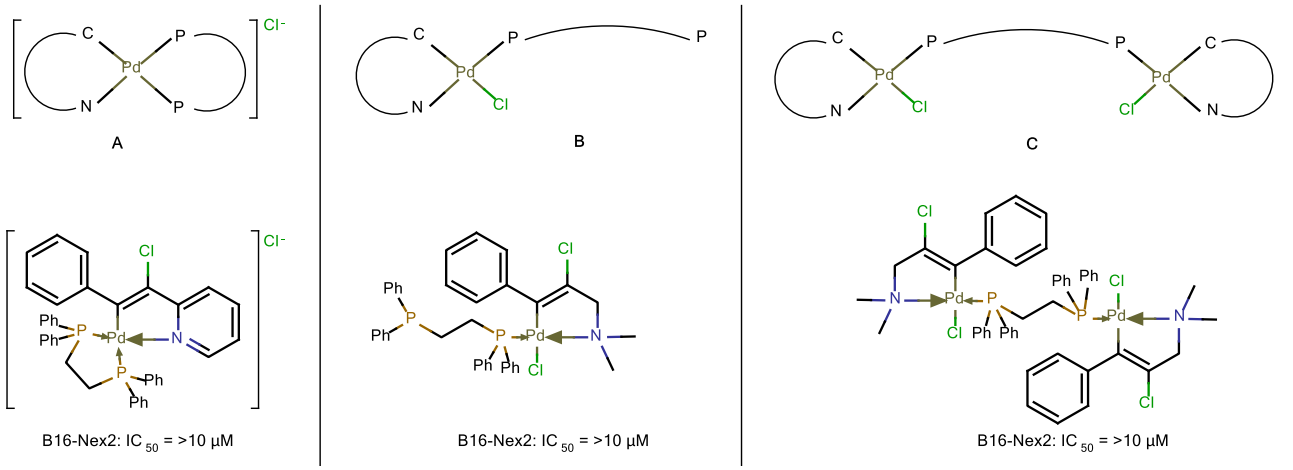

Figure 1.36: The different classes of compounds investigated by Travassos and colleagues[51] and the resulting palladacycles tested.

Ruiz et al.[54] investigated palladacycles with 9-aminoacridine ligands against the leukaemia cell line, HL60. The inclusion of the acridine moiety was done in order to predisposition the compounds towards intercalation with DNA as its biological mechanism. They found that the palladacycles were more active than cisplatin under the same conditions. The two most potent compounds in this series are shown in Figure 1.37.

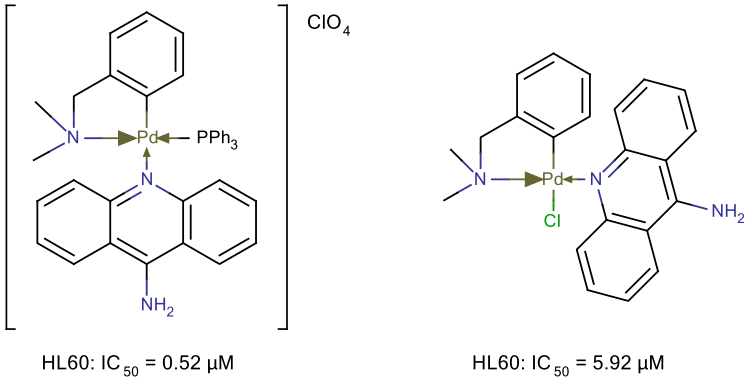

Figure 1.37: The 9-aminoacridine palladacycles investigated by Ruiz et al.[54]

The bis(diphenylphosphino) ethane (dppe) moiety appeared again in 2009 with the compounds investigated by Spencer et al.[55] (Figure 1.38). The dinuclear compounds performed better than the monomeric compounds under the same conditions, and the bis(diphenylphosphino) ethane moieties performed better than the bis(diphenylphosphino) ferrocene (dppf) moieties, indicating that the type of bridging ligand is important.

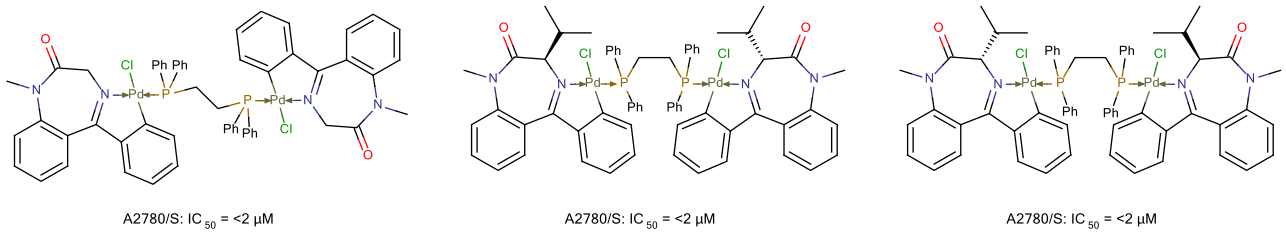

Figure 1.38: The dimeric compounds investigated by Spencer et al.[55]

Another prominent moiety with palladacycles is the use of α-diimines to form pincer type palladacycles, as demonstrated by Gutiérrez and co-workers[56] in 2009 (Figure 1.39). Although the cytotoxicity profiles of the compounds obtained were not as potent compared to cisplatin, the compounds showed some selectivity towards leukaemia and central nervous system (CNS) cancers as compared to prostate, colon and breast cancer.

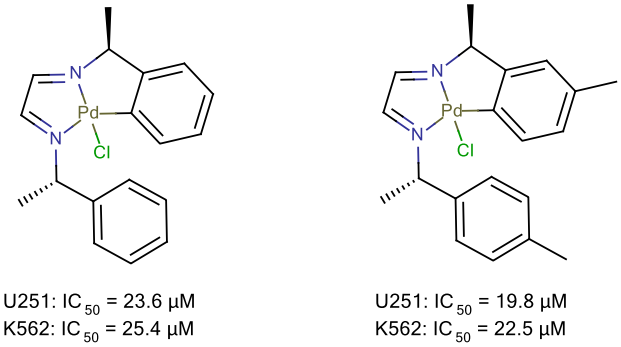

Figure 1.39: The α-diimines investigated by Gutiérrez and co-workers.[56]

One of the most prominent issues with palladacycles is their low water solubility, which was overcome by Contel and colleagues[57] with the use of water-soluble iminophosphorane ligands. Two of their most promising compounds are shown in Figure 1.40. DNA binding studies revealed that these compounds' main target is not DNA, but rather human serum albumin (HSA), which is different from that of cisplatin and thus more favourable. With the advent of platinum resistant cancers, it is necessary to develop anti-cancer agents with biological mechanisms different from that of cisplatin in order to circumvent the rapid onset of resistant cancers. HSA is a carrier protein that has the ability to bind various therapeutic drugs, including metal cations and thus provides an ideal alternative anti-cancer mechanism.[57]

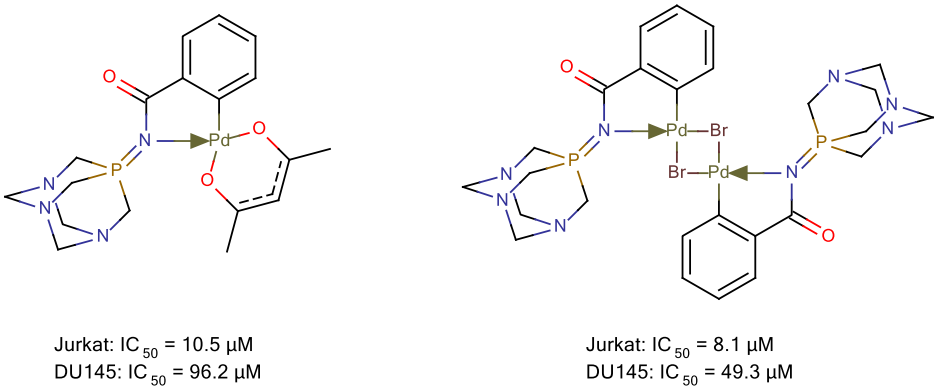

Figure 1.40: The water-soluble iminophosphorane palladacycles that showed improved anti-cancer activity when compared to cisplatin.[57]

Recently our own research group investigated the cytotoxic capabilities of a dppe bridged palladacycle **AJ5**, basing the synthesis on the palladacycles investigated by Spencer et al.[55] and Travassos and colleagues[51] The *in vitro* and *in vivo* cytotoxicity of **AJ5** have been fully investigated and indicate remarkably potent anti-cancer activity.[58] This has sparked intense investigation into similar compounds.

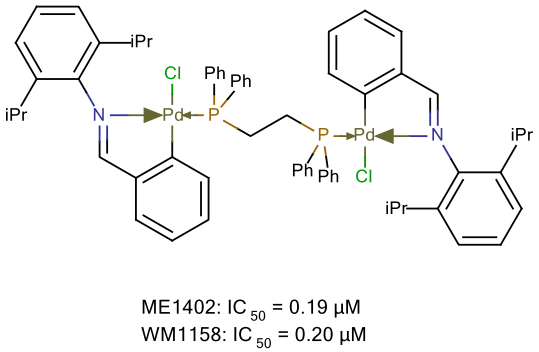

Figure 1.41: The binuclear palladacycle AJ5 which displayed highly potent activity against malignant melanoma cell lines.[58]

The same year that AJ5 was published, an independent research group published their investigation into a number of benzylamines, two mononuclear compounds and one dinuclear compound (Figure 1.42). Karami et al.[59] found that the dinuclear compounds were generally more potent than their mononuclear counterparts. Nonetheless, all their compounds showed significant anti-cancer activity against various cell lines.

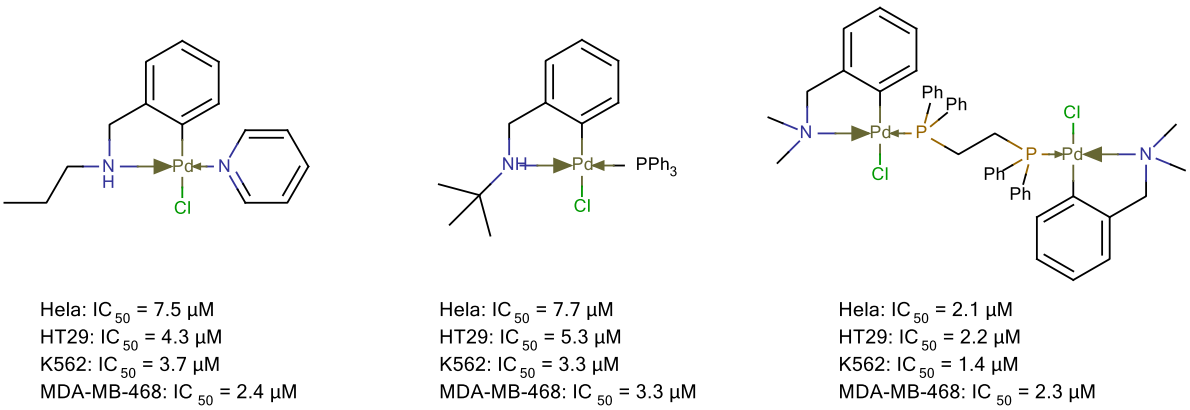

Hela: IC_{50} = 7.5 µM
HT29: IC_{50} = 4.3 µM
K562: IC_{50} = 3.7 µM
MDA-MB-468: IC_{50} = 2.4 µM

Hela: IC_{50} = 7.7 µM
HT29: IC_{50} = 5.3 µM
K562: IC_{50} = 3.3 µM
MDA-MB-468: IC_{50} = 3.3 µM

Hela: IC_{50} = 2.1 µM
HT29: IC_{50} = 2.2 µM
K562: IC_{50} = 1.4 µM
MDA-MB-468: IC_{50} = 2.3 µM

Figure 1.42: The compounds investigated by Karami et al.[59]

In 2014 Albert et al.[60] investigated the effect of the co-ligand in dinuclear palladacycles with a range of differently substituted compounds. The most effective of their compounds is shown in Figure 1.43. Interestingly they found that the length of the co-linker chain does have a remarkable effect on the anti-cancer activity that can be contributed to the increased flexibility and lipophilicity of the molecule.

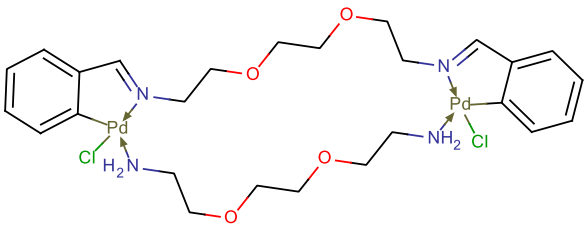

HCT116: IC_{50} = 30 µM
MCF7: IC_{50} = 5.5 µM
MDA-MB-231: IC_{50} = 7.8 µM

Figure 1.43: The most effective compound investigated by Albert et al.[60]

From the information above it appears that the dinuclear compounds outperform the mononuclear compounds when one simply considers the IC_{50} values. Since it is the metal adducts formed between the DNA and the compound that results in the cytotoxic effect observed, one should not only consider the IC_{50} value determined, but rather the metal centre to DNA ratio. When that is considered, the IC_{50} values of the dinuclear compounds can be considered as half that reported, which would mean that per metal centre the mononuclear compounds are more potent that the dinuclear compounds.

In summary, Pd(II) compounds have found extensive use as anti-cancer agents, but the structure-activity relationship is still vague. This necessitates further investigation into these compounds and the creation of larger libraries with the aim of generating enough data from which a more definitive structure-activity relationship can be elucidated.

1.3.4 Structure-Activity Relationships

As mentioned extensively throughout this chapter, the structure-activity relationships governing palladium based anti-cancer agents are vague and indefinite. In a comprehensive review by Alam and Huq[61] published in 2016, a number of general structure-activity guidelines were presented based on the trends observed in literature. The most relevant conclusions are summarized below:

1. In general, *trans* palladium complexes display greater anti-cancer activity than their *cis* counterparts.
2. Bulkier ligands lead to increased activity due to a greater distortion of the DNA.
3. Within a series of analogous palladium complexes, an increase in the lipophilicity of a complex generally leads to an increase in the anti-cancer activity of the complex.
4. Chlorides are generally used as leaving groups in order to yield the active species in solution.

These conclusions are still quite general and there are exceptions to the rule in all cases. It is thus important to focus more on the development of structure-activity relationships within a class or series of compounds

1.4 Proposed compounds

The proposed compounds for this project were *trans*-Pd(II) complexes and *N,N'*-bidentate Pd(II) complexes with 1,2,3-triazole scaffolds similar to that of Trivedi and co-workers.[49]

The azide substituents were kept simple in order to investigate the steric, electronic and hydrophilic influences on the anti-cancer activities of the compounds. It was decided to investigate simple substituents, as their anti-cancer activity has, to the best of our knowledge, not been investigated, but more complex substituents, such as carbohydrate substituents, have been investigated before.[49]

The general structures of the proposed compounds are shown in Figure 1.44. The *trans*-Pd(II)-1-substituted-4-phenyl-1,2,3-triazolyl complexes and some of the *N,N'*-bidentate Pd(II)-1-substituted-4-pyridyl-1,2,3-triazolyl complexes are to the best of our knowledge new.

The structure of the ligands was chosen in such a manner as to utilize the 1,2,3-triazole as a coordinating ligand. 1,2,3-Triazoles are metabolically stable, have hydrogen bonding and coordination capabilities and are pharmacophores in their own right, thus making them suitable for medicinal applications.[62]

The *trans*-Pd(II)-1,4-disubstituted-1,2,3-triazolyl complexes include a phenyl ring in the 4-position, as there is literature precedent which indicates that planar ligands facilitate DNA-binding interaction through intercalation.

For the *N,N'*-bidentate Pd(II)-1,4-disubstituted-1,2,3-triazolyl complexes the phenyl ring was exchanged for a pyridine ring, as it would maintain the planar structure of the substituent while facilitating chelation to the metal centre.

The N-bound substituents were varied in order to investigate the effect of sterics, hydrophilicity and electronics on the anticancer activity of the complexes. The choice of substituents is fully addressed in Chapter 2.

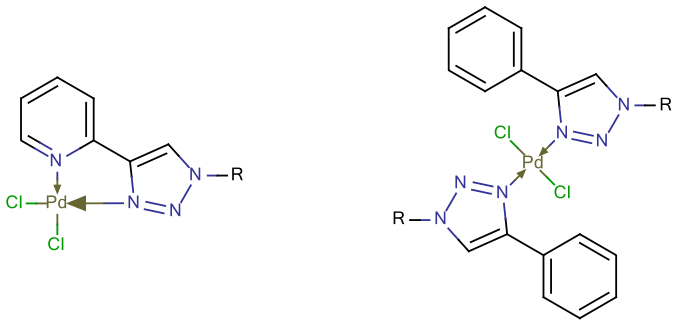

R = mesityl, phenyl, 4-nitrophenyl, cyclohexyl, C_8H_{17}, CH_2OH, $C_6H_{12}OH$, $(CH_2CH_2O)CH_2CH_2OH$, $(CH_2CH_2O)_2CH_2CH_2OH$.

Figure 1.44: The general structures of the proposed compounds.

1.5 Aims and Objectives

The aim of this project was to synthesized the two libraries of proposed complexes, as shown in Section 1.4, and to investigate their cytotoxicity against two breast cancer cell lines.

In order to achieve this aim, the following objectives were identified:

1. To synthesize of a series of 1,4-disubstituted 1,2,3-triazole ligands obtained from click chemistry methods. This includes the synthesis of the organo-azides used for the synthesis of the ligands.
2. To synthesize and characterize the *trans*-Pd(II)-1-substituted-4-phenyl-1,2,3-triazolyl complexes.
3. To synthesize and characterize the *N,N'*-bidentate Pd(II)-1-substituted-4-pyridyl-1,2,3-triazolyl complexes.
4. To investigate of the compounds' interaction with DNA by utilizing UV-Vis spectrometry and horizontal gel electrophoresis.
5. To assess the anti-cancer activity of the compounds against breast cancer cell lines (MCF-7 and MDA-MB-231) with MTT Assays.

1.6 Overview of thesis content by chapter

Chapter 2: The synthesis and characterization of the ligands and their precursors are described in this chapter.

Chapter 3: The synthesis and characterization of the *trans*-Pd(II)- and *N,N'*-bidentate Pd(II) complexes.

Chapter 4: The investigation into the DNA binding modes of the compounds are discussed as well as the results from the *in vitro* testing on the breast cancer cell lines.

Chapter 5: This chapter includes the final summary and concluding remarks of each preceding chapter as well as some suggestions for future work to be conducted.

1.7 References

1. *International Agency for Research on Cancer: Biennial Report*, Lyon France, 2013.
2. A. Sudhakar, *J. Cancer Sci. Ther.*, 2009, **1**, i–iv.
3. R. L. Siegel, K. D. Miller, and A. Jemal, *CA Cancer J Clin*, 2015, **65**, 5–29.
4. American Cancer Society, *Cancer Facts Fig. 2016*, 2016, 1–9.
5. S. Mukherjee, *The Emperor of all Maladies*, Scribner, New York, 2010.
6. American cancer Society, *The History of Cancer*, 2014.
7. V. T. DeVita and E. Chu, *Cancer Res.*, 2008, **68**, 8643–8653.
8. B. A. Chabner and T. G. Roberts, *Nat. Rev. Cancer*, 2005, **5**, 65–72.
9. S. Crawford, *Front. Pharmacol.*, 2013, **4**, 1–18.
10. I. S. Johnson, J. G. Armstrong, M. Gorman, and J. P. Burnett, *Cancer Res.*, 1963, **23**, 1390–1427.
11. B. Rosenberg, L. Van Camp, J. E. Trosok, and V. H. Monsour, *Nature*, 1969, **222**, 385–386.
12. M. Cleare, *Coord. Chem. Rev.*, 1974, **12**, 349–405.
13. L. M. Weiner, R. Surana, and S. Wang, *Nat. Rev. Immunol.*, 2010, **10**, 317–327.
14. I. Haiduc and C. Silvestru, *Coord. Chem. Rev.*, 1990, **99**, 253–296.
15. W. A. Collier and F. Krauss, *Z. Krebsforsch.*, 1931, **34**, 526–530.
16. B. Rosenberg, *Anticancer Chemother.*, 1984, **55**, 2303–2316.
17. A. R. Kapdi and I. J. S. Fairlamb, *Chem. Soc. Rev.*, 2014, **43**, 4751–4777.
18. M. Stern and R. Herrmann, *Crit. Rev. Oncol. Hematol.*, 2005, **54**, 11–29.
19. N. Iqbal and N. Iqbal, *Chemother. Res. Pract.*, 2014, **2014**, 1–9.
20. B. D. Smith, *JNCI J. Natl. Cancer Inst.*, 2011, **103**, 527–529.
21. B. Rosenberg, *Platin. Met. Rev.*, 1971, **15**, 42–51.
22. A. C. F. Caires, *Anticancer. Agents Med. Chem.*, 2007, **7**, 484–491.
23. L. Tušek-Božic, I. Matijašić, G. Bocelli, G. Calestani, A. Furlani, V. Scarcia, and A.

Papaioannou, *J. Chem. Soc. Dalton. Trans.*, 1991, 195–201.

24. T. A. K. Al-Allaf and L. J. Rashan, *Eur. J. Med. Chem.*, 1998, **33**, 817–820.
25. A. S. Abu-Surrah, T. A. K. Al-allaf, L. J. Rashan, and M. Klinga, *Eur. J. Med. Chem.*, 2002, **37**, 919–922.
26. M. A. Peláez, T. Ramírez, M. Martínez, P. Sharma, C. Álvarez, and R. Gutiérrez, *Zeitschrift für Anorg. und Allg. Chemie*, 2004, **630**, 1489–1494.
27. L. Szucová, Z. Trávnícek, M. Zatloukal, and I. Popa, *Bioorg. Med. Chem.*, 2006, **14**, 479–491.
28. A. S. Abu-surrah, H. H. Al-sa, and M. Y. Abdalla, *Cancer Ther.*, 2008, **6**, 1–10.
29. N. Poklar, D. S. Pilch, S. J. Lippard, E. A. Redding, S. U. Dunham, and K. J. Breslauer, *Proc. Natl. Acad. Sci. U. S. A.*, 1996, **93**, 7606–7611.
30. P. M. Takahara, A. C. Rosenzweig, C. A. Frederick, and S. J. Lippard, *Nature*, 1995, **377**, 649–652.
31. Z. Trávníček, L. Szučová, and I. Popa, *J. Inorg. Biochem.*, 2007, **101**, 477–492.
32. F. Huq, H. Tayyem, P. Beale, and J. Q. Yu, *J. Inorg. Biochem.*, 2007, **101**, 30–35.
33. M. E. H. Mazumder, P. Beale, C. Chan, J. Q. Yu, and F. Huq, *ChemMedChem*, 2012, **7**, 1840–1846.
34. E. Guerrero, S. Miranda, S. Lüttenberg, N. Fröhlich, J. M. Koenen, F. Mohr, E. Cerrada, M. Laguna, and A. Mendía, *Inorg. Chem.*, 2013, **52**, 6635–6647.
35. J. Vázquez, S. Berns, P. Sharma, J. Pérez, G. Hernández, A. Tovar, U. Peña, and R. Gutiérrez, *Polyhedron*, 2011, **30**, 2514–2522.
36. S. Ray, R. Mohan, J. K. Singh, M. K. Samantaray, M. M. Shaikh, D. Panda, and P. Ghosh, *J. Am. Chem. Soc.*, 2007, **129**, 15042–15053.
37. R. A. Haque, A. W. Salman, S. Budagumpi, A. A. Abdulla, and A. M. S. A. Majid, *Metallomics*, 2013, **5**, 760–769.
38. G. R. Newkome, F. R. Fronczek, and W. A. Deutsch, *Inorg. Chem*, 1985, **24**, 811–826.
39. H. Mansuri-Torshizi, R. Mital, T. S. Srivastava, H. Parekh, and M. P. Chitnis, *J. Inorg. Biochem*, 1991, **44**, 239–241.
40. G. Zhao, H. Sun, H. Lin, S. Zhu, X. Su, and Y. Chen, *J. Inorg. Biochem*, 1998, **72**, 173–177.
41. A. Valentini, F. Conforti, A. Crispini, A. De Martino, R. Condello, C. Stellitano, G. Rotilio, M. Ghedini, G. Federici, S. Bernardini, and D. Pucci, *J. Med. Chem.*, 2009, **52**, 484–491.
42. E. Gao, M. Zhu, L. Liu, Y. Huang, L. Wang, C. Shi, W. Zhang, and Y. Sun, *Inorg. Chem.*, 2010, **49**, 3261–3270.
43. C. Navarro-Ranninger, J. M. Pérez, F. Zamora, V. M. González, J. R. Masaguer, and C. Alonso, *J. Inorg. Biochem.*, 1993, **52**, 37–49.
44. G. Zhao, H. Lin, S. Zhu, H. Sun, and Y. Chen, *J. Inorg. Biochem.*, 1998, **70**, 219–226.
45. G. Zhao, H. Lin, P. Yu, H. Sun, S. Zhu, X. Su, and Y. Chen, *J. Inorg. Biochem.*, 1999, **73**, 145–149.
46. H. Mansouri-Torshizi, M. Saeidifar, G. R. Rezaei-behbehani, A. Divsalar, and A. A. Saboury, *J. Chin. Chem. Soc.*, 2010, **57**, 1299–1308.
47. H. Mansouri-Torshizi, M. Saeidifar, A. Divsalar, A. A. Saboury, and S. Shahraki, *Bull. Korean Chem. Soc.*, 2010, **31**, 435–441.
48. M. Frik, J. Jiménez, V. Vasilevski, M. Carreira, A. de Almeida, E. Gascon, F. Benoit, M. Sanau,

A. Casini, and M. Contel, *Inorg. Chem. Front.*, 2014, **1**, 231–241.

49. S. B. Deepthi, R. Trivedi, P. Sujitha, C. G. Kumar, B. Sridhar, and S. K. Bhargava, *J. Chem. Sci.*, 2012, **124**, 1405–1413.

50. M. Tanaka, H. Kataoka, S. Yano, H. Ohi, K. Kawamoto, T. Shibahara, T. Mizoshita, Y. Mori, S. Tanida, T. Kamiya, and T. Joh, *BMC Cancer*, 2013, **13**, 1–9.

51. E. G. Rodrigues, L. S. Silva, D. M. Fausto, M. S. Hayashi, S. Dreher, E. L. Santos, J. B. Pesquero, L. R. Travassos, and A. C. F. Caires, *Int. J. Cancer*, 2003, **107**, 498–504.

52. J. D. Higgins III, L. Neely, and S. Fricker, *J. Inorg. Biochem*, 1993, **49**, 149–156.

53. J. Ruiz, N. Cutillas, C. Vincente, M. D. Villa, and G. López, *Inorg. Chem*, 2005, **44**, 7365–7376.

54. J. Ruiz, J. Lorenzo, C. Vicente, G. López, J. M. López-de-Luzuriaga, M. Monge, F. X. Avilés, D. Bautista, V. Moreno, and A. Laguna, *Inorg. Chem.*, 2008, **47**, 6990–7001.

55. J. Spencer, A. Casini, O. Zava, R. Rathnam, S. Velhanda, M. Pfeffer, S. Callear, M. B. Hursthouse, and P. J. Dyson, *Dalton Trans.*, 2009, 10731–10735.

56. S. Cruz, S. Bernès, P. Sharma, R. Vazquez, G. Hernández, R. Portillo, and R. Gutiérrez, *Appl. Organomet. Chem.*, 2010, **24**, 8–11.

57. M. Carreira, R. Calvo-Sanjuán, M. Sanaú, I. Marzo, and M. Contel, *Organometallics*, 2012, **31**, 5772–5781.

58. S. Aliwaini, A. J. Swarts, A. Blanckenberg, S. Mapolie, and S. Prince, *Biochem. Pharmacol.*, 2013, **86**, 1650–1663.

59. K. Karami, M. H. Kharat, H. Sadeghi-Aliabadi, J. Lipkowski, and M. Mirian, *Polyhedron*, 2013, **50**, 187–192.

60. J. Albert, R. Bosque, M. Cadena, L. D'Andrea, J. Granell, A. González, J. Quirante, C. Calvis, R. Messeguer, J. Badía, L. Baldomà, T. Calvet, and M. Font-Bardia, *Organometallics*, 2014, **33**, 2862–2873.

61. M. N. Alam and F. Huq, *Coord. Chem. Rev.*, 2016, **316**, 36–67.

62. S. G. Agalave, S. R. Maujan, and V. S. Pore, *Chem. - An Asian J.*, 2011, **6**, 2696–2718.

Chapter 2: Synthesis and Characterization of substituted-phenyl-1,2,3-triazole and substituted-pyridine-1,2,3-triazole ligands

2.1 Introduction

Click chemistry is a term that is widely used to describe reactions that tend to conform to a number of specifications as outlined by Sharpless et al.[1]. These stipulate that a click reaction must take place under *simple reaction conditions*, use *readily available starting materials*, take place in a *benign or readily removable solvent* and finally result in *simple product isolation*[1].

When these conditions are considered, there are a number of reaction types that adhere to the criteria, such as cycloadditions, nucleophilic substitutions, non-aldol type carbonyl reactions and additions to multiple carbon-carbon bonds[2].

The most prominent of the so-called 'click' reactions, is the copper-catalysed 1,3-dipolar Huisgen cycloaddition (CuAAC). Traditionally the 1,3-dipolar Huisgen cycloaddition reaction is slow, requiring very high temperatures and long reaction times. Sharpless et al.[1] demonstrated in 2001 that the reaction rates and conditions can be greatly improved with the addition of a Cu(I) catalyst in benign solvents such as water, thus ensuring that the reaction conditions conform to the click chemistry criteria.

The 1,3-dipolar Huisgen cycloaddition utilizes an alkyne and an azide in the presence of a copper catalyst to afford a 1,4-disubstituted 1,2,3-triazole. Figure 2.1 shows the revised mechanism[3] for a CuAAC reaction. The 1,5-disubstituted 1,2,3-triazole can also be obtained with the use of a ruthenium catalyst[4,3].

Since then, great strides have been made in the application of 1,2,3-triazoles in drug development[2] due to the fact that they provide the opportunity for rapid library expansion and have proven to 'mimic' known pharmacophores, thus making them biologically relevant. Recently, CuAAC 1,2,3-triazoles have also found application in materials science[4], bioconjugation[4] and photoelectronics[5].

1,2,3-Triazoles have also recently been described as a pharmacophore, as they can resist metabolic degradation and have hydrogen bonding capabilities, which are responsible for interactions with biomolecules and might improve aqueous solubility.[6] There is thus a possibility that the ligands themselves might display some anti-cancer activity of their own.

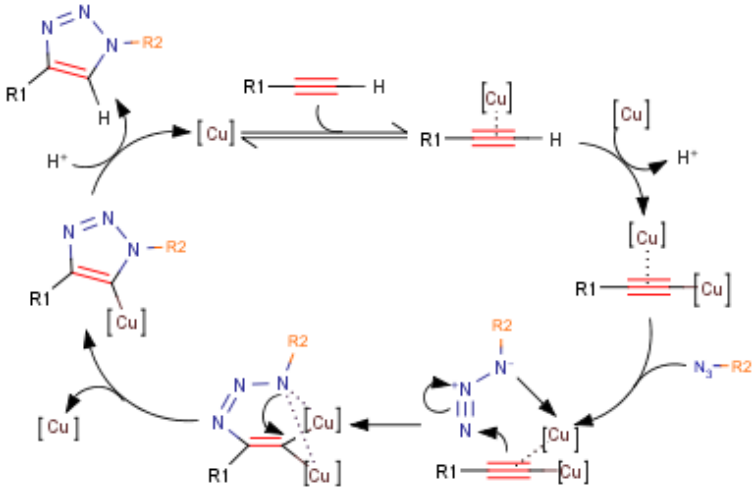

Figure 2.1: The revised mechanism for the CuAAC reaction as determined by Worrell et al.[3] in 2013, showing the involvement of two different Cu-centres.

As discussed in Section 1.6, this chapter contains the synthesis and characterization of the different triazole ligands and their precursors. This includes the synthesis of the various organoazides, 1-substituted-4-phenyl-1,2,3-triazoles and 1-substituted-4-pyridyl-1,2,3-triazoles

2.2 Results and Discussion

2.2.1 Synthesis of organoazides precursors

The azides chosen were selected in order to ultimately investigate the steric and electronic influences of the ligands on the anti-cancer activity of the complex. It was decided to investigate simple substituents, as their anti-cancer activity has, to the best of our knowledge, not been investigated, although complex substituents, such as carbohydrate functionalities have been investigated before.[7] Azides **1** and **2** were selected for their electron donating abilities as well as steric bulk. Both azides are not explosive in nature and allows for a comparison between a flexible aliphatic chain versus the more rigid cyclohexane functionality. Azides **3** – **6** were chosen for their increasing hydrophilicity and hydrocarbon chain lengths. Azides **7** and **8** were chosen for their aromaticity and steric bulk. Azide **9** was chosen as it is strongly electron withdrawing while **7** is only weakly electron withdrawing.

Organoazides are considered explosive and decompose with the release of nitrogen at the slightest external provocation such as heat, pressure or impact. Care was thus taken to synthesize azides that are not considered explosive. The general rule is that if the sum of carbon and oxygen atoms is less than threefold the number of nitrogen atoms, the organoazide is considered explosive. Equation 2.1 shows the relationship required for the synthesis of non-explosive organoazides.[8] There are however some exceptions to the rule.

$$\frac{(N_c + N_O)}{N_N} \geq 3 \qquad N = number\ of\ atoms \tag{2.1}$$

The synthesis of the organoazides was all based on literature procedures as outlined in the experimental section of this chapter (Section 2.4).

The aliphatic and hydrophilic azides were prepared through the nucleophilic substitution of the halogen analogues, and the aromatic azides were prepared from the diazotization of the analogous amines with $NaNO_2$, followed by the conversion of the diazonium salts into azides with the addition of NaN_3. A summary of all the organoazides synthesized is shown in

Table 2.1.

Table 2.1: Summary of all the organoazides synthesized.

Steric bulk	Increased hydrophilicity	Electronic effects
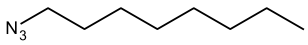 1	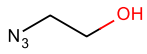 3	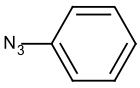 7
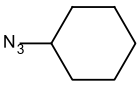 2	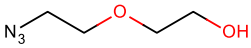 4	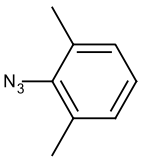 8
	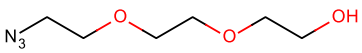 5	
	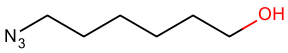 6	

FTIR provides the most valuable means of characterization regarding the synthesis of azides, due to the strong asymmetric N≡N stretch that can be observed around 2100 cm^{-1}.[9] For this reason, FTIR was used to track the synthesis of the azides and NMR was used to simply confirm that the organic structure had remained intact.

The table below contains a comparison of the azide stretches of the various ligands synthesized.

Table 2.2: A comparison of the N≡N stretches of each organoazide as observed with FTIR.

Azide	FTIR (ATR) N≡N stretch (cm^{-1})
1	2089
2	2085
3	2097
4	2091
5	2097
6	2087
7[a]	2123 (sym.), 2091 (asym.)
8	2092
9	2121

[a] A split in the azide stretch was observed for this organoazide, which can be attributed to the symmetric and asymmetric stretches of the azide.

It was observed that with a decrease in the electron donating ability of the substituent, an increase in the wavenumber for the azide stretch is observed. This can be attributed to a decrease in the stabilization of the azide, leading to an increase in the vibrational energy and thus an increase in the stretching frequency.

2.2.2 Synthesis of 1,2,3-triazole ligands

2.2.2.1 Substituted-phenyl-1,2,3-triazole ligands

All substituted phenyl-1,2,3-triazole ligands prepared are summarized in Table 2.3. Of these, **4a**, **5a** and **6a** are, to the best of our knowledge, new compounds.

Table 2.3: A summary of the substituted phenyl-1,2,3-triazole ligands synthesized. Compound numbers in italics indicate novelty.

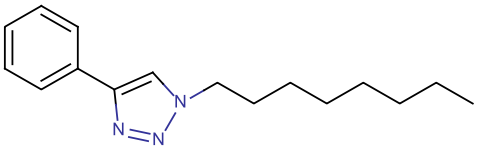 **1a**	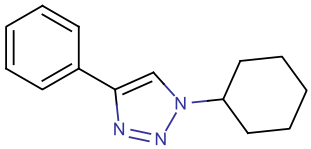 **2a**	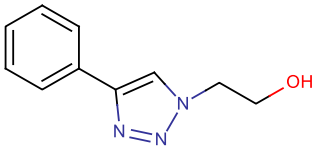 **3a**
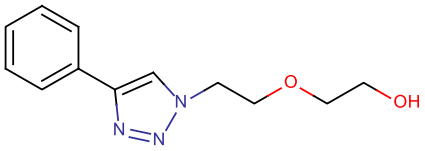 ***4a***	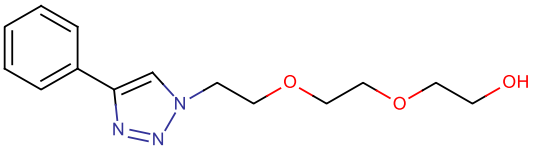 ***5a***	
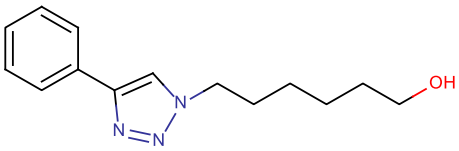 ***6a***	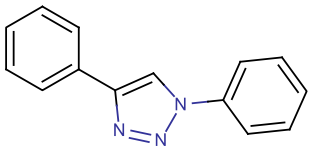 **7a**	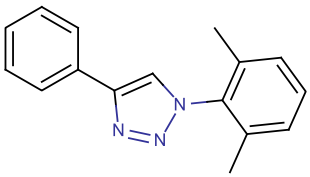 **8a**
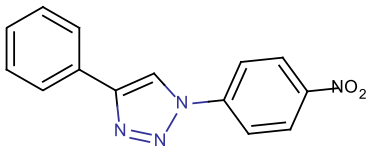 **9a**		

The ^{1}H NMR spectroscopic data for the ligands are summarized in Table 2.4. Additional analytical characterization are summarized in Table 2.5.

From the ^{1}H NMR spectroscopic data in Table 2.4 it should be noted that the triazole proton resonates as a singlet shifts downfield with a decrease in the electron donating ability of the *N*-substituent. This corresponds to the trend that was observed with the N≡N stretch in the FTIR spectra of the azides, as discussed in Section 2.2.1, and also corresponds to the shift in the wavenumber of the C-H triazole stretch in the FTIR spectra of the ligands, as shown in Table 2.5.

Table 2.4: A summary of the ^{1}H NMR characterization for the substituted-phenyl-1*H*-1,2,3-triazole ligands. [a]

Compound	CH triazole (ppm)	Aromatic region (ppm)	Aliphatic region (ppm)	
			$CH_3/CH_2/CH$	OH
1a	7.74 (s, 1H)	7.85-7.81 (m, 2H, 2 × C*H* Ar), 7.45-7.39 (m, 2H, 2 × C*H* Ar), 7.35-7.29 (m, 1H, C*H* Ar)	4.39 (t, 2H, ^{3}J = 7.2 Hz, CH_2), 1.94 (quint., 2H, ^{3}J = 7.3 Hz, CH_2), 1.35-1.26 (m, 10H, 5 × CH_2), 0.87 (t, 3H, ^{3}J = 6.8 Hz, CH_3)	
2a	7.76 (s, 1H)	7.81 (d, 2H, ^{3}J = 8.0 Hz, 2 × C*H* Ar), 7.42 (t, 2H, ^{3}J = 7.5 Hz, 2 × C*H* Ar), 7.32 (t, 1H, ^{3}J = 7.2 Hz, C*H* Ar)	2.28-1.93 (m, 4H, 2 × CH_2), 1.82-1.76 (m, 2H, CH_2), 1.54-1.44 (m, 2H, CH_2), 1.67 (s, 1H, C*H*), 1.36-1.29 (m, 2H, CH_2)	
3a	7.76 (s, 1H)	7.61-7.59 (m, 2H, C*H* Ar), 7.34-7.26 (m, 3H, C*H* Ar),	4.43 (t, ^{3}J = 4.8 Hz, 2H, CH_2), 4.07 (bs, 2H, CH_2)	4.43 (bs,1H)
4a	7.93 (s, 1H)	7.77 (d, ^{3}J = 8.0 Hz, 2H, C*H* Ar), 7.36 (t, ^{3}J = 7.8 Hz, 2H, C*H* Ar), 7.27 (t, ^{3}J = 6.9 Hz, 1H, C*H* Ar)	4.51 (t, ^{3}J = 4.7 Hz, 2H, CH_2), 3.84 (t, ^{3}J = 5.4 Hz, 2H, CH_2), 3.69 (t, ^{3}J = 4.5 Hz, 2H, CH_2), 3.53 (t, ^{3}J = 4.74 Hz, 2H, CH_2)	3.04 (s, 1H).
5a	7.95 (s, 1H)	7.79-7.76 (m, 2H, C*H* Ar), 7.39-7.33 (m, 2H, C*H* Ar), 7.29-7.23 (m, 1H, C*H* Ar),	4.49 (t, ^{3}J = 5.1 Hz, 2H, CH_2), 3.82 (t, ^{3}J = 5.1 Hz, 2H, CH_2), 3.65 (t, ^{3}J = 4.6 Hz, 2H, CH_2), 3.54 (s, 4H, 2 × CH_2), 3.49 (t, 3*J* = 4.6 Hz, 2H, CH_2),	3.14 (bs, 1H).
6a	8.57 (s, 1H)	7.84 (dd, 2H, ^{3}J = 7.5 Hz, C*H* Ar), 7.44 (dt, 2H, ^{3}J = 7.6 Hz, C*H* Ar), 7.32 (dt, 1H, ^{3}J = 7.3 Hz, C*H* Ar),	4.38 (t, 2H, ^{3}J = 7.0 Hz, CH_2), 3.37 (q, 2H, ^{3}J = 6.0 Hz, CH_2), 1.86 (quintet, 2H, ^{3}J = 7.4 Hz, CH_2), 1.40 (quintet, 2H, ^{3}J = 7.0 Hz, CH_2), 1.35-1.24 (m, 4H, 2 × CH_2)	4.34 (t, 1H, ^{3}J = 5.0 Hz)
7a[b]	9.30 (s, 1H)	7.97-7.96 (m, 2H, 2 × C*H* Ar), 7.96-7.95 (m, 2H, 2 × C*H* Ar), 7.66-7.62 (m, 2H, 2 × C*H* Ar), 7.54-7.49 (m, 3H, 2 × C*H* Ar + C*H* Ar overlapped), 7.39 (tt, 1H, ^{3}J = 7.4 Hz, ^{4}J = 1.2 Hz, C*H* Ar).		
8a	7.87 (s, 1H)	7.94-7.92 (m, 2H, 2 × C*H* Ar), 7.48-7.44 (m, 2H, 2 × C*H* Ar), 7.38-7.34 (m, 1H, C*H* Ar), 7.32 (d, 1H, ^{3}J = 7.4 Hz, C*H* Ar), 7.19 (d, 2H, , ^{3}J = 7.8 Hz, 2 × C*H* Ar)	2.05 (s, 6H, 2 × CH_3)	
9a[b]	9.53 (s, 1H)	8.51 (d, 2H, ^{3}J = 8.8 Hz, 2 × C*H* Ar), 8.28 (d, 2H, ^{3}J = 9.2 Hz, 2 × C*H* Ar), 7.97 (d, 2H, ^{3}J = 7.6 Hz, 2 × C*H* Ar), 7.53 (t, 2H, ^{3}J = 7.6 Hz, 2 × C*H* Ar), 7.42 (t, 1H, ^{3}J = 7.4 Hz		

[a] All spectra run in $CDCl_3$ at 25 °C, except where indicated. Chemical shifts reported as ppm values, referenced to the residual solvent peak

[b] Spectrum run in DMSO-d^6 at 25 °C

Table 2.5: The analytical data pertaining to the substituted-phenyl-1,2,3-triazole ligands.

Compound	Mp (°C)[a]	FTIR C-H triazole stretch (cm^{-1})[b]	ESI-MS $[M + H]^+$ (m/z)[c]
1a	80 – 81	3120	-
2a	107 – 110	3125	227.1495 $[M + H]^+$
3a	89 – 93	3130	189.0983 $[M + H]^+$
4a	62 – 70	3129	234.1238 $[M + H]^+$
5a	34- 36	3133	278.1506 $[M + H]^+$
6a	97 – 98	3120	246.1602 $[M + H]^+$
7a	188 – 190	3121	-
8a	128 - 130	3132	-
9a	238 - 239	3122	-

[a] Reported as uncorrected. [b] Recorded neat with a ZnSe ATR accessory. [c] Reported fragments agree with the predicted spectra.

For the purposes of this thesis, only the synthesis and characterization of **6a** will be discussed in detail. The experimental procedures for all the ligands synthesized are reported in Section 2.4.3.

The ligand, **6a**, was synthesized via two different methods. The first was based on the synthesis described Romeo et al.[10] which utilizes the traditional $CuSO_4 \cdot 5H_2O$ catalyst in the presence of sodium ascorbate. The second was based on the synthesis described by Man et al.[11] which utilizes a less conventional $Cu(PPh_3)_3Br$ catalyst. Both synthetic routes are shown in Scheme 2.1.

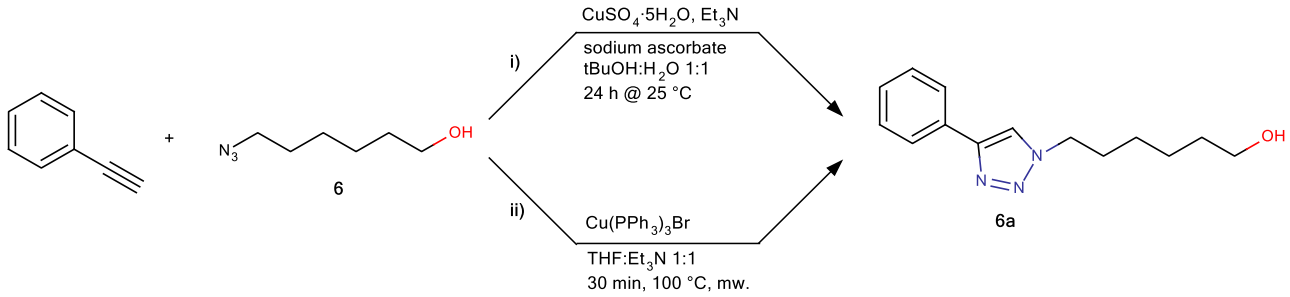

Scheme 2.1: A representation of the synthetic schemes used to synthesize ligand 6a. i) follows the synthesis based on Romeo et al.[10] and ii) follows the synthesis based on Man et al.[11]

The synthesis published by Romeo et al.[10] was used to synthesize **3a**, with a reaction time of 4 hours and without chromatographic purification steps. The same conditions were followed for ligands **4a**, **5a** and **6a** but the reaction time had to be extended to 24 hours and the product had to be purified with column chromatography in order to remove the copper catalyst from the product. This did not conform to the principles of click chemistry and, in addition to this, very low yields (36 %) were achieved.

The synthesis of **6a** thus employed the procedure reported by Man and co-workers.[11] The reported synthesis was previously used for siloxane functionalized triazole ligands and had to be kept completely water free in order to prevent the condensation of the siloxane functionalities. In the case of **6a** the reaction time was changed from the reported 5 minutes to 30 minutes with the hope of

increasing the yield of the product. There was no chromatographic purification required as the product could be purified with recrystallization from DCM:Et_2O, without the copper contamination that was observed with the previous method, thus conforming to the click chemistry principles. The product was obtained in high purity and good yield (74 %).

The product was characterized with FTIR, ^{1}H NMR, ^{13}C NMR, ESI-MS and elemental analysis.

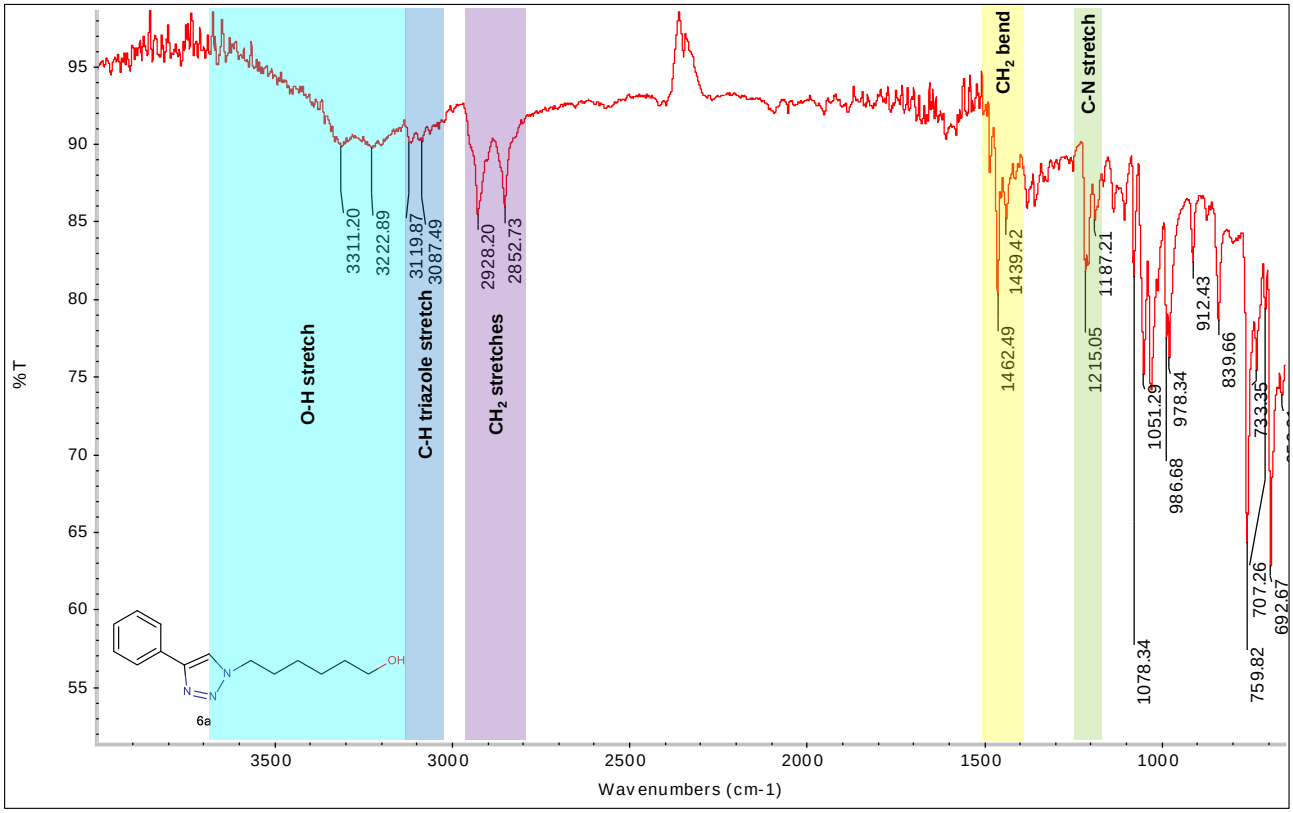

Figure 2.2: The FTIR spectrum of 6a with the signals assigned. All assignments were made in accordance with correlation tables compiled by Pavia et al.[12]

The FTIR spectrum of **6a** (Figure 2.2) shows that the triazole had formed with the appearance of the alkene C-H stretch at 3117 cm^{-1} and the appearance of the mono-substituted aromatic ring overtones[12,13].

The structure of the triazole was confirmed with ^{1}H NMR since the triazole proton exhibits a very prominent singlet at 8.57 ppm, as shown in Figure 2.3. Interestingly, the proton on the hydroxyl group shows fine coupling to the neighbouring CH_2, resulting in a triplet at 4.34 ppm. The structure was confirmed with ^{13}C NMR (Figure 2.4).

ESI-MS confirmed the formation of the product with the base peak representing the parent ion $[M + H]^+$ at 246.1602 m/z (calculated at 246.1606 m/z). $[M + Na]^+$ and $[M + K]^+$ adducts were also identified and matched the predicted cluster patterns as indicated in Figure 2.5.

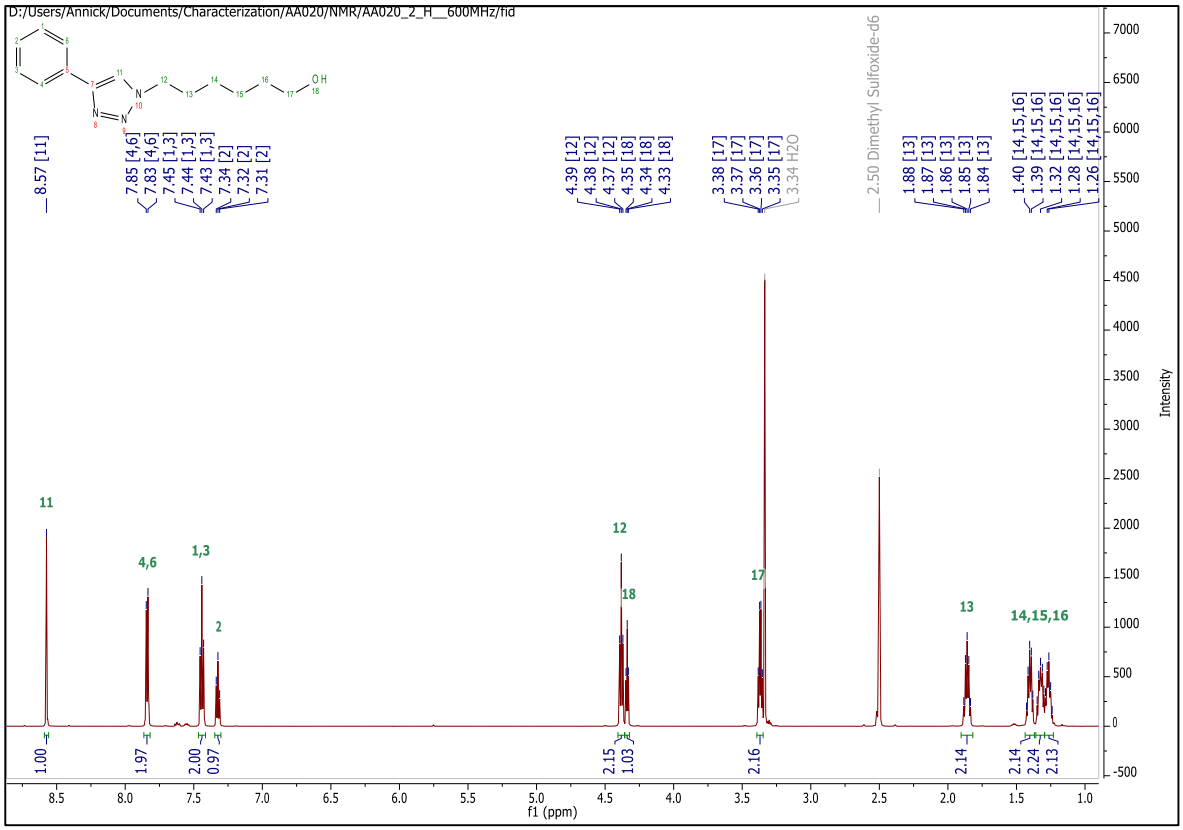

Figure 2.3: The ^{1}H NMR (600 MHz, DMSO-*d*^{6}) spectrum of 6a. Assignments have been made according to the molecular structure as indicated.

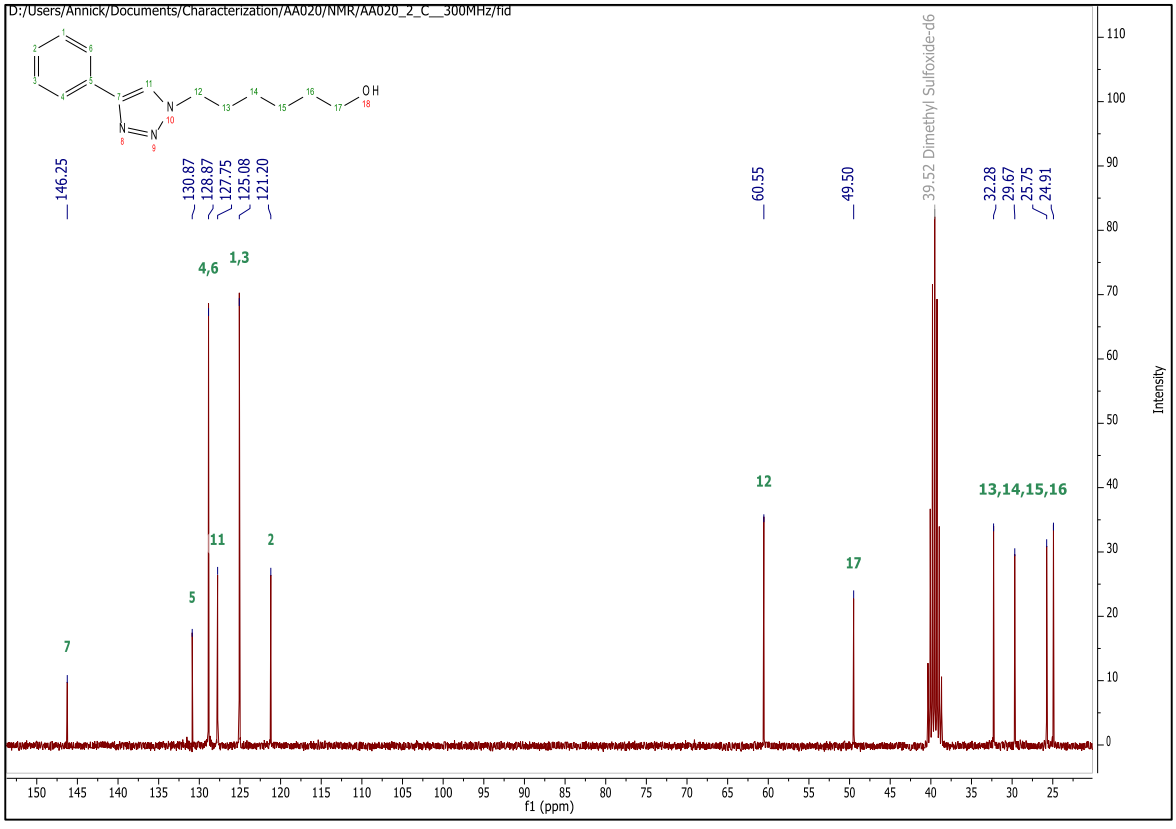

Figure 2.4: The ^{13}C NMR (75 MHz, DMSO-*d*^{6}) spectrum of 6a. Assignments have been made according to the molecular structure as indicated.

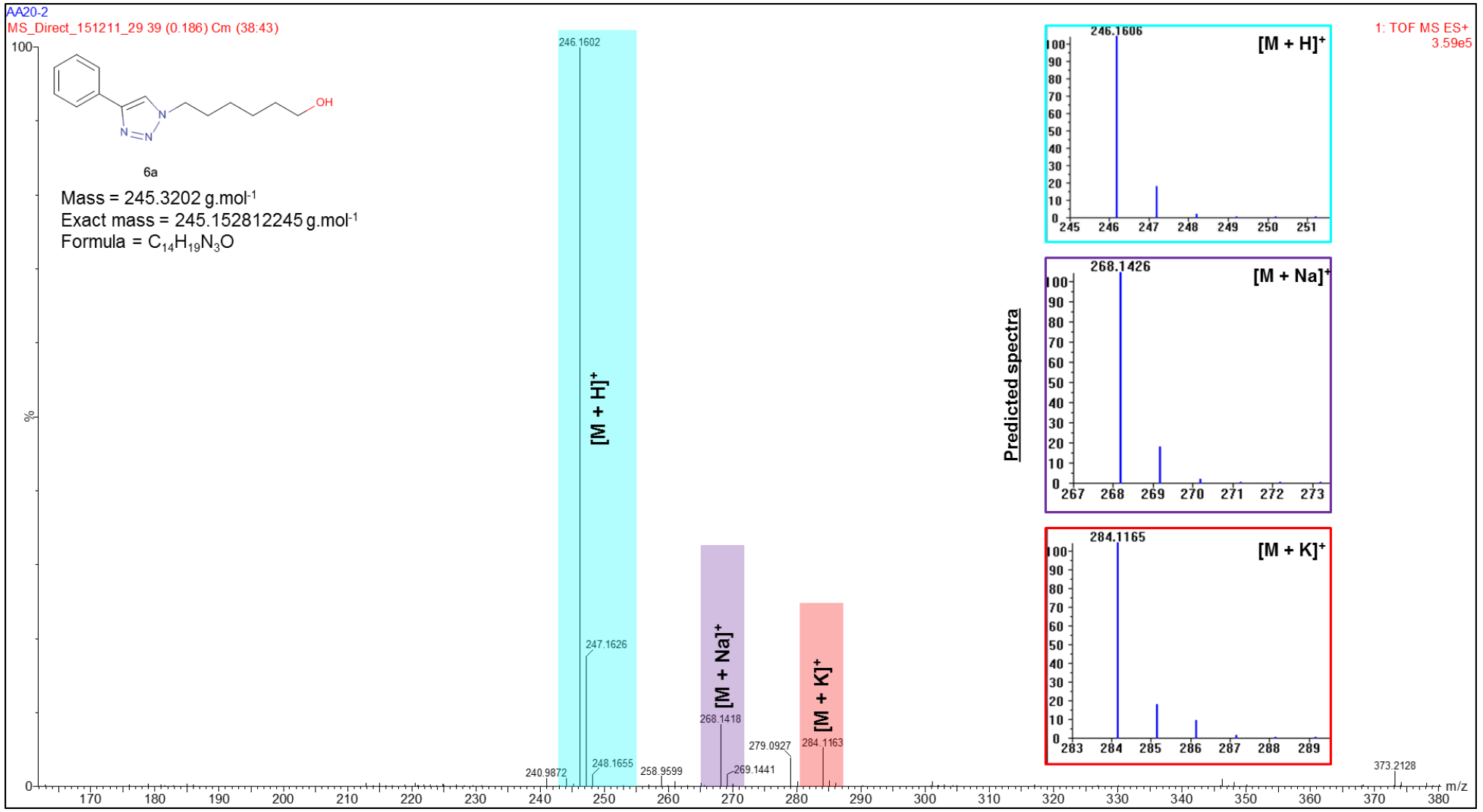

Figure 2.5: The ESI-MS spectrum of the product obtained with the predicted spectra for each identified signal. The prediction was performed on Molecular Weight Calculator freeware[14]

The elemental analysis of the **6a** is summarized in Table 2.6.

Table 2.6: The elemental analysis of 6a.

	% C	% H	% N
Calculated	67.4	7.41	17.7
Found	67.3	7.17	16.8

Molecular formula found: $C_{14}H_{19}N_3O \cdot 0.25H_2O$

The ligand contained a small amount of water despite extensive *in vacuo* drying, and the percentage nitrogen is not within percentage error, but combined with all the other characterization techniques it can be concluded that the ligand was successfully synthesized.

2.2.2.2 Substituted-pyridine-1,2,3-triazole ligands

All substituted pyridine-1,2,3-triazole ligands are summarized in Table 2.7. Of these ligands **4b**, **5b**, **6b** and **8b** are to the best of our knowledge new.

Table 2.7: A summary of the substituted pyridine-1*H*-1,2,3-triazole ligands synthesized. Compound numbers of new ligands are indicated in italics.

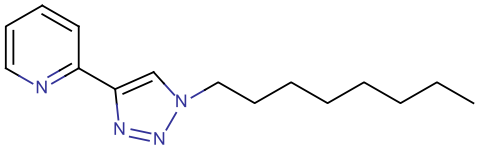 **1b**	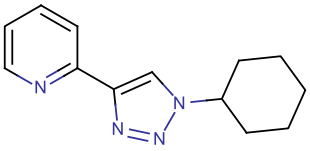 **2b**	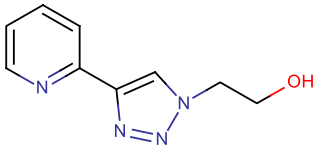 **3b**
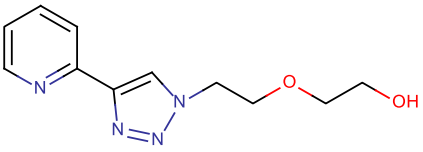 ***4b***	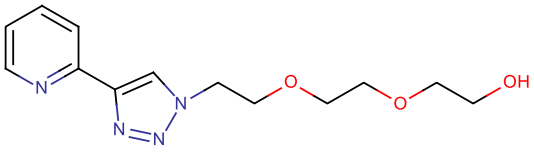 ***5b***	
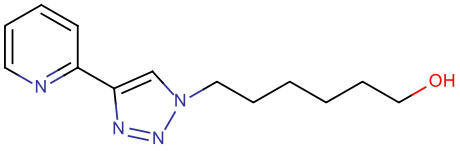 ***6b***	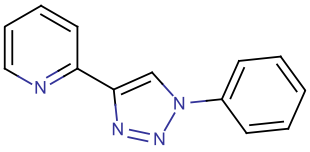 **7b**	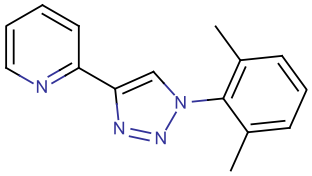 ***8b***
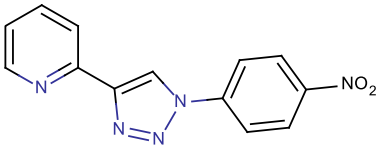 9b **9b**		

The ^{1}H NMR characterization of the all the ligands synthesized is summarized in Table 2.9. Additional analytical characterization are summarized in Table 2.8.

From the ^{1}H NMR data in Table 2.9, a similar trend is observed as for the substituted-phenyl-1*H*-1,2,3-triazole ligands. With a decrease in the donating ability of the substituent, derived from the original azide, there is an increase in the deshielding of the triazole proton.

Table 2.8: The analytical data pertaining to the substituted-pyridyl-1,2,3-triazole ligands

Compound	Mp (°C)[a]	FTIR C-H triazole stretch (cm^{-1})[b]	ESI-MS $[M + H]^+$ (m/z)[c]
1b	75 – 77	3128	-
2b	84 – 86	3061	-
3b	108 – 109	3211	191.0928 $[M + H]^+$
4b	53 – 54	3314	235.1192 $[M + H]^+$
5b	-[d]	3365	279.1457 $[M + H]^+$
6b	70 – 72	3419	247.1553 $[M + H]^+$
7b	90.- 91	3114	-
8b	-[d]	3051	251.1302 $[M + H]^+$
9b	247 - 248	3126	-

[a] Reported as uncorrected. [b] Recorded neat with a ZnSe ATR accessory. [c] Reported fragments agree with the predicted spectra.
[d] Compounds isolated as viscous oils.

Table 2.9: A summary of the ^{1}H NMR characterization of the substituted-pyridine-1,2,3-triazole ligands. [a]

Compound	CH triazole (ppm)	Aromatic region (ppm)	Aliphatic region (ppm)	
			$CH_2/CH_3/CH$	OH
1b	8.04 (s, 1H)	8.45-8.44 (m, 1H, C*H* Ar), 8.55 (d, 1H, ^{3}J = 7.9 Hz, C*H* Ar), 7.63 (dd, 1H, ^{3}J = 7.7 Hz, ^{4}J = 1.8 Hz, C*H* Ar), 7.08 (dd, 1H, ^{3}J = 7.4 Hz, ^{4}J = 1.1 Hz, C*H* Ar)	4.28 (t, 2H, ^{3}J = 7.2 Hz, CH_2), 1.81 (qt, 2H, ^{3}J = 7.2 Hz, CH_2), 1.20-1.12 (m, 10H, 5 × CH_2), 0.74 (t, 3H, ^{3}J = 7.1 Hz, CH_2).	
2b	8.12-8.11 (m, 2H, C*H* Ar overlap C*H* triazole)	8.50 (d, 1H, ^{3}J = 4.5 Hz, C*H* Ar), 7.69 (dd, 1H, ^{3}J = 7.7 Hz, ^{4}J = 1.7 Hz, C*H* Ar), 7.14 (m, 1H, C*H* Ar), 4.44 (tt, 1H, ^{3}J = 11.7 Hz, ^{4}J = 3.8 Hz, C*H* Ar)	2.21-2.17 (m, 2H, CH_2), 1.89-1.64 (m, 5H), 1.48-1.13 (m, 3H)	
3b[b]	8.54 (s, 1H)	8.60 (d, 1H, ^{3}J = 4.4 Hz, C*H* Ar), 8.03 (dd, 1H, ^{3}J = 8.0 Hz, C*H* Ar), 7.89 (dd, 1H, ^{3}J = 7.7 Hz, C*H* Ar), 7.33 (dd, 1H, ^{3}J = 7.0 Hz, C*H* Ar)	4.48 (t, 2H, ^{3}J = 5.5 Hz, CH_2), 3.84 (q, 2H, ^{3}J = 5.0 Hz, CH_2)	5.07 (t, 1H, ^{3}J = 5.2 Hz)
4b	8.58 (s, 1H)	8.60-8.59 (m, 1H, C*H* Ar), 8.04 (dd, 1H, ^{3}J = 7.9 Hz, ^{4}J = 1.0 Hz, C*H* Ar), 7.89 (dd, 1H, ^{3}J = 9.6 Hz, ^{4}J = 1.8 Hz, C*H* Ar), 7.34 (dd, 1H, ^{3}J = 7.5 Hz, ^{4}J = 1.1 Hz, C*H* Ar)	4.63-4.60 (m, 4H, 2 × CH_2), 3.88 (t, 2H, ^{3}J = 5.3 Hz, CH_2), 3.49-3.44 (m, 5H,CH_2 + OH)	
5b	8.58 (s, 1H)	8.46 (dd, 1H, ^{3}J = 4.9 Hz, ^{4}J = 0.9 Hz, C*H* Ar), 8.15 (dd, 1H, ^{3}J = 8.1 Hz, ^{4}J = 0.95 Hz, C*H* Ar), 7.70 (dd, 1H, ^{3}J = 7.5 Hz, ^{4}J = 1.75 Hz, C*H* Ar), 7.16 (dd, 1H, ^{3}J = 7.5 Hz, ^{4}J = 1.1 Hz, C*H* Ar)	4.55 (t, 2H, ^{3}J = 4.8 Hz, CH_2), 3.83 (t, 2H, ^{3}J = 4.8 Hz, CH_2), 3.72 (t, 2H, ^{3}J = 4.4 Hz, CH_2), 3.57 (s, 4H, 2 × CH_2), 3.52 (t, 2H, ^{3}J = 4.4 Hz, CH_2)	5.02 (bs,1H),
6b[b]	8.61 (s, 1H)	8.59 (dd, 1H, ^{3}J = 1.7 Hz, ^{4}J = 0.9 Hz, C*H* Ar), 8.03-8.02 (m, 1H, C*H* Ar), 7.88 (dd, ^{3}J = 7.7 Hz, ^{4}J = 1.9 Hz, C*H* Ar), 7.33 (dd, 1H, ^{3}J = 4.8 Hz, ^{4}J = 1.2 Hz, C*H* Ar)	4.42 (t, 2H, ^{3}J = 7.1 Hz, CH_2), 3.37 (q, 2H, ^{3}J = 5.3 Hz, CH_2), 1.87 (quintet, 2H, ^{3}J = 7.2 Hz, CH_2), 1.39 (quintet, 2H, ^{3}J = 6.5 Hz, CH_2), 1.34-1.22 (m, 4H, 2 × CH_2).	4.33 (t, 1H, ^{3}J = 5.0 Hz)
7b[b]	9.33 (s, 1H)	8.67-8.65 (m, 1H, C*H* Ar), 8.13 (dd, 1H, ^{3}J = 7.9 Hz, ^{4}J = 1.0 Hz, C*H* Ar), 8.04-8.01 (m, 2H, C*H* Ar), 7.95 (dd, 1H, ^{3}J = 7.8 Hz, ^{4}J = 1.8 Hz, C*H* Ar), 7.64-7.60 (m, 2H, C*H* Ar), 7.52 (m, 1H, C*H* Ar), 7.41 (dd, 1H, ^{3}J = 4.8 Hz, ^{4}J = 1.2 Hz, C*H* Ar)		
8b[b]	8.88 (s, 1H)	8.64-8.62 (m, 1H, C*H* Ar), 8.15 (d, 1H, ^{3}J = 7.9 Hz, C*H* Ar), 7.94 (dd, 1H, ^{3}J = 7.8 Hz, ^{4}J = 1.8 Hz, C*H* Ar), 7.44-7.36 (m, 2H, C*H* Ar), 7.31-7.29 (m, 2H, C*H* Ar)	1.98 (s, 6H, 2 × CH_3)	

Compound	CH triazole (ppm)	Aromatic region (ppm)	Aliphatic region (ppm)	
			$CH_2/CH_3/CH$	OH
9b[b]	9.55 (s, 1H)	8.69-8.67 (m, 1H, C*H* Ar), 8.46 (dd, 2H, ^3J = 9.1 Hz, ^4J = 2.1 Hz, C*H* Ar), 8.35 (dd, 2H, ^3J = 9.2 Hz, ^4J = 2.2 Hz, C*H* Ar), 8.14 (d, 1H, ^3J = 7.9 Hz, C*H* Ar), 7.97 (td, 1H, ^3J = 7.7 Hz, ^4J = 1.8 Hz, C*H* Ar), 7.43 (dd, 1H, ^3J = 7.6 Hz, ^4J = 1.2 Hz, C*H* Ar)		

[a] All spectra run in $CDCl_3$ at 25 °C, except where indicated. Chemical shifts reported as ppm values, referenced to the residual solvent peak

[b] Spectrum run in DMSO-d^6 at 25 °C

For the purposes of this thesis, only the synthesis of **4b** will be discussed in detail. As with **6a**, two different synthetic methods were used to synthesize **4b**, of which the modified microwave assisted method yielded the purer product in better yield (Scheme 2.2).

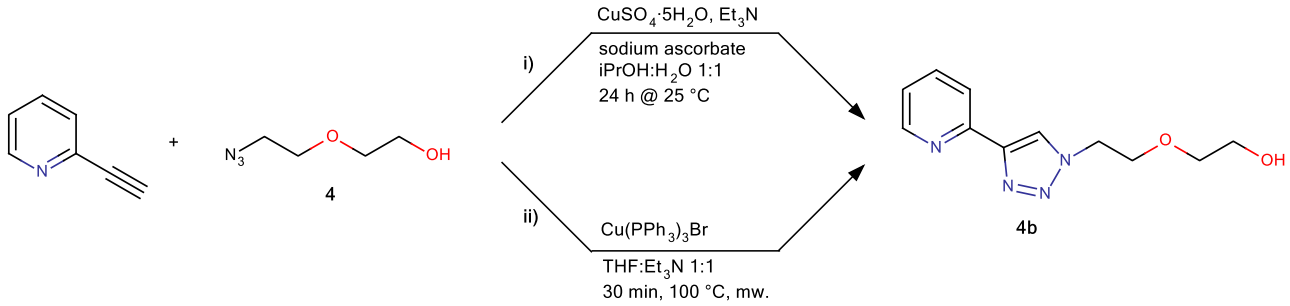

Scheme 2.2: A representation of the synthetic schemes used to synthesize ligand 6a. i) follows the synthesis based on Romeo et al.[10] and ii) follows the synthesis based on Man et al.[11]

The method reported by Romeo et al.[10] yielded the product in a moderate yield (41 %) as a yellow oil with a small number of impurities. Using the procedure described by Man et al.[11] and extending the reaction time to 30 minutes, the product was isolated in good yield (86 %) as an off-white powder. The difference between the two isolated products could possibly be ascribed to the chelation of the copper to the desired product, a phenomenon that is known to occur for these types of ligands[15]. The copper was not completely stripped from the ligand during the extraction step using the first method, thus resulting in a final product that consisted of free ligand and copper complexed ligand. The method reported by Man et al.[11] utilizes a sterically hindered catalyst in a much lower molar ratio, thus circumventing the chelation problem and yielding a pure white powder rather than the impure yellow oil.

The compound (**4b**) was characterized with FTIR, ^{1}H NMR and ^{13}C NMR spectroscopy as well as ESI-MS and elemental analysis.

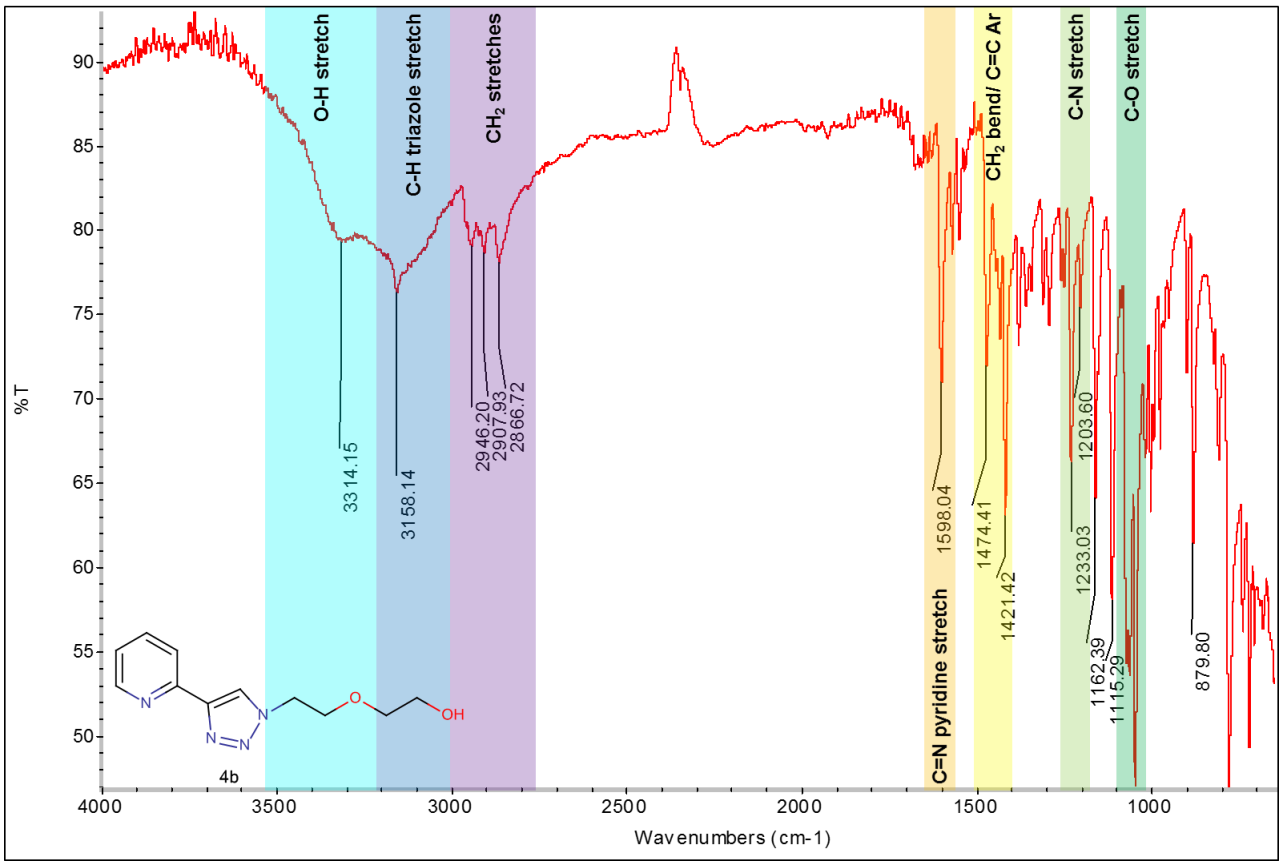

Figure 2.6: The assigned FTIR spectrum of *4b*.

From the FTIR spectrum of **4b** (Figure 2.6) it is evident that the desired product was synthesized. The appearance of the C-H triazole stretch at 3158 cm^{-1} indicates the formation of the triazole ring along with the disappearance of the azide stretch of the starting material at 2091 cm $^{-1}$.

The structure of the ligand was confirmed with ^{1}H NMR, as shown in Figure 2.7, and was integrated relative to the triazole proton at 8.58 ppm. The integration of all the signals matched the molecular structure except for the multiplet at 3.49 – 3.44 ppm. This can be attributed to an overlap of the OH-signal with that of the protons on the neighbouring carbon which results in a broader signal with a higher integration.

^{13}C NMR spectroscopy and ESI-MS were used to confirm the structure of the ligand, as shown in Figure 2.8 and Figure 2.9, respectively.

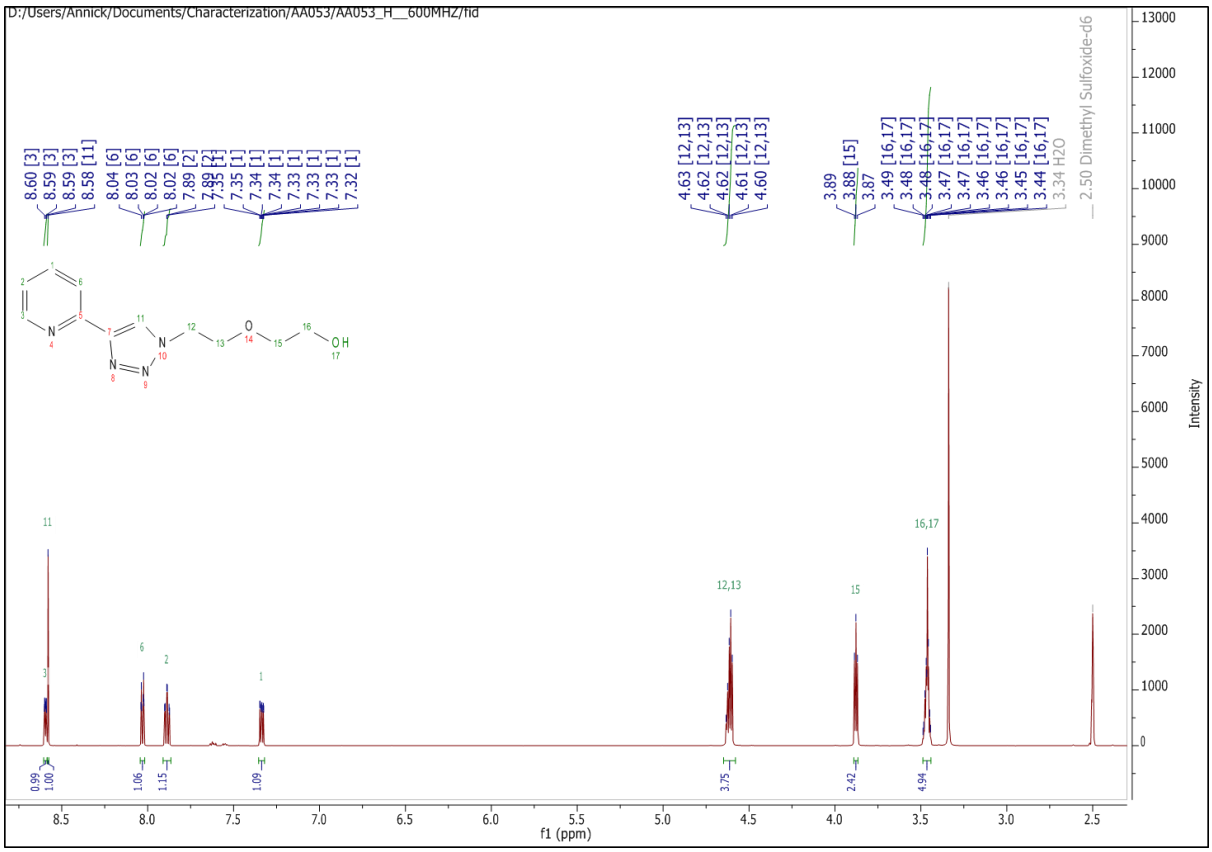

Figure 2.7: The assigned ^{1}H NMR (600 MHz, DMSO-d^{6}) spectrum of *4b*. Assignments have been made according to the molecular structure as indicated.

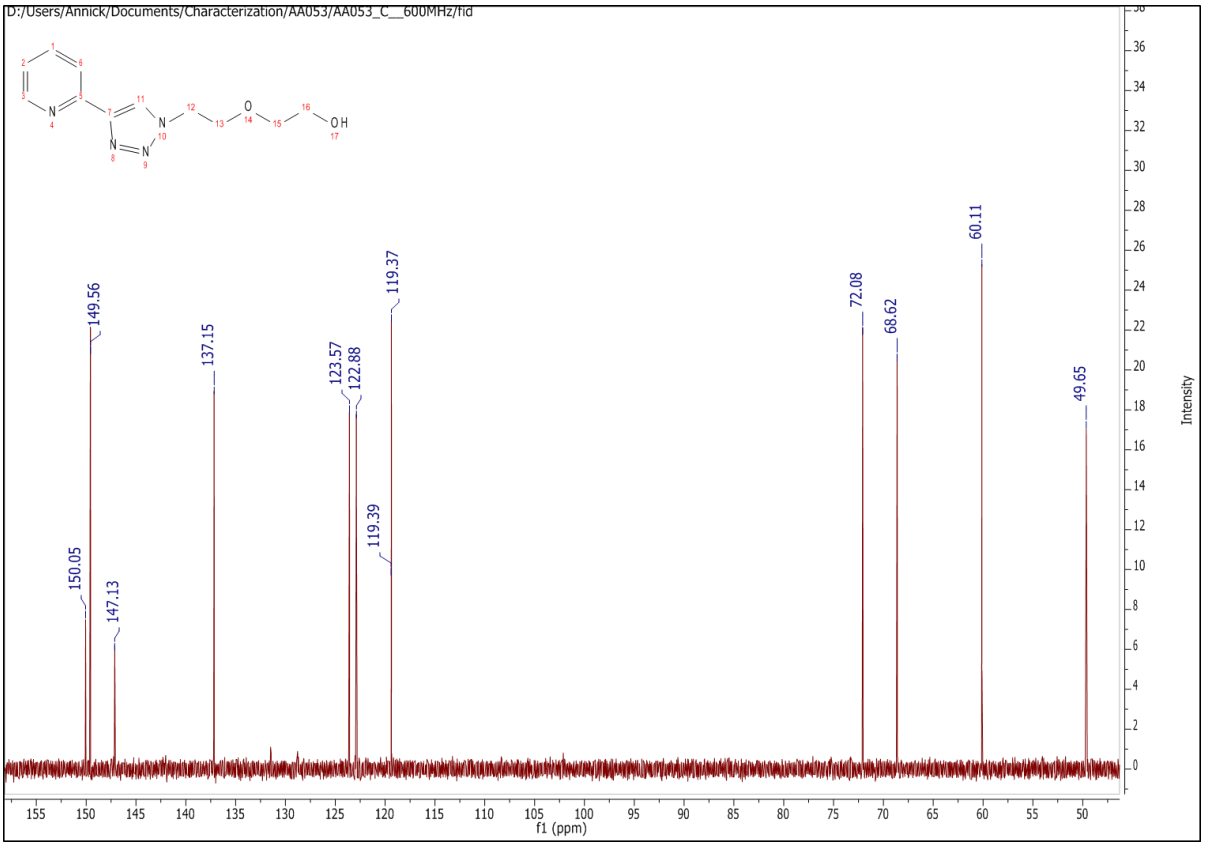

Figure 2.8: The ^{13}C NMR (600 MHz, DMSO-d^{6}) spectrum of *4b*.

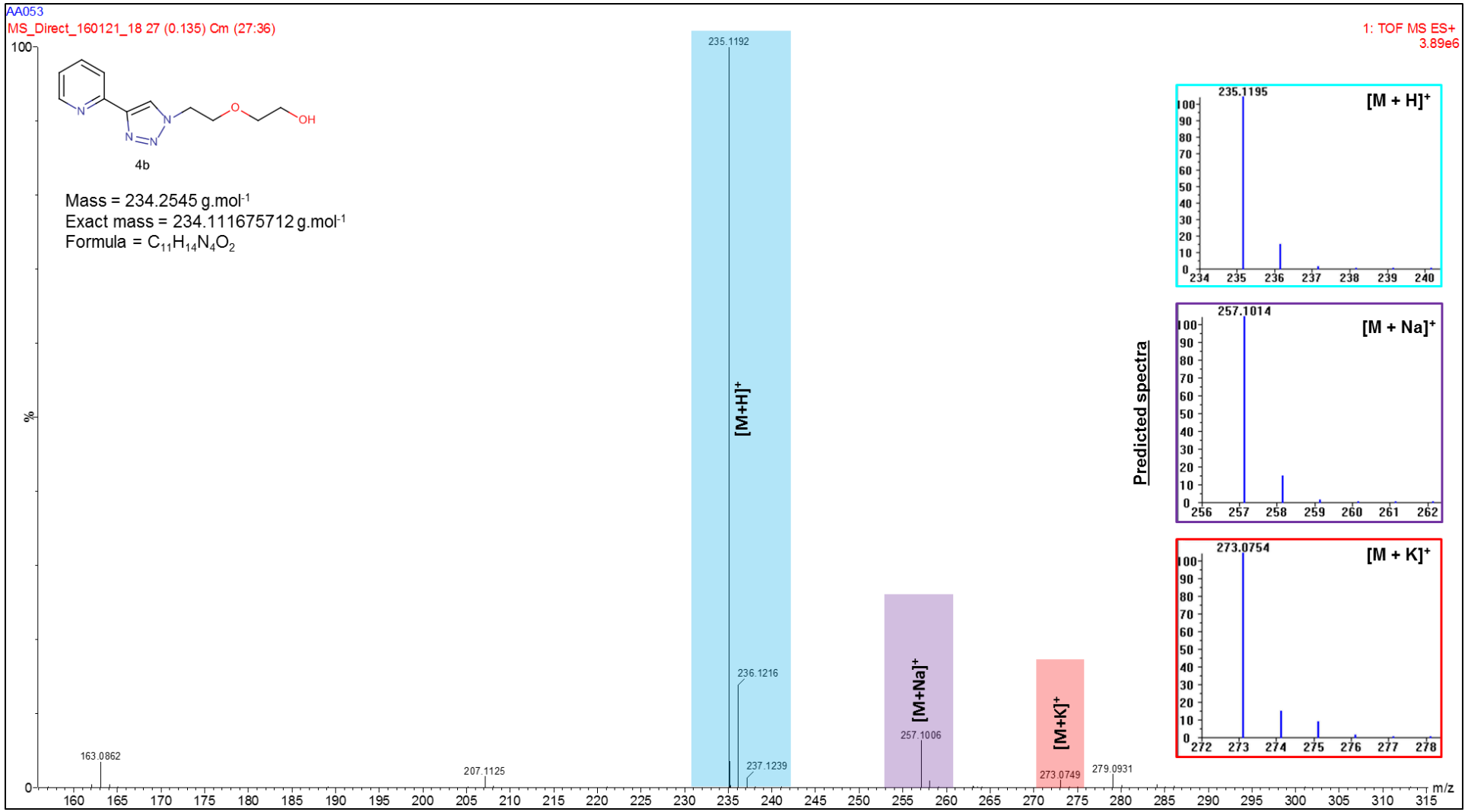

Figure 2.9: The ESI-MS spectrum of the product obtained with the predicted spectra for each identified signal. The prediction was performed on Molecular Weight Calculator freeware[14]

The elemental analysis of the **4a** is summarized in Table 2.6.

Table 2.10: The elemental analysis of 4a.

	% C	% H	% N
Calculated	52.5	5.57	22.6
Found	52.4	6.39	22.2
Molecular formula found: $C_{11}H_{14}N_4O_2 \cdot H_2O$			

As with ligand **6a**, ligand **4b** also contained a small amount of water despite extensive *in vacuo* drying. In this case the percentage hydrogen is not within experimental error, but combined with all the other characterization techniques it can be concluded that the ligand was successfully synthesized.

2.3 Conclusion

A number of known and new ligands were synthesized from their respective organoazide moieties, and fully characterized. Within both series of ligands, it was noted that a decrease in the electron donating abilities of the substituent lead to an increase in the deshielding of the triazole proton, as observed with ^{1}H NMR. The ligands were then complexed to a Pd(II) precursor, as discussed in the next chapter.

2.4 Experimental Section

2.4.1 General Methods and Materials

The synthetic procedures were all performed under standard Schlenk conditions in a nitrogen atmosphere unless otherwise noted. Literature procedures were used where indicated. All starting materials used were obtained from Merck and Sigma-Aldrich and used without additional purification. Solvents used were obtained from Merck, Protea Chemicals, Kimix and Sigma-Aldrich and purified accordingly. THF, DCM, hexane, and diethyl ether were purified and degassed with PureSolv Micro purifiers. Acetonitrile, methanol and ethanol were distilled over the appropriate drying agents. Acetonitrile was distilled over phosphorous pentoxide and both methanol and ethanol were distilled over magnesium filings and iodine. The copper catalyst, $Cu(PPh_3)_3Br$, was prepared using a literature procedure[16]. Where applicable, reactions were performed in a CEM Discover SP microwave reactor at a fixed voltage of 150 W.

FTIR data was collected on a Thermo Nicolet 350 ATR-FTIR spectrometer with a Smart Performance ATR (Zn/Se) accessory. ^{1}H NMR and ^{13}C NMR spectroscopy were performed on 300, 400 and 600 MHz Agilent NMR spectrometers as indicated. Chemical shifts were taken in reference to residual

solvent peaks in which the compound was dissolved. Coupling constants (*J*) are reported in Hz. Mass Spectrometry data was collected on a Waters Synapt G2 mass spectrometer (ESI +, 15 V). Microanalysis was performed at the UCT Department of Chemistry on a Thermo Elemental Analyser CHNS-O instrument. Melting points were determined on a Bibby Stuart Scientific Melting Point Apparatus SMP3.

2.4.2 Synthesis of azides

2.4.2.1 Synthesis of 1: 1-azido-octane

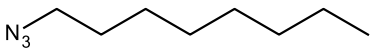

1

Based on the synthesis published by Yao and Lear et al.[17] NaN_3 (0.250 g, 3.85 mmol) was added to DMF (1.00 mL) and stirred vigorously in an inert atmosphere. To this 1-bromooctane (0.440 mL, 2.54 mmol) was added drop wise. The reaction solution was allowed to stir at room temperature for 23 h, after which TLC (eluted with EtOAc) indicated that the reaction has reached completion. The reaction mixture was diluted with water (20 mL) and the organic products extracted with EtOAc (5 × 10 mL). The combined organic layers were washed with brine (10 mL) and dried over anhydrous $MgSO_4$. After filtration the solvent was removed with rotary evaporation to yield a pale yellow oil (0.331 g, 84 %). FTIR (ATR): 2089 cm^{-1} (N≡N stretch). ^{1}H NMR (600 MHz, $CDCl_3$): *δ* (ppm) = 3.25 (t, 2H, ^3J = 7.2 Hz, CH_2), 1.59 (quint, 2H, ^3J = 7.1 Hz, CH_2), 1.37-1.27 (m, 10H, 5 × CH_2), 0.88 (t, 3H, ^3J = 7.0 Hz, CH_3). ^{13}C NMR (151 MHz, $CDCl_3$): *δ* (ppm) = 51.62, 31.88, 29.28, 29.25, 28.97, 26.85, 22.75, 14.17. The characterization data agrees with that reported in literature and the product was used without further purification.

2.4.2.2 Synthesis of 2: 1-azidocyclohexyl

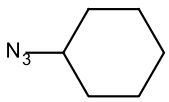

2

Based on the synthesis published by Renaud et al.[18] Bromocyclohexane (0.500 mL, 4.00 mmol) and NaN_3 (0.650 g, 10.0 mmol) were added to DMF (20.0 mL). The saturated solution was allowed to stir at 80 °C for 18 h in an inert atmosphere. The reaction mixture was then diluted with EtOAc (20.0 mL) and washed with water (6 × 10.0 mL). The combined organic layers were dried over anhydrous $MgSO_4$, filtered and concentrated under reduced pressure to yield a clear oil (0.412 g, 82 %). FTIR (ATR): 2085 cm^{-1} (N≡N stretch)). ^{1}H NMR (300 MHz, $CDCl_3$): δ (ppm) = 3.30-3.22 (m, 1H, C*H*), 1.85-1.66 (m, 5H, CH_2), 1.53-1.47 (m, 1H, CH_2), 1.36-1.26 (m, 4H, CH_2). ^{13}C NMR (75 MHz, $CDCl_3$): *δ* (ppm) = 30.76, 25.22, 24.15, 0.92. The characterization data agrees with that reported in literature and the product was used without further purification.

2.4.2.3 Synthesis of 3: 1-azido-ethanol

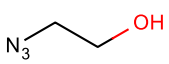

3

Based on the synthesis reported by Murphy et al.[19] To a stirring solution of 2-chloroethanol (0.380 mL, 5.74 mmol) in DMF (20.0 mL) was added NaN_3 (0.523 g, 8.04 mmol). The saturated solution was allowed to stir at 80 °C for 64h in an inert atmosphere. After

cooling to room temperature, some DMF was removed on the rotary evaporator. The product was then extracted from the remaining solvent with Et_2O (5 × 10.0 mL). The combined organic layers were washed with water (10 × 10.0 mL) dried over anhydrous $MgSO_4$, and filtered. The solvent was then removed under reduced pressure to yield a clear colourless oil (0.464 g, 93 %). FTIR (ATR): 2097 cm^{-1} (N≡N stretch). ^{1}H NMR (400 MHz, $CDCl_3$): δ (ppm) = 4.25 (bs, 1H, O*H*), 2.99 (t, 2H, ^3J = 5.0 Hz, CH_2), 2.59 (t, 2H, ^3J = 5.1 Hz, CH_2). The characterization data agrees with that reported in literature and the product was used without further purification.

2.4.2.4 Synthesis of 4: 2-(2-azido-ethoxy) ethanol

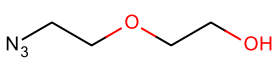

4

Synthesized according to a literature procedure[20]. 2-(2-chloroethoxy) ethanol (1.61 mL, 15.3 mmol) was added to a stirring solution of NaN_3 (1.98 g, 30.5 mmol) in water (6.35 mL). The solution was stirred at 90 °C for 16 h after which it was cooled to room temperature. The product was then extracted with DCM (5 × 5 mL). The organic phase was dried over anhydrous $MgSO_4$ and the solvent removed under vacuum. A clear, colourless oil was obtained (1.75 g, 88 %). FTIR (ATR): 2091 cm^{-1}(N≡N stretch). ^{1}H NMR (400 MHz, $CDCl_3$): δ (ppm) = 3.59-3.56 (m, 2H), 3.53 (t, 2H, *J* = 5.0 Hz), 3.44 (t, 2H, *J* = 4.7 Hz), 3.26 (t, 2H, *J* = 5.0 Hz), 3.19 (t, 1H, *J* = 5.8 Hz). ^{13}C NMR (101 MHz, $CDCl_3$): δ (ppm) = 72.05, 69.34, 60.95, 50.24. The characterization data agrees with that reported in literature and the product was used without further purification.

2.4.2.5 Synthesis of 5: 2-(2-(2-azidoethoxy)ethoxy)ethanol

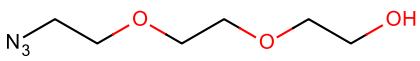

5

Synthesized according to a literature procedure[21]. 2-(2-(2-chloroethoxy)ethoxy)ethanol (0.860 mL, 6.00 mmol) was added to a stirring solution of NaN_3 (0.780 g, 12.0 mmol) in DMF (8.00 mL). The solution was allowed to reflux at 90 °C for 24 h. Some of the DMF was then removed under vacuum. The remaining solution was then diluted with water (20 mL) and the product extracted with EtOAc (4 × 10 mL). The organic phase was then washed with brine (10.0 mL), dried over anhydrous $MgSO_4$, filtered and the solvent removed under vacuum. A clear, slightly green oil was obtained (1.04 g, 96 %). FTIR (ATR): 2097 cm^{-1}(N≡N stretch). ^{1}H NMR (600 MHz, $CDCl_3$): δ (ppm) = 3.66 (bs, 1H, O*H*), 3.25-3.24 (m, 4H, 2 × CH_2), 3.23-3.20 (m, 4H, 2 × CH_2), 3.14 (t, 2H, ^3J = 5.0 Hz, CH_2), 2.96 (t, 2H, ^3J = 5.1 Hz, CH_2). ^{13}C NMR (101 MHz, $CDCl_3$): δ (ppm) = 71.50, 69.21, 69.05, 68.65, 59.93, 49.39. The characterization data agrees with that reported in literature and the product was used without further purification.

2.4.2.6 Synthesis of 6: 6-azidohexanol

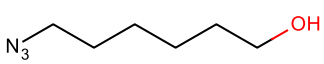

6

Synthesized according to a literature procedure[22]. 6-chlorohexanol (0.466 mL, 3.49 mmol) was added to a stirring solution of NaN_3 (0.567 g, 8.725 mmol) in DMF (1.11 mL). The solution was then allowed to stir at 90 °C for 24 h after which ether was added to the reaction mixture. The organic layer was then

washed with brine (5 × 5 mL) and water (5 × 5 mL). The organic layer was then dried over anhydrous $MgSO_4$, filtered and the solvent removed under reduced pressure. A clear, off-white oil was obtained (0.362 g, 72 %). FTIR (ATR): 2087 cm^{-1} (N≡N stretch). ^{1}H NMR (600 MHz, $CDCl_3$): δ (ppm) = 3.45 (t, 2H, ^3J = 6.7 Hz, CH_2), 3.30 (bs, 1H, O*H*), 3.13 (t, 2H, ^3J = 7.0 Hz, CH_2), 1.48 (q, 2H, ^3J = 7.0 Hz, CH_2), 1.42 (q, 2H, ^3J = 6.8 Hz, CH_2), 1.29-1.22 (m, 4H, 2 × CH_2). ^{13}C NMR (151 MHz, $CDCl_3$): δ (ppm) = 61.97, 51.10, 32.18, 28.53, 26.27, 25.10. The characterization data agrees with that reported in literature and the product was used without further purification.

2.4.2.7 Synthesis of 7: 1-azidobenzene

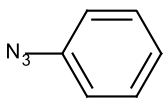

7

Based on the synthesis reported by Ye et al.[23] Aniline (0.382 mL, 4.20 mmol) was dissolved in rapidly stirring 10 % (v/v) HCl (5.0 mL) at 0 °C. $NaNO_2$ (0.435 g, 6.30 mmol) was dissolved in water (3 mL) and added dropwise over 10 minutes to the aniline solution. The reaction was allowed to stir at 0 °C for 30 minutes. NaN_3 (1.09 g, 16.8 mmol) was dissolved in water (3 mL) and added dropwise over 15 minutes to the reaction mixture. Each addition of the azide resulted in the reaction bubbling and foaming rapidly. The reaction mixture was then allowed to warm up to room temperature where it was stirred for 3 h until TLC (eluent 30 % EtOAc: PE) showed that the reaction had reached completion. EtOAc (20 mL) was added to the reaction mixture and stirred vigorously. The organic phase was then washed with water (5 × 15 mL). The organic phase was isolated, dried over Na_2SO_4, filtered and the solvent removed under reduced pressure. This yielded a yellow oil (0.462 g, 92.4 %). FTIR (ATR): 2123 cm^{-1} (N≡N sym. stretch), 2091 cm^{-1} (N=N=N asym. stretch). ^{1}H NMR (600 MHz, $CDCl_3$): δ (ppm) = 7.38-7.35 (m, 2H, 2 × C*H* Ar), 7.16 (tt, 1H, ^3J = 7.4 Hz, ^4J = 1.1 Hz, C*H* Ar), 7.06-7.04 (m, 2H, 2 × C*H* Ar). The characterization data agrees with that reported in literature and the product was used without further purification.

2.4.2.8 Synthesis of 8: 2-azido-1,3-dimethylbenzene

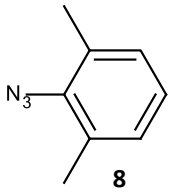

8

Synthesized according to a literature procedure[24] 2,6-dimethylaniline (1.54 mL, 12.5 mmol) was dissolved in a 1:1 mixture of AcOH:H_2O at 0 °C. A saturated aqueous solution of $NaNO_2$ (1.294 g, 18.75 mmol) was added drop-wise to the solution. The solution was allowed to stir in air at 0 °C until all the starting material was confirmed consumed via TLC (eluent DCM). NaN_3 (1.219 g, 18.75 mmol) was dissolved in water (3 mL) and the solution added dropwise over 15 minutes to the reaction mixture. Each addition of the azide resulted in the reaction bubbling and foaming vigorously. The solution was allowed to reach room temperature and then stirred for an additional 60 minutes. The solution was then diluted with H_2O (15 mL) and Et_2O (15 mL) which resulted in a bright red organic phase. The pH of the solution was adjusted to neutral with the addition of solid Na_2CO_3 and measured with universal indicator strips. The organic phase was then separated and the aqueous layer further extracted with Et_2O (2 × 15 mL). The combined organic phases were washed with H_2O (10 mL) and saturated brine (10

mL), dried over anhydrous $MgSO_4$, filtered and the solvent removed under reduced pressure to yield a dark yellow oil (1.41 g, 76 %). FTIR (ATR): 2092 cm^{-1} (N≡N stretch). ^1H NMR (400 MHz, $CDCl_3$): δ (ppm) = 7.06-7.02 (m, 3H, 3 × C*H* Ar), 2.39 (s, 6H, 2 × CH_3). ^{13}C NMR (75 MHz, $CDCl_3$): δ (ppm) = 136.97, 132.13, 128.86, 125.71, 18.15. The characterization data agrees with that reported in literature and the product was used without further purification.

2.4.2.9 Synthesis of 9: 1-azido-4-nitrobenzene

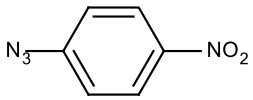

9

Based on synthesis published by Yao and Lear et al.[17] 4-nitroaniline (1.38 g, 10.0 mmol) was dissolved in a 10 % (v/v) HCl at 0 °C. A saturated aqueous solution of $NaNO_2$ (0.690 g, 10.0 mmol) was added to the solution. The solution was then allowed to stir in air at 0 °C until all the starting material had disappeared on TLC (eluted with 20 % (v/v) DCM:Hex). To the foaming mixture was added a saturated aqueous solution of NaN_3 (1.219 g, 18.75 mmol), dropwise over 15 min. With each addition of the azide the solution bubbled furiously, forming white foam. In order for the solution to reach homogeneity, EtOAc (10 mL) was added to dissolve the foam, resulting in a biphasic system. After the addition of all the azide the solution was allowed to reach room temperature and then stirred for an additional hour. The product was then extracted with EtOAc (3 × 20 mL). The combined organic fractions were washed with brine (30 mL), dried over anhydrous $MgSO_4$, filtered and the solvent removed. A bright yellow powder was obtained (1.419 g, 87 %). Melting point: 74-75 °C. FTIR (ATR): 2120.90 cm^{-1} (N≡N stretch). ^1H NMR (400 MHz, $CDCl_3$): δ (ppm) = 8.25-8.22 (m, 2H, 2 × C*H* Ar), 7.26 - 7.12 (m, 2H, 2 × C*H* Ar). ^{13}C NMR (151 MHz, $CDCl_3$): δ (ppm) = 146.99, 144.76, 125.73, 119.51. The characterization data agrees with that reported in literature and the product was used without further purification.

2.4.3 Synthesis of substituted-phenyl-1,2,3-triazole ligands

2.4.3.1 Synthesis of 1a: 1-octyl-4-phenyl-1,2,3-triazole

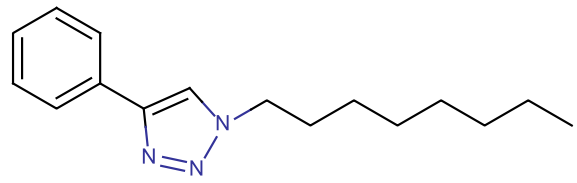

1a

Based on synthesis published by Hu et al.[25] Phenylacetylene (0.162 L, 1.48 mmol) and compound **1** (286 mg, 1.48 mmol) were added to DIPEA (0.011 mL, 0.062 mmol), HOAc (0.004 mL, 0.062 mmol) and CuI (0.0059 g, 0.031 mmol) in DCM (1.0 mL). The solution was allowed to stir at 25 °C for 24 h. The solution was filtered through a 0.45 µm syringe filter to remove the copper precipitate that had formed and the solvent removed on a rotary evaporator. The product was purified with a short silica column to remove any residual copper catalyst (30% EtOAc: PE (40-60°C). The relevant fractions were collected and the solvent removed to yield a white powder (0.240 g, 63 %). Mp = 80-81 °C (lit. 78-80 °C) FTIR (ATR): 3120 cm^{-1} (C-H triazole stretch). ^1H NMR (300 MHz, $CDCl_3$): δ (ppm) = 7.85-7.81 (m, 2H, 2 × C*H* Ar), 7.74 (s, 1H, C*H* triazole), 7.45-7.39 (m, 2H, 2 × C*H* Ar), 7.35-

7.29 (m, 1H, C*H* Ar), 4.39 (t, 2H, ^{3}J = 7.2 Hz, CH_2), 1.94 (quint., 2H, ^{3}J = 7.3 Hz, CH_2), 1.35-1.26 (m, 10H, 5 × CH_2), 0.87 (t, 3H, ^{3}J = 6.8 Hz, CH_3). ^{13}C NMR (75 MHz, $CDCl_3$): δ (ppm) = 147.85 (*C* quat.), 130.88 (*C* quat.), 128.95 (2 × *C*H Ar), 128.19 (*C*H triazole), 125.82 (2 × *C*H Ar), 119.49 (*C*H Ar), 50.58, 31.84, 30.50, 29.18, 26.65, 22.73, 14.19 (7 × *C*H_2), 1.16 (*C*H_3). The characterization data agrees with that reported in literature.

2.4.3.2 Synthesis of 2a: 1-cyclohexyl-4-phenyl-1H-1,2,3-triazole

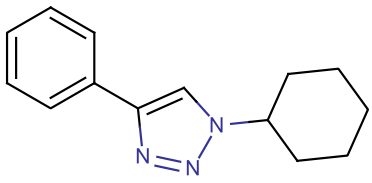

2a

Based on synthesis published by Hu et al.[25] Phenylacetylene (0.111 mL, 1.00 mmol) and compound **2** (0.076 g, 0.607 mmol) were added to DIPEA (0.007 mL, 0.04 mmol), HOAc (0.0023 mL, 0.04 mmol) and CuI (0.0038 g, 0.02 mmol) in DCM (1.0 mL). The solution was allowed to stir at 25 °C for 24 h in an inert atmosphere. The solution was then filtered through a syringe filter to remove the copper impurity. The solvent was removed under vacuum to yield an off-white powder. The product was purified via column chromatography (30 % EtOAc: PE (40-60°C)) to yield a white powder (0.116 g, 84 %). Mp = 107-110 °C (lit. 106-110.0°C). FTIR (ATR): 3125 cm^{-1} (C-H triazole stretch). ^{1}H NMR (400 MHz, $CDCl_3$): δ (ppm) = 7.81 (d, 2H, ^{3}J = 8.0 Hz, 2 × C*H* Ar), 7.76 (s, 1H, C*H* triazole), 7.42 (t, 2H, ^{3}J = 7.5 Hz, 2 × C*H* Ar), 7.32 (t, 1H, ^{3}J = 7.2 Hz, C*H* Ar), 2.28-1.93 (m, 4H, 2 × CH_2), 1.82-1.76 (m, 2H, CH_2), 1.67 (s, 1H, C*H*), 1.54-1.44 (m, 2H, CH_2), 1.36-1.29 (m, 2H, CH_2). ^{13}C NMR (101 MHz, $CDCl_3$): δ (ppm) =147.35, 130.99, 128.86, 128.03, 125.71, 117.40, 60.22, 33.68, 25.27, 25.23. ESI-MS: found: 227.1495 $[M + H]^+$ (calc. 227.3093). The characterization data agrees with that reported in literature.

2.4.3.3 Synthesis of 3a: 2-(4-phenyl-1H-1,2,3-triazol-1-yl)ethanol

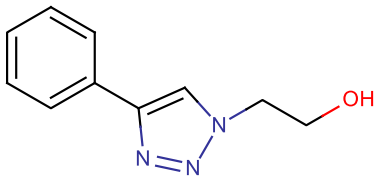

3a

Based on synthesis published by Romeo at al.[10] Phenylacetylene (0.120 mL, 1.10 mmol), compound **3** (0.087 g, 1.00 mmol) and Et_3N (0.139 mL, 1.00 mmol) were added to ^{i}PrOH (1.15 mL). In a separate container $CuSO_4 \cdot 5H_2O$ (0.065 g, 0.26 mmol) was reduced with sodium ascorbate (0.103 g, 0.52 mmol) in water (1.15 mL). The copper solution was then added to the isopropanol solution. The reaction mixture was allowed to stir at 25 °C for 24 h. The solution was filtered through a syringe filter to remove the copper impurity and the ^{i}PrOH was removed under reduced pressure. The residue obtained was then diluted with water (20 mL) and the product was extracted with EtOAc (5 × 10 mL). The organic phase was dried over anhydrous $MgSO_4$, filtered and the solvent removed under reduced pressure. This resulted in a yellow oil that was purified via column chromatography (5 % Et_3N: EtOAc) to yield a white powder (0.101 g, 53 %). Mp = 89-93 °C (lit. 89-92°C). FTIR (ATR): 3130 cm^{-1} (C-H triazole stretch). ^{1}H NMR (400 MHz, $CDCl_3$): δ (ppm) = 7.76 (s, 1H, C*H* triazole), 7.61-7.59 (m, 2H, C*H* Ar), 7.34-7.26 (m, 3H, C*H* Ar), 4.43 (t, *J* = 4.8 Hz, 2H, CH_2), 4.43 (bs overlapped, 1H, O*H*), 4.07 (bs, 2H, CH_2). ^{13}C NMR (151 MHz, $CDCl_3$): δ (ppm) = 147.37, 130.25, 128.88, 128.21, 125.58, 121.17, 61.10, 53.14. ESI-

MS: found: 189.0983 m/z $[M + H]^+$ (calc. 189.2169). The characterization data agrees with that reported in literature.

2.4.3.4 Synthesis of 4a: 2-[2-(4-phenyl-1H-1,2,3-triazolyl)ethoxy]ethanol

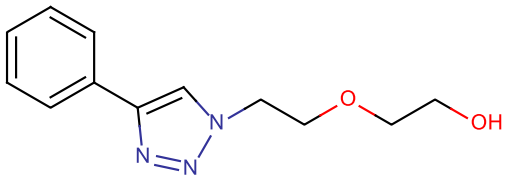

4a

Synthesized using the same method as for compound **3a** (Section 2.4.3.3). A lustrous golden powder was obtained (0.176 g, 76 %). Mp = 62-70 °C. FTIR (ATR): 3129 cm^{-1} (C-H triazole stretch). ^1H NMR (400 MHz, $CDCl_3$): δ (ppm)= 7.93 (s, 1H, C*H* triazole), 7.77 (d, ^3J = 8.0 Hz, 2H, C*H* Ar), 7.36 (t, ^3J = 7.8 Hz, 2H, C*H* Ar), 7.27 (t, ^3J = 6.9 Hz, 1H, C*H* Ar), 4.51 (t, ^3J = 4.7 Hz, 2H, CH_2), 3.84 (t, ^3J = 5.4 Hz, 2H, CH_2), 3.69 (t, ^3J = 4.5 Hz, 2H, CH_2), 3.53 (t, ^3J = 4.74 Hz, 2H, CH_2), 3.04 (s, 1H, O*H*). ^{13}C NMR (101 MHz, $CDCl_3$): δ (ppm) = 147.66, 130.54, 128.82, 128.11, 125.67, 120.98, 72.69, 69.27, 61.47, 50.30. ESI-MS: found: 234.1238 m/z $[M + H]^+$ (calc. 233.1164), 256.1053 m/z $[M + Na]^+$ (calc. 256.1062). Elemental analysis: % Found (% calc.) for $C_{12}H_{15}N_3O_2$: C: 61.36 (61.79); H: 6.63 (6.48); N: 17.32 (18.01).

2.4.3.5 Synthesis of 5a: 2-(2-[2-(4-phenyl-1H-1,2,3-triazolyl)ethoxy]ethoxy)ethanol

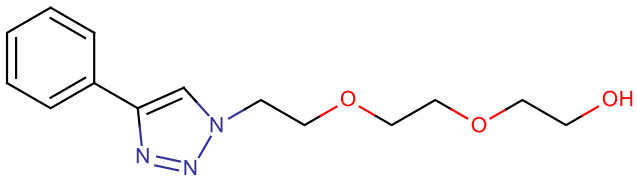

5a

Synthesized using the same method as used for compound **3a** (Section 2.4.3.3). A hygroscopic white solid was obtained (0.251 g, 91 %). Mp = 34-36 °C. FTIR (ATR) = 3133 cm^{-1} (C-H triazole stretch), 3364 (O-H stretch). ^1H NMR (300 MHz, $CDCl_3$): δ (ppm) = 7.95 (s, 1H, C*H* triazole), 7.79-7.76 (m, 2H, C*H* Ar), 7.39-7.33 (m, 2H, C*H* Ar), 7.29-7.23 (m, 1H, C*H* Ar), 4.49 (t, ^3J = 5.1 Hz, 2H, CH_2), 3.82 (t, ^3J = 5.1 Hz, 2H, CH_2), 3.65 (t, ^3J = 4.6 Hz, 2H, CH_2), 3.54 (s, 4H, 2 × CH_2), 3.49 (t, ^3J = 4.6 Hz, 2H, CH_2), 3.14 (bs, 1H, O*H*). ^{13}C NMR (101 MHz, $CDCl_3$): δ (ppm) = 147.42 (*C* quat.), 130.49 (*C* quat.), 128.71 (2 × *CH* Ar), 127.96 (*CH* triazole), 125.52 (2 × *CH* Ar), 121.03 (*CH* Ar), 72.43, 70.39, 70.05, 69.27, 61.36, 50.13 (6 × CH_2). ESI-MS: found: 278.1506 m/z $[M + H]^+$ (calc. 278.1505), 300.1324 m/z $[M + Na]^+$ (calc. 300.1324). Elemental analysis: % Found (% calc.) for $C_{14}H_{19}N_3O_3 \cdot H_2O$: C: 56.94 (57.72); H: 7.16 (6.49); N: 14.22 (13.98).

2.4.3.6 General synthesis of 6a, 7a and 9a

The synthesis is based on a procedure described by Man and co-workers.[11] The azide (1 eq.), 2-ethynylpyridine (1 eq.) and $Cu(PPh_3)_3Br$ (0.005 mmol) were added to a solvent system of THF:Et_3N (1:1, 500 µL:500µL) in a 10 mL microwave reactor tube. The reaction mixture was irradiated for 30 minutes at 100 °C under nitrogen. The solvent was removed under reduced pressure. The resulting residue was washed with Et_2O and the solvent decanted. The solvent was removed to yield the crude product. The product was then recrystallized from DCM:Et_2O to produce the purified product.

2.4.3.6.1 Synthesis of 6a: 6-(4-phenyl-1H-1,2,3-triazol-1-yl)hexan-1-ol

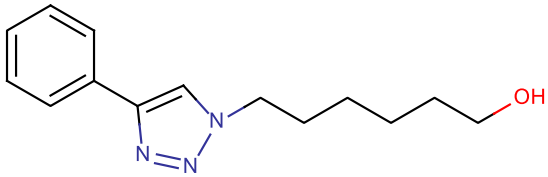

6a

White opalescent flakes were isolated (0.132 g, 74 %). Mp = 97 – 98 °C. FTIR (ATR): 3208 cm^{-1} (O-H stretch), 3120 cm^{-1} (C-H triazole). ^{1}H NMR (600 MHz, DMSO-d^6): δ (ppm) = 8.57 (s, 1H, C*H* triazole), 7.84 (dd, 2H, ^{3}J = 7.5 Hz, 2 × C*H* Ar), 7.44 (dt, 2H, ^{3}J = 7.6 Hz, 2 × C*H* Ar), 7.32 (dt, 1H, ^{3}J = 7.3 Hz, C*H* Ar), 4.38 (t, 2H, ^{3}J = 7.0 Hz, CH_2), 4.34 (t, 1H, ^{3}J = 5.0 Hz, O*H*), 3.37 (q, 2H, ^{3}J = 6.0 Hz, CH_2), 1.86 (quintet, 2H, ^{3}J = 7.4 Hz, CH_2), 1.40 (quintet, 2H, ^{3}J = 7.0 Hz, CH_2), 1.35-1.24 (m, 4H, 2 × CH_2). ^{13}C NMR (75 MHz, DMSO-d^6): δ (ppm) = 146.24 (*C* quat.), 130.87 (*C* quat.), 128.86 (2 × *C*H_2), 127.75 (*C*H triazole), 125.08 (2 × *C*H Ar), 121.20 (*C*H Ar), 60.55 (*C*H_2), 49.49 (*C*H_2), 32.28 (*C*H_2), 29.67 (*C*H_2), 25.75 (*C*H_2), 24.91 (*C*H_2). ESI-MS: found: 246.1602 m/z [M + H]$^+$ (calc. 246.1606), 268.1418 m/z [M + Na]$^+$ (calc. 268.1426), 284.1163 m/z [M + K]$^+$ (calc. 284.1165). Elemental analysis: % Found (% calc.) for $C_{14}H_{19}N_3O \cdot 0.25H_2O$: C: 67.31 (67.38); H: 7.17 (7.41); N: 16.82 (17.73).

2.4.3.6.2 Synthesis of 7a: 1,4-diphenyl-1H-1,2,3-triazole

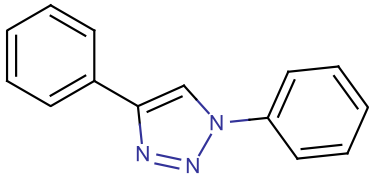

7a

White opalescent flakes were isolated (0.127 g, 57 %). Mp = 188-190 °C (lit. 184-186 °C). FTIR (ATR): 3121 cm^{-1} (C-H triazole). ^{1}H NMR (600 MHz, DMSO-d^6): δ (ppm) = 9.30 (s, 1H, C*H* triazole), 7.97-7.96 (m, 2H, 2 × C*H* Ar), 7.96-7.95 (m, 2H, 2 × C*H* Ar), 7.66-7.62 (m, 2H, 2 × C*H* Ar), 7.54-7.49 (m, 3H, 2 × C*H* Ar + C*H* Ar overlapped), 7.39 (tt, 1H, ^{3}J = 7.4 Hz, ^{4}J = 1.2 Hz, C*H* Ar). ^{13}C NMR (151 MHz, DMSO-d^6): δ (ppm) = 147.30, 136.64, 130.24, 129.94, 129.00, 128.72, 128.24, 125.36, 125.31, 120.03, 119.98, 119.63, 119.59. The characterization data agrees with that reported in literature.

2.4.3.6.3 Synthesis of 9a: 1-(4-nitrophenyl)-4-phenyl-1H-1,2,3-triazole

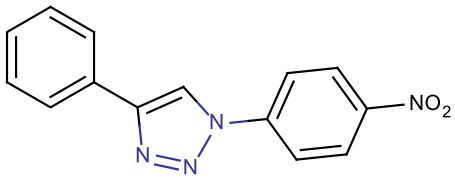

9a

Orange powder isolated (0.243 g, 91 %). Mp = 238 – 239 °C (lit. 237-238 °C). FTIR (ATR): 3122 cm^{-1} (C-H triazole stretch), 1597 cm^{-1} (N=O stretch), 1347 cm^{-1} (N=O stretch). ^{1}H NMR (600 MHz, DMSO-d^6): δ (ppm) = 9.53 (s, 1H, C*H* triazole), 8.51 (d, 2H, ^{3}J = 8.8 Hz, 2 × C*H* Ar), 8.28 (d, 2H, ^{3}J = 9.2 Hz, 2 × C*H* Ar), 7.97 (d, 2H, ^{3}J = 7.6 Hz, 2 × C*H* Ar), 7.53 (t, 2H, ^{3}J = 7.6 Hz, 2 × C*H* Ar), 7.42 (t, 1H, ^{3}J = 7.4 Hz, C*H* Ar). ^{13}C NMR (101 MHz, DMSO-d^6): δ (ppm) = 147.83 (*C* quat), 146.71 (*C* quat), 140.86 (*C* quat), 122.77 (*C* quat), 129.09 (2 × *C*H Ar), 128.56 (*C*H Ar), 125.67 (2 × *C*H Ar), 125.42 (2 × *C*H Ar), 120.46 (2 × *C*H Ar), 120.01 (*C*H triazole). The characterization data agrees with that reported in literature.

2.4.3.7 Synthesis of 8a: 1-(2,6-dimethylphenyl)-4-phenyl-1H-1,2,3-triazole

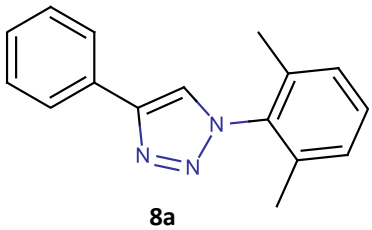

8a

Synthesized according to a literature procedure[26]. Phenylacetylene (0.362 mL, 3.30 mmol), azide **8** (0.456 g, 3.10 mmol), $CuSO_4 \cdot 5H_2O$ (0.899 g, 3.60 mmol) and sodium ascorbate (1.43 g, 7.20 mmol) were added to the solvent system of ^{t}BuOH: H_2O (4:1, 20 mL: 5.0 mL) and stirred at 25 °C for 43 hours. After 43 h the ^{t}BuOH was removed under reduced pressure and the resulting residue diluted with water (20 mL). The product was extracted with EtOAc (5 × 20 mL) and the combined organic fractions were washed with saturated NH_4Cl (25 mL). The organic phase was dried over $MgSO_4$, filtered and the solvent removed under reduced pressure. The product was then purified with silica gel chromatography (column length 12 cm) in petroleum ether (40 – 60 °C) with increasing amounts of EtOAc. The relevant fractions were combined and the solvent removed under reduced pressure to yield an opalescent orange powder (0.635 g, 82 %). Mp = 128 - 130 °C. FTIR (ATR): 3132 cm^{-1} (C-H triazole stretch). ^{1}H NMR (400 MHz, $CDCl_3$): δ (ppm) = 7.94-7.92 (m, 2H, 2 × C*H* Ar), 7.87 (s, 1H, C*H* triazole), 7.48-7.44 (m, 2H, 2 × C*H* Ar), 7.38-7.34 (m, 1H, C*H* Ar), 7.32 (d, 1H, ^3J = 7.4 Hz, C*H* Ar), 7.19 (d, 2H, , ^3J = 7.8 Hz, 2 × C*H* Ar), 2.05 (s, 6H, 2 × CH_3). ^{13}C NMR (75 MHz, $CDCl_3$): δ (ppm) = 147.66, 135.94, 135.48, 130.41, 130.08, 128.95, 128.49, 128.33, 125.76, 121.34, 17.43. The characterization data agrees with that reported in literature.

2.4.4 Synthesis of substituted-pyridine-1*H*-1,2,3-triazole ligands

2.4.4.1 Synthesis of 1b: 2-(1-octyl-1H-1,2,3-triazol-4-yl) pyridine

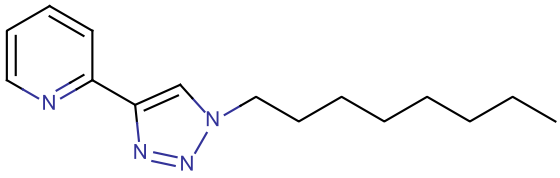

1b

Synthesized according to a literature procedure[27]. To a stirring solution of 2-ethynylpyridine (0.607 L, 6.0 mmol) in DMF:H_2O (4:1, 15 mL) was added Na_2CO_3 (0.650 g, 6.0 mmol), NaN_3 (0.470 g, 7.2 mmol), $CuSO_4 \cdot 5H_2O$ (0.300 g, 1.2 mmol) and sodium acetate (1.05 g, 6.0 mmol). 1-bromo-octane (1.14 mL, 6.6 mmol) was added to this solution. The reaction was allowed to stir at 95 °C for 20 h. The reaction mixture was washed with disodium-EDTA (1M, 100 mL) in order to remove the copper catalyst. The product was extracted with DCM (5 × 20 mL). The combined organic phases were washed with water (100 mL) and brine (100 mL), and then dried over anhydrous $MgSO_4$, filtered, and the solvent removed under reduced vacuum. The product was then purified by means of silica gel chromatography (eluted with DCM followed by 10 % acetone in DCM). The relevant fractions were collected and the solvent removed under reduced vacuum. This yielded an off-white powder (0.607 g, 48 %). Melting point: 75 -77°C. FTIR (ATR): 3128 cm^{-1} (C-H triazole). ^{1}H NMR (600 MHz, $CDCl_3$): δ (ppm) = 8.45-8.44 (m, 1H, C*H* Ar), 8.55 (d, 1H, ^3J = 7.9 Hz, C*H* Ar),8.04 (s, 1H, C*H* triazole), 7.63 (dd, 1H, ^3J = 7.7 Hz, ^4J = 1.8 Hz, C*H* Ar), 7.08 (dd, 1H, ^3J = 7.4 Hz, ^4J = 1.1 Hz, C*H* Ar), 4.28 (t, 2H, ^3J = 7.2 Hz, CH_2), 1.81 (qt, 2H, ^3J = 7.2 Hz, CH_2), 1.20-1.12

(m, 10H, 5 × C*H*$_2$), 0.74 (t, 3H, ^3J = 7.1 Hz, C*H*$_2$). ^{13}C NMR (151 MHz, $CDCl_3$): δ (ppm) = 150.32, 149.21, 148.15, 136.68, 122.58, 121.17, 119.98, 50.32, 31.54, 30.09, 28.87, 28.80, 26.30, 22.43, 13.90. The characterization data agrees with that reported in literature.

2.4.4.2 Synthesis of 2b: 2-(1-cyclohexyl-1H-1,2,3-triazol-4-yl) pyridine

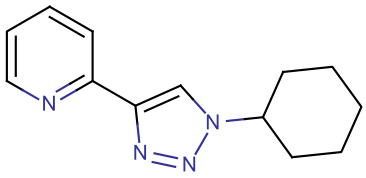

2b

Based on the synthesis published by Sarkar et al.[28] The azide **2** (0.250 g, 2.00 mmol) and 2-ethynylpyridine (0.202 mL, 2.00 mmol) were added to a solvent system of DCM: H_2O: ^{t}BuOH (2.5 mL: 2.5 mL: 5.0 mL) while stirring. To this was added $CuSO_4 \cdot 5H_2O$ (0.025 g, 0.10 mmol), sodium ascorbate (0.079 g, 0.40 mmol) and DIPEA (0.00348 mL, 0.02 mmol). The solution was allowed to reflux at 50 °C for 48h. Water (50 mL) was added to quench the solution and the product was extracted with DCM (3 × 20 mL). The organic phase was then dried over anhydrous Na_2SO_4, filtered, and the solvent removed under reduced pressure. The product was then purified with silica gel chromatography (eluted with DCM followed by 10 % acetone in DCM). The solvent was removed under reduced pressure to yield an off white powder (0.145 g, 32 %). Melting point: 84 - 86 °C. FTIR (ATR): 3061 cm^{-1} (C-H triazole). ^{1}H NMR (300 MHz, C*D*Cl_3): δ (ppm) = 8.50 (d, 1H, ^3J = 4.5 Hz, C*H* Ar), 8.12-8.11 (m, 2H, C*H* Ar overlap C*H* triazole), 7.69 (dd, 1H, ^3J = 7.7 Hz, ^4J = 1.7 Hz, C*H* Ar), 7.14 (m, 1H, C*H* Ar), 4.44 (tt, 1H, ^3J = 11.7 Hz, ^4J = 3.8 Hz, C*H* Ar), 2.21-2.17 (m, 2H, C*H*$_2$), 1.89-1.64 (m, 5H, C*H*$_2$), 1.48-1.13 (m, 3H, C*H*$_2$). ^{13}C NMR (75 MHz, C*D*Cl_3): δ (ppm) = 150.51, 149.29, 147.85, 136.85, 122.67, 120.09, 119.66, 60.13, 33.51, 25.11. The characterization agrees with literature.

2.4.4.3 General synthesis of 3b – 6b.

The synthesis is based on a procedure described by Man et al.[11] The azide (1 eq.), 2-ethynylpyridine (1 eq.) and $Cu(PPh_3)_3Br$ (0.005 mmol) were added to a solvent system of THF:Et_3N (1:1, 500 µL:500µL) in a 10 mL microwave reactor tube. The reaction mixture was irradiated for 30 minutes at 100 °C under nitrogen. The solvent was removed under reduced pressure. The resulting residue was washed with Et_2O and the solvent decanted. The solvent was removed to yield the crude product. The product was then recrystallized from DCM:Et_2O to produce the purified product.

2.4.4.3.1 Synthesis of 3b: 2-[4-(pyridine-2-yl)-1H-1,2,3-triazol-1-yl] ethan-1-ol

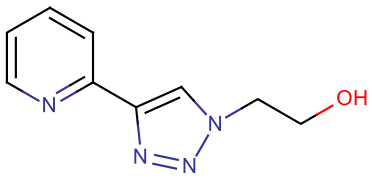

3b

Pale brown crystals were isolated (0.171 g, 90 %). Mp = 108 – 109 °C. FTIR (ATR): 3211 cm^{-1} (O-H stretch), 3132 cm^{-1} (C-H triazole). ^{1}H NMR (600 MHz, DMSO-d^6): δ (ppm) = 8.60 (d, 1H, ^3J = 4.4 Hz, C*H* Ar), 8.54 (s, 1H, C*H* triazole), 8.03 (dd, 1H, ^3J = 8.0 Hz, C*H* Ar), 7.89 (dd, 1H, ^3J = 7.7 Hz, C*H* Ar), 7.33 (dd, 1H, ^3J = 7.0 Hz, C*H* Ar), 5.07 (t, 1H, ^3J = 5.2 Hz, O*H*), 4.48 (t, 2H, ^3J = 5.5 Hz, C*H*$_2$), 3.84 (q, 2H, ^3J = 5.0 Hz, C*H*$_2$). ^{13}C NMR (151 MHz, DMSO-d^6): δ (ppm) = 150.12 (*C* quat.), 149.55 (*C*H triazole), 147.01 (*C* quat.), 137.14 (*C*H Ar), 123.60 (*C*H Ar), 122.83 (*C*H Ar), 119.30 (*C*H Ar), 59.79 (*C*H$_2$), 52.36 (*C*H$_2$). ESI-MS: found: 191.0928

m/z $[M + H]^+$ (calc. 191.0933), 213.0747 m/z $[M + Na]^+$ (calc. 213.0752). Elemental analysis: % Found (% calc.) for $C_9H_{10}N_4O$: C: 57.03 (56.68); H: 4.85 (5.29); N: 29.16 (29.35).

2.4.4.3.2 Synthesis of 4b: 2-{2-[4-(pyridine-2-yl)-1H-1,2,3-triazol-1-yl]ethoxy}ethan-1-ol

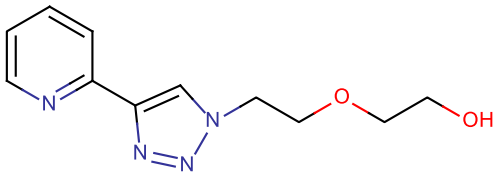

4b

An off white powder was isolated (0.201 g, 86 %). Mp = 53 - 54 °C. FTIR (ATR): 3314 cm^{-1} (O-H stretch), 3155 cm^{-1} (C-H triazole). ^1H NMR (600 MHz, $CDCl_3$): δ (ppm) = 8.60-8.59 (m, 1H, C*H* Ar), 8.58 (s, 1H, C*H* triazole), 8.04 (dd, 1H, ^3J = 7.9 Hz, ^4J = 1.0 Hz, C*H* Ar), 7.89 (dd, 1H, ^3J = 9.6 Hz, ^4J = 1.8 Hz, C*H* Ar), 7.34 (dd, 1H, ^3J = 7.5 Hz, ^4J = 1.1 Hz, C*H* Ar), 4.63-4.60 (m, 4H, 2 × CH_2), 3.88 (t, 2H, ^3J = 5.3 Hz, CH_2), 3.49-3.44 (m, 5H,CH_2 + OH). ^{13}C NMR (600 MHz, $CDCl_3$): δ (ppm) = 150.05 (*C* quat.), 149.56 (*C*H triazole), 147.13 (*C* quat.), 137.15 (*C*H Ar), 123.57 (*C*H Ar), 122.88 (*C*H Ar), 119.37 (*C*H Ar), 72.08 (CH_2), 68.62 (CH_2), 60.11 (CH_2), 49.65 (CH_2). ESI-MS: found: 235.1192 m/z $[M + H]^+$ (calc. 235.1195), 257.1006 m/z $[M + Na]^+$ (calc. 257.1014), 273.0749 m/z $[M + K]^+$ (calc. 273.0754). Elemental analysis: % Found (% calc.) for $C_{11}H_{14}N_4O_2 \cdot H_2O$: C: 52.37 (52.50); H: 6.39 (5.57); N: 22.21 (22.62).

2.4.4.3.3 Synthesis of 5b: 2-(2-{2-[4-(pyridine-2-yl)-1H-1,2,3-triazol-1-yl]ethoxy}ethoxy)ethan-1-ol

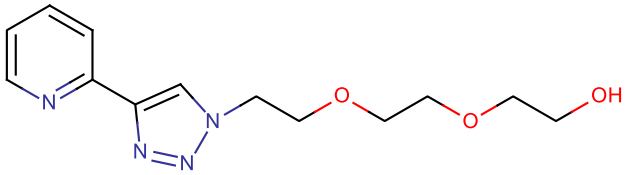

5b

A brown oil was obtained after the Et_2O was removed (0.151 g, 84 %). FTIR (ATR): 3365 cm^{-1} (O-H stretch), 1112 and 1060 cm^{-1} (overlapping C-O stretches). ^1H NMR (600 MHz, $CDCl_3$): δ (ppm) = 8.58 (s, 1H, C*H* triazole), 8.46 (dd, 1H, ^3J = 4.9 Hz, ^4J = 0.9 Hz, C*H* Ar), 8.15 (dd, 1H, ^3J = 8.1 Hz, ^4J = 0.95 Hz, C*H* Ar), 7.70 (dd, 1H, ^3J = 7.5 Hz, ^4J = 1.75 Hz, C*H* Ar), 7.16 (dd, 1H, ^3J = 7.5 Hz, ^4J = 1.1 Hz, C*H* Ar), 5.02 (bs, O-*H*), 4.55 (t, 2H, ^3J = 4.8 Hz, CH_2), 3.83 (t, 2H, ^3J = 4.8 Hz, CH_2), 3.72 (t, 2H, ^3J = 4.4 Hz, CH_2), 3.57 (s, 4H, 2 × CH_2), 3.52 (t, 2H, ^3J = 4.4 Hz, CH_2). ^{13}C NMR (600 MHz, $CDCl_3$): δ (ppm) = 150.26 (*C* quat.), 148.87 (*C*H triazole), 147.60 (*C* quat.), 137.35 (*C*H Ar), 123.77 (*C*H Ar), 122.79 (*C*H Ar), 120.48 (*C*H Ar), 72.85 (CH_2), 70.10 (CH_2), 70.08 (CH_2), 68.98 (CH_2), 61.27 (CH_2), 50.12 (CH_2). ESI-MS: found: 279.1457 m/z $[M + H]^+$ (calc. 279.1457). Elemental analysis: % Found (% calc.) for $C_{13}H_{18}N_4O_3 \cdot 2$ EtOAc: C: 53.55 (53.51); H: 5.96 (7.09); N: 13.00 (13.14).

2.4.4.3.4 Synthesis of 6b: 6-[4-(pyridine-2-yl)-1H-1,2,3-triazol-1-yl] hexan-1-ol

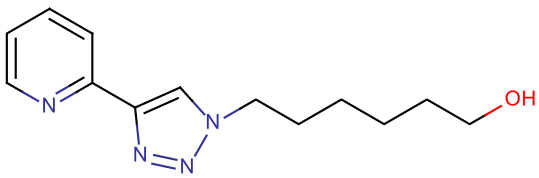

6b

Fine white crystals were obtained (0.213 g, 86 %). Mp = 70 - 72 °C. FTIR (ATR): 3419 cm^{-1} (O-H stretch), 3127 cm^{-1} (CH triazole). ^1H NMR (600 MHz, DMSO-d^6): δ (ppm) = 8.61 (s, 1H, C*H* triazole), 8.59 (dd, 1H, ^3J = 1.7 Hz, ^4J = 0.9 Hz, C*H* Ar), 8.03-8.02 (m, 1H, C*H* Ar), 7.88 (dd, ^3J = 7.7 Hz, ^4J = 1.9 Hz, C*H* Ar), 7.33 (dd, 1H, ^3J =

4.8 Hz, ^{4}J = 1.2 Hz, C*H* Ar), 4.42 (t, 2H, ^{3}J = 7.1 Hz, CH_2), 4.33 (t, 1H, ^{3}J = 5.0 Hz, O*H*), 3.37 (q, 2H, ^{3}J = 5.3 Hz, CH_2), 1.87 (quintet, 2H, ^{3}J = 7.2 Hz, CH_2), 1.39 (quintet, 2H, ^{3}J = 6.5 Hz, CH_2), 1.34-1.22 (m, 4H, 2 × CH_2). ^{13}C NMR (75 MHz, DMSO-d^6): δ (ppm) = 150.09 (*C* quat.), 149.55 (*C*H triazole), 147.15 (*C* quat.), 137.15 (*C*H Ar), 123.13 (*C*H Ar), 122.88 (*C*H Ar), 119.35 (*C*H Ar), 60.55 (*C*H_2), 49.54 (*C*H_2), 32.30 (*C*H_2), 29.68 (*C*H_2), 25.72 (*C*H_2), 24.90 (*C*H_2). ESI-MS: found: 247.1553 m/z [M + H]$^+$ (calc. 247.1559), 269.1374 m/z [M + Na]$^+$ (calc. 269.1378). Elemental analysis: % Found (% calc.) for $C_{13}H_{18}N_4O$: C: 63.39 (63.33); H: 7.37 (6.91); N: 22.75 (24.71).

2.4.4.4 Synthesis of 7b: 2-(1-phenyl-1H-1,2,3-triazol-4-yl)pyridine

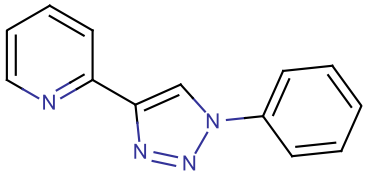

7b

Based on the synthesis reported by Crowly et al.[29] Phenylboronic acid (0.279 g, 2.88 mmol), NaN_3 (0.800 g, 12.3 mmol) and $Cu(OAc)_2 \cdot H_2O$ (0.164 g, 0.820 mmol) were added to MeOH (5.0 mL) and allowed to reflux at 55 °C for 2 hours. After 2 hours, sodium ascorbate (0.174 g, 0.880 mmol) and 2-ethynylpyridine (0.245 mL, 2.42 mmol) were added to the reaction mixture. The reaction was then allowed to stir at 25 °C for 16 hours. The reaction was then quenched with 1.5 M Na_2EDTA/NaOH at pH = 8 (300 mL) and stirred for 1 hour. The solution was filtered through a Büchner filter and the yellow precipitate suspended in 25% NH_3 solution (50 mL). The organic compounds were then extracted with DCM (2 × 20 mL). The combined organic fractions were dried over anhydrous $MgSO_4$, filtered and the solvent removed under reduced pressure. This yielded an off white powder (0.223 g, 41 %). Mp: 90 – 91 °C (lit. 90-91°C). FTIR (ATR): 3114 cm^{-1} (C-H triazole stretch).^{1}H NMR (300 MHz, DMSO-d^6): δ (ppm) = 9.33 (s, 1H, C*H* triazole), 8.67-8.65 (m, 1H, C*H* Ar), 8.13 (dd, 1H, ^{3}J = 7.9 Hz, ^{4}J = 1.0 Hz, C*H* Ar), 8.04-8.01 (m, 2H, C*H* Ar phenyl ring), 7.95 (dd, 1H, ^{3}J = 7.8 Hz, ^{4}J = 1.8 Hz, C*H* Ar), 7.64-7.60 (m, 2H, C*H* Ar phenyl ring), 7.52 (m, 1H, C*H* Ar phenyl ring), 7.41 (dd, 1H, ^{3}J = 4.8 Hz, ^{4}J = 1.2 Hz, C*H* Ar). ^{13}C NMR (75 MHz, DMSO-d^6): δ (ppm) = 149.67 (*C*H triazole), 149.50 (*C* quat.), 148.20 (*C* quat), 137.34 (*C*H Ar), 136.56 (*C* quat.), 129.90 (2 × *C*H Ar), 128.84 (*C*H Ar), 123.35 (*C*H Ar), 121.24 (*C*H Ar), 120.19 (2 × *C*H Ar), 119.81 (*C*H Ar). The characterization data agrees with that reported in literature.

2.4.4.5 Synthesis of 8b: 2-[1-(2,6-dimethylphenyl)-1H-1,2,3-triazol-4-yl]pyridine

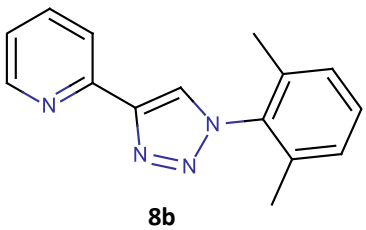

8b

Based on the synthesis reported by Sarkar et al.[30] The azide **8** (0.294 g, 2.00 mmol) and 2-ethynylpyridine (0.202 mL, 2.00 mmol) were added to a solvent system of DCM: H_2O: ^{t}BuOH (2.5 mL: 2.5 mL: 5.0 mL). To the rapidly stirring mixture was added $CuSO_4 \cdot 5H_2O$ (0.025 g, 0.10 mmol), sodium ascorbate (0.079 g, 0.40 mmol) and DIPEA (0.0035 mL, 0.02 mmol). The reaction mixture was allowed to stir at room temperature for 48 hours after which it was diluted with H_2O (50 mL). The organic compounds were extracted with DCM (3 × 20 mL) and the combined organic fractions washed with H_2O (20 mL) and saturated NH_4Cl (20 mL). The organic phase was then dried over anhydrous Na_2SO_4, filtered

and the solvent removed under reduced pressure. The resulting viscous red oil was purified with silica gel chromatography (eluted with DCM followed by 10 % acetone in DCM). The solvent was removed under reduced pressure to yield a viscous red oil (0.230 g, 46 %). FTIR (ATR): 3051 cm^{-1} (C-H triazole stretch). ^{1}H NMR (300 MHz, DMSO-d^6): δ (ppm): 8.88 (s, 1H, C*H* triazole), 8.64-8.62 (m, 1H, C*H* Ar), 8.15 (d, 1H, ^{3}J = 7.9 Hz, C*H* Ar), 7.94 (dd, 1H, ^{3}J = 7.8 Hz, ^{4}J = 1.8 Hz, C*H* Ar), 7.44-7.36 (m, 2H, C*H* Ar), 7.31-7.29 (m, 2H, C*H* Ar), 1.98 (s, 6H, 2 × CH_3). ^{13}C NMR (75 MHz, DMSO-d^6): δ (ppm) = 149.78, 149.61, 147.39, 137.27, 135.76, 134.87, 130.02, 028.40, 125.08, 123.17, 119.72, 16.95. ESI-MS: found: 251.1302 m/z $[M + H]^+$ (calc. 251.1297). Elemental analysis: % Found (% calc.) for $C_{15}H_{14}N_4$: C: 70.60 (70.78); H: 5.41 (5.57); N: 21.56 (21.92).

2.4.4.6 Synthesis of 9b: 2-[1-(4-nitrophenyl)-1H-1,2,3-4-yl]pyridine

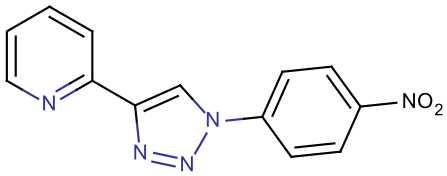

9b

Synthesized according to a literature procedure[15]. The azide **9** (1.38 g, 8.350 mmol) was added to rapidly stirring MeCN (30 mL) to which was added 2-ethynylpyridine (0.770 mL, 7.59 mmol), $Cu(OAc)_2 \cdot H_2O$ (0.300 g, 4.510 mmol) and sodium ascorbate (0.600 g, 3.05 mmol). The solution was allowed to stir for 24 hours at room temperature. The reaction mixture was diluted with CH_3Cl (50 mL) and washed with Na_2EDTA (1M) (2 × 50 mL). The organic compounds were extracted with CH_3Cl (3 × 10 mL) and the combined organic phases washed with H_2O (50 mL) and brine (50 mL). The organic phase was dried over anhydrous $MgSO_4$, filtered and the solvent removed under reduced pressure. The resulting red powder was purified with silica gel chromatography (eluted with DCM followed by 10 % acetone in DCM). The solvent was removed under reduced pressure to yield a yellow powder (0.729 g, 36 %). Mp: 247 – 248 °C. FTIR (ATR): 3126 cm^{-1} (C-H triazole stretch). ^{1}H NMR (600 MHz, DMSO-d^6): δ (ppm) = 9.55 (s, 1H, C*H* triazole), 8.69-8.67 (m, 1H, C*H* Ar), 8.46 (dd, 2H, ^{3}J = 9.25 Hz, ^{4}J = 1.92 Hz, C*H* Ar), 8.35 (dd, 2H, ^{3}J = 8.83 Hz, ^{4}J = 2.25 Hz, C*H* Ar), 8.14 (d, 1H, ^{3}J = 8.08 Hz, C*H* Ar), 7.97 (td, 1H, ^{3}J = 7.66 Hz, ^{4}J = 1.74 Hz, C*H* Ar), 7.43 (dd, 1H, ^{3}J = 7.53 Hz, ^{4}J = 1.13 Hz, C*H* Ar). ^{13}C NMR (101 MHz, DMSO-d^6): δ (ppm) = 149.80, 149.05, 148.69, 146.83, 140.80, 137.46, 125.53, 123.64, 121.79, 120.81, 120.00. The characterization agrees with literature.

2.5 References

1. H. C. Kolb, M. G. Finn, and K. B. Sharpless, *Angew. Chem. Int. Ed. Engl.*, 2001, **40**, 2004–2021.
2. H. C. Kolb and K. B. Sharpless, *Drug Discov. Today*, 2003, **8**, 1128–1137.
3. B. T. Worrell, J. A. Malik, and V. V Fokin, *Science.*, 2013, **340**, 457–460.
4. J. E. Moses and A. D. Moorhouse, *Chem. Soc. Rev.*, 2007, **36**, 1249–1262.
5. V. Hornillos, F. Amat-Guerri, and A. U. Acuña, *J. Photochem. Photobiol. A Chem.*, 2012, **243**, 56–60.

6. S. G. Agalave, S. R. Maujan, and V. S. Pore, *Chem. - An Asian J.*, 2011, **6**, 2696–2718.
7. S. B. Deepthi, R. Trivedi, P. Sujitha, C. G. Kumar, B. Sridhar, and S. K. Bhargava, *J. Chem. Sci.*, 2012, **124**, 1405–1413.
8. S. Bräse, C. Gil, K. Knepper, and V. Zimmermann, *Angew. Chem. Int. Ed. Engl.*, 2005, **44**, 5188–5240.
9. E. Lieber, C. N. R. Rao, T. S. Chao, and C. W. W. Hoffman, *Anal. Chem.*, 1957, **29**, 916–918.
10. R. Romeo, S. V. Giofrè, C. Carnovale, A. Campisi, R. Parenti, L. Bandini, and M. A. Chiacchio, *Bioorg. Med. Chem.*, 2013, **21**, 7929–7937.
11. N. Moitra, J. J. E. Moreau, X. Cattoën, and M. Wong Chi Man, *Chem. Commun.*, 2010, **46**, 8416–8418.
12. D. L. Pavia, G. M. Lampman, G. S. Kriz, and J. R. Vyvyan, *Introduction to Spectrometry*, Brooks/Cole Cengage Learning, Belmont:USA, 4th edn., 2010.
13. F. Billes, H. Endrédi, and G. Keresztury, *J. Mol. Struct. THEOCHEM*, 2000, **530**, 183–200.
14. F. Antolasic, *Molecular Weight Calculator Version 1.0*, 2005.
15. M. Wolff, L. Munoz, A. François, C. Carrayon, A. Seridi, N. Saffon, C. Picard, B. Machura, and E. Benoist, *Dalton Trans.*, 2013, **42**, 7019–7031.
16. Z. Yu, L. Tan, and E. Fossum, *ARKIVOC*, 2009, **xiv**, 255–265.
17. M. H. Ngai, P.-Y. Yang, K. Liu, Y. Shen, M. R. Wenk, S. Q. Yao, and M. J. Lear, *Chem. Commun.*, 2010, **46**, 8335–8337.
18. J. Maury, L. Feray, M. P. Bertrand, A. Kapat, and P. Renaud, *Tetrahedron*, 2012, **68**, 9606–9611.
19. F. Macleod, S. Lang, and J. Murphy, *Synlett*, 2010, **2010**, 529–534.
20. V. Aucagne, I. E. Valverde, P. Marceau, M. Galibert, N. Dendane, and A. F. Delmas, *Angew. Chem. Int. Ed. Engl.*, 2012, **51**, 11320–11324.
21. L. Deng, O. Norberg, S. Uppalapati, M. Yan, and O. Ramström, *Org. Biomol. Chem.*, 2011, **9**, 3188–3198.
22. S.M. Chang, Z. Tu, H.M. Jan, J.F. Pan, and C.H. Lin, *Chem. Commun.*, 2013, **49**, 4265–4267.
23. Z.C. Dai, Y.F. Chen, M. Zhang, S.K. Li, T.T. Yang, L. Shen, J.X. Wang, S.S. Qian, H.L. Zhu, and Y.H. Ye, *Org. Biomol. Chem.*, 2015, **13**, 477–486.
24. D. Brown, P. Schauer, J. Borau-Garcia, B. Fancy, and C. Berlinguette, *J. Am. Chem. Soc.*, 2013, **135**, 1692–1695.
25. C. Shao, X. Wang, Q. Zhang, S. Luo, J. Zhao, and Y. Hu, *J. Org. Chem.*, 2011, **76**, 6832–6836.
26. K. Ogata, S. Inomata, and S. Fukuzawa, *Dalton. Trans.*, 2013, **42**, 2362–2365.
27. J. D. Crowley, P. H. Bandeen, and L. R. Hanton, *Polyhedron*, 2010, **29**, 70–83.
28. D. Schweinfurth, S. Strobel, and B. Sarkar, *Inorg. Chim. Acta*, 2011, **374**, 253–260.
29. K. J. Kilpin, E. L. Gavey, C. J. McAdam, C. B. Anderson, S. J. Lind, C. C. Keep, K. C. Gordon, and J. D. Crowley, *Inorg. Chem.*, 2011, **50**, 6334–6346.
30. D. Schweinfurth, R. Pattacini, S. Strobel, and B. Sarkar, *Dalton Trans.*, 2009, 9291–9297.

Chapter 3: Synthesis and Characterization of *trans*- and *N,N'*-bidentate Pd(II) complexes

3.1 Introduction

As discussed in Chapter 1, palladium complexes have been investigated extensively as anti-cancer agents. It is thus prudent to revisit the most relevant literature examples and discuss their studies in more detail.

3.1.1 *Trans*-Pd(II) complexes based on 1-substituted-4-phenyl-1,2,3-triazolyl ligands

From Chapter 1 it is clear that the structures of *trans*-Pd(II) complexes are highly varied and that there are no clear structure-activity-relationships established as of yet. To the best of our knowledge, no *trans*-Pd(II) complexes with substituted-1,2,3-triazole ligands have been evaluated for their anti-cancer activities, but there are a few examples of these compounds reported in literature.

Owing to the discovery of the CuAAC reaction, there has been an exponential increase in the number of 1,4-disubstituted-1,2,3-triazole compounds synthesized. Despite the popularity of these compounds, investigation into their coordination properties has surprisingly not kept pace, although these compounds have the potential for a wide array of coordination modes (Figure 3.1).[1]

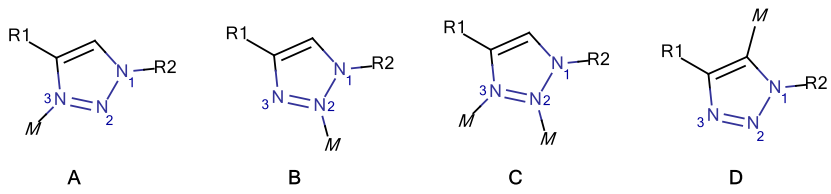

Figure 3.1: The various coordination modes of 1,4-substituted-1,2,3-triazole ligands.

Only coordination modes A, C and D have been observed. Coordination to N3 is preferred over N2 due to the fact that N3 is more electron rich than N2.[1,2]

Additionally, the CH-acidity in position 5 gives the 1,2,3-triazole a hydrogen bond donor-strength similar to a prototypical amide, depending on its substituents. Owing to the triazole's aromatic character it is thus an ideal moiety for bioinorganic applications, as it allows for simultaneous hydrogen bonding and metal coordination.[3]

Van Koten and co-workers[4] published the first complexes with substituted-1,2,3-triazoles as monodentate ligands. It was shown that the electronic and steric characteristics of the ligands can

easily be tuned and that these characteristics influence the coordination behaviour of the ligands. With the inclusion of an electron withdrawing substituent on the N1-atom of the triazole, the coordination strength of the ligand decreased, while the reverse was true for an electron donating substituent. This was established by using competition experiments between the complex and a number of commonly used Lewis bases, such as PPh_3 and DMSO. It was shown that the strength of the 1,2,3-triazole coordination bond is similar to that of pyridine, depending on the substituents on the triazole ring (Figure 3.2).[4]

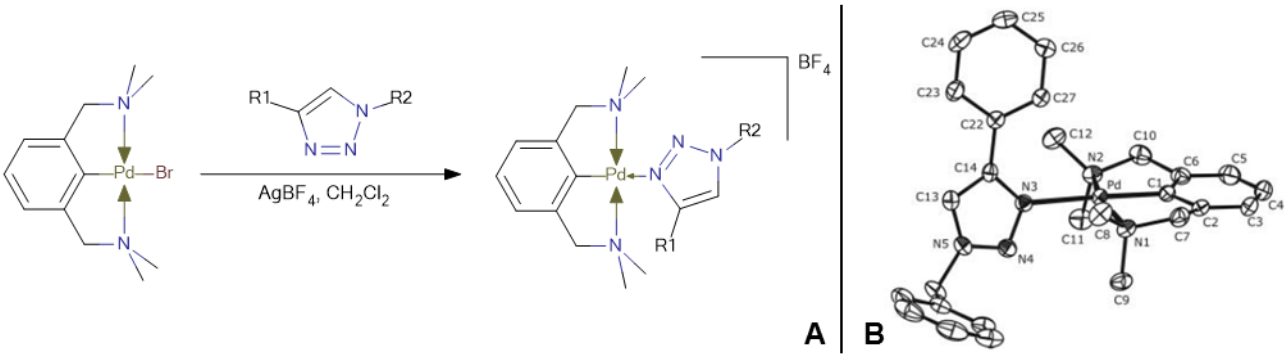

Figure 3.2: A) The first monodentate 1,4-disubstituted-1,2,3-triazole Pd(II) complex synthesized by Van Koten and co-workers.[4] and B) the crystal structure obtained for the product.

Astruc and co-workers[5] synthesized the first monodentate triazole complex of the type PdL_2X_2 complex in 2008 with a ferrocenyl substituent on the triazole ring. This complex was not evaluated for any anti-cancer activity, but, nevertheless, displayed interesting ^1H NMR characteristics (see Section 3.2.1.1).

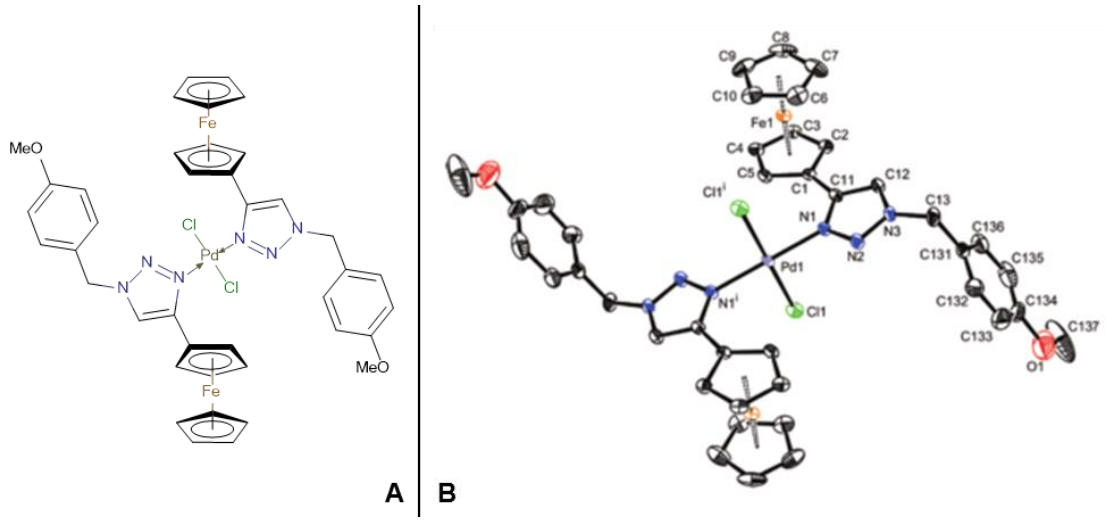

Figure 3.3: A) The PdL_2X_2 complex synthesized by Astruc and co-workers[5] and B) the crystal structure obtained of the complex.

More recently Crowley and McMorran.[6] showed that these *trans*-Pd(II) complexes can be manipulated into supramolecular structures. They started out by showing that the Pd(II) centre can

sterically accommodate up to four disubstituted-1,2,3-triazole ligands, and exploited this phenomenon to prepare quadruply stranded helicate cages (Figure 3.4).[6]

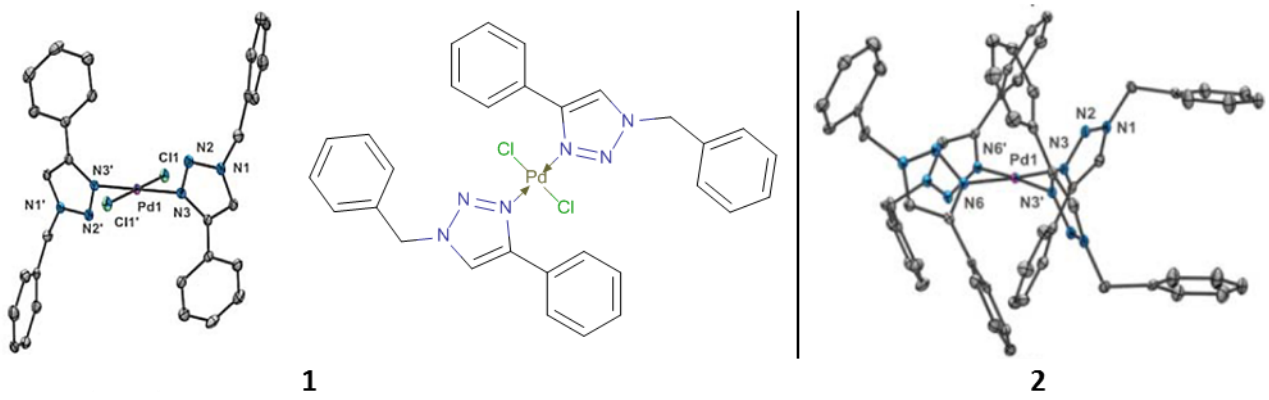

Figure 3.4: The complexes investigated by Crowley and McMorran.[1] with 1) the disubstituted complex and 2) the crystal structure of the tetra substituted complex.

The examples briefly discussed above are the most structurally relevant *trans*-Pd(II) complexes with disubstituted-1,2,3-triazole ligands to date, but none of them have been evaluated as anti-cancer agents, nor have they found application in other fields. This motivated us to investigate the same type of complexes for their anti-cancer activity.

3.1.2 *N,N'*-bidentate Pd(II) complexes based on 1-substituted-4-pyridyl-1,2,3-triazolyl ligands

Unlike the substituted-1,2,3-triazolyl *trans*-Pd(II) complexes, there are examples of *N,N'*-bidentate substituted-1,2,3-triazolyl Pd(II) complexes in the literature as discussed in Chapter 1 (Section 1.3.3.2). Although no structure-activity relationship has been established for these compounds, there have been a few promising candidates.

The most recent examples of *N,N'*-bidentate substituted-1,2,3-triazolyl Pd(II) complexes used as antiproliferative agents were published by Trivedi et al.[7] in which they synthesized a number of *N,N'*-bidentate-1,2,3-triazolyl Pd(II) complexes with carbohydrate substituents. These complexes showed significant anti-cancer activity against a number of cancer cell lines while the ligands themselves were non-toxic.[7] The structures investigated are shown in Table 3.1.

Table 3.1: The carbohydrate substituted-pyridyl-1,2,3-triazole Pd(II) complexes investigated by Trivedi et al.[7] for their anti-cancer activity.

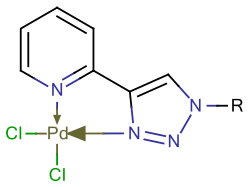

R =

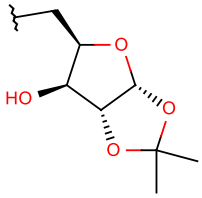

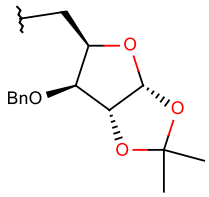

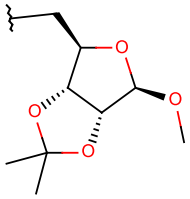

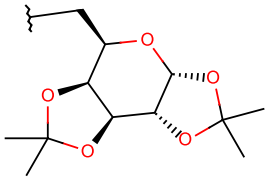

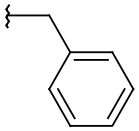

Cell line	A	B	C	D	E
	IC_{50} (μM)	IC_{50} (μM)	IC_{50} (μM)	IC_{50} (μM)	IC_{50} (μM)
A549	6.4	-[a]	7.7	6.9	-
Neuro2a	7.8	5.6	7.1	-	-
HeLa	8.3	7.9	-	9.2	-
MDA-MBA-231	9.9	7.9	-	12.1	-
MCF-7	5.5	8.9	-	-	-

[a] Inactive at concentrations evaluated.

Although it was shown that the carbohydrate moiety was necessary for the anti-cancer activity displayed[7], there is to the best of our knowledge no literature that investigates the steric, solubility or electronic effects on the anti-cancer activity of the compounds.

This chapter covers the synthesis and characterization of the *trans*- and *N,N'*-bidentate Pd(II) complexes derived from substituted-phenyl- and pyridyl 1,2,3-triazolyl ligands, respectively, reported in Chapter 2.

3.2 Results and Discussion

3.2.1 *Trans*-Pd(II) complexes based on 1-substituted-4-phenyl-1,2,3-triazolyl ligands

All the *trans*-Pd(II) complexes synthesized are to the best of our knowledge new and were synthesized in a similar manner (see Section 3.4.2).

The complexes were synthesized by reacting the ligand with $(MeCN)_2PdCl_2$ at room temperature. All complexes were isolated in moderate to good yields as indicated in Scheme 3.1.

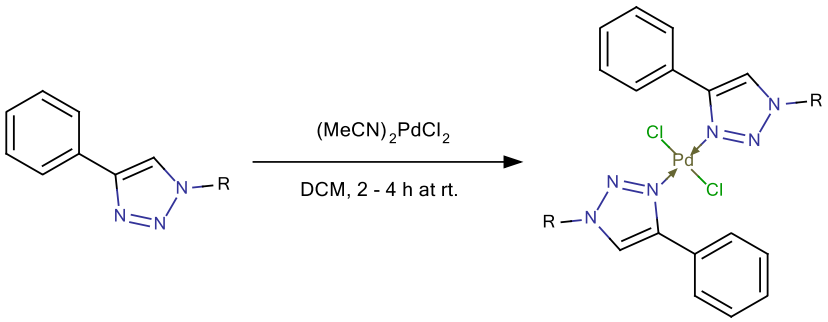

T1a:	R =	Octyl	(65 %)
T2a:	R =	Cyclohexyl	(63 %)
T3a:	R =	Ethanol	(95 %)
T4a:	R =	2-(2-ethoxy) ethanol	(87 %)
T5a:	R =	2-(2-(2-ethoxy) ethoxy) ethanol	(90 %)
T6a:	R =	Hexanol	(60 %)
T7a:	R =	Phenyl	(76 %)
T8a:	R =	2,6-dimethylphenyl	(63 %)
T9a:	R =	4-nitrophenyl	(90 %)

Scheme 3.1: The general structure of the *trans*-Pd(II) substituted-phenyl-1,2,3-triazolyl complexes synthesized, with the percentage yield indicated in brackets.

The complexation of the ligands to the Pd-precursor was monitored with FTIR spectroscopy, where a small shift in the C-H triazole stretch was observed upon the formation of the complex, as shown in Table 3.2. Ideally, the N=N stretch would result in the best confirmation of complexation and indication of bond strength. Unfortunately, the N=N signal is very weak in FTIR spectra and ^{15}N substitution is required for unambiguous assignment.[8] Thus the C-H triazole stretch was monitored.

Complexes **T1a**, **T2a** and **T5a** were soluble in DCM, $CHCl_3$ and DMSO while all of the other complexes prepared were only soluble in DMSO.

There is no trend in the FTIR shift of the C-H triazole signals upon complexation, so complexation had to be confirmed with ^{1}H NMR spectroscopy. However, it appeared that the complexes were in equilibrium with uncoordinated ligand in solution, as shown in Figure 3.5 with **T4a** as example. Irrespective of the batch of compound and concentration of the NMR sample, the ratio between the complex signals and the dissociated ligand signal remained the same. This phenomenon was investigated in more detail with a short NMR study, as discussed in Section 3.2.1.1.

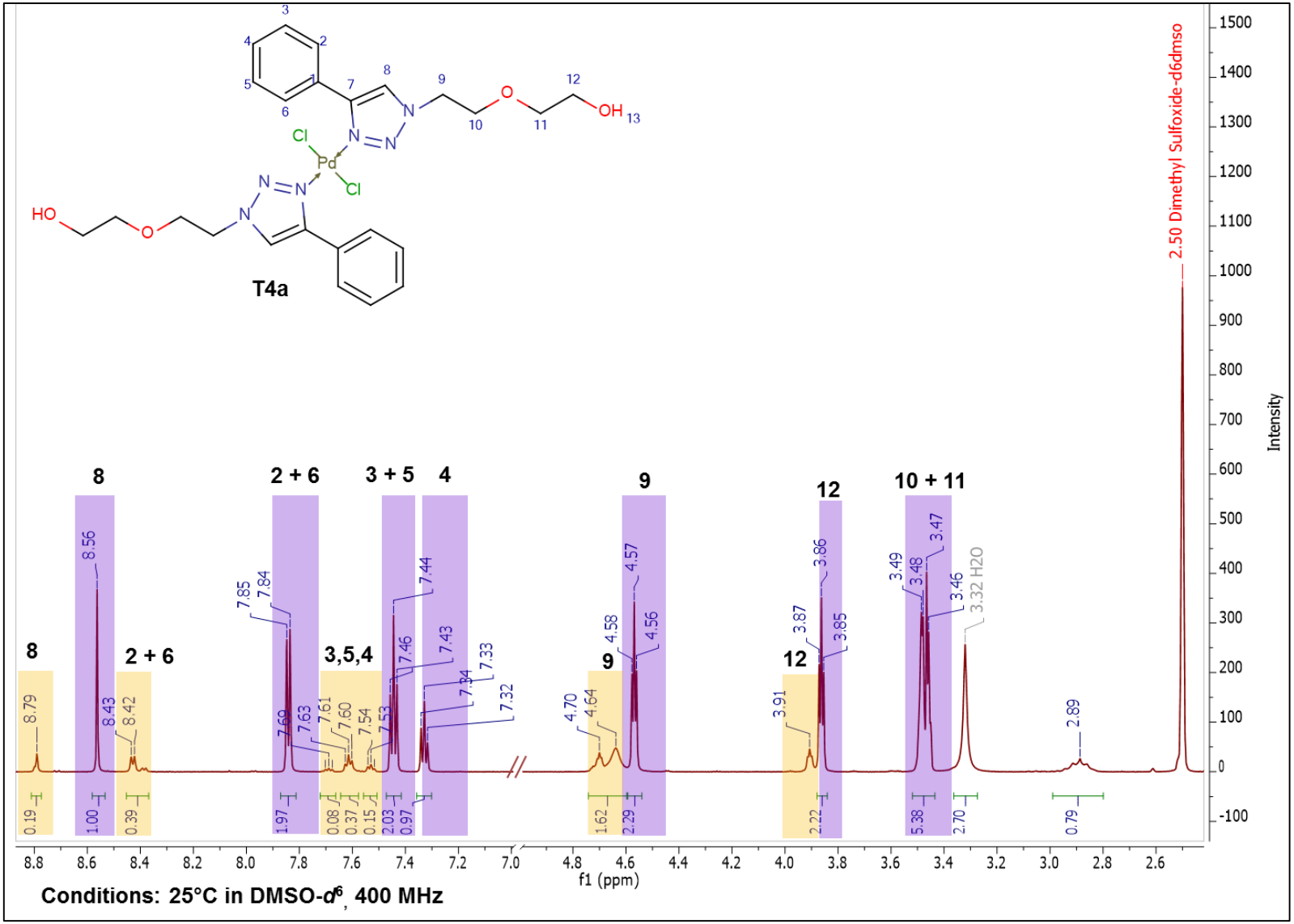

Figure 3.5: The ^{1}H NMR (600 MHz, DMSO-*d*^{6}) of *T4a* with the dissociated ligand indicated in purple, and the complex in orange. Assignment aided by Marvin Suite prediction software.

Table 3.2: Characterization data of the *trans*-Pd(II) substituted-phenyl-1,2,3-triazolyl complexes with a comparison of the FTIR C–H triazole stretch between the ligand and the corresponding complex.

Compound	Mp (°C)	FTIR C-H triazole stretch (cm^{-1})		ESI-MS (m/z)
		Metal complexes	Ligands	
T1a	180 – 181	3128	3120	435.2332 $[M – L]^+$
T2a	155 – 157	3134	3125	597.1552 $[M – Cl]^+$
T3a	239 – 240	3130	3130	521.0526 $[M – Cl]^+$
T4a	191[a]	3098	3129	609.1058 $[M – Cl]^+$
T5a	131 – 132	3129	3133	697.1556 $[M – Cl]^+$
T6a	123 – 124	3096	3120	633.1762 $[M – Cl]^+$
T7a	160[a]	3114	3121	619.1668 $[M – H]^+$
T8a	213[a]	3132	3132	426.1011 $[M – L]^+$
T9a	304 – 305[b]	3126	3122	638.9197 $[M – 2Cl]^-$

[a] Decomposition without melting
[b] Decomposition with melting

The ESI mass spectra of these complexes generally showed the daughter ions, $[M – Cl]^+$. The detection of fragments of this type is not unusual as they are normally observed for Pd-Cl compounds.[9] It was also noted that performing the mass spectral analysis at low cone voltages, yielded spectra which showed ions that could only be assigned to ligand fragments. An increase in the cone voltage resulted in increased fragmentation which allowed for the identification of the $[M – Cl]^+$ fragments.

Figure 3.6 shows the assigned ESI mass spectrum of complex **T4a** with the predicted spectra of each identified fragment superimposed onto the spectrum. The base peak has been assigned to the $[M – 2Cl – H]^+$ daughter ion while the parent ion $[M – H]^+$ is visible at 643.0611 m/z. Since the complex is only soluble in DMSO, the $[M – Cl + DMSO]^+$ ion is also observed at 685.1174 m/z. The acetonitrile adduct to the $[M – Cl]^+$ daughter ion has also been identified at 650.1307 m/z. All identified fragments displayed the expected isotope clusters for Pd-containing complexes.

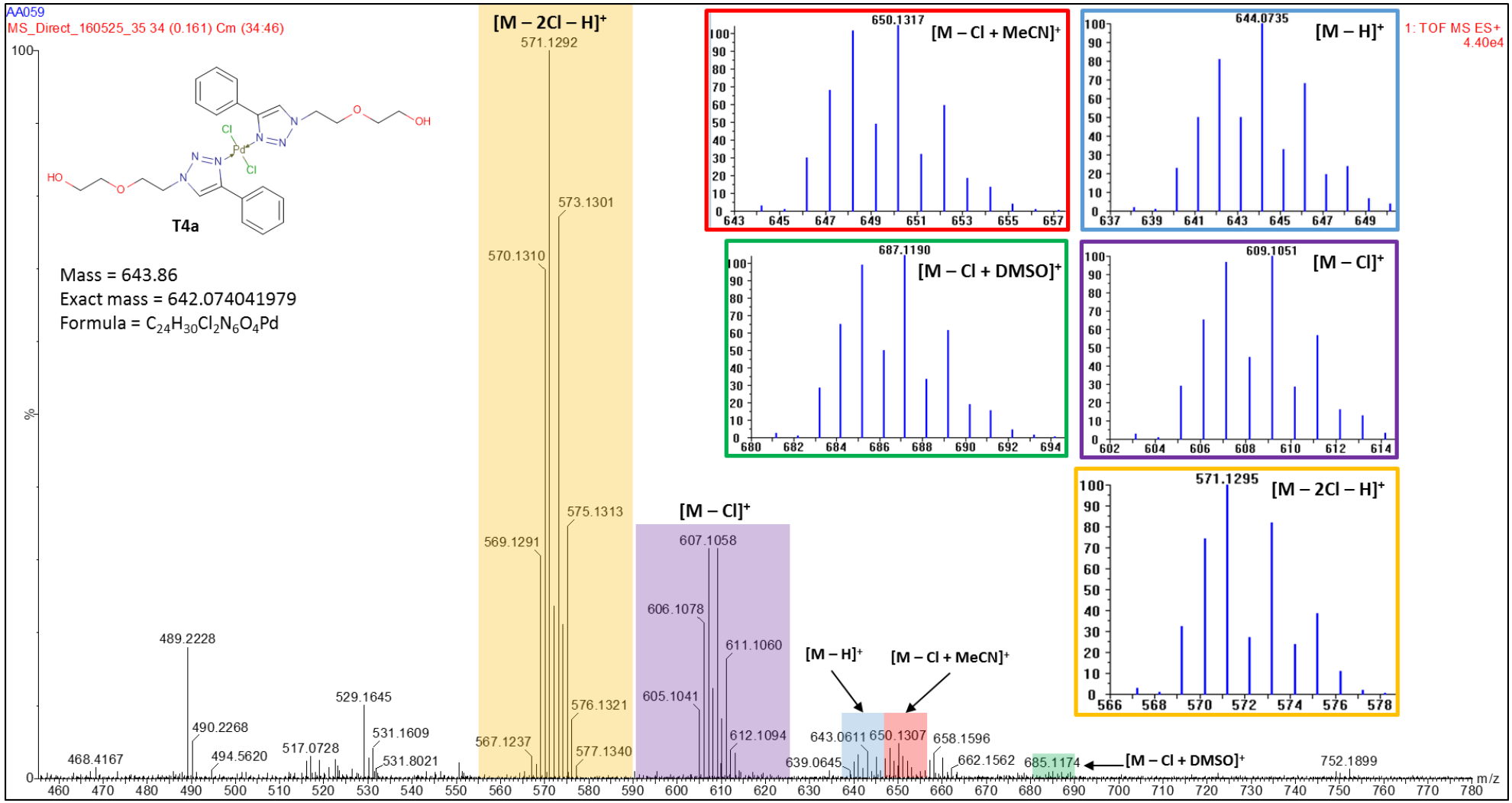

Figure 3.6: The ESI-MS spectrum of T4a obtained, with the predicted spectra for each identified signal. The prediction was performed on Molecular Weight Calculator freeware.[10]

The elemental analysis of the *trans*-Pd(II) complexes revealed the PdL_2Cl_2 nature of these compounds with the results summarized in Table 3.3

Table 3.3: A summary of the elemental analysis results obtained for the *trans*-Pd(II) complexes.

	Calculated			Found			Molecular formula calculated for:
	% C	% H	% N	% C	% H	% N	
T1a	55.54	6.70	12.14	55.57	6.69	12.43	$C_{32}H_{46}Cl_2N_6Pd$
T2a	52.47	5.50	13.11	52.37	5.27	13.11	$C_{28}H_{34}Cl_2N_6Pd{\cdot}0.5H_2O$
T3a	42.15	3.93	14.57	42.49	3.75	14.80	$C_{20}H_{22}Cl_2N_6Pd{\cdot}0.25DCM$
T4a	44.77	4.70	13.05	44.76	4.91	12.58	$C_{24}H_{30}O_4Cl_2N_6Pd$
T5a	45.05	5.15	11.16	45.43	5.47	10.16	$C_{28}H_{38}O_6N_6Cl_2Pd$
T6a	47.20	5.44	11.49	46.89	5.28	10.97	$C_{28}H_{38}Cl_2N_6PdO_2{\cdot}0.75DCM$
T7a	40.05	3.15	8.76	39.66	2.89	8.40	$C_{28}H_{22}Cl_2N_6Pd{\cdot}4DCM$
T8a	56.86	4.47	12.43	56.22	4.87	10.92	$C_{32}H_{30}Cl_2N_6Pd$
T9a	46.89	2.83	15.55	47.27	2.65	14.61	$C_{28}H_{20}N_8O_4PdCl_2{\cdot}0.125DCM$

As with the elemental analysis of the ligands in Chapter 2, there is in some cases a discrepancy between the calculated % N and that found. There are also trace amounts of solvent present in some of the samples despite extensive drying. Combined with the other characterization results, it can be concluded that the intended *trans*-Pd(II) complexes have been successfully synthesized.

It is, however, necessary to mention that the exact geometry of the complexes have not been confirmed, as we were unable to obtain a crystal structure. There are a number of isomers that could be present for the PdL_2Cl_2 complexes, as shown in Figure 3.7 with **T1a** as an example. The complexes synthesized are described as *trans*-Pd(II) complexes since bulky monodentate ligands generally result in a *trans* geometry around the Pd-centre, due to steric influences playing the determining role in the geometry of the complexes.[11,12] In solution, it is possible that any one of these isomers are present, although a *trans* geometry is preferred, and further investigation in this regard is required.

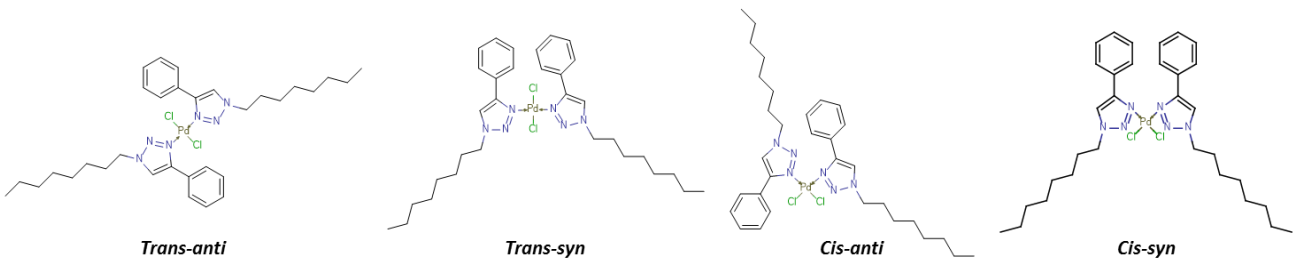

Figure 3.7: The various conformational isomers that are possible for the PdL_2Cl_2 complexes.

3.2.1.1 NMR study on *trans*-Pd(II) phenyl-1,2,3-triazolyl complexes

As mentioned in Section 3.2.1, it was observed that the substituted-1,2,3-triazolyl *trans*-Pd(II) complexes dissociate in DMSO. This phenomenon was observed with varying degrees of ligand dissociation/exchange depending on the nature of the substituents.

The extent of dissociation was greater for complexes with electron withdrawing aromatic N-bound substituents, than for aliphatic groups, as shown in Figure 3.8. This could possibly be attributed to the decrease in the electron density around the coordinating N-atom caused by the electron withdrawing nature of the aromatic substituents, ultimately leading to a lower coordination ability of the ligand. This phenomenon has been studied previously and it was found that the coordination strength of the triazole depends on the C- and N-bound substituents, and increases in the order phenyl < H < benzyl < alkyl. [3,4]

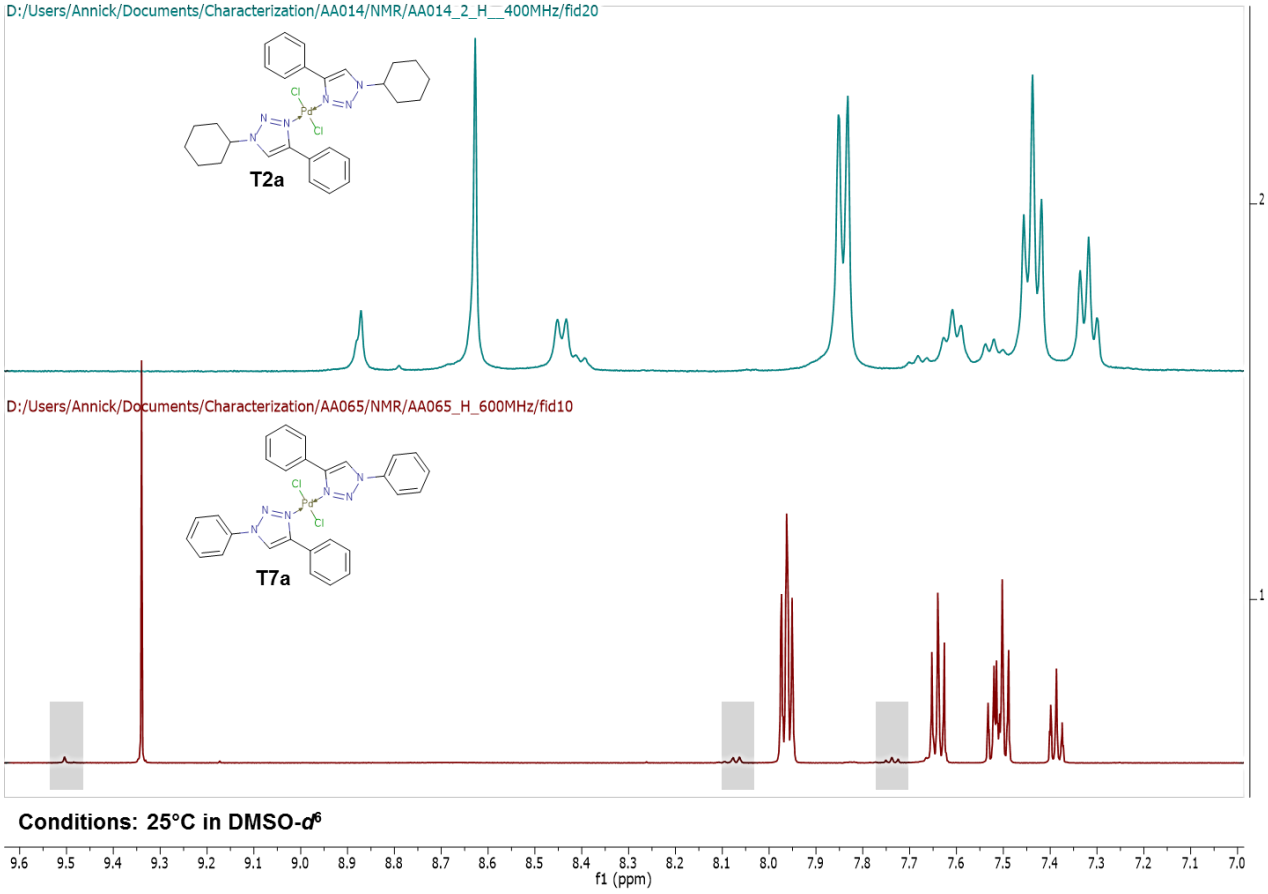

Figure 3.8: A comparison of the aromatic region of the ^{1}H NMR spectra of T2a, with an aliphatic substituent, and T7a, with an aromatic substituent. The signals attributed to the complex of T7a are shown in grey blocks.

To the best of our knowledge, there is a single literature precedent for this phenomenon as documented by Astruc and co-workers[5] for ferrocenyl-1,2,3-triazolyl complexes. Ligand dissociation/exchange was confirmed with the addition of varying equivalents of Pd-precursor to a solution of the ligand in DMSO-*d*^{6}. The results of their experiment are shown in Figure 3.9. Ligand dissociation was still observed at a ratio of 2 equivalents Pd-precursor to ligand.[5]

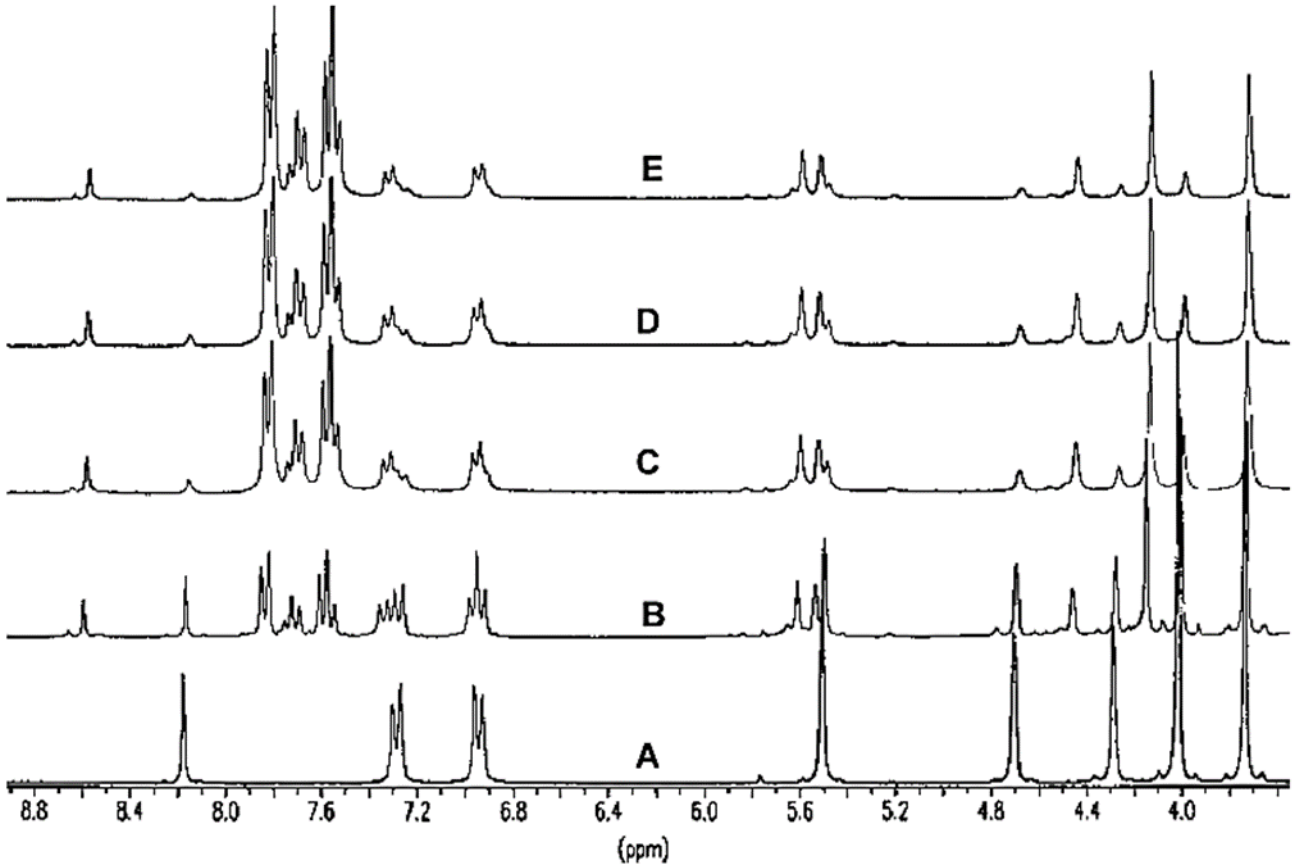

Figure 3.9: The ^{1}H NMR spectroscopy experiment conducted by Astruc and co-workers[5] in which they dissolved their ligand in DMSO-d^6 and added sequential amounts of $(C_6H_5CN)_2PdCl_2$: (A) ligand alone, (B) 1eq. of ligand and 0.5eq. of $(C_6H_5CN)_2PdCl_2$, (C) 1eq. of ligand with 1eq. of $(C_6H_5CN)_2PdCl_2$. (D) 1eq. of ligand and 1.5eq. of $(C_6H_5CN)_2PdCl_2$, (E) 1eq. of ligand and 2eq. of $(C_6H_5CN)_2PdCl_2$.

The experiment outlined by Astruc and co-workers[5] was performed with the **T4a** system. This was done by preparing a sample of the corresponding ligand **4a** in DMSO-d^6 and adding increasing molar equivalents of $(MeCN)_2PdCl_2$ in order to monitor the effect on the ^{1}H NMR spectrum. The resulting spectra are shown in Figure 3.10 and the experimental details are given in Section 3.4.4.

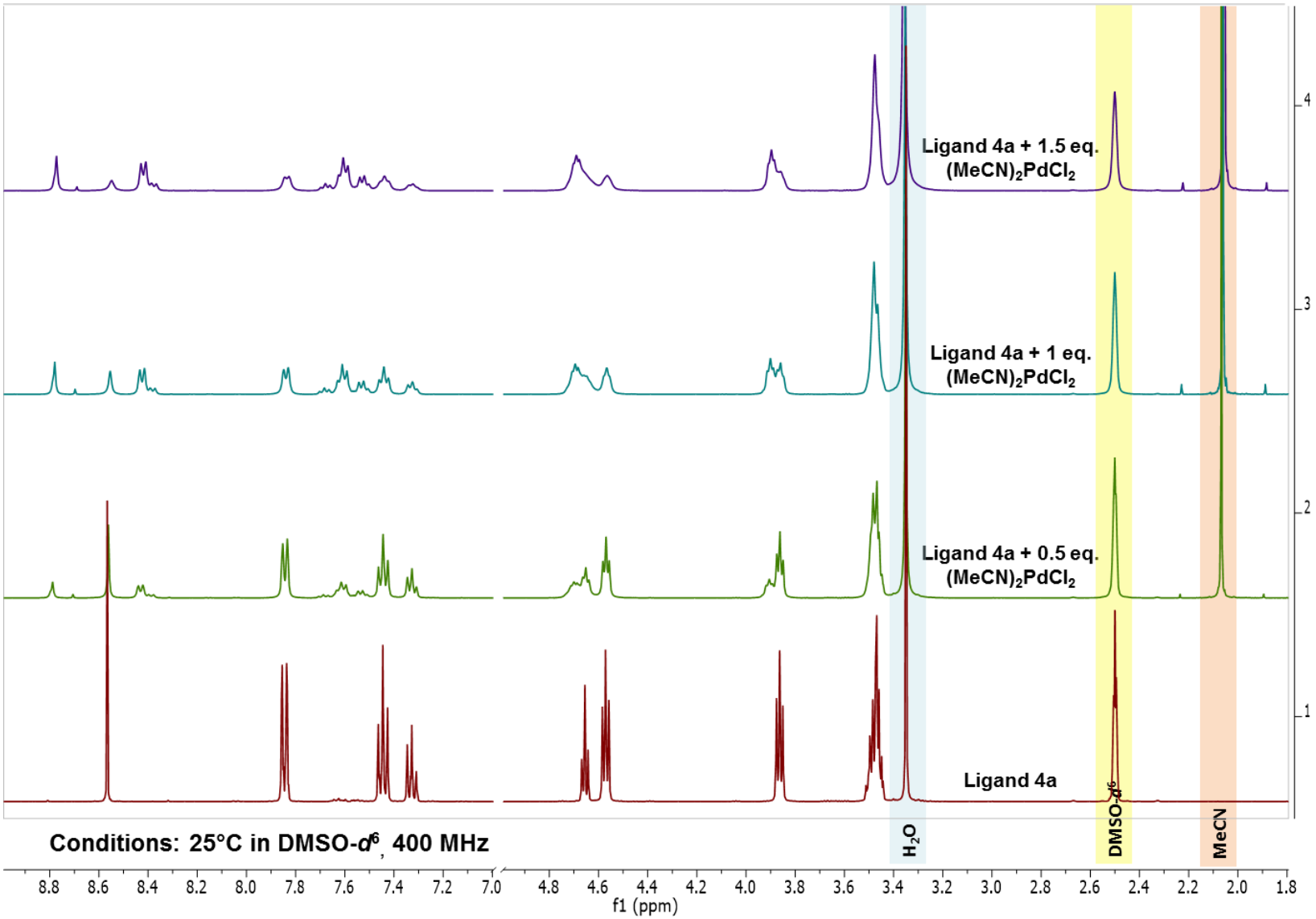

Figure 3.10: The results from the $(MeCN)_2PdCl_2$ addition to 1 eq. *4a* experiments. Since the ratio of ligand to metal in the complex is 2:1, the addition of 0.5 eq. of the Pd-precursor would result in the complex ratio.

As seen in Figure 3.10, with each addition of the Pd-precursor to the ligand sample, there is an increase in the intensity of the signals associated with the complex and a corresponding decrease in the signals associated with the ligand, similar to what was reported by Astruc and co-workers[5]. It was noted that despite the addition of 1.5 eq. Pd-precursor to the ligand, three times the stoichiometric ratio, there are still free ligand signals observed. At 1.5 eq. Pd-precursor, the NMR sample became so concentrated that precipitation of the Pd-precursor was observed and the experiment could not be continued.

The effect of temperature was also investigated by running a variable temperature experiment on **T4a**. Since the sample was only soluble in DMSO, low temperature NMR was not practical, thus only 20 °C, 40 °C and 60 °C ^{1}H NMR experiments were performed. The resulting spectra are shown in Figure 3.11.

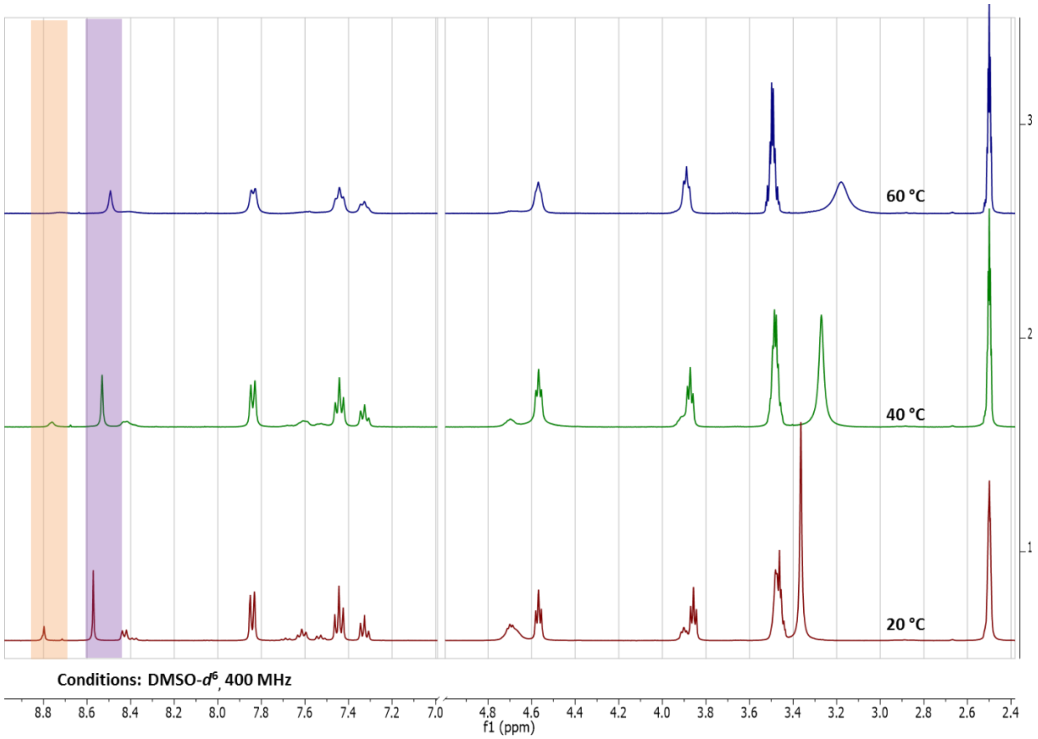

Figure 3.11: The ^{1}H NMR spectroscopy variable temperature experiment of *T4a*. The ligand C*H*-triazole is shown in purple and the complex C*H*-triazole is shown in orange.

The variable temperature NMR spectra (Figure 3.11) shows a pronounced increase in the dissociation with an increase in temperature, evidenced by the decrease of the complex signals and an increase in the free ligand signals, as expected. There is also a marked loss of fine coupling and broadening in the signals with an increase in temperature.

The next logical question was whether this process is reversible, i.e. could the formation of the complex in solution be reversed to bring about ligand dissociation by diluting the saturated NMR sample again. The results from this experiment are shown in Figure 3.12 where the concentration of the Pd-precursor is used to indicate the process.

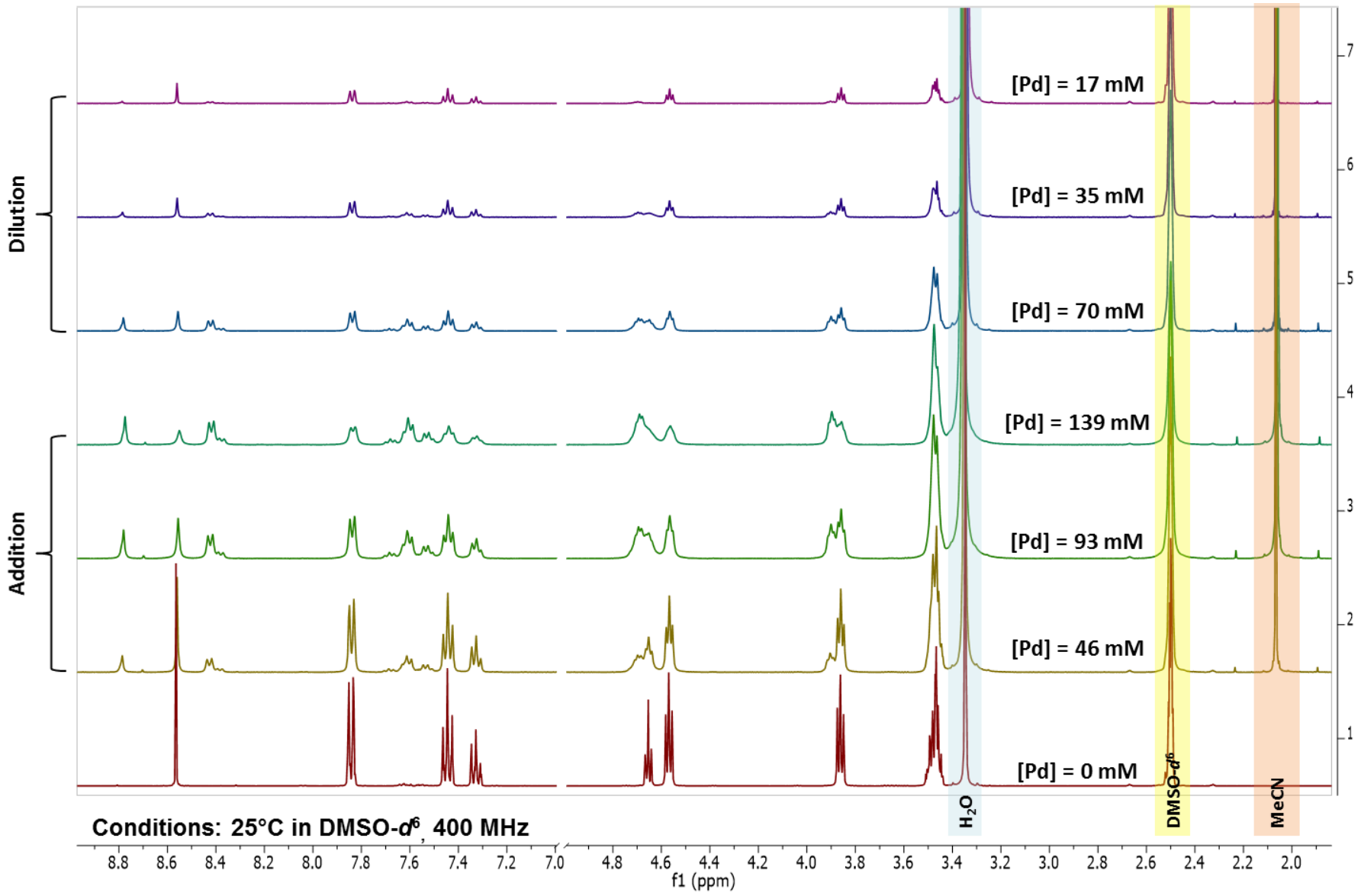

Figure 3.12: The results from the addition-dilution experiment performed in order to determine the reversibility of the process.

The addition-dilution experiment indicated that the dissociation of the ligand from the saturated solution will take place upon dilution of the sample with additional DMSO-d^6. Upon dilution, the complex signals decrease and the ligand signals increase once more.

From the addition-dilution experiment a few interesting observations were made, as shown in Figure 3.13. It was observed that with an increase in the Pd-concentration there is a decrease in the intensity of the ligand CH-triazole signal with a corresponding increase in the complex CH triazole signal, as is expected. This is coupled with a very slight (0.0004 ppm) upfield shift of the signals for both the complex and the free ligand. The opposite is observed when the sample is diluted, and the signals return to their usual positions.

As for the aromatic signals, there is a remarkable decrease in the fine coupling of the ligand signals upon addition of $(MeCN)_2PdCl_2$ and a general broadening of the signals throughout the spectrum. It should also be noted that the signals for protons 2 and 6 (according to the numbering scheme in Figure 3.5) shifts drastically from 7.84 ppm for the free ligand, to 8.43 ppm for the complex. This is interesting when taking into consideration that the downfield shift for the CH triazole signal is only 0.22 ppm. This would indicate that the complexation of the metal centre to the ligand has a greater effect on the two signals of the adjacent phenyl ring than on the triazole itself.

The final observation pertains to the solvents present within the NMR sample, i.e. the residual DMSO signal and the H_2O signal. In the case of the latter, this could potentially be employed to probe any interaction of the complex and water. This could be useful since these products are aimed at a biological application, which usually takes place in aqueous media. Interestingly, in the ^1H NMR spectra of these complexes in DMSO, the H_2O signal shifts downfield with an increase in the Pd-precursor concentration and upfield upon dilution, a trend that is the opposite from the other ligand and complex signals. This interaction with H_2O indicates that the complex might not stable in the presence of H_2O and some species in solution could potentially be attributed to the aqua complexes. As for the residual DMSO signal, only a loss in fine coupling is observed with an increase in the Pd-precursor concentration. Upon dilution the fine coupling returns.

Due to the fact that these spectra are referenced relative to the residual DMSO signal, any shift in this signal is not discernible. It is reasonably expected that, upon ligand dissociation, the vacant sites on the Pd-centre would be occupied by DMSO-molecules, thus resulting in the formation of $(DMSO)_2PdCl_2$. Theoretically, this should result in a shift of the residual DMSO signals, which cannot be observed using this particular setup.

It thus became necessary to repeat the above process using an external reference. It was also decided to switch to an analogous complex that is soluble in both DMSO and $CDCl_3$ in order to investigate the effect of dissociation in a system where the DMSO is not in excess, and to investigate whether the phenomenon observed will hold in a different solvent system. The addition-dilution

experiment was thus repeated on the **T2a** system with $CDCl_3$ as an external reference. The resulting spectra are shown in Figure 3.14.

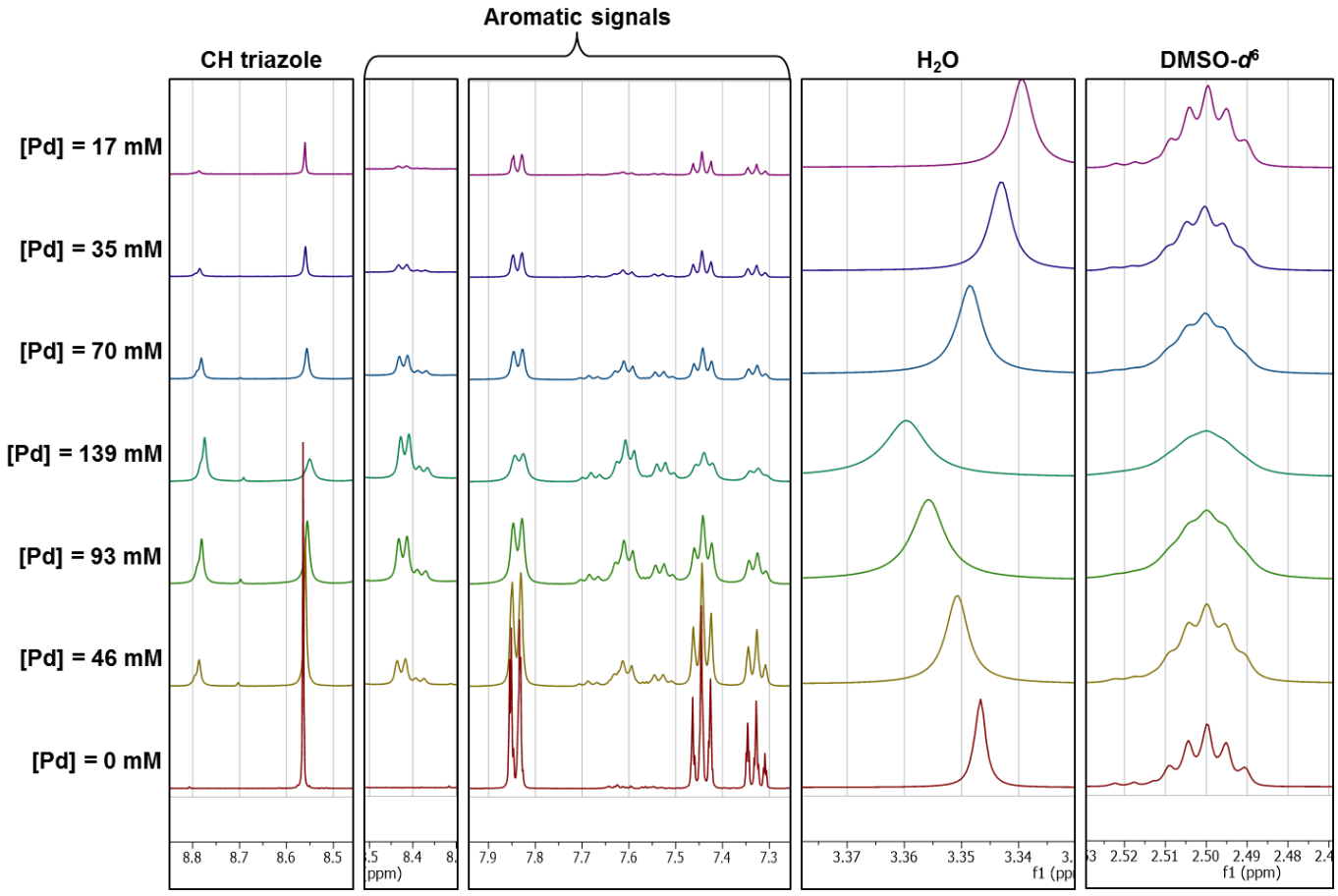

Figure 3.13: A collection of the interesting changes observed in the NMR spectrum of 4a arranged according to increasing Pd-precursor concentration.

From Figure 3.14, it is also seen that the ligand signals decrease as the complex signals increase with the addition of the Pd-precursor and the opposite is observed upon dilution, similar to what was observed for the **T4a** system.

It was interesting to note that the external $CDCl_3$ signals appeared at 6.72 ppm (indicated in grey in Figure 3.14) rather than the expected 8.32 ppm[13], where it should occur if the $CDCl_3$ is in contact with the DMSO-d^6. Nevertheless, the spectra were all referenced to the signal at 6.72 ppm in order to investigate the effect the Pd-precursor addition has on the residual DMSO-d^6 shift.

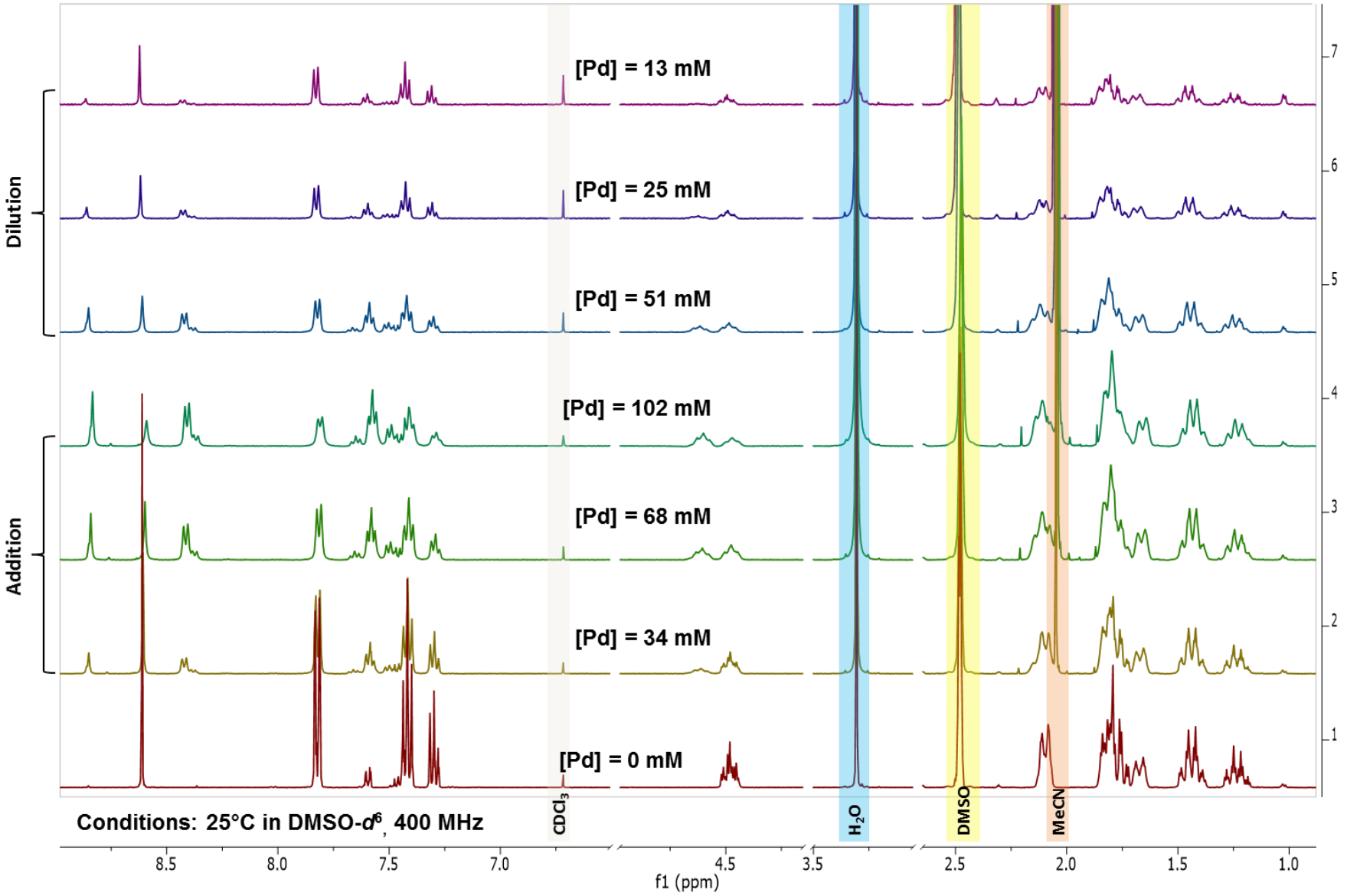

Figure 3.14: The ^{1}H NMR spectra of the addition-dilution experiment of 2a with the addition of $(MeCN)_2PdCl_2$ in order to synthesize T2a *in situ*.

The more relevant signals from the addition-dilution study on the **T2a** system have been summarized in Figure 3.15.

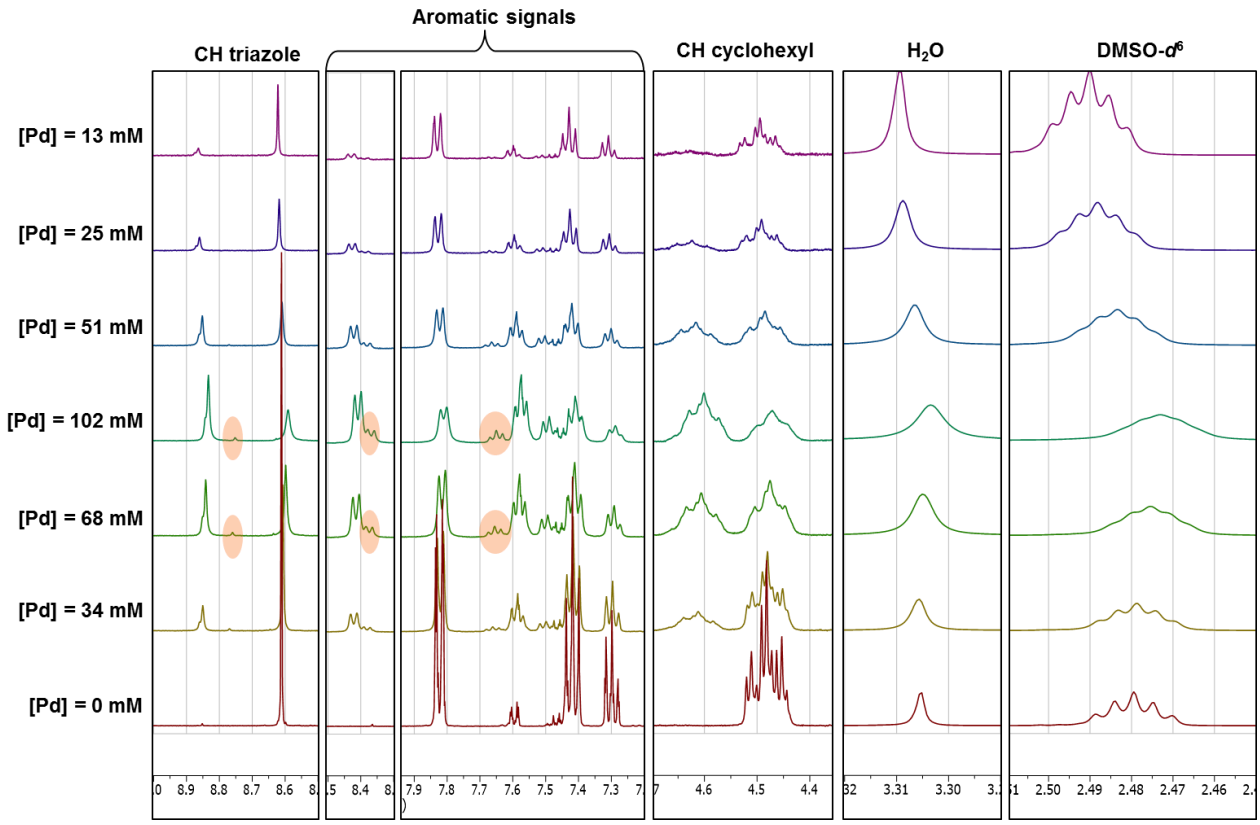

Figure 3.15: A collection of the interesting changes observed in the addition-dilution experiment of the T2a system, arranged according to the Pd-precursor concentration.

It was found that the trends observed for the **T4a** system were also observed with the **T2a** system. The signal of the CH cyclohexyl substituent is included in Figure 3.15 since it clearly shows the disappearance of fine coupling present in the spectrum of the ligand as the intensity of the signals assigned to complex increases. A slight upfield shift of the complex signals are also observed as the Pd-precursor concentration increases and the reversal of the process is seen upon dilution.

Owing to the external referencing used, a similar shift is now observed in the residual DMSO signal. It is assumed that this is due to the coordination of the DMSO to the metal centre.

In addition to the signals arising from the free ligand and the complex, there is a third set of signals that mimics the complex signals (indicated within orange ovals in Figure 3.15). Similarly, Astruc and co-workers[5] observed the same low intensity signals in their system and hypothesized that it could be due to a chloro-bridged dimer forming in solution.[14,15] This hypothesis is still not completely proven, but since the ratio of the third set of signals to that of the complex and the ligand remain the same irrespective of the Pd-concentration, it is unlikely that they can be attributed to the mono-substituted (DMSO)Pd(L)Cl_2 species.[5]

Since the **T2a** complex is also soluble in $CDCl_3$ where ligand dissociation is not observed, it was decided that the effect of the addition of DMSO to the system would be investigated as well, since it would be interesting to see at which concentration the ligand is displaced from the metal centre. In $CDCl_3$ the signals for the aromatic rings are broad and lack fine structure, which could potentially be the exchange of the ligands around the metal centre. A summary of the resulting spectra is shown in Figure 3.16.

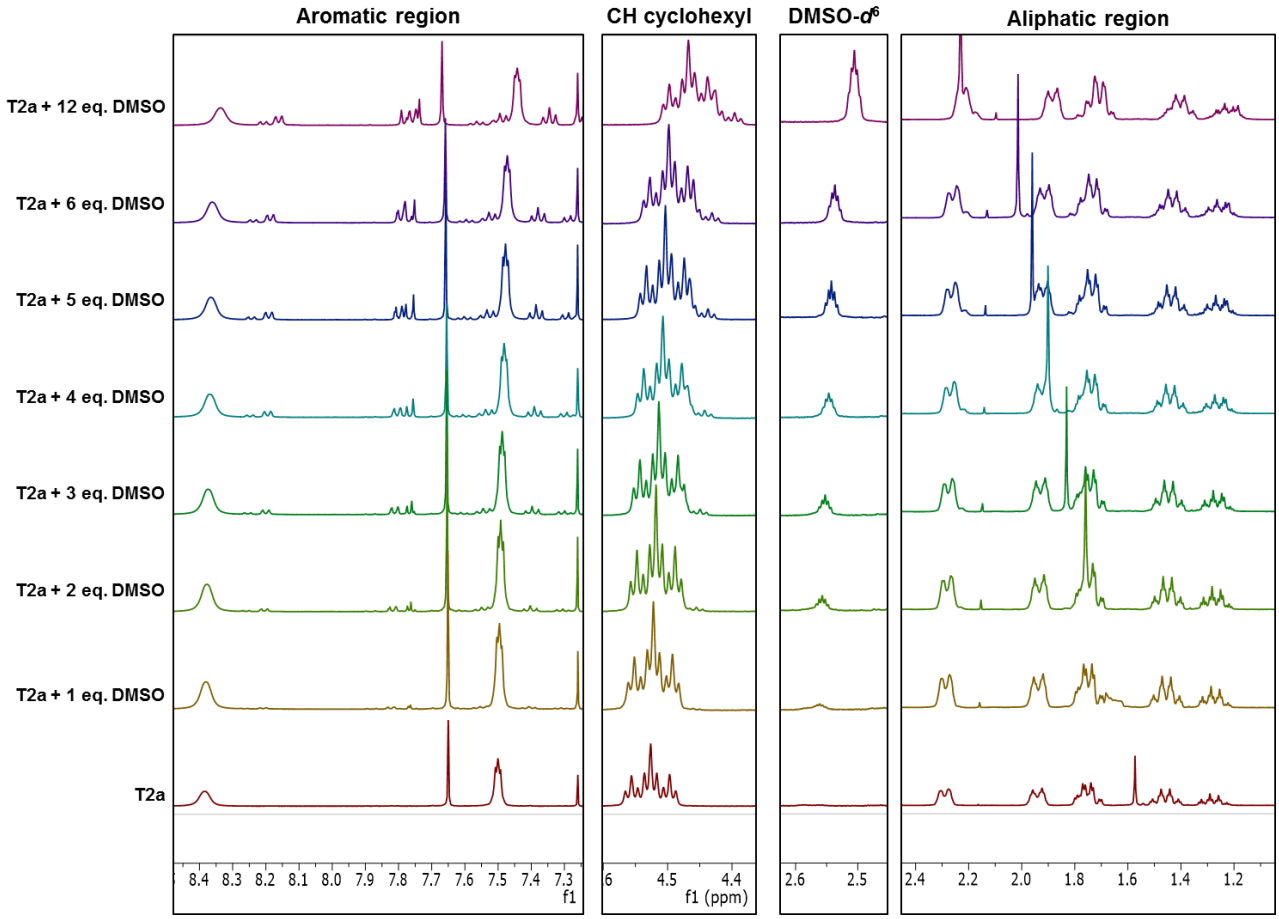

Figure 3.16: A summary of the spectra obtained for the addition of DMSO to *T2a* in $CDCl_3$.

As seen in Figure 3.16, even the addition of one equivalent DMSO to the complex in solution results in the formation of new species in solution. This is accompanied by a small upfield shift for all the complex signals, apart from the CH-triazole signal (7.65 – 7.67 ppm) which has a slight downfield shift. The most noticeable shift is that of the water signal which shifts downfield from 1.58 ppm to 2.23 ppm as the concentration of DMSO increases. This could be attributed to the hydrogen bonding interaction between DMSO and water.

When one considers the products that could form during a ligand dissociation/exchange process, the number of possible interactions become more difficult to distinguish from the NMR spectrum alone. Owing to the presence of water in the DMSO-d^6 solvent, the complexes also have the potential to form the aqua-species with the loss of a labile Cl^- ion. A summary of all the potential species that could be present is shown in Scheme 3.2, with the addition of the chloro-bridged species.

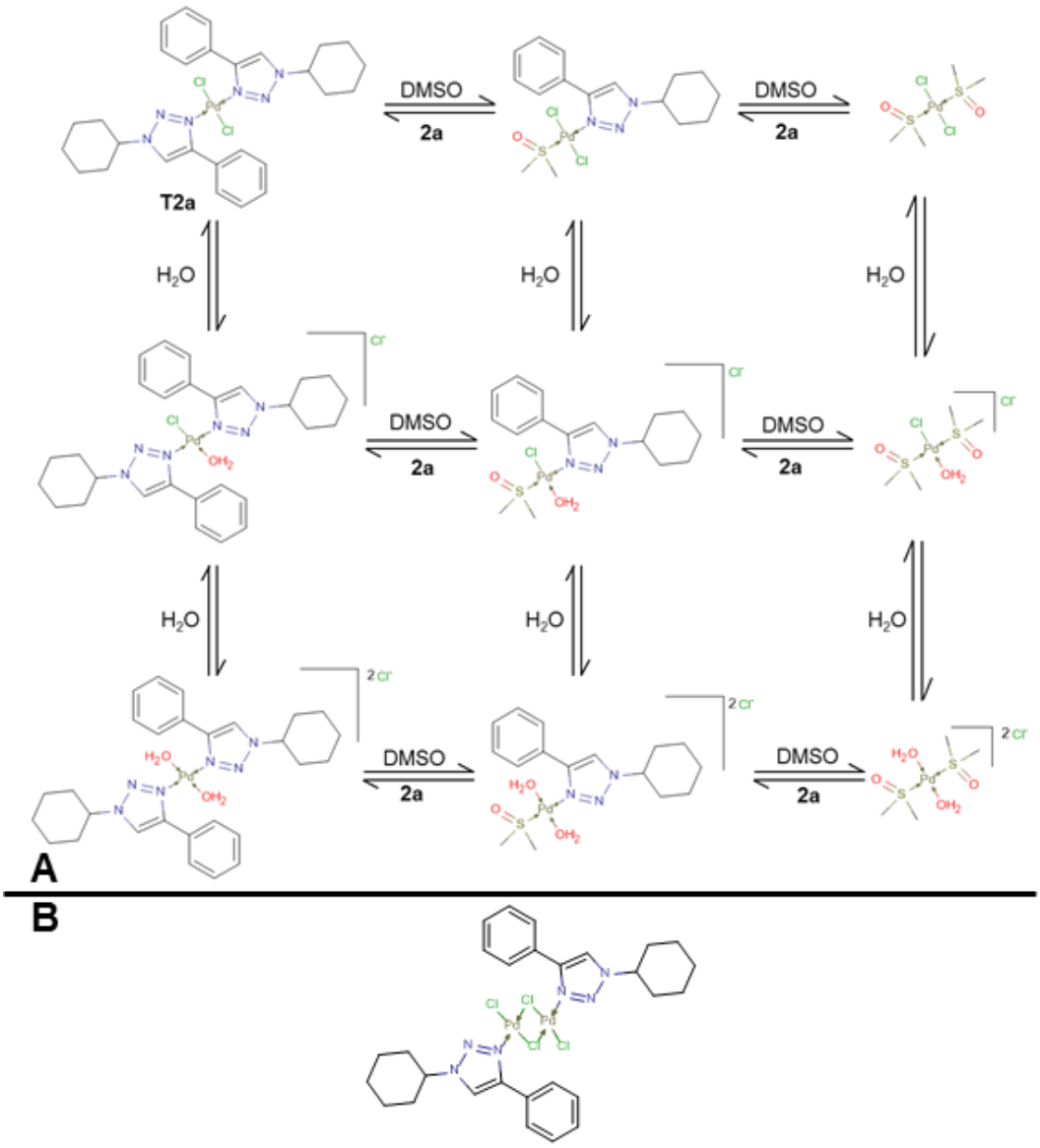

Scheme 3.2: A) a summary of all the species that could potentially be present when T2a is dissolved in DMSO and B) the structure of the proposed chloro-bridged dimer that could form in solution.

Since the aim of these compounds were to be evaluated as anti-cancer agents, their stability in DMSO was crucial. The protocol for evaluating the anti-cancer activity involves the preparation of a stock solution of the compound in DMSO (see Chapter 4). If any ligand dissociation and subsequent solvent coordination occurs, then any anti-cancer activity that is observed is more than likely not attributable to the original palladium complex alone, but rather to a combination of species present within the solution. Additionally, the extent of ligand dissociation has an influence on the concentration of each of the possible components. Should the intact complex have any anti-cancer activity of its own, its concentration within the dissociated solution could be lower than the detection limit, thus resulting in false negatives.

The DMSO-mediated dissociation of N-coordinating ligands in drug-like molecules is generally not reported and thus this presumably results in inaccurate representation of biological activity, as

discussed by Gasser and co-workers.[16] To the best of our knowledge, the complete ligand dissociation of N-containing ligands has only been documented for Ru-complexes.[17]

From the NMR study it can thus be concluded that in the case of the *trans*-Pd(II) phenyl-1,2,3-triazolyl complexes the extent of ligand dissociation should be considered when interpreting anti-cancer assay results. This will be discussed in more detail in Chapter 4.

3.2.2 *N,N'*-bidentate Pd(II) pyridyl-1,2,3-triazolyl complexes derived from pyridyl-1,2,3-triazolyl ligands

The *N,N'*-bidentate complexes are to the best of our knowledge all new, except for **N7b** which has been reported previously[18] but not investigated for its activity as an anti-cancer agent.

The synthesis of these compounds was similar to that of the *trans*-Pd(II) phenyl-1,2,3-triazolyl complexes (Section 3.2.1) and is summarized in Section 3.4.3.1. All complexes were isolated in moderate to good yields, as indicated in Scheme 3.3, and all complexes were only soluble in DMSO.

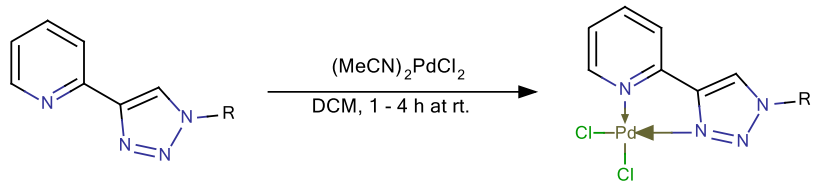

N1b:	R =	Octyl	(82 %)
N2b:	R =	Cyclohexyl	(78 %)
N3b:	R =	Ethanol	(87 %)
N4b:	R =	2-(2-ethoxy) ethanol	(88 %)
N5b:	R =	2-(2-(2-ethoxy) ethoxy) ethanol	(36 %)
N6b:	R =	Hexanol	(89 %)
N7b:	R =	Phenyl	(88 %)
N8b:	R =	2,6-dimethylphenyl	(77 %)
N9b:	R =	4-nitrophenyl	(86 %)

Scheme 3.3: The general structure of the *N,N'*-bidentate Pd(II) pyridyl-1,2,3-triazolyl complexes synthesized with the percentage yields indicated in brackets.

The reaction of the ligands with the Pd-precursor, $(MeCN)_2PdCl_2$, was monitored with FTIR and ^1H NMR spectroscopy, where a significant shift in the CH-triazole proton signal was observed following complex formation. The FTIR and ^1H NMR characterization data for the *N,N'*-bidentate complexes are summarized in Table 3.4 and Table 3.5 respectively.

Table 3.4: Characterization data for the *N,N'*-bidentate-Pd(II) pyridyl-1,2,3-triazolyl complexes with a comparison of the FTIR C–H triazole stretch between the ligand and the corresponding complex.

Compound	Mp (°C)	FTIR C-H triazole stretch (cm^{-1})		ESI-MS (m/z)
		Metal complexes	Ligands	
N1b	279 - 280	3080	3128	459.01 $[M + Na]^+$
N2b	304[b]	3087	3061	428.97 $[M + Na]^+$
N3b	249[a]	3091	3211	297.00 $[M – 2Cl + H]^+$
N4b	202 - 203	3090	3314	376.98 $[M – Cl]^+$
N5b	160 – 161	3099	3365	421.01 $[M – Cl]^+$
N6b	220 - 221	3095	3419	389.02 $[M – Cl]^+$
N7b	252[a]	3593	3114	362.96 $[M – Cl]^+$
N8b	327[a]	3117	3051	434.02 $[M + Li]^+$
N9b	335[b]	3135	3126	450.97 $[M + Li]^+$

[a] Decomposition without melting
[b] Decomposition with melting

There is no apparent correlation between the C-H triazole stretch of the ligand and the complex for the compounds with the aliphatic tethers (**N1b** and **N2b**). For the aromatic complexes, **N7b**, **N8b** and **N9b**, there is an increase in the frequency of the C-H triazole band while the opposite can be seen for the complexes with the hydrophilic tethers, **N3b**, **N4b**, **N5b** and **N6b**.

Upon complexation, a distinct downfield shift in the CH triazole singlet was observed in the ^{1}H NMR spectra, as illustrated in Table 3.5. This can be attributed to the shift of electron density from the N3-atom to the metal centre, which results in a decrease in electron density around the triazole proton. This results in a downfield shift or the triazole proton resonance.

Table 3.5: A comparison of the ^{1}H NMR signals of the CH triazole peaks of the ligands and the *N,N'*-bidentate Pd(II) complexes.

Substituted Pyridine-1,2,3-triazolyl ligands		*N,N'*-bidentate Pd(II)-pyridyl-1,2,3-triazolyl complexes	
Ligand	CH triazole (ppm)	Complex	CH triazole (ppm)
1b	8.04 (s, 1H)	**N1b**	9.21 (s, 1H)
2b[b]	8.12-8.11 (m, 2H, C*H* Ar overlap C*H* triazole)	**N2b**	9.30 (s, 1H)
3b	8.60 (s, 1H)	**N3b**	9.20 (s, 1H)
4b	8.58 (s, 1H)	**N4b**	9.19 (s, 1H)
5b[b]	8.58 (s, 1H)	**N5b**	9.16 (s, 1H)
6b	8.61 (s, 1H)	**N6b**	9.22 (s, 1H)
7b	9.33 (s, 1H)	**N7b**	9.88 (s, 1H)
8b	8.88 (s, 1H)	**N8b**	9.47 (s, 1H)
9b	9.55 (s, 1H)	**N9b**	10.10 (s, 1H)

[a] All spectra run in DMSO-d^6 at 25 °C, except where indicated. Chemical shifts reported as ppm values, referenced to the residual solvent signal
[b] Spectrum recorded in $CDCl_3$ at 25 °C

Table 3.6: The ^{1}H NMR characterization of the *N,N'*-bidentate-Pd(II) pyridyl-1,2,3-triazolyl complexes.

Compound	CH triazole (ppm)	Aromatic region (ppm)	Aliphatic region (ppm)	
			$CH_2/CH_3/CH$	OH
N1b	9.21 (s, 1H)	8.96 (d, 1H, ^{3}J = 5.3 Hz, C*H* Ar), 8.30 (dd, 1H, ^{3}J = 7.6 Hz, ^{4}J = 1.4 Hz, C*H* Ar), 8.15 (d, 1H, ^{3}J = 7.5 Hz, C*H* Ar).	7.69 (m, 1H, CH_2), 1.91-1.88 (m, 2H, CH_2), 1.30-1.24 (m, 10H, 5 × CH_2), 0.85 (t, 3H, ^{3}J = 7.0 Hz, CH_3)	
N2b	9.30 (s, 1H)	8.95 (d, 1H, ^{3}J = 5.7 Hz, C*H* Ar), 8.30 (ddd, 1H, ^{3}J = 7.6 Hz, ^{4}J = 1.2 Hz, C*H* Ar), 8.12 (d, 1H, ^{3}J = 7.9 Hz, C*H* Ar).	4.72 (tt, 1H, ^{3}J = 11.3 Hz, ^{4}J = 3.9 Hz, C*H*), 2.21-2.18 (m, 2H, CH_2), 1.86-1.67 (m, 5H, 2 × CH_2), 1.53-1.43 (m, 2H, CH_2), 1.31-1.20 (m, 1H, C*H*)	
N3b	9.20 (s, 1H)	8.98 (d, 1H, ^{3}J = 5.5 Hz, C*H* Ar), 8.30 (t, 1H, ^{3}J = 7.5 Hz, C*H* Ar), 8.24 (d, 1H, ^{3}J = 7.7 Hz, C*H* Ar), 7.69 (t, 1H, ^{3}J = 7.1 Hz, C*H* Ar).	4.62 (t, 2H, ^{3}J = 5.1 Hz, CH_2), 3.85 (m, 2H, CH_2).	5.22 (bs, 1H)
N4b	9.19 (s, 1H)	8.96-8.94 (m, 1H, C*H* Ar), 8.30 (dd, 1H, ^{3}J = 7.7 Hz, ^{4}J = 1.4 Hz, C*H* Ar), 8.21-8.19 (dd, 1H, C*H* Ar), 7.68 (dd, 1H, ^{3}J = 8.9 Hz, ^{4}J = 1.5 Hz, C*H* Ar).	4.55 (t, 2H, ^{3}J = 4.9 Hz, CH_2), 3.90 (t, 2H, ^{3}J = 4.9 Hz, CH_2), 3.49 (s, 4H, 2 × CH_2)	
N5b	9.16 (s, 1H)	8.98 (d, 1H, ^{3}J = 5.2 Hz, C*H* Ar), 8.29 (td, 1H, ^{3}J = 7.7 Hz, ^{4}J = 1.1 Hz, C*H* Ar), 8.23 (d, 1H, ^{3}J = 7.3 Hz, C*H* Ar), 7.70 (td, 1H, ^{3}J = 7.4 Hz, ^{4}J = 1.4 Hz, C*H* Ar)	4.77 (t, 2H, ^{3}J = 4.8 Hz, CH_2), 3.90 (t, 2H, ^{3}J = 4.9 Hz, CH_2), 3.60-3.57 (m, 2H, *CH₂*), 3.53-3.50 (m, 2H, CH_2), 3.49-3.44 (m, 2H, CH_2), 3.40-3.38 (m, 2H, CH_2)	4.58 (t, 1H, ^{3}J = 5.5 Hz)
N6b	9.22 (s, 1H)	8.96 (d, 1H, ^{3}J = 6.0 Hz, C*H* Ar), 8.29 (t, 1H, ^{3}J = 7.8 Hz, C*H* Ar), 8.16 (d, 1H, ^{3}J = 7.8 Hz, C*H* Ar), 7.68 (t, 1H, ^{3}J = 7.2 Hz, C*H* Ar).	4.56 (t, 2H, ^{3}J = 7.1 Hz, CH_2), 3.38 (q, 2H, ^{3}J = 6.3 Hz, CH_2), 1.90 (multiplet, 2H, CH_2), 1.44-1.39 (m, 2H, CH_2), 1.36-1.31 (m, 4H, 2 × CH_2).	4.34 (t, 1H, ^{3}J = 5.2 Hz)
N7b	9.88 (s, 1H)	9.04-9.02 (m, 1H, C*H* Ar), 8.38 (dd, 1H, ^{3}J = 7.8 Hz, ^{4}J = 1.4 Hz, C*H* Ar), 8.19-8.16 (m, 1H, C*H* Ar), 7.94-7.90 (m, 2H, 2 × C*H* Ar), 7.78-7.66 (m, 4H, 4 × C*H* Ar).		
N8b	9.47 (s, 1H)	9.04 (d, 1H, ^{3}J = 6.2 Hz, C*H* Ar), 8.35 (dd, 1H, ^{3}J = 7.8 Hz, ^{4}J = 1.3 Hz, C*H* Ar), 8.14 (d, 1H, ^{3}J = 7.5 Hz, C*H* Ar), 7.78-7.73 (m, 1H, C*H* Ar), 7.55-7.50 (m, 1H, C*H* Ar), 7.38 (d, 2H, ^{3}J = 7.8 Hz, 2 × C*H* Ar).	2.06 (s, 6H, 2 × CH_3)	
N9b	10.09 (s, 1H)	8.97 (d, 1H, ^{3}J = 5.5 Hz, C*H* Ar), 8.58 – 8.55 (m, 2H, 2 × C*H* Ar), 8.38 (td, 1H, ^{3}J = 7.9 Hz, ^{4}J = 1.5 Hz, C*H* Ar), 8.21 – 8.18 (m, 3H, 3 × C*H* Ar), 7.75 (td, 1H, ^{3}J = 7.3 Hz, ^{4}J = 1.3 Hz, C*H* Ar).		

[a] All spectra run in DMSO-d^6 at 25 °C, except where indicated. Chemical shifts reported as ppm values, referenced to the residual solvent peak

The ESI-MS spectra of the complexes typically yielded the $[M - Cl]^+$ fragments, which is commonly observed for Pd-Cl compounds. The loss of chloride is brought on by the protonation of the mass ion, followed by the loss of HCl.[9] The $[M - Cl + MeCN]^+$ fragments were also observed and a possible fragmentation pattern, using complex **N7b** as an example, is shown in Scheme 3.4 in order to illustrate the loss of the chloride ion and the formation of the $[M - Cl + MeCN]^+$ fragment.

Assuming that the Pd-N (triazole) bond has not been severed (as indicated by the $[M + H]^+$ fragment in Scheme 3.4), it is expected that the proton would reside on the medial N-atom, as it is the next most basic atom, after the coordinating proximal N-atom.[1,2,3]

Additionally, a Na adduct was also observed in some cases. The observed fragments displayed the characteristic isotopic clusters expected for Pd(II) complexes. An example of a typical ESI-MS spectrum for the *N,N'*-bidentate Pd(II) pyridyl-1,2,3-triazolyl complexes is shown in Figure 3.17.

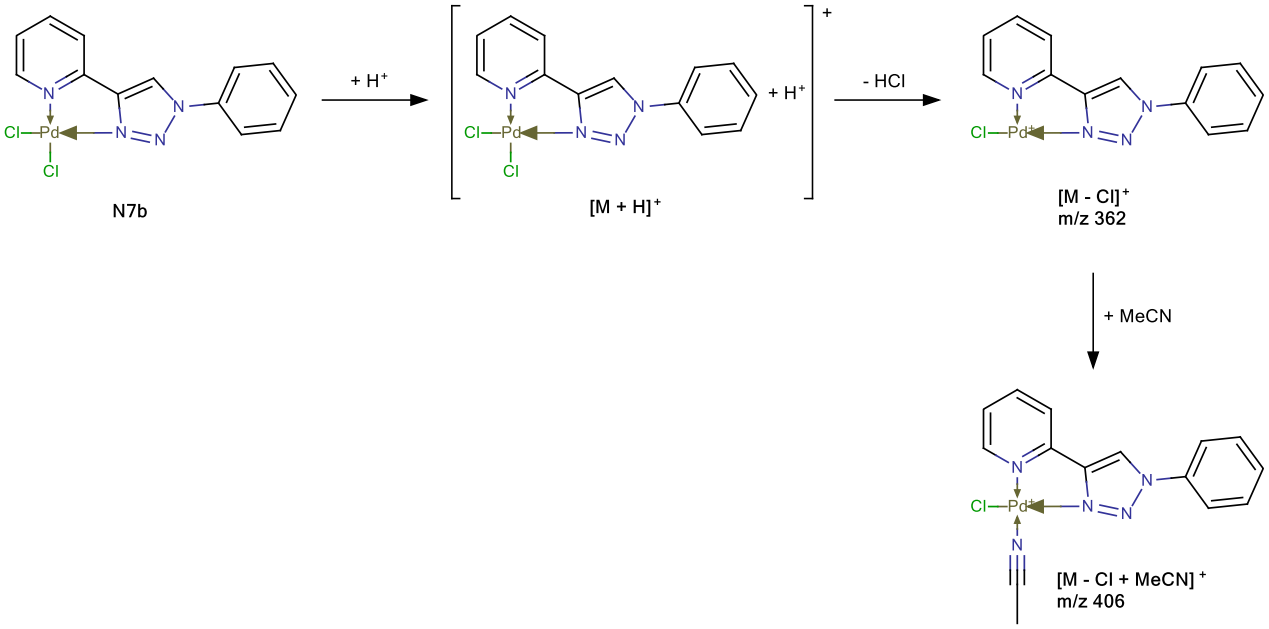

Scheme 3.4: The fragmentation pattern observed for the *N,N'*-bidentate Pd(II) pyridyl-1,2,3-triazolyl complexes, with N7b as an example.

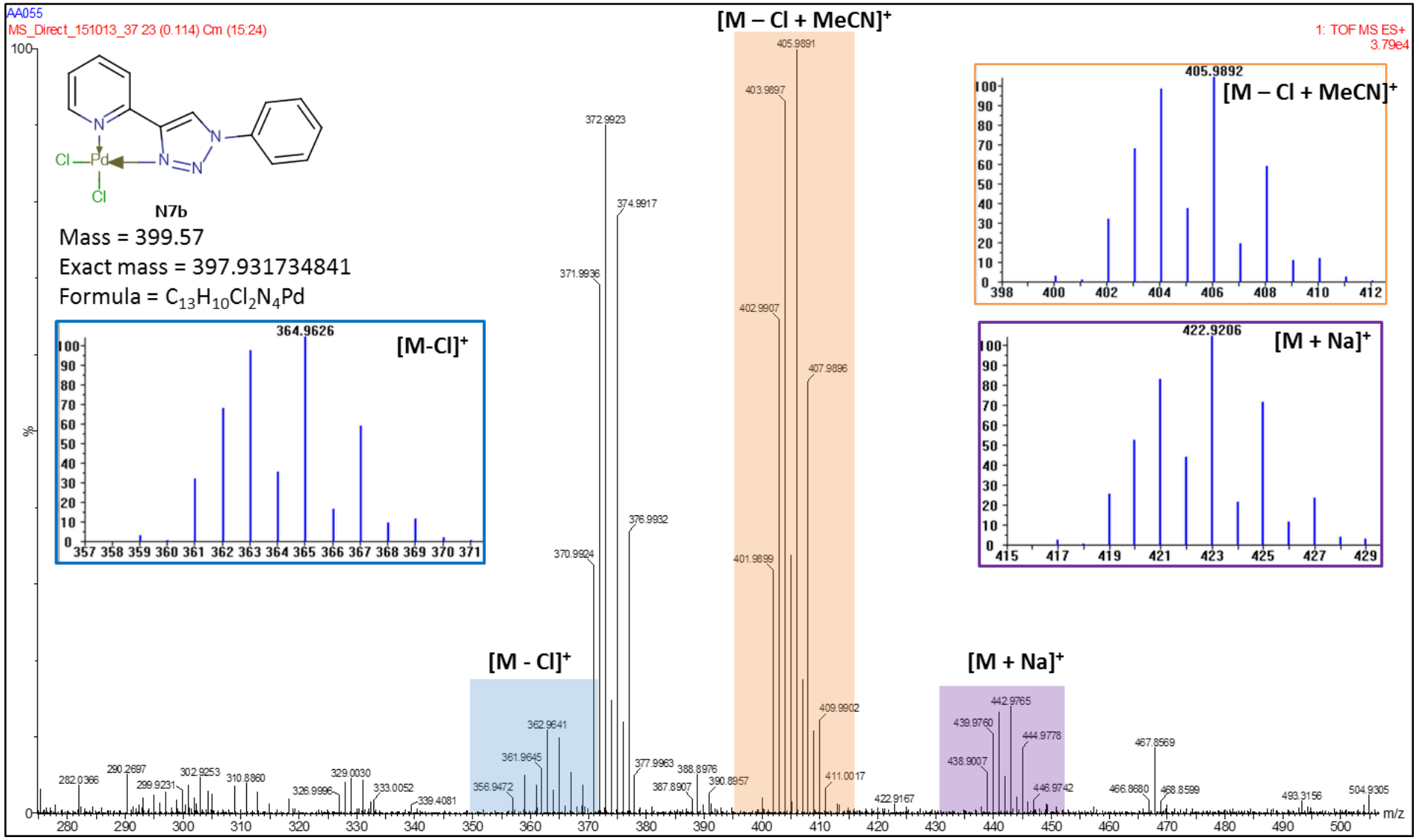

Figure 3.17: The ESI-MS spectrum of N7b obtained with the predicted spectra for each identified signal. The prediction was performed on Molecular Weight Calculator freeware.[10]

The identity of the complexes was also confirmed with elemental analysis, as summarized in Table 3.7. Efforts to obtain single crystals suitable for single crystal X-ray diffraction (SCXRD) analysis were fruitless as amorphous powders were obtained in all cases. A summary of the elemental analysis is given in Table 3.7.

Table 3.7: A summary of the elemental analysis results of all the *N,N'*-bidentate Pd(II)-complexes.

	Calculated			Found			Molecular formula found
	% C	% H	% N	% C	% H	% N	
N1b	41.35	5.09	12.86	41.01	4.84	12.40	$C_{15}H_{22}Cl_2N_4Pd$
N2b	38.49	3.98	13.81	38.12	4.17	12.44	$C_{13}H_{16}Cl_2N_4Pd$
N3b	28.04	3.14	15.27	28.34	3.32	14.53	$C_9H_{10}Cl_2N_4Pd{\cdot}H_2O$
N4b	38.49	3.98	13.81	38.12	4.17	12.44	$C_{13}H_{16}O_2Cl_2N_4Pd$
N5b	31.11	3.73	10.36	30.79	3.30	10.67	$C_{13}H_{18}O_2Cl_2N_4Pd$
N6b	36.47	4.36	13.09	36.12	5.41	14.16	$C_{13}H_{18}Cl_2N_4O_2Pd{\cdot}0.25H_2O$
N7b	37.80	2.80	13.56	37.60	2.27	14.10	$C_{13}H_{10}Cl_2N_4Pd{\cdot}0.75H_2O$
N8b	42.13	3.30	13.10	40.32	2.84	12.01	$C_{15}H_{14}Cl_2N_4Pd$
N9b	34.17	2.06	15.04	34.59	1.71	14.42	$C_{13}H_9N_5O_2PdCl_2{\cdot}0.25DCM$

In the cases of **N3b**, **N6b** and **N7b** trace amounts of water was detected despite extensive *in vacuo* drying.

3.3 Conclusion

The *trans*-Pd(II) phenyl-1,2,3-triazolyl complexes and *N,N'*-bidentate Pd(II) pyridyl-1,2,3-triazolyl complexes were both successfully synthesized and characterized. It was noted that the 1,2,3-triazole ligands of the *trans*-Pd(II) complexes dissociated in DMSO and that the extent of dissociation is dependent on the N-bound substituents of the 1,2,3-triazole ring, with aromatic substituents leading to a greater extent of dissociation than the aliphatic and hydrophilic substituents. As discussed in Section 3.2.1.1, it is suspected that the increase in the electron withdrawing capabilities of the aromatic R-groups result in a decrease in the electron donating abilities of the coordinating proximal N-atom. This results in a weakening of the coordination strength of the N-atom, which increases the extent of ligand dissociation observed. This phenomenon has been studied previously and it was found that the coordination strength of the triazole depends on the C- and N-bound substituents, and increases in the order phenyl < H < benzyl < alkyl. [3,4]

3.4 Experimental Section

3.4.1 General Methods and Materials

The synthetic procedures were all performed under standard Schlenk conditions under a nitrogen atmosphere unless otherwise noted. Literature procedures were used where indicated. All starting materials used were obtained from Merck and Sigma-Aldrich and used without additional purification. Solvents used were obtained from Merck, Protea Chemicals, Kimix and Sigma-Aldrich and purified accordingly. THF, DCM, hexane, and diethyl ether were dried and degassed using PureSolv Micro purifiers. Acetonitrile, methanol and ethanol were distilled over the appropriate drying agents. Acetonitrile was distilled over phosphorous pentoxide and both methanol and ethanol were distilled over magnesium filings and iodine. The Pd(II) precursor, $(MeCN)_2PdCl_2$, was prepared according to a literature procedure[19].

FTIR data was collected on a Thermo Nicolet 350 ATR-FTIR spectrometer with a Smart Performance ATR (Zn/Se) attachment. ^{1}H NMR and ^{13}C NMR spectroscopy experiments were performed on 300, 400 and 600 MHz Agilent NMR spectrometers as indicated. Chemical shifts were recorded in reference to the residual solvent signals. The coupling constants (*J*) are reported in Hz. ESI Mass Spectra were recorded in positive mode, unless otherwise stated, using a Waters Synapt G2 mass spectrometer and employing a cone voltage of 15 V unless otherwise noted. Microanalysis was performed at the University of Cape Town's Department of Chemistry on an Thermo Scientific Flash 2000 CHNS-O Analyzer. Melting points were determined on a Bibby Stuart Scientific Melting Point Apparatus SMP3.

3.4.2 Synthesis of *trans*-Pd(II) complexes based on 1-substituted-4-phenyl-1,2,3-triazolyl ligands

3.4.2.1 General synthesis for *trans*-Pd(II) phenyl-1,2,3-triazolyl complexes

$(MeCN)_2PdCl_2$ (1 eq.) was dissolved in DCM (9.0 mL) at 25 °C. A solution of the ligand (2 eq.) dissolved in DCM (1.0 mL) was added to a solution of the Pd-precursor. The reaction mixture was allowed to stir at 25 °C for 2-4 hours after which the resulting precipitate was filtered off. The precipitate was washed with DCM (3 × 2 mL) to remove any residual ligand and Pd-precursor, followed by Et_2O (3 × 2 mL) in order to remove the residual solvent. The product was then dried under vacuum overnight.

3.4.2.1.1 Synthesis of T1a

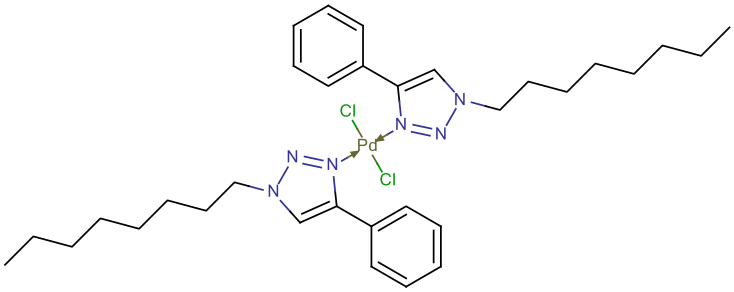

T1a

An opalescent yellow powder was recrystallized by layering hexane onto a DCM solution of the compound (0.093 g, 65 %). Mp = 180 – 181 °C. FTIR (ATR): 3128.45 cm^1 (C-H triazole stretch). ^{1}H NMR (600 MHz, DMSO-d^6): δ (ppm) = 8.81 (s, 1H C*H* triazole), 8.44 (d, 2H, ^3J = 7.6 Hz, 2 × C*H* Ar), 7.61 (t, 2H, ^3J = 7.5 Hz, 2 × C*H* Ar), 7.53 (t, 1H, ^3J = 7.4 Hz, C*H* Ar), 4.53 – 4.48 (m, 2H, CH_2), 1.90 – 1.83 (m, 3H, CH_2 + C*H*), 1.27-1.22 (m, 14H, 5 × CH_2), 0.84 (t, 3H, ^3J = 7.0 Hz, CH_3), (severe overlap with dissociated ligand signals). ^{13}C NMR (151 MHz, DMSO-d^6): δ (ppm) = 147.03 (C quat), 129.47 (C quat), 128.94 (2 × C*H* Ar), 127.77 (2 × C*H* Ar), 127.45 (C*H* triazole), 124.87 (C*H* Ar), 51.42 (CH_2), 31.11 (CH_2), 29.04 (CH_2), 29.01 (CH_2), 28.45 (CH_2), 28.22 (CH_2), 25.58 (CH_2), 13.91 (CH_3), (severe overlap with dissociated ligand signals). ESI-MS: found: 435.2332 m/z $[M – L]^+$ (calc. 435.0296 m/z). Elemental analysis: % Found (% calc.) for $C_{32}H_{46}Cl_2N_6Pd$: C: 55.57 (55.54); H: 6.69 (6.70); N: 12.43 (12.14).

3.4.2.1.2 Synthesis of T2a

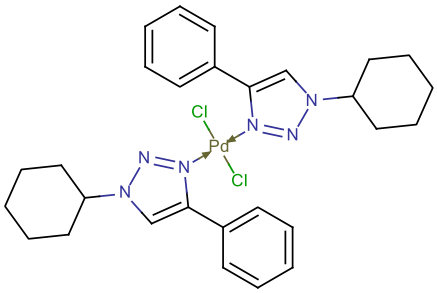

T2a

A pale yellow powder was recrystallized by layering hexane onto a DCM solution of the compound (89 mg, 63 %). Mp = 155 - 157 °C. FTIR (ATR): 3134 cm^{-1} (C-H triazole stretch). ^{1}H NMR (400 MHz, DMSO-d^6): δ (ppm) = 8.87 (s, 1H, C*H* triazole), 8.44 (d, 2H, ^3J = 7.7 Hz, 2 × C*H* Ar), 7.61 (t, 2H, ^3J = 7.5 Hz, 2 × C*H* Ar), 7.52 (t, 1H, ^3J = 7.4 Hz, C*H* Ar), 4.66 - 4.60 (m, 1H, C*H*), 2.12 (d, 2H, ^3J = 13.1 Hz, CH_2), 1.85-1.75 (m, 5H, 2 × CH_2 + C*H*), 1.50 – 1.41 (q, 3H, ^3J = 12.8 Hz, CH_2 + C*H*), 1.31 – 1.21 (m, 1H, C*H*), (severe overlap with dissociated ligand signals). ^{13}C NMR (101 MHz, DMSO-d^6): δ (ppm) = 146.85 (*C* quat), 129.44 (*C* quat), 128.91 (2 × *C*H Ar), 127.84 (2 × *C*H Ar), 127.45 (*C*H Ar), 123.33 (*C*H triazole), 59.11 (*C*H), 54.90 (*C*H_2) 32.86 (*C*H_2), 32.28 (*C*H_2), 24.73 (*C*H_2), 24.57 (*C*H_2), (severe overlap with dissociated ligand signals). Confirmed with HSQC. ESI-MS: found: 597.1552 m/z $[M – Cl]^+$ (calc. 597.1568 m/z). Elemental analysis: % Found (% calc.) for $C_{28}H_{34}Cl_2N_6Pd·0.5H_2O$: C: 52.37 (52.47); H: 5.27 (5.50); N: 11.90 (13.11).

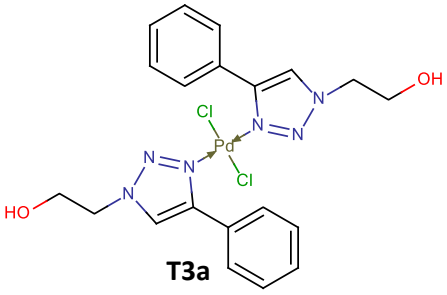

T3a

3.4.2.1.3 Synthesis of T3a

A pale yellow powder was obtained (0.053 g, 95 %). Mp =.232 °C (turns brown), 239 – 240 °C (decomposes). FTIR (ATR): 3469 (O-H stretch), 3130 (C-H triazole stretch), 1229 (C-N), 1071 (C-O). ^{1}H NMR (600 MHz. DMSO-*d*^{6}): *δ* (ppm) = 8.76 (s, 1H, C*H* triazole), 8.43 (d, 2H, ^{3}J = 7.5 Hz, 2 × C*H* Ar), 7.61 (t, 2H, ^{3}J = 7.6 Hz, 2 × C*H* Ar), 7.52 (t, 1H, ^{3}J = 8.0 Hz, C*H* Ar), 5.22 (t, 1H, ^{3}J = 5.0 Hz, O*H*), 4.58 – 4.55 (m, 2H, CH_2), 3.89 – 3.86 (m, 2H, CH_2), (severe overlap with dissociated ligand signals). ^{13}C NMR (101 MHz, DMSO-*d*^{6}): *δ* (ppm) = 146.92 (*C* quat), 129.43 (*C* quat), 128.93 (2 × C*H* Ar), 127.88 (2 × C*H* Ar), 127.45 (C*H* triazole), 125.43 (C*H* Ar), 59.12 (CH_2), 54.28 (CH_2). ESI-MS: found: 483.0766 m/z [M – 2Cl - H]$^{+}$ (calc. 483.0769 m/z), 521.0526 m/z [M – Cl]$^{+}$ (calc. 521.0526 m/z). Elemental analysis: % Found (% calc.) for $C_{20}H_{22}N_6O_2Cl_2Pd$·0.25DCM: C: 42.49 (42.15); H: 3.75 (3.93); N: 14.80 (14.57).

3.4.2.1.4 Synthesis of T4a

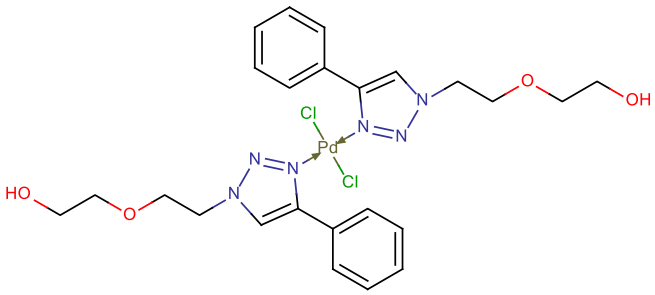

T4a

A pale yellow powder was obtained (0.121 g, 87 %). Mp = 191 °C decomposes. FTIR (ATR): 3422 cm^{-1} (O-H stretch), 3098 cm^{-1} (C-H triazole). ^{1}H NMR (600 MHz, DMSO-*d*^{6}): *δ* (ppm) = 8.79 (s, 1H, C*H* triazole), 8.43 (d, 2H, ^{3}J = 7.3 Hz, 2 × C*H* Ar), 7.61 (t, 2H, ^{3}J = 7.5 Hz, 2 × C*H* Ar), 7.53 (t, 1H, ^{3}J = 7.3 Hz, C*H* Ar), 4.73 – 4.67 (m, 5H, 2 × CH_2 + O*H*), 3.90 (t, 4H, ^{3}J = 4.8 Hz, 2 × CH_2), 3.50 – 3.47 (m, 2H, CH_2), (severe overlap with dissociated ligand signals). ^{13}C NMR (101 MHz, DMSO-*d*^{6}): *δ* (ppm) = 147.04 (*C* quat), 146.18 (*C* quat), 129.50 (2 × *C*H Ar), 129.15 (2 × *C*H Ar), 127.49 (*C*H triazole), 125.39 (*C*H Ar), 67.81 (CH_2), 67.80 (CH_2), 51.50 (CH_2), 51.46 (CH_2), (severe overlap with dissociated ligand signals). HRMS: found: 571.1292 m/z [M – 2Cl - H]$^{+}$ (calc. 571.1295 m/z), 609.1058 m/z [M – Cl]$^{+}$ (calc. 609.1051), 643.0611 m/z [M – H]$^{+}$ (calc. 644.0735), 650.1307 m/z [M – Cl + MeCN]$^{+}$ (calc. 650.1317), 685.1174 m/z [M – Cl + DMSO]$^{+}$ (calc. 685.1198). Elemental analysis: % Found (% calc.) for $C_{24}H_{30}N_6O_4Cl_2Pd$: C: 44.76 (44.77); H: 4.91 (4.70); N: 12.58 (13.05).

3.4.2.1.5 Synthesis of T5a

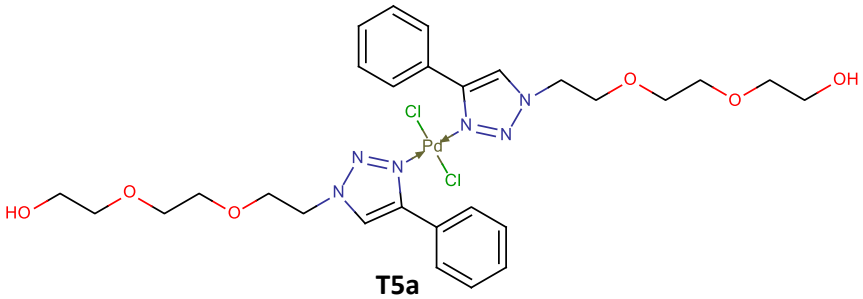

T5a

A pale yellow powder was crystallized from a layered solution of DCM and hexane (0.119 g, 90 %). Mp = 131 – 132 °C. FTIR (ATR): 3447 cm^{-1} (O-H stretch), 3129 cm^{-1} (C-H

triazole stretch). ^{1}H NMR (600 MHz, DMSO-d^6): δ (ppm) = 8.75 (s, 1H, C*H* triazole), 8.43 (d, 2H, ^{3}J = 7.1 Hz, 2 × C*H* Ar), 7.61 (t, 2H, ^{3}J = 7.6 Hz, 2 × C*H* Ar), 7.53 (t, 1H, ^{3}J = 7.4 Hz, C*H* Ar), 4.70 – 4.69 (m, 3H, CH_2 + O*H*), 3.92 (t, 3H, ^{3}J = 4.8 Hz, CH_2), 3.56-3.55 (m, 2H, CH_2), 3.51-3.49 (m, 2H, CH_2), 3.46 (q, 2H, ^{3}J = 5.1 Hz, CH_2), 3.39 (t, 2H, ^{3}J = 5.2 Hz, CH_2), (severe overlap with dissociated ligand signals). ^{13}C NMR (75 MHz, DMSO-d^6): δ (ppm) = 129.50 (*C* quat), 128.95 (*C* quat), 128.54 (2 × *C*H Ar), 127.49 (2 × *C*H Ar), 125.21 (*C*H Ar), 121.76 (*C*H triazole), 72.36 (*C*H_2), 69.74 (*C*H_2), 69.53 (*C*H_2), 67.87 (*C*H_2), 67.84 (*C*H_2), 49.66 (*C*H_2), (severe overlap with dissociated ligand signals). ESI-MS: found: 659.1819 m/z [M – 2Cl - H]$^+$ (calc. 659.1821 m/z), 697.1556 m/z [M – Cl]$^+$ (calc. 697.1577 m/z). Elemental analysis: % Found (% calc.) for $C_{28}H_{38}N_6O_6PdCl_2$: C: 45.43 (45.05); H: 5.47 (5.15); N: 10.16 (11.16).

3.4.2.1.6 Synthesis of T6a

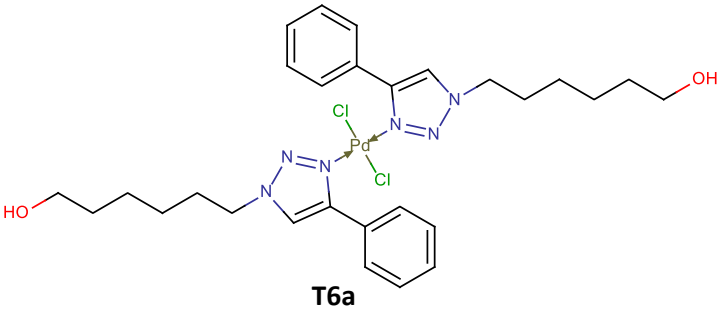

T6a

A pale yellow powder was obtained (0.041 g, 60 %). Mp = 123 – 124 °C. FTIR (ATR): 3369 cm^{-1} (O-H stretch), 3096 cm^{-1} (C-H triazole stretch). ^{1}H NMR (600 MHz, DMSO-d^6): δ (ppm) = 8.81 (s, 1H, C*H* triazole), 8.44 (d, 2H, ^{3}J = 7.5 Hz, 2 × C*H* Ar), 7.61 (t, 2H, ^{3}J = 7.5 Hz, 2 × C*H* Ar), 7.53 (t, 1H, ^{3}J = 7.2 Hz, C*H* Ar), 4.54 – 4.49 (m, 3H, CH_2 + O*H*), 3.36 (q, 3H, ^{3}J = 6.4 Hz, CH_2), 1.92 – 1.84 (m, 3H, CH_2), 1.43 – 1.38 (m, 3H, CH_2), 1.35-1.24 (m, 4H, 2 × CH_2), (severe overlap with dissociated ligand signals). ^{13}C NMR (101 MHz, DMSO-d^6): δ (ppm) = 147.04 (*C* quat), 129.48 (*C* quat), 129.14 (2 × *C*H Ar), 128.95 (2 × *C*H Ar), 127.45 (*C*H Ar), 124.88 (*C*H triazole), 51.41 (*C*H_2), 29.09 (*C*H_2), 25.52 (*C*H_2), 24.81 (*C*H_2), (severe overlap with dissociated ligand signals). ESI-MS: found: 595.2024 m/z [M – 2Cl - H]$^+$ (calc. 595.2024 m/z), 633.1762 m/z [M – Cl]$^+$ (calc. 633.1780 m/z). Elemental analysis: % Found (% calc.) for $C_{28}H_{38}N_6O_2PdCl_2$·0.75DCM: C: 46.89 (47.20); H: 5.28 (5.44); N: 10.97 (11.49).

3.4.2.1.7 Synthesis of T7a

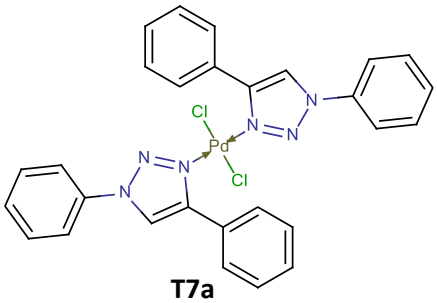

T7a

A pale brown powder was obtained (114 mg, 76 %). Mp = 160 °C decomposes. FTIR (ATR): 3113.98 cm^{-1} (C-H triazole). ^{1}H NMR (400 MHz, DMSO-d^6): δ (ppm) = 9.50 (s, 1H, C*H* triazole, 8.07 (t, 2H, ^{3}J = 7.9 Hz, 2 × C*H* Ar), 7.74 (t, 2H, ^{3}J = 7.5 Hz, 2 × C*H* Ar), ligand dissociation is so extensive that complex signals are mostly obscured. HRMS: found: 619.1668 m/z [M – H]$^+$ (calc. 619.0234 m/z). Elemental analysis: % Found (% calc.) for $C_{28}H_{22}Cl_2N_6Pd$·4DCM: C: 39.66 (40.05); H: 2.89 (3.15); N: 8.40 (8.76).

3.4.2.1.8 Synthesis of T8a

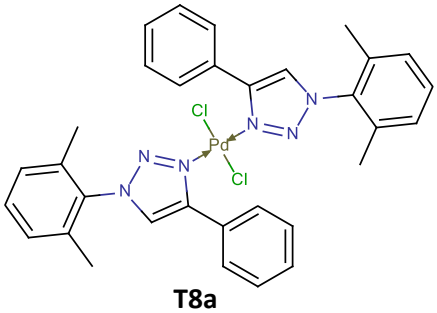

T8a

A pale brown powder was obtained (82 mg, 63 %). Mp = 213 °C decomposes. FTIR (ATR): 3131.64 cm^{-1} (C-H triazole). ^{1}H NMR (300 MHz, DMSO-d^6): δ (ppm) = ligand dissociation is so extensive that complex signals are mostly obscured. ESI-MS: found: 426.1011 m/z $[M - L]^+$ (calc. 426.9670 m/z), found: 603.1541 m/z $[M - 2Cl]^+$ (calc. 604.1579 m/z). Elemental analysis: % Found (% calc.) for $C_{32}H_{30}Cl_2N_6Pd$: C: 56.22 (56.86); H: 4.87 (4.47); N: 10.92 (12.43).

3.4.2.1.9 Synthesis of T9a

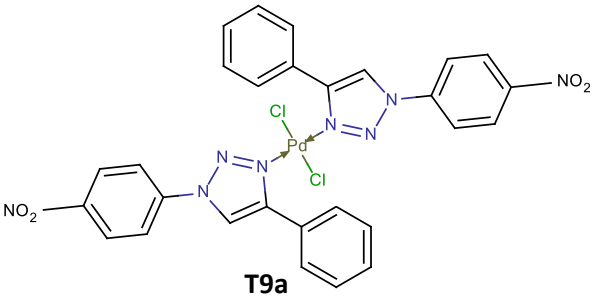

T9a

The precipitate was too fine to filter. The reaction mixture was thus divided into two centrifuge tubes and the samples centrifuged at 6000 rpm for 15 minutes. The supernatant was siphoned off and fresh DCM (4 mL) was added. The process was repeated until the supernatant was clear. A bright orange powder was obtained (0.241 g, 90 %). Mp = 304 – 305 °C decomposes with melting. FTIR (ATR): 3126 cm^{-1} (C-H triazole stretch), 1597 cm^{-1} (N=O stretch), 1343 cm^{-1} (N=O stretch). ^{1}H NMR (600 MHz, DMSO-d^6): δ (ppm) = ligand dissociation is so extensive that complex signals are mostly obscured. ESI-MS: found: 638.9182 m/z $[M - 2Cl]^-$ (calc. 638.0653 m/z). Elemental analysis: % Found (% calc.) for $C_{28}H_{20}N_8O_4PdCl_2 \cdot 0.125DCM$: C: 47.27 (46.89); H: 2.65 (2.83); N: 14.61 (15.55).

3.4.3 Synthesis of *N,N'*-bidentate Pd(II) complexes based on 1-substituted-4-pyridyl-1,2,3-triazolyl ligands

3.4.3.1 General synthesis for *N,N'*-bidentate Pd(II) pyridyl-1,2,3-triazolyl complexes

$(MeCN)_2PdCl_2$ (1 eq.) was dissolved in DCM (9.0 mL) at 25 °C. The ligand (1 eq.) was dissolved in DCM (1.0 mL) and added to the Pd-precursor. The reaction mixture was allowed to stir at 25 °C for 2-4 hours after which the resulting precipitate was filtered off. The precipitate was washed with DCM (3 × 2 mL) to remove any residual ligand and Pd-precursor, followed by Et_2O (3 × 2 mL) in order to remove the residual solvent. The product was then dried under vacuum overnight.

3.4.3.1.1 Synthesis of N1b

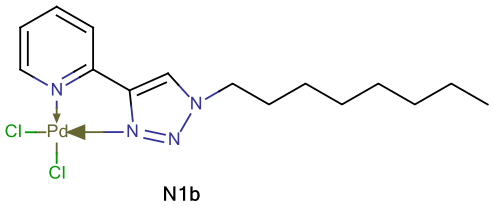

N1b

A pale orange powder was obtained (0.082 g, 82 %). Mp = 279 – 280 °C decomposes with melting. FTIR (ATR): 3080 cm^{-1} (C-H triazole). ^{1}H NMR (400 MHz, DMSO-d^6): δ (ppm) = 9.21 (s, 1H, C*H* triazole), 8.96 (d, 1H, ^{3}J = 5.3 Hz, C*H* Ar), 8.30 (dd, 1H, ^{3}J = 7.6 Hz, ^{4}J = 1.4 Hz, C*H* Ar), 8.15 (d, 1H, ^{3}J = 7.5 Hz, C*H* Ar), 7.69 (m, 1H, CH_2), 1.91-1.88 (m, 2H, CH_2), 1.30-1.24 (m, 10H, 5 × CH_2), 0.85 (t, 3H, ^{3}J = 7.0 Hz, CH_3). ^{13}C NMR (101 MHz, DMSO-d^6): δ (ppm) = 149.49, 148.32, 147.36, 141.40, 125.57, 125.52, 122.04, 52.19, 31.18, 24.11, 28.46, 28.36, 25.62, 22.07, 13.96. ESI-MS: found: 459.01 m/z $[M + Na]^+$ (calc. 459.0146 m/z), found: 442.08 m/z $[M – Cl + MeCN]^+$ (calc. 442.0831 m/z). Elemental analysis: % Found (% calc.) for $C_{15}H_{22}Cl_2N_4Pd$: C: 41.01 (41.35); H: 4.84 (5.09); N: 12.40 (12.86).

3.4.3.1.2 Synthesis of N2b

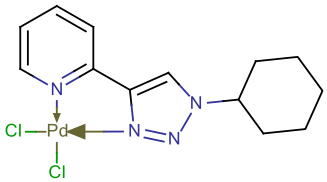

N2b

A pale orange powder was obtained (0.078 g, 78 %). Mp = 304 °C decomposes. FTIR (ATR): 3087 cm^{-1} (C-H triazole). ^{1}H NMR (400 MHz, DMSO-d^6): δ (ppm) = 9.30 (s, 1H, C*H* triazole), 8.95 (d, 1H, ^{3}J = 5.7 Hz, C*H* Ar), 8.30 (ddd, 1H, ^{3}J = 7.6 Hz, ^{4}J = 1.2 Hz, C*H* Ar), 8.12 (d, 1H, ^{3}J = 7.9 Hz, C*H* Ar), 4.72 (tt, 1H, ^{3}J = 11.3 Hz, ^{4}J = 3.9 Hz, C*H*), 2.21-2.18 (m, 2H, CH_2), 1.86-1.67 (m, 5H, 2 × CH_2), 1.53-1.43 (m, 2H, CH_2), 1.31-1.20 (m, 1H, C*H*). ^{13}C NMR (101 MHz, DMSO-d^6): δ (ppm) = 149.50, 148.38, 147.21, 141.41, 125.49, 123.97, 121.90, 61.84, 32.36, 24.48, 24.26. ESI-MS: found: 428.97 m/z $[M + Na]^+$ (calc. 428.9676 m/z), found: 412.04 m/z $[M – Cl + MeCN]^+$ (calc. 412.0361 m/z), found: 371.01 m/z $[M-Cl]^+$ (calc. 371.0095 m/z). Elemental analysis: % Found (% calc.) for $C_{13}H_{16}Cl_2N_4Pd$: C: 38.12 (38.49); H: 4.17 (3.98); N: 12.44 (13.81).

3.4.3.1.3 Synthesis of N3b

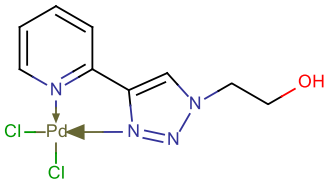

N3b

A pale orange powder was obtained (0.087 g, 87 %). Mp = 249 °C decomposes. FTIR (ATR): 3446 cm^{-1} (O-H stretch), 3091 (C-H stretch). ^{1}H NMR (600 MHz, DMSO-d^6): δ (ppm): 9.20 (s, 1H, C*H* triazole), 8.98 (d, 1H, ^{3}J = 5.5 Hz, C*H* Ar), 8.30 (t, 1H, ^{3}J = 7.5 Hz, C*H* Ar), 8.24 (d, 1H, ^{3}J = 7.7 Hz, C*H* Ar), 7.69 (t, 1H, ^{3}J = 7.1 Hz, C*H* Ar), 5.22 (bs, 1H, O*H*), 4.62 (t, 2H, ^{3}J = 5.1 Hz, CH_2), 3.85 (m, 2H, CH_2). ^{13}C NMR (151 MHz, DMSO-d^6): δ (ppm): 149.50 (*C*H triazole), 148.30 (*C* quat.), 147.16 (*C* quat.), 141.39 (*C*H Ar), 126.25 (*C*H Ar), 125.48 (*C*H Ar), 121.97 (*C*H Ar), 59.26 (*C*H_2), 55.05 (*C*H_2). ESI-MS: found: 296.9956 m/z $[M – 2Cl + H]^+$ (calc. 296.9972 m/z), found: 371.9851 m/z $[M – Cl + MeCN]^+$ (calc. 371.9845 m/z). Elemental analysis: % Found (% calc.) for $C_9H_{10}Cl_2N_4Pd·H_2O$: C: 28.34 (28.04); H: 3.32 (3.14); N: 14.53 (15.27).

3.4.3.1.4 Synthesis of N4b

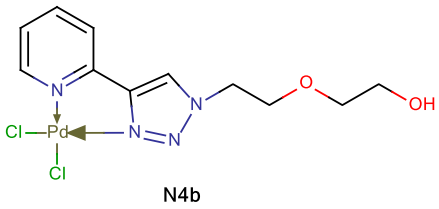

N4b

A pale orange powder was obtained (0.232 g, 88%). Mp = 202 - 203 °C decomposes. FTIR (ATR): 3458 cm^{-1} (O-H stretch), 3090 cm^{-1} (C-H triazole). ^{1}H NMR (300 MHz, DMSO-d^6): δ (ppm) = 9.19 (s, 1H, C*H* triazole), 8.96-8.94 (m, 1H, C*H* Ar), 8.30 (dd, 1H, ^{3}J = 7.7 Hz, ^{4}J = 1.4 Hz, C*H* Ar), 8.21-8.19 (dd, 1H, C*H* Ar), 7.68 (dd, 1H, ^{3}J = 8.9 Hz, ^{4}J = 1.5 Hz, C*H* Ar), 4.55 (t, 2H, ^{3}J = 4.9 Hz, CH_2), 3.90 (t, 2H, ^{3}J = 4.9 Hz, CH_2), 3.49 (s, 4H, 2 × CH_2). ^{13}C NMR (101 MHz, DMSO-d^6): δ (ppm) = 149.49 (*C*H triazole.), 148.26 (*C* quat), 147.27 (*C* quat.), 141.39 (*C*H Ar), 126.18 (*C*H Ar), 125.54 (*C*H Ar), 122.07 (*C*H Ar), 72.19 (*C*H_2), 67.88 (*C*H_2), 60.04 (*C*H_2), 52.31 (*C*H_2). ESI-MS: found: 376.9839 m/z $[M - Cl]^+$ (calc. 376.9837 m/z), 418.0099 m/z $[M - Cl + MeCN]^+$ (calc. 418.0103 m/z). Elemental analysis: % Found (% calc.) for $C_{13}H_{16}O_2Cl_2N_4Pd$: C: 38.12 (38.49); H: 4.17 (3.98); N: 12.44 (13.81).

3.4.3.1.5 Synthesis of N5b

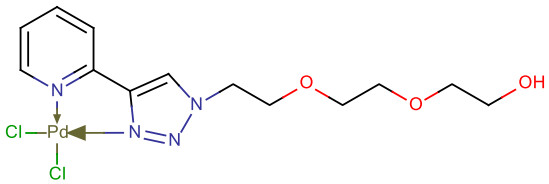

N5b

A pale brown powder was obtained (0.072 g, 36 %). Mp = 160 – 161 °C decomposes. FTIR (ATR): 3535 cm^{-1} (O-H stretch), 3099 cm^{-1} (C-H triazole stretch). ^{1}H NMR (400 MHz, DMSO-d^6): δ (ppm) = 9.16 (s, 1H, C*H* triazole), 8.98 (d, 1H, ^{3}J = 5.2 Hz, C*H* Ar), 8.29 (td, 1H, ^{3}J = 7.7 Hz, ^{4}J = 1.1 Hz, C*H* Ar), 8.23 (d, 1H, ^{3}J = 7.3 Hz, C*H* Ar), 7.70 (td, 1H, ^{3}J = 7.4 Hz, ^{4}J = 1.4 Hz, C*H* Ar), 4.77 (t, 2H, ^{3}J = 4.8 Hz, CH_2), 4.58 (t, 1H, ^{3}J = 5.5 Hz, O*H*), 3.90 (t, 2H, ^{3}J = 4.9 Hz, CH_2), 3.60-3.57 (m, 2H, *CH*$_2$), 3.53-3.50 (m, 2H, CH_2), 3.49-3.44 (m, 2H, CH_2), 3.40-3.38 (m, 2H, CH_2). ^{13}C NMR (101 MHz, DMSO-d^6): δ (ppm) = 149.51, 148.24, 147.26, 141.38, 126.10, 125.55, 122.07, 72.30, 69.64, 69.51, 67.90, 60.19, 52.25. ESI-MS: found: 421.0098 m/z $[M - Cl]^+$ (calc. 421.0100 m/z). Elemental analysis: % Found (% calc.) for $C_{13}H_{18}O_2Cl_2N_4Pd$: C: 30.79 (31.11); H: 3.30 (3.73); N: 10.67 (10.36).

3.4.3.1.6 Synthesis of N6b

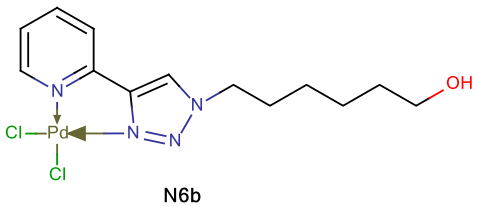

N6b

A yellow-orange powder was obtained (0.134 g, 89 %). Mp = 220 – 221 °C decomposes. FTIR (ATR): 3472 cm^{-1} (O-H stretch), 3095 (C-H triazole stretch). ^{1}H NMR (600 MHz, DMSO-d^6): δ (ppm) = 9.22 (s, 1H, C*H* triazole), 8.96 (d, 1H, ^{3}J = 6.0 Hz, C*H* Ar), 8.29 (t, 1H, ^{3}J = 7.8 Hz, C*H* Ar), 8.16 (d, 1H, ^{3}J = 7.8 Hz, C*H* Ar), 7.68 (t, 1H, ^{3}J = 7.2 Hz, C*H* Ar), 4.56 (t, 2H, ^{3}J = 7.1 Hz, CH_2), 4.34 (t, 1H, ^{3}J = 5.2 Hz, O*H*), 3.38 (q, 2H, ^{3}J = 6.3 Hz, CH_2), 1.90 (quintet, 2H, ^{3}J = 7.1 Hz, CH_2), 1.44-1.39 (m, 2H, CH_2), 1.36-1.31 (m, 4H, 2 × CH_2). ^{13}C NMR (151 MHz, DMSO-d^6): δ (ppm) = 149.44, 148.29, 147.32, 141.35, 125.55, 125.47, 122.01, 60.50, 52.15, 32.18, 29.12, 25.48, 24.90. ESI-MS: found: 389.0191 m/z $[M - Cl]^+$ (calc. 389.0201 m/z), 406.0662 m/z $[M - OH]^+$ (calc. 406.9856 m/z), found: 430.0455

m/z [M – Cl + MeCN]$^+$ (calc. 430.0467 m/z). Elemental analysis: % Found (% calc.) for $C_{13}H_{18}Cl_2N_4Pd{\cdot}0.25H_2O$: C: 36.12 (36.47); H: 5.41 (4.36); N: 14.16 (13.09).

3.4.3.1.7 Synthesis of N7b

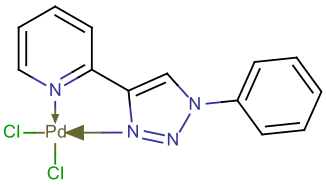

N7b

A pale orange powder was isolated (0.316 g, 88 %). Mp = 252 °C decomposes. FTIR (ATR): 3593 cm^{-1} (C-H triazole). ^{1}H NMR (300 MHz, DMSO-*d*^{6}): *δ* (ppm) = 9.88 (s, 1H, C*H* triazole), 9.04-9.02 (m, 1H, C*H* Ar), 8.38 (dd, 1H, ^3J = 7.8 Hz, ^4J = 1.4 Hz, C*H* Ar), 8.19-8.16 (m, 1H, C*H* Ar), 7.94-7.90 (m, 2H, 2 × C*H* Ar), 7.78-7.66 (m, 4H, 4 × C*H* Ar). ^{13}C NMR (75 MHz, DMSO-*d*^{6}): *δ* (ppm) = 149.67, 148.28, 148.08, 141.62, 135.84, 130.65, 130.26, 125.88, 124.28, 122.07, 121.22. ESI-MS: found: 362.9641 m/z [M – Cl]$^+$ (calc. 362.963118 m/z), found: 405.9891 m/z [M – Cl + MeCN]$^+$ (calc. 405.9892 m/z), found: 422.9167 m/z [M + Na]$^+$ (calc: 422.9206 m/z). Elemental analysis: % Found (% calc.) for $C_{13}H_{10}Cl_2N_4Pd{\cdot}0.75H_2O$: C: 37.60 (37.80); H: 2.27 (2.80); N: 14.10 (13.56).

3.4.3.1.8 Synthesis of N8b

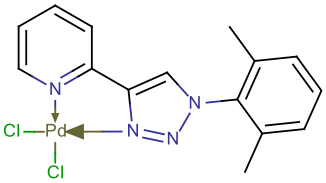

N8b

A pale orange powder was obtained (0.196 g, 77 %). Mp = 327 °C decomposes. FTIR (ATR): 3117 cm^{-1} (C-H triazole). ^{1}H NMR (300 MHz, DMSO-*d*^{6}): *δ* (ppm) = 9.47 (s, 1H, C*H* triazole), 9.04 (d, 1H, ^3J = 6.2 Hz, C*H* Ar), 8.35 (dd, 1H, ^3J = 7.8 Hz, ^4J = 1.3 Hz, C*H* Ar), 8.14 (d, 1H, ^3J = 7.5 Hz, C*H* Ar), 7.78-7.73 (m, 1H, C*H* Ar), 7.55-7.50 (m, 1H, C*H* Ar), 7.38 (d, 2H, ^3J = 7.8 Hz, 2 × C*H* Ar), 2.06 (s, 6H, 2 × CH_3). ^{13}C NMR (75 MHz, DMSO-*d*^{6}): *δ* (ppm) = 149.86, 148.26, 148.15, 141.44, 134.91, 134.55, 131.36, 128.88, 127.70, 125.83, 122.34, 16.89. ESI-MS: found: 434.0217 m/z [M – Cl + MeCN]$^+$ (calc. 434.0205 m/z). Elemental analysis: % Found (% calc.) for $C_{15}H_{14}Cl_2N_4Pd{\cdot}H_2O$: C: 40.32 (40.43); H: 2.84 (3.62); N: 12.01 (12.57).

3.4.3.1.9 Synthesis of N9b

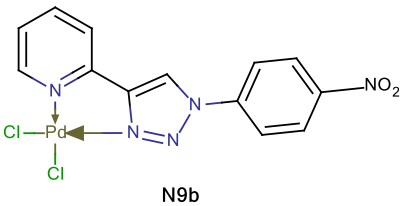

N9b

A pale yellow powder was obtained (0.093 g, 86 %). Mp = 335 °C decomposes. FTIR (ATR): 3135 cm^{-1} (C-H triazole), 1596 (C=N pyridine stretch), 1523 (N=O stretch), 1346 (N=O stretch). ^{1}H NMR (600 MHz, DMSO-*d*^{6}): *δ* (ppm) = 10.09 (s, 1H, C*H* triazole), 8.97 (d, 1H, ^3J = 5.5 Hz, C*H* Ar), 8.58 – 8.55 (m, 2H, 2 × C*H* Ar), 8.38 (td, 1H, ^3J = 7.9 Hz, ^4J = 1.5 Hz, C*H* Ar), 8.21 – 8.18 (m, 3H, 3 × C*H* Ar), 7.75 (td, 1H, ^3J = 7.3 Hz, ^4J = 1.3 Hz, C*H* Ar). ^{13}C NMR (151 MHz, DMSO-*d*^{6}): *δ* (ppm) = 149.62, 148.60, 147.94, 147.72, 141.69, 139.90, 126.06, 125.79, 124.75, 122.28, 121.95. ESI-MS: found: found: 450.9749 m/z [M – Cl + MeCN]$^+$ (calc. 450.9743 m/z). Elemental analysis: % Found (% calc.) for $C_{13}H_9N_5O_2PdCl_2{\cdot}0.25DCM$: C: 34.59 (34.17); H: 1.71 (2.06); N: 14.42 (15.04).

3.4.4 The NMR study of the *trans*-Pd(II) 1-substituted-4-phenyl-1,2,3-triazolyl complexes

All the ^{1}H NMR experiments performed in this study were conducted on a 400 MHz Agilent NMR instrument at 25 °C, unless otherwise indicated.

3.4.4.1 Addition of $(MeCN)_2PdCl_2$ to 4a in DMSO-d^6

4a (0.01 g, 0.042 mmol) was dissolved in DMSO-d^6 (0.65 mL). The ^{1}H NMR spectrum was recorded immediately. The sample was then removed from the spectrometer and added to 0.5 eq. $(MeCN)_2PdCl_2$ (0.0056 mg. 0.021 mmol). The ^{1}H NMR spectrum of the resulting mixture was collected immediately. The process was repeated by adding two more equivalents of the Pd-precursor. With the addition of the third equivalent of the Pd-precursor, the solution showed signs of saturation and required extensive heating to dissolve the Pd-precursor.

3.4.4.2 Addition of $(MeCN)_2PdCl_2$ to 4a in DMSO-d^6 followed by the dilution of the sample

4a (0.014 g, 0.06 mmol) was dissolved in DMSO-d^6 (0.65 mL). The ^{1}H NMR spectrum was recorded immediately. The sample was then removed from the spectrometer and added to 0.5 eq. $(MeCN)_2PdCl_2$ (0.0077 g. 0.03 mmol). The ^{1}H NMR spectrum of the resulting mixture was collected immediately. The process was repeated by adding two more equivalents of the Pd-precursor. With the addition of the third equivalent of Pd-precursor, the solution showed signs of saturation and required extensive heating to dissolve the Pd-precursor. The solution was then diluted by half by adding it to an additional 0.65 mL DMSO-d^6. The NMR sample was prepared again and the ^{1}H NMR spectrum collected immediately. This was repeated twice.

3.4.4.3 Addition of $(MeCN)_2PdCl_2$ to 2a in DMSO-d^6 followed by the dilution of the sample

2a (0.01 g, 0.044 mmol) was dissolved in DMSO-d^6 (0.65 mL). To this was added $CDCl_3$ as an external standard in a sealed glass capillary. The ^{1}H NMR spectrum was recorded immediately. The sample was then removed and added to 0.5 eq. $(MeCN)_2PdCl_2$ (0.0057 g. 0.022 mmol). The ^{1}H NMR spectrum was collected immediately. The process was repeated by adding two more equivalents of Pd-precursor in the presence of the external reference. With the addition of the third equivalent, the solution showed signs of saturation and required extensive heating to dissolve the Pd-precursor. The solution was then diluted by half by adding it to an additional 0.65 mL DMSO-d^6. The NMR sample was prepared again and the ^{1}H NMR spectrum collected immediately. This was repeated twice.

3.4.4.4 Titration of T2a in $CDCl_3$ with DMSO-d^6

The ^{1}H NMR spectrum of the DMSO-d^6 was recorded in order to determine the H_2O/DMSO ratio of the solvent. Through the integration of the resulting H_2O and DMSO-d^6 signals, it was found that the DMSO-d^6 contained 25 % (v/v) H_2O, thus the DMSO equivalents to be added was calculated for a 75 % (v/v) DMSO solution. A NMR sample of **T2a** (0.01 g, 0.024 mmol) in $CDCl_3$ (0.65 mL) was

prepared and the spectrum acquired. To the sample was added one equivalent 75 % DMSO-d^6 (2.25 µL, 0.024 mmol). The sample was inverted 4 times in order to ensure thorough mixing of the DMSO-d^6 the metal-containing solution. The spectrum was acquired immediately. The process was repeated until 6 eq. DMSO-d^6 added. The 12 eq. spectrum was obtained by adding 13.5 µL DMSO-d^6 to the sample and collecting the spectrum immediately after mixing.

3.5 References

1. J. D. Crowley and D. A. McMorran, *Top Heterocycl. Chem.*, 2012, **2012**, 31–84.
2. P. I. P. Elliott, *Organomet. Chem.*, 2014, **39**, 1–25.
3. B. Schulze and U. S. Schubert, *Chem. Soc. Rev.*, 2014, **43**, 2522–2571.
4. B. M. J. M. Suijkerbuijk, B. N. H. Aerts, H. P. Dijkstra, M. Lutz, A. L. Spek, G. van Koten, and R. J. M. Klein Gebbink, *Dalton Trans.*, 2007, **1**, 1273–1276.
5. S. Badèche, J. C. Daran, J. Ruiz, and D. Astruc, *Inorg. Chem.*, 2008, **47**, 4903–4908.
6. J. D. Crowley and E. L. Gavey, *Dalton Trans.*, 2010, **39**, 4035–4037.
7. S. B. Deepthi, R. Trivedi, P. Sujitha, C. G. Kumar, B. Sridhar, and S. K. Bhargava, *J. Chem. Sci.*, 2012, **124**, 1405–1413.
8. G. W. Rayner-Canham and D. Sutton, *Can. J. Chem.*, 1971, **49**, 3994–3996.
9. J. Flapper, P. Wormald, M. Lutz, A. L. Spek, P. W. N. M. Van Leeuwen, C. J. Elsevier, and P. C. J. Kamer, *Eur. J. Inorg. Chem.*, 2008, 4968–4976.
10. F. Antolasic, *Molecular Weight Calculator Version 1.0*, 2005.
11. A. S. Abu-Surrah, H. H. Al-Sa, and M. Y. Abdalla, *Cancer Ther.*, 2008, **6**, 1–10.
12. A. R. Kapdi and I. J. S. Fairlamb, *Chem. Soc. Rev.*, 2014, **43**, 4751–4777.
13. G. R. Fulmer, A. J. M. Miller, N. H. Sherden, H. E. Gottlieb, A. Nudelman, B. M. Stoltz, J. E. Bercaw, and K. I. Goldberg, *Organometallics*, 2010, **29**, 2176–2179.
14. H. C. Clark, G. Ferguson, V. K. Jain, and M. Parvez, *Inorg. Chem.*, 1985, **24**, 1477–1482.
15. W. Kitching, C. J. Moore, and D. Doddrell, *Inorg. Chem.*, 1970, **9**, 541–549.
16. M. Patra, T. Joshi, V. Pierroz, K. Ingram, M. Kaiser, S. Ferrari, B. Spingler, J. Keiser, and G. Gasser, *Chem. - A Eur. J.*, 2013, **19**, 14768–14772.
17. A. Castonguay, C. Doucet, M. Juhas, and D. Maysinger, *J. Med. Chem.*, 2012, **55**, 8799–8806.
18. D. Schweinfurth, R. Pattacini, S. Strobel, and B. Sarkar, *Dalton Trans.*, 2009, 9291–9297.
19. M. Rimoldi, F. Ragaini, E. Gallo, F. Ferretti, P. Macchi, and N. Casati, *Dalton Trans.*, 2012, **41**, 3648–58.

Chapter 4: Biological evaluation of *trans*- and *N,N'*-bidentate Pd(II) complexes

4.1 Introduction

The development of a novel drug-like compound takes approximately 12 – 15 years from conceptualization to clinical application.[1,2] With research costs exceeding $1 billion (approximately R13.5 billion), it becomes clear that the drug development process is not ideal when taking into account that only 10 % of compounds that enter clinical trials reach the market.[2]

The drug discovery process is multi-faceted with various areas that are interlinked. Kerns et al. summed the process up in the form of a flow diagram (Figure 4.1).[3]

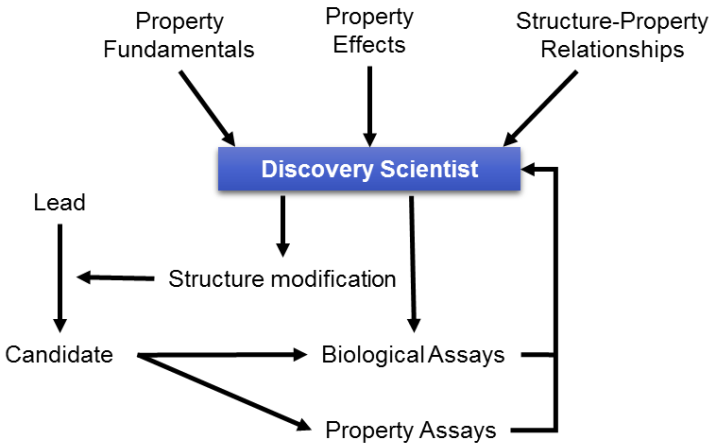

Figure 4.1: The drug discovery process as outlined by Kerns et al.[3]

As is visible from Figure 4.1, property assays play an important role within the early drug discovering process. Property assays involve the evaluation of five physiochemical properties: absorption, distribution, metabolism, excretion and toxicity (ADMETox). Without a good understanding of these properties for each potential drug-like molecule, the chances of that drug progressing beyond the laboratory are limited.[4]

There is some debate within the literature as to whether the ADMETox properties of potential drug-like molecules should be evaluated before the biological screening is performed, or whether it should be the other way around.[5] The current trend is to evaluate certain aspects of the ADMETox properties, specifically properties that would influence absorption, and to perform the biological screening in between the property evaulations.[1]

In general, the majority of Pd(II)-compounds for anti-cancer applications have not progressed into clinical trials due to two reasons, 1) that there is no real structure-activity-relationship established for these compounds and 2) that their mode of action is not yet understood. It is thus necessary to

investigate libraries of compounds in order to determine a structure-activity-relationship and to investigate the mode of anti-cancer activity.[4]

Within the field of bioinorganic chemistry, it has become practice to evaluate the interaction of potential anti-cancer compounds with DNA. Metal complexes can form covalent bonds to DNA, or interact with DNA in a variety of non-covalent manners[6], as discussed in Section 4.2.3.

This chapter summarizes the evaluation of the complexes described in Chapter 3 as anti-cancer agents and the investigations into their solubility and DNA binding modes.

4.2 Results and Discussion

4.2.1 Turbidimetric Assay

Solubility is one of the key elements that influence the absorption properties of a compound, and it is thus prudent that the aqueous solubility of a potential drug-like compound is determined early within the discovery stages. Some would argue that the solubility of a compound should be determined prior to its biological evaluation.[7]

Conventionally, one can define two types of solubility, thermodynamic solubility and kinetic solubility. The measurement of thermodynamic solubility involves the addition of the aqueous phase directly to the solid followed by a long incubation period (24 – 72 hours) in order to establish an equilibrium between the dissolved material and the undissolved material. Thermodynamic solubility is generally determined in late stage drug development rather than early drug discovery due to the fact that it is dependent on the crystalline form of the compound and can thus vary between batches.[3]

In order to determine the kinetic solubility of a compound, the compound is dissolved in DMSO and the resulting solution added to an aqueous buffer solution. Equilibrium is not reached between the undissolved material and the dissolved material and the compound is allowed to precipitate out of solution.[3] Kinetic solubility testing mimics the protocols typically applied when carrying out biological assays in which a stock solution in DMSO is prepared and then added to the aqueous buffered solution, thus making it more suitable for early drug discovery. After incubation (2 – 4 hours), the turbidity of the sample is assessed with UV-Vis spectroscopy by recording the extent of light scattering at 620[a] nm.[3]

The kinetic solubility of the *trans*-Pd(II) phenyl-1,2,3-triazolyl complexes and *N,N'*-bidentate Pd(II) pyridyl-1,2,3-triazolyl complexes were determined with a turbidimetric assay, the details of which is outline in Section 4.4.2. The results are summarized in Table 4.2. As discussed in Chapter 3, the

[a] The extent of light scattering caused by particulates in solution can be assessed with wavelengths ranging from 600 – 820 nm,[49] depending on the absorbance of the particles themselves. It is protocol to assess the turbidity of drug-like molecules in solution at 620 nm, as few drug-like molecules absorb in this region.[3,49,50]

trans-Pd(II) phenyl-1,2,3-triazolyl complexes undergo ligand dissociation/exchange in DMSO, thus in reality what we were determining was the kinetic solubility of the various species in solution.

The degree of the solubility of the compounds is classified according to the criteria outlined in Table 4.1.

Table 4.1: The classification of compounds according to their solubility.

< 10 µg/mL	Sparingly soluble
10 – 60 µg/mL	Partially soluble
> 60 µg/mL	Soluble

Table 4.2: A summary of the kinetic solubility obtained for the *trans*-Pd(II) and *N,N'*-bidentate Pd(II) complexes.

Compound	Functionality	µM (2 % DMSO/PBS)[a]		µg/mL (2 % DMSO/PBS)[a]	
		25 °C	37 °C	25 °C	37 °C
T1a	Octyl	10 - 20	10 - 20	6.92 - 13.84	6.92 - 13.84
T2a	Cyclohexyl	5 - 10	5 - 10	3.16 - 6.32	3.16 - 6.32
T3a	Ethanol	> 200	> 200	> 111.15	> 111.15
T4a	2-(2-ethoxy)ethanol	> 200	> 200	> 128.77	> 128.77
T5a	2-(2-(2-ethoxy) ethoxy)ethanol	> 200	> 200	> 146.39	> 146.39
T6a	Hexanol	80 - 120	80 - 120	53.44 - 80.16	53.44 - 80.16
T7a	Phenyl	20 - 40	5 - 10	0 - 3.10	3.10 - 6.20
T8a	2,6-dimethyl phenyl	20 - 40	60 - 80	13.52 - 27.04	40.56 - 54.08
T9a	Nitrophenyl	0 - 5	0 - 5	0 - 3.55	0 - 3.55
N1b	Octyl	5 - 10	5 - 10	2.18 - 4.36	2.18 - 4.36
N2b	Cyclohexyl	20 - 40	40 - 80	8.11 - 16.23	16.23 - 32.45
N3b	Ethanol	40 - 80	> 200	14.70 - 29.40	> 73.51
N4b	2-(2-ethoxy)ethanol	160 - 200	> 200	65.85 - 82.31	> 82.32
N5b	2-(2-(2-ethoxy)ethoxy)ethanol	>200	> 200	> 91.13	> 91.13
N6b	Hexanol	160 - 200	> 200	67.78 - 84.73	> 84.73
N7b	Phenyl	40 - 60	40 - 80	15.98 - 23.97	15.98 - 31.97
N8b	2,6-dimethyl phenyl	10 - 20	40 - 80	4.28 - 8.55	17.11 - 34.21
N9b	Nitrophenyl	10 - 20	20 - 40	4.45 – 8.89	8.89 - 17.78
	$(MeCN)_2PdCl_2$	> 200	> 200	> 51.89	> 51.89
	Hydrocortisone	>200	>200	> 72.49	> 72.49
	Reserpine	20 - 40	10 - 20	12.17 - 24.35	6.09-12.17

[a] Percentage expressed as v/v.

The results obtained for the controls, Hydrocortisone and Reserpine, agree with literature values[8] and thus the assay is validated.

From the solubility results obtained it is clear that the complexes with the ethanol moieties (**3**, **4**, **5** and **6**) are more soluble than their aliphatic and aromatic counterparts (**1**, **2**, **7**, **8** and **9**) as was

expected. It was also interesting to note that the **T2a** is less soluble than **N2b** although both have cyclohexyl moieties, and the reverse is observed for **T1a** versus **N1b** with the octyl moieties. For both the *trans*-Pd(II) phenyl-1,2,3-triazolyl and *N,N'*-bidentate Pd(II) pyridyl-1,2,3-triazolyl complexes it is also observed that an increase in temperature results in an increase in solubility, as expected.

In general, all complexes are soluble at the MTT Assay test concentrations (0 – 20 µM) apart from those indicated in red in Table 4.2.

Treatment of cells with the complexes of poor solubility were thus done with suspensions, just to assess whether they have some anti-cancer activity as nanosuspensions. The use of nanosuspensions as a drug delivery method has become an active area of research recently, as this allows for the utilization of previous disregarded drug candidates. The IC_{50} values of nanosuspensions are not reported as molar concentrations, due to the nature of the suspensions, but rather as mass/volume concentrations.[9]

4.2.2 *In Vitro* cytotoxic evaluation

The cytotoxicity of the *trans*-Pd(II) and *N,N'*-bidentate Pd(II) complexes was evaluated against advanced human breast cancer, MCF-7, and metastatic human breast cancer, MDA-MB-231, using a standard MTT Assay. The concentration range tested was 0 – 20 µM and the treatment time was kept constant at 48 hours. The results are summarized in Table 4.3.

Among the *trans*-Pd(II) phenyl-1,2,3-triazolyl complexes, only **T8a** showed some anti-cancer activity at the concentration tested. It should be noted that since the *trans*-Pd(II) phenyl-1,2,3-triazolyl complexes dissociate in DMSO, it is suspected that what was being tested is a mixture of ligand, complex and various, thus far unidentified, Pd-species present in solution.

The inactivity of the *trans*-Pd(II) phenyl-1,2,3-triazolyl complexes could possibly be explained by the dissociation of the complex in solution. As mentioned in Chapter 1, the main hypothesis for the inactivity for most Pd-compounds is their faster hydrolysis rates (10^5 times faster than for Pt).[10] This can be overcome with strongly binding ligands. Since the *trans*-Pd(II) complexes described in this thesis appears to readily dissociate in DMSO, even before cell treatment takes place, the percentage of the original complex that might ultimately reach the cellular target is so small that, even if it is cytotoxic, the concentration is below detectable limits.

Interestingly, the *N,N'*-bidentate Pd(II) pyridyl-1,2,3-triazolyl complexes were also inactive. This is slightly surprizing since analogous pyridine triazole complexes reported by Trivedi and colleagues.[11] showed reasonable activity. These complexes however have carbohydrate moieties incorporated into their ligand scaffolds and these play a role in cellular uptake.

Table 4.3: A summary of the MTT Assay results obtained for the *trans*-Pd(II) and *N,N'*-bidentate Pd(II) complexes.

Functionality	Pd(II) complexes	IC_{50} (μM)[a]	
		MCF7	MDA-MB-231
Octyl	**T1a**	Inactive[b]	Inactive
Cyclohexyl	**T2a**	Inactive	Inactive
Ethanol	**T3a**	Inactive	Inactive
2-ethoxy ethanol	**T4a**	Inactive	Inactive
2-ethoxy-ethoxy-ethanol	**T5a**	Inactive	Inactive
Hexanol	**T6a**	Inactive	Inactive
Phenyl	**T7a**	Inactive	Inactive
2,6-dimethyl phenyl	**T8a**	40.7 ± 1.1	Inactive
4-nitrophenyl	**T9a**	Inactive	Inactive
Octyl	**N1b**	Inactive	Inactive
Cyclohexyl	**N2b**	Inactive	Inactive
Ethanol	**N3b**	Inactive	Inactive
2-ethoxy ethanol	**N4b**	Inactive	Inactive
2-ethoxy-ethoxy-ethanol	**N5b**	Inactive	Inactive
Hexanol	**N6b**	Inactive	Inactive
Phenyl	**N7b**	Inactive	Inactive
2,6-dimethyl phenyl	**N8b**	Inactive	Inactive
4-nitrophenyl	**N9b**	Inactive	Inactive
Cisplatin		19.6 ± 4.3[c]	43.5 ± 3.0[d]

[a] IC_{50}: Concentration at which 50 % cell growth is inhibited

[b] No growth inhibition observed at the maximum concentration tested (20 μM)

[c] From Trávníček et al.[12]

[d] From Canada et al.[13]

It was then decided to evaluate the cytotoxicity of the ligands in order to see whether the free ligand itself has any anti-cancer activity. The results of the MTT Assays conducted with the ligands are summarized in Table 4.4. Since the complexes did not show any activity against MDA-MB-231, it was decided that the cytotoxicity of the ligands would only be evaluated against MCF-7, and should they show activity against the less aggressive MCF-7 cell line, only then would they be evaluated against MDA-MB-231.

Owing to time-constraints, **9a** and **8b** were not evaluated for their cytotoxicity, but it was interesting to note that among the phenyl-1,2,3-triazole ligands there were some active compounds, while the pyridine analogues were completely inactive. This could possibly indicate that the phenyl ring in that position plays a role in the mode of cytotoxicity that cannot be replicated by the pyridine moiety.

Table 4.4: A summary of the MTT Assay results obtained for the substituted phenyl- and pyridyl-1,2,3-triazole ligands.

Functionality	Ligands	IC_{50} (μM)[a]	
		MCF7	MDA-MB-231
Octyl	**1a**	80.0 ± 1.2	Inactive[b]
Cyclohexyl	**2a**	33.3 ± 1.3	Inactive
Ethanol	**3a**	24.5 ± 1.1	Inactive
2-(2-ethoxy) ethanol	**4a**	65.2 ± 2.5	Inactive
2-(2-(2-ethoxy) ethoxy) ethanol	**5a**	Inactive	-[c]
Hexanol	**6a**	Inactive	-
Phenyl	**7a**	13.0 ± 1.2	Cytotoxic[f]
2,6-dimethyl phenyl	**8a**	Inactive	-
4-nitrophenyl	**9a**	-	-
Octyl	**1b**	Inactive	-
Cyclohexyl	**2b**	Inactive	-
Ethanol	**3b**	Inactive	-
2-(2-ethoxy) ethanol	**4b**	Inactive	-
2-(2-(2-ethoxy) ethoxy) ethanol	**5b**	Inactive	-
Hexanol	**6b**	Inactive	-
Phenyl	**7b**	Inactive	-
2,6-dimethyl phenyl	**8b**	-	-
4-nitrophenyl	**9b**	Inactive	-
Cisplatin		19.6±4.3[d]	43.5 ± 3.0[e]

[a] IC_{50}: Concentration at which 50 % cell growth is inhibited

[b] No growth inhibition observed at the maximum concentration tested (20 μM)

[c] Not tested

[d] From Trávníček et al.[12]

[e] From Canada et al.[13]

[f] Cytotoxicity observed is not concentration dependent.

When the compounds are arranged in order of decreasing cytotoxicity (Figure 4.2), it becomes more apparent that there is a structure-activity-relationship.

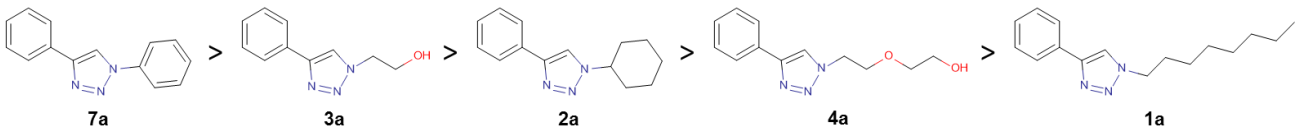

$$Phenyl\ (7\boldsymbol{a}) > Ethanol\ (3\boldsymbol{a}) > Cyclohexyl\ (2\boldsymbol{a}) > 2-(2-ethoxy)ethanol\ (4\boldsymbol{a}) > Octyl\ (1\boldsymbol{a})$$

Figure 4.2: The structures of the active ligands arranged in order of decreasing cytotoxicity.

Since ligand **7a** has the more planar structure due to the presence of a phenyl ring on each side of the 1,2,3-triazole ring, it was expected that the compound could perhaps intercalate with the DNA, thus preventing cell replication from taking place. Compounds **1a** – **4a** have only one aromatic ring compared to **7a**. This is expected to reduce the possibility of these species from being DNA

intercalators. It would appear that the flexibility of the N-bound substituent is playing a role in the cytotoxicity. **7a**, whilst having the least flexible N-bound substituent, is the more active, and **1a**, with the most flexible N-bound substituent, is the least active. **3a**, **2a** and **4a** have similarly flexible N-bound substituents and display higher IC_{50} values. The exact reason for the difference of activity is not clear and thus would require further investigation. From the results it is also clear that those complexes with highly flexible substituents are less active, showing higher IC_{50} values.

It was also interesting to note that the ligand **8a** does not show any cytotoxicity while its *trans*-Pd(II) complex **T8a** does show some activity. Since **T8a** dissociates in solution and the ligand itself is not active, it can be concluded that the activity could potentially be attributed to the small amount of intact complex present in solution or by any one of the other Pd-species present.

It was however concerning to see that **7a** has concentration independent cytotoxicity for the MDA-MB-231 cell line. This could potentially indicate that the compound is not genotoxic enough in order to bring about cell death, but rather only supresses cell growth. This however requires further investigations.

It was then decided to investigate the type of interaction the active compounds have with DNA by means of horizontal agarose gel electrophoresis and UV-Vis DNA titration studies.

4.2.3 DNA binding studies

The anti-cancer activity of most chemotherapeutic compounds can often be attributed to the direct interaction of the compound with DNA. This interaction usually results in the prevention of mitosis and ultimately leads to cell death.[6,14] Cisplatin's activity can be attributed to the fact that it cross-links DNA strands by preferentially binding to the guanine and cytosine base pairs.[15–17]

Compounds can interact with DNA covalently or non-covalently. Among the non-covalent interactions there are three distinct ways in which compounds can interact with the DNA (Figure 4.3):

1. Intercalation during which the compound enters the DNA helix and, through π-stacking interactions, positions itself between the base pairs.
2. Groove binding during which the compound aligns itself in either the major or minor groove of the DNA helix through weak electrostatic interactions caused by hydrogen bonding.
3. Electrostatic interaction whereby a positively charged compound interacts with the negatively charged phosphate backbone of the DNA.[6]

In general, non-covalent interactions are preferred clinically since covalent interactions are irreversible, leading to an increase in toxicity due to non-selectivity and the appearance of secondary growths.[18]

Drug-DNA interactions can be investigated with a variety of analytical techniques, including agarose gel electrophoresis, UV-Vis spectroscopy, circular dichroism, fluorescence

spectroscopy, enzymatic assays and viscometry.[6,14] These techniques are all sensitive to buffer composition, pH and temperature, and thus it is advised that direct comparisons are made.[14]

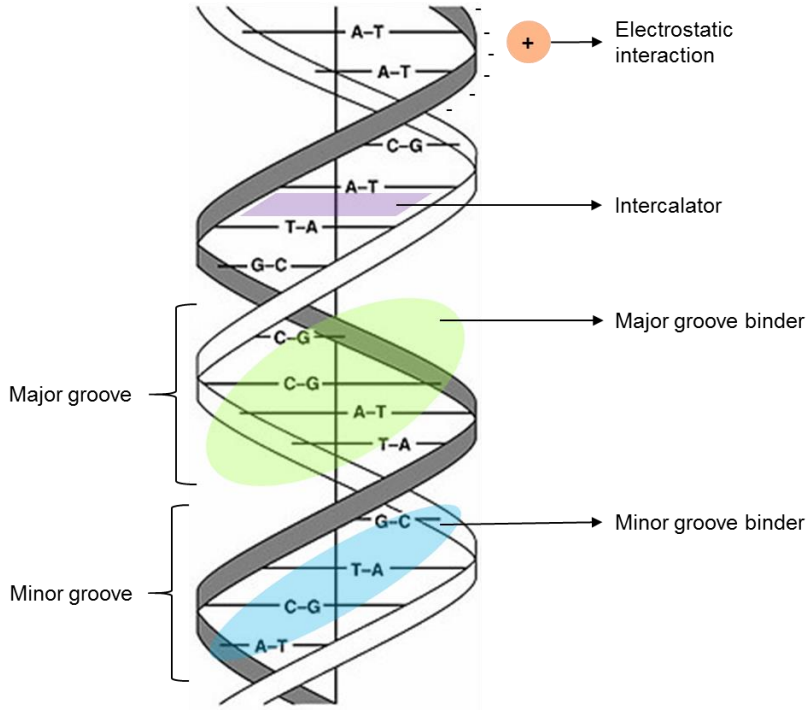

Figure 4.3: The various modes of non-covalent DNA-drug interactions.[b]

No single method can be used to unambiguously determine the DNA binding mode of the test compound and thus, for the purposes of this thesis, horizontal agarose gel electrophoresis and UV-Vis spectroscopy were used to investigate the DNA binding modes of the compounds that displayed cytotoxicity in the MTT Assays.

4.2.3.1 DNA migration study: Horizontal agarose gel electrophoresis

The use of gel electrophoresis in the determination of DNA-drug interactions has gained increasing popularity in recent years.[19–23]

Bacterial plasmids separate into two distinct bands in an electrical field. The first is the open circular (OC) band which has the lower electrophoretic mobility (thus appears near the top of the gel) and the second is the supercoiled closed circular (CCC) band, which has the higher electrophoretic mobility of the two bands (appears below the OC band). In some cases, a third band is observed between the OC and CCC bands, which is attributed to the linear plasmid DNA (L). Changes in the electrophoretic mobilities of the plasmid bands in the presence of the test compounds indicate

[b] DNA structure template obtained from http://www.scienceclarified.com/scitech/Genetics/Genes-and-DNA.html

interaction of the compounds with the DNA. DNA damage can also be assessed by a decrease/increase in a band's intensity or in the extent of streaking of the bands through the gel.[24,6]

This is a simple, robust method used to investigate preliminary DNA interactions, but the interpretation could be ambiguous in cases where more than one type of binding mode is observed.[6] However, by comparing the changes observed to those of known control compounds in the same system, an approximate idea of the DNA interaction mode can be obtained.

A recent example of the use of horizontal gel electrophoresis in the characterization of DNA-drug interactions was published by Albert el al.[24]

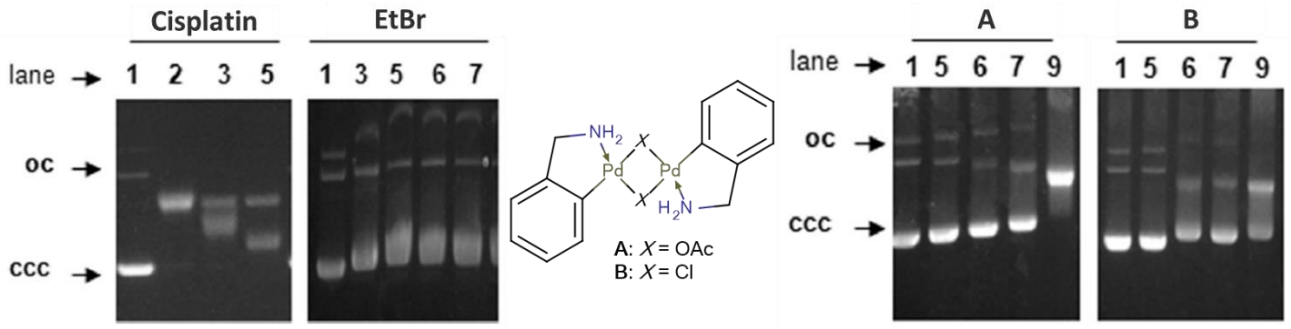

Figure 4.4: The horizontal gel electrophoresis of the palladacycles investigated by Albert et al.[24] with pBluescript DNA using cisplatin and ethidium bromide (EB) as control compounds. Lane 1 of each gel shown does not contain test compound. Lanes 2 – 9 show increases in the concentration of the compound while the DNA loading remains constant.[24]

From Figure 4.4 it is observed that neither palladacycle **A** nor **B** have the same effect as that of cisplatin on DNA. It is thus possible to concluded that the palladacycles are not cross-linking the DNA. Ethidium bromide, as a known intercalator, shows a slight decrease in the electrophoretic mobility of both the OC and the CCC band. The same trend is observed for **A** and, to a lesser extent, **B**, along with a general increase in streaking with an increase in concentration. It can thus be concluded from these gels that **A** and **B** could possibly be intercalators but that they are also contributing to indiscriminate DNA damage, as observed from the increase in band streaking.[24]

A similar study was thus performed with the compounds prepared in the current work that displayed some cytotoxicity, namely **1a** – **4a**, **7a** and **T8a**. The agarose gels were stained with ethidium bromide for visualization purposes after electrophoresis had taken place, in order to prevent competitive binding. Figure 4.5 shows the image obtained of the pBluescript migration study in the presence of ethidium bromide (EtBr), **7a**, **2a**, **4a** and **3a**.

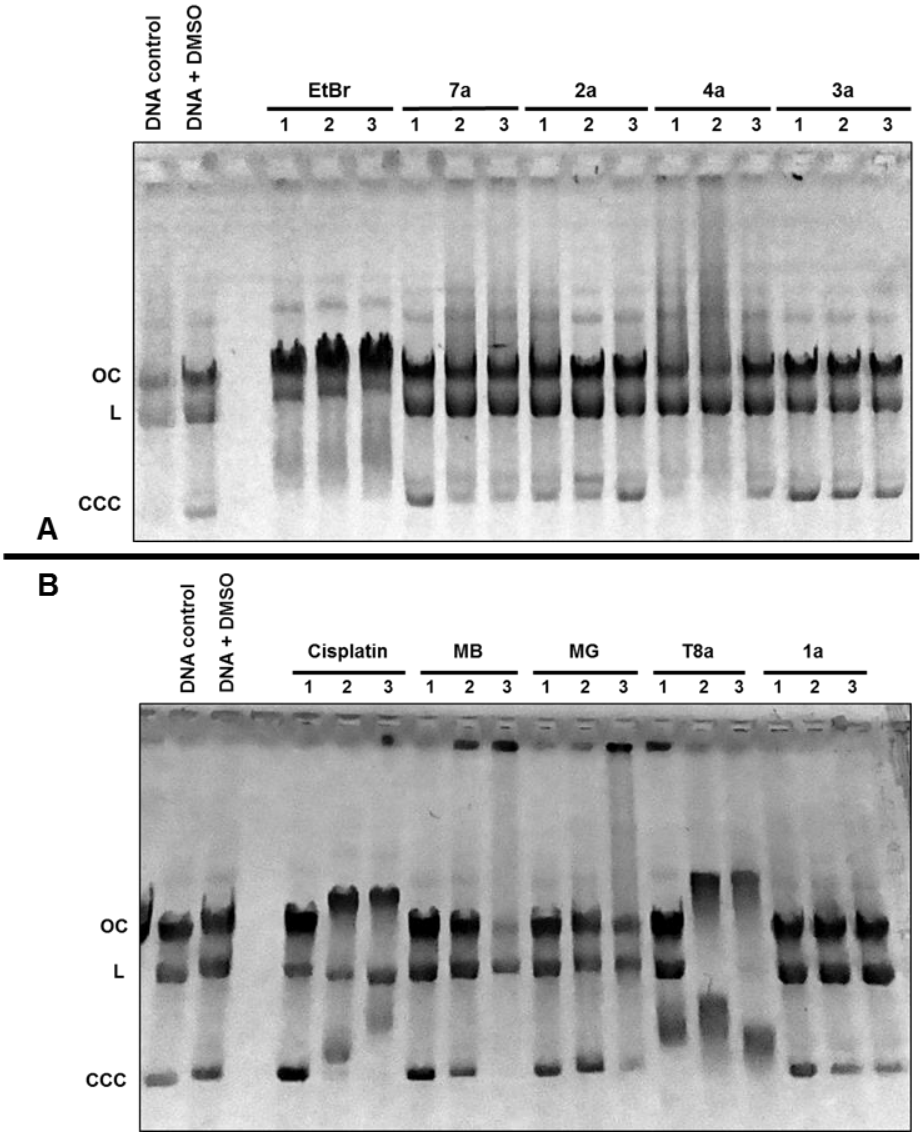

Figure 4.5: The photos obtained from the horizontal agarose gel electrophoresis of pBluescript (40 ug/mL), with (A) showing different concentrations of EtBr and compounds *7a*, *2a*, *4a* and *3a* as indicated and (B) with cisplatin, methylene blue, methyl green and compounds *T8a* and *1a*. Each compound was investigated at three different concentrations, 10 μM (Lane 1), 100 μM (Lane 2) and 200 μM (Lane 3) as shown.

From Figure 4.5A and Figure 4.5B, it can be seen that the DMSO has a limited influence on the DNA itself, causing a slight retardation in all three DNA bands. Since all the compound were prepared in DMSO-containing stock solutions, the resulting DNA interactions were analysed in reference to the DNA + DMSO band. Ethidium bromide was used as a classical intercalator control compound[25], and causes retardation of all three plasmid bands. A decrease in the intensity of the CCC and L bands in the favour of the OC band is observed with an increase in concentration. A decrease in the intensity of the CCC band is due to DNA unwinding into the larger OC form, indicating that intercalation has taken place.

None of the ligands investigated in Figure 4.5A altered the DNA migration as drastically as ethidium bromide, possibly indicating that the ligands have a lower affinity towards DNA than ethidium

bromide. All the ligands cause a slight retardation in all three plasmid DNA bands and exhibit higher concentrations of L DNA than present in the control, indicating that the ligands could possibly cause double stranded DNA breaks.[6]

7a and **4a** display concentration dependent reduction in the amount of the CCC form and an increase in band smearing, indicating a fair amount of DNA degradation at higher concentrations. At higher concentrations, **4a** has more of the CCC form than **7a**, which could indicate the CCC band uncoils to the OC form at lower concentrations and recoils at higher concentrations. The uncoiling and recoiling of CCC DNA is usually attributed to the transition between negative supercoiled DNA (CCC-) and positive supercoiled DNA (CCC+).[24,26] Due to the excessive smearing observed for **4a**, it is not possible to definitively attribute the increase in the CCC form to the transition between CCC- and CCC+ forms. This could further be investigated by performing an unwinding experiment, in which the compound is incubated in the presence of CCC- alone and the formation of the OC band is monitored.

Ligands **2a** and **3a** do not entirely eradicate the CCC band, but a lower intensity of the CCC band with an increase in the OC band intensity indicates that the supercoiled DNA unwinds to the more relaxed OC form. The same trend is observed for ligand **1a** in Figure 4.5B.

In Figure 4.5B, cisplatin and methyl green (MG) were included as controls for intra-strand crosslinking[27] and major groove binding,[28] respectively. The DNA binding mechanism for methylene blue (MB) is under some debate, with some studies indicating semi-intercalative binding[29] while others conclude that minor groove binding is observed.[30] The current consensus is that methylene blue displays multimode binding, including intercalation and minor groove binding depending on the nucleotide sequence.[31]

Cisplatin causes concentration dependent retardation of both the OC and CCC bands, along with slight increase in the electrophoretic mobility of the L band. With an increase in concentration, the CCC band becomes less intense in favour of precipitation in the wells, indicating the formation of high molecular weight aggregates forming due to intra-strand crosslinking.[32]

MB also shows high molecular weight aggregates in the wells, possibly indicating the that DNA has been saturated with compound. A concentration dependent increase in electrophoretic mobility is observed for the OC band while the opposite is observed for the L band. At the highest concentration, 200 μM, the CCC band has completely disappeared in favour of precipitation in the wells.

The trends observed for MG are similar to that of MB but less intense. Smearing of the DNA is observed at higher concentrations indicating severe DNA damage.

T8a behaves similarly to cisplatin, causing concentration dependent retardation of the OC and the CCC bands, while the electrophoretic mobility of the L band increases. Coalescence of the L and CCC bands are observed with a reversal of retardation observed for the coalesced band at 200 μM.

Similar behaviour has been discussed in literature and is attributed to counter-twisting of the negatively supercoiled DNA to the positively supercoiled DNA.[33]

From the DNA migration studies it can thus be concluded that ligands **1a** - **4a** and **7a** show similar behaviour to that observed for EtBr, but to a lesser extent, thus possibly indicating that the ligands are weak intercalators or have weak electronic interactions with the DNA. **T8a** shows behaviour similar to that of cisplatin, thus indicating a cross-linking mode of action. It should be noted that **T8a** dissociates in solution and that it is a mixture of species responsible for the DNA interaction observed, and not the discrete complex alone, as discussed in Chapter 3.

4.2.3.2 UV-Vis DNA binding study: Electronic absorption titration

Electronic absorption spectroscopy is the most common method utilized for the investigation of drug-DNA interactions. Practically, there are a number of methods that can be used to investigate the DNA-drug interactions. The DNA concentration can be kept constant and increasing amounts of compound can be added, thus the effect on the DNA spectrum is monitored.[34] Alternatively, the compound concentration can be kept constant and increasing amounts of DNA can be added, thus monitoring the effect on the compound spectrum.[20,23,35] These methods are known as electronic absorption titration experiments.

Changes observed in the absorbance spectrum corresponds to certain types of drug-DNA interactions. Intercalation results in hypochromism in the absorbance spectrum, due to the coupling of the π^*-orbitals of the ligand and the π-orbitals of the base pairs, resulting in a decreased $\pi - \pi^*$ transition energy.[36] Intercalation can also result in bathochromism in some cases, which is attributed to a decrease in the energy gap between the HOMO and LUMO molecular orbitals after binding of the compound to the DNA.[37]

Electrostatic and groove binding interactions both result in hyperchromism. This is considered to be due to the change that these interactions cause in the DNA structure. The partial unwinding of the DNA or distortion of the helix, results in the destabilization of the stacking interaction of the base pairs, resulting in an increase of absorbance.[37,38]

The method used in this study is based on that published by Yang et al.[39] in which aliquots of DNA are added to both the reference cell (containing the buffer solution) and the sample cell (containing a fixed concentration of compound). This results in the observation of changes in the compound spectrum alone, from which the binding constant can be calculated.

The intrinsic binding constants, K_b, were calculated, where possible, by the model developed by Wolfe et al.[40]

The Wolfe-model originates from the Benesi-Hildebrand method[41], which was developed to describe host-guest interactions. This model assumes that the UV-Vis absorbance of the compound tested and its resulting, or apparent spectrum, upon DNA addition, obeys the Beer-Lambert Law. It also

assumes that if reagent A (compound) is in great excess to reagent B (DNA), the absorption spectrum of reagent B will be negligible.[41] Thus, by measuring the absorption spectra of the reaction before and after the formation of the product, the association constant of the reaction can be determined. The method unfortunately results in systematic deviations depending on the chosen concentration scale.[42] The Benesi-Hildebrand equation is shown in Equation 4.1.

$$\frac{1}{\Delta A} = \frac{1}{l\Delta\varepsilon C_T[DNA]K_b} + \frac{1}{l\Delta\varepsilon[DNA]}$$

Where $[DNA]$ denotes the DNA concentration in base pairs and K_b represents the binding coefficient to be calculated. ΔA is the difference between the absorbance of two titrations, C_T is the compound concentration, $\Delta\varepsilon$ the difference in the extinction coefficient between two titrations and l represents the path length of the sample.

Schmechel and Crothers[43] modified the Benisi-Hildebrand method in order to address the concentration scale problem. This was done by rearranging Equation 4.1 to use the extinction coefficients rather than the absorbance units. From each titration compound absorbance obtained, from which the extinction coefficient can be calculated. The difference between the extinction coefficient of the free compound and that of the spectrum obtained from the interaction of the compound with DNA, serves as an indication of the degree of drug-DNA interaction. The binding constant can be determined from a double-reciprocal plot[c] of the apparent extinction coefficient of the compound versus the DNA concentration, as shown in Equation 4.2.[40]

$$\frac{1}{|\varepsilon_a - \varepsilon_f|} = \frac{1}{|\varepsilon_b - \varepsilon_f|} + \frac{1}{K_b|\varepsilon_b - \varepsilon_f|[DNA]} \tag{4.2}$$

Where ε_a denotes the apparent extinction coefficient, ε_f the free compound extinction coefficient and ε_b the fully bound extinction coefficient. However, the double reciprocal plot is biased towards data points obtained at low DNA concentrations.[42]

In order to correct for this, Wolfe et al.[40] rearranged the double reciprocal plot to a half-reciprocal[d] form. This was done by multiplying Equation 4.2 with the concentration of DNA,[40] as shown by Equation 4.3. In this form, the binding constant can be easily calculated from the *y*-intercept equal to $1/|\varepsilon_b - \varepsilon_f|K_b$.

$$\frac{[DNA]}{|\varepsilon_a - \varepsilon_f|} = \frac{[DNA]}{|\varepsilon_b - \varepsilon_f|} + \frac{1}{K_b|\varepsilon_b - \varepsilon_f|} \tag{4.3}$$

[c] A double reciprocal plot refers to any plot in which the reciprocal of the dependent variable (in this case the change in extinction coefficients) is plotted against the reciprocal of the independent variable (the concentration of DNA). This method is generally employed in enzyme kinetics.[42]

[d] A half-reciprocal plot is obtained from a double reciprocal plot when the independent variable is multiplied throughout and is no longer a reciprocal.

This model is however not suited for compounds with more than one binding mode, in which case a linear relationship is not obtained and the binding constant cannot be calculated. The Wolfe-model is the prevalent method used to interpret electronic absorption titrations.[44,19,45]

It should also be noted that if the compound displays multi-mode binding, the fit of the model to the experimental data will not be good. The Wolfe-model was designed to evaluate any interaction between a host (DNA) and a guest (compound), but not classify the type of interaction. The type of interaction is determined by comparing the binding constant calculated to that of a known binder, such of ethidium bromide ($K_b = 1.3 \times 10^6$ M^{-1}).[29]

As an example, the study by Icsel et al.[22] (Figure 4.6) followed the same assay and kinetic analysis and concluded that the binding constant is lower than that of the classical intercalators such as ethidium bromide, indicating the complex is probably not an intercalator. When combined with the information obtained from the other drug-DNA investigations, they concluded that the complex probably forms covalent bonds to the DNA, similar to that observed for cisplatin.[22]

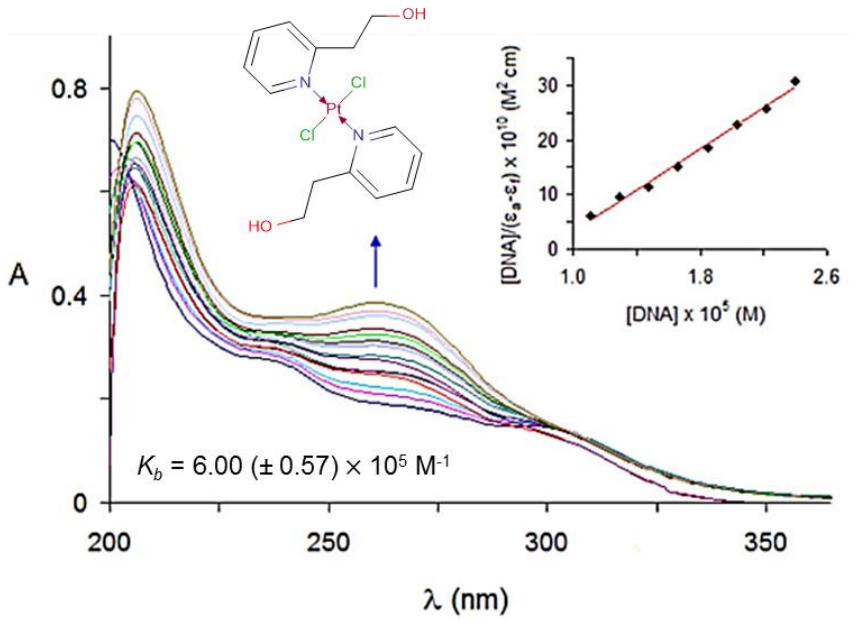

Figure 4.6: The UV-Vis spectra obtained by Icsel et al.[22] for the absorption titration performed with *trans*-[$PtCl_2$(2-hepy)$_2$] with increasing amounts of FS-DNA (fish sperm DNA). The arrow indicates the general change in absorption upon DNA addition and the inset shows the $[DNA]/|\varepsilon_a - \varepsilon_f|$ vs $[DNA]$ plot, from which the K_b value was obtained, as indicated.

The electronic absorption titrations were conducted at 25 °C rather than 37 °C. This is due to the fact that accelerated DNA denaturation was observed at 37 °C in the absence of the compounds investigated. The data was also corrected for the small dilution effect that is inherent in this assay, as is described in Section 4.4.4.2.

The titration spectra of ligand **2a** are shown in Figure 4.7, with the inset depicting the kinetic analysis of the Wolfe-model. Hypochromism is observed, as opposed to the hyperchromism which is observed for the example in Figure 4.6. The UV-Vis spectrum of the ligand alone shows two local absorption maxima at 307 nm and 327.5 nm respectively, as well as a shoulder around 247 nm. With an increase in the DNA concentration, a hypochromic shift is observed throughout the spectrum. The kinetic analysis was done with the absorbance at 327.5 nm. The binding constant determined (K_b = 0.06 × 10^6 M^{-1}) is smaller than that of ethidium bromide (K_b = 1.3 × 10^6 M^{-1})[29], indicating that the compound has a lower affinity for DNA than ethidium bromide and can be described as a weak intercalator. Similarly, ligand **3a** showed hypochromism with an increase in the DNA concentration. Thus indicating an intercalative interaction, as shown in

Figure 4.8. As evidenced by the kinetic plot inserted, the Wolfe-model does not fit this compound, as there are systematic errors in the data. This might suggest that multi-mode binding is taking place.

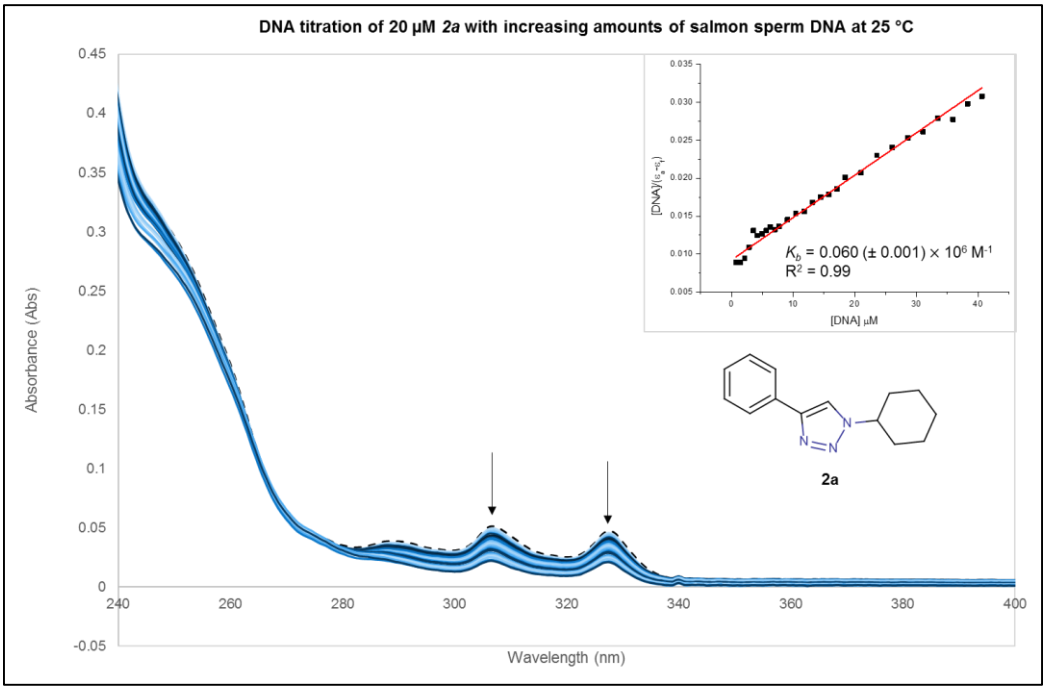

Figure 4.7: The spectra obtained for the titration of 20 µM *2a* with increasing amounts of 0.47 mM salmon sperm DNA. The arrows indicate the general change in absorption upon the addition of DNA. The inset shows the $[DNA]/|\varepsilon_a - \varepsilon_f|$ vs $[DNA]$ plot, from which the K_b value was obtained, as indicated. The dotted line represents the spectrum of *2a* in the absence for DNA.

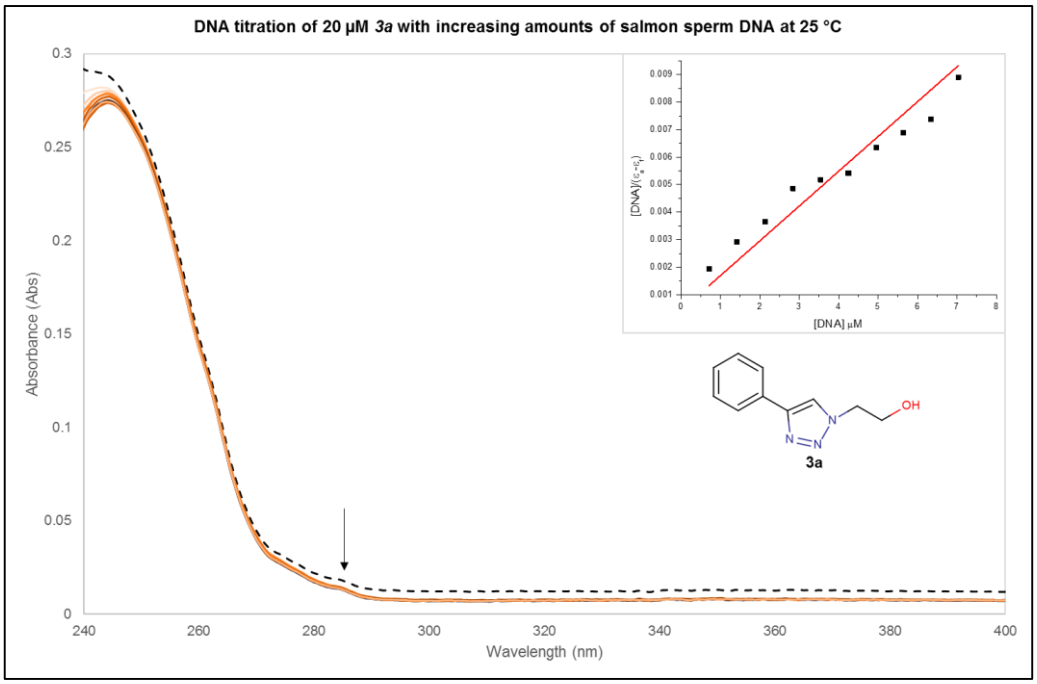

Figure 4.8: The spectra obtained for the titration of 20 µM 3a with increasing amounts of 0.47 mM salmon sperm DNA. The arrow indicates the general change in die absorption upon DNA addition. The inset shows the $[DNA]/|\varepsilon_a - \varepsilon_f|$ vs $[DNA]$ plot. The dotted line shows the spectrum of 3a in the absence for DNA.

It was interesting to note that **4a**, while being less cytotoxic than both **2a** and **3a**, shows a higher affinity for DNA than **2a**, displaying a binding constant of $K_b = 4.35 \times 10^6$ M^{-1} (Figure 4.9). It should however be noted that there are slight systematic deviations in the kinetic plot for 4a, but the model fit is still acceptable. The K_b value is thus just an approximate indication of DNA affinity.

The DNA titration of **1a** resulted in the most drastic hypochromism observed for all the compounds investigated, as shown in Figure 4.10. This agrees with the higher binding constant ($K_b = 6.39 \times 10^6$ M^{-1}) obtained for the ligand, despite the fact that the compound shower the weakest cytotoxicity among the ligands. There is also an isobestic point observed at 270 nm. This usually indicates that there are two different species in solution that are at equilibrium with one another.[46] These species could be due to more than one binding site that is being occupied or a combination of bound and free species in solution, but more information is required.

From the ligands discussed thus far it can be concluded that they display intercalative properties, as indicated by the binding constants obtained for some of the ligands, the hypochromism observed in the DNA titration studies and the results of the DNA migration studies. The other two compounds investigated, **7a** and **T8a**, yielded unexpected results.

The titration spectrum for **T8a** is shown in Figure 4.11. It was interesting to note that despite the significant effect the complex had on the plasmid DNA in the DNA migration study (Figure 4.5B), it displayed no significant hypochromism upon the addition of DNA.

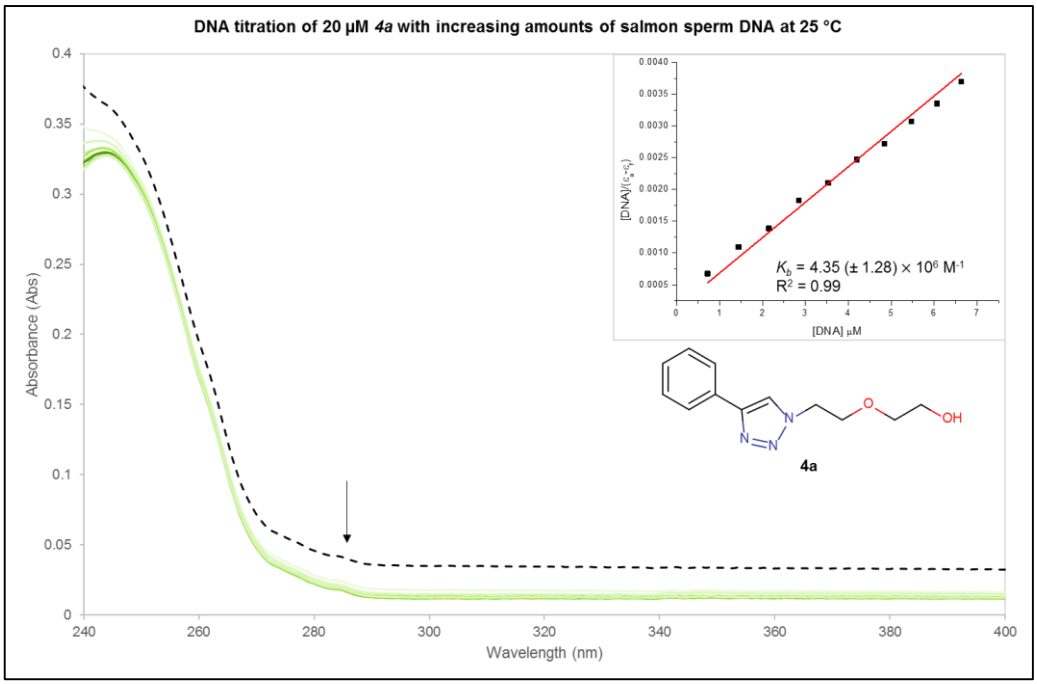

Figure 4.9: The spectra obtained for the titration of 20 µM *4a* with increasing amounts of 0.47 mM salmon sperm DNA. The arrow indicates the general change in die absorption upon DNA addition. The insets show the $[DNA]/|\varepsilon_a - \varepsilon_f|$ vs $[DNA]$ plot, from which the K_b value was obtained, as indicated. The dotted line shows the spectrum of *4a* in the absence for DNA.

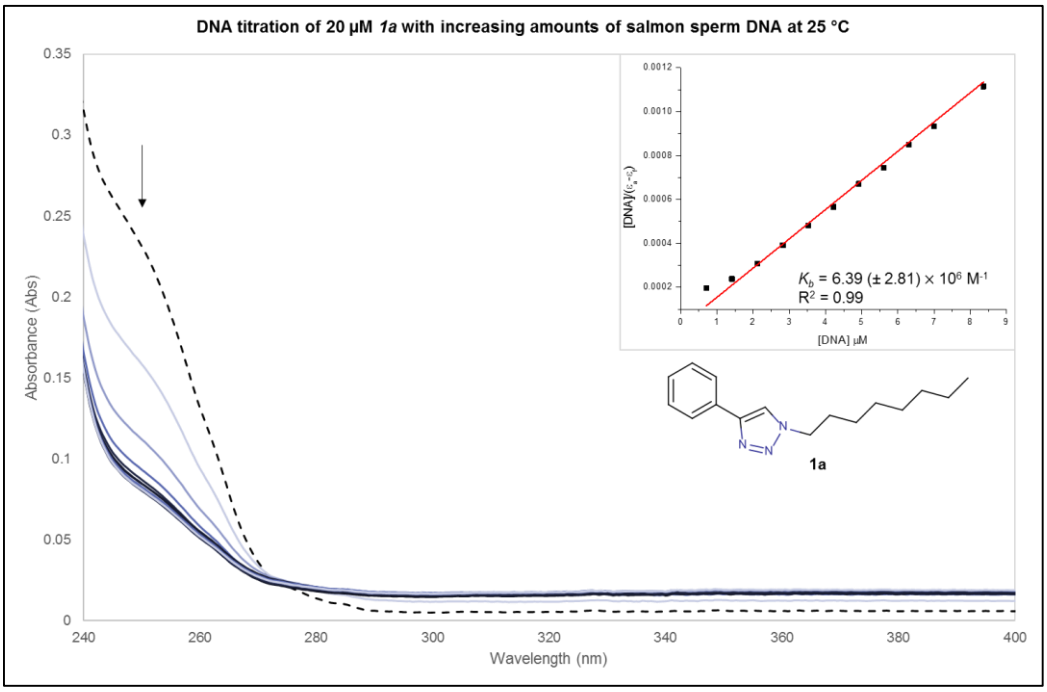

Figure 4.10: The spectra obtained for the titration of 20 µM *1a* with increasing amounts of 0.47 mM salmon sperm DNA. The arrow indicates the general change in die absorption upon DNA addition. The insets show the $[DNA]/|\varepsilon_a - \varepsilon_f|$ vs $[DNA]$ plot, from which the K_b value was obtained, as indicated. The dotted line shows the spectrum of *1a* in the absence for DNA.

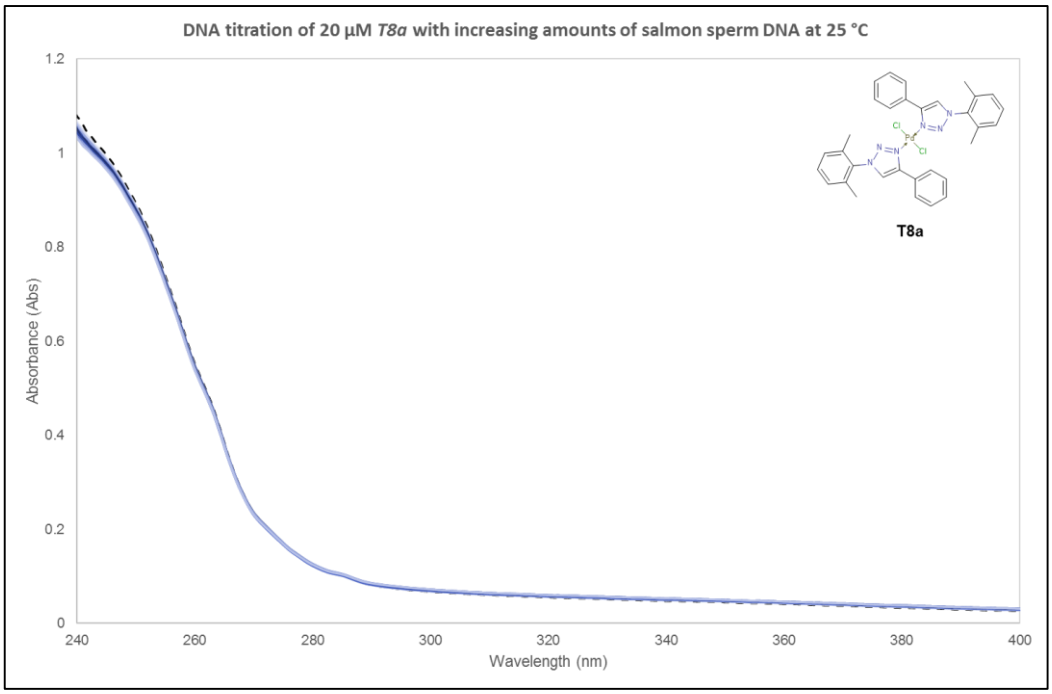

Figure 4.11: The spectra obtained for the titration of 20 µM *T8a* with increasing amounts of 0.47 mM salmon sperm DNA. The dotted line shows the spectrum of *T8a* in the absence for DNA.

The lack of hypochromism was surprising considering the extent of DNA alteration observed in the DNA migration study. The lack of interaction prevented the calculation of a binding constant for **T8a**. However, it should be noted that the DNA migration study uses pBluescript plasmid DNA and the samples are incubated for 24 hours, while the DNA titration uses salmon sperm DNA and incubates for 5 minutes after each DNA addition.

In order to evaluate the effect of the incubation time, 20 µM **T8a** was incubated with 20 µL salmon sperm DNA (0.47 mM) over 22 hours at 25 °C, with an absorbance spectrum collected every hour. The resulting spectra are shown in Figure 4.12.

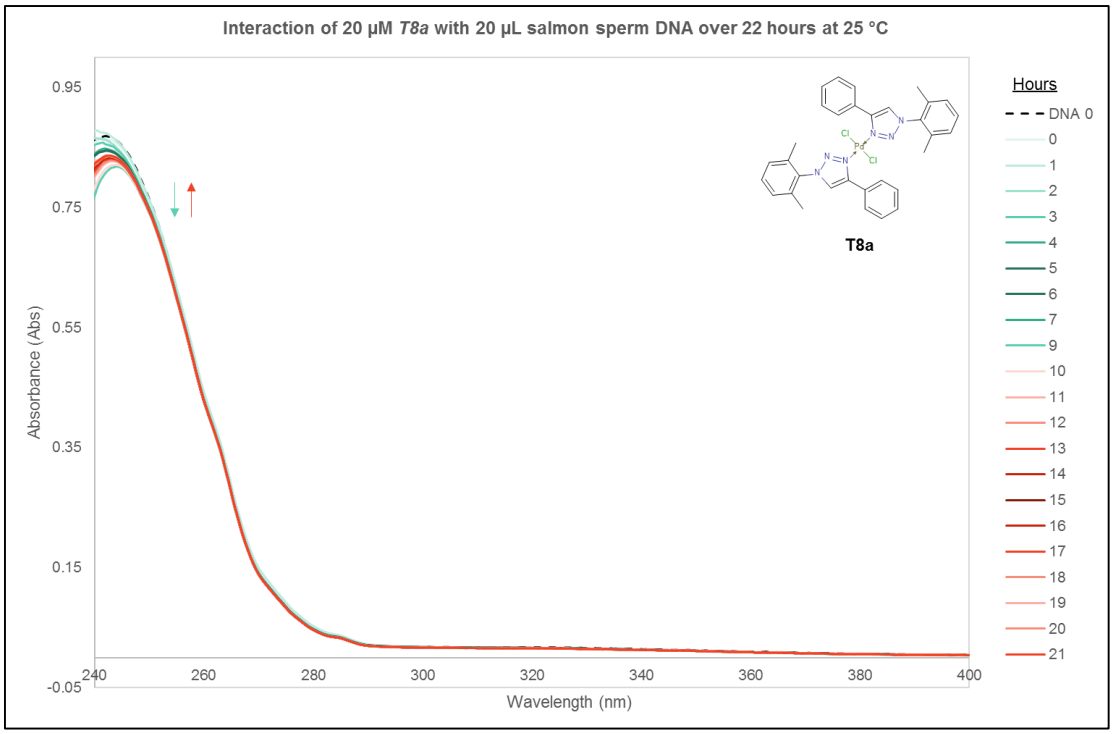

Figure 4.12: The spectra obtained for the interaction of 20 µM *T8a* with 20 µL 0.47 mM salmon sperm DNA over 22 hours. The arrows indicate the general trend of the complex spectrum.

Slight hypochromism was observed for the first 9 hours of incubation and slight hyperchromism for the final 11 hours of incubation. Hyperchromism is generally an indication of DNA denaturation or weak electronic interactions, but the changes in the spectrum are so small that the results can be deemed insignificant. Thus indicating that the incubation time is not the determining factor.

The DNA migration study indicated that **T8a** binds DNA in a similar fashion to cisplatin, thus it would appear that **T8a** binds covalently to DNA. The lack of activity in the titration study can thus potentially be explained by the difference in DNA sources between the DNA migration and DNA titration studies.

DNA migration studies are used to observe how the compound affects the tertiary structure of DNA[6], i.e. how the double helix shapes itself. In order to visualize this, plasmid DNA is used as it separates into three distinct forms that can easily be distinguished from one another. Thus, any changes in the DNA structure are readily visualized.

DNA titration investigations use linear DNA sources, such as salmon sperm DNA or calf thymus DNA.[6] Since these DNA sources have only linear DNA strands in solution, they do not produce distinct bands in DNA migration studies, but rather one large smeared band, and are thus unsuitable for tertiary structure evaluations. They are however better suited towards the observation of secondary structure changes, such as those investigated in DNA titration studies, due to the fact that there is only one form (linear) in solution and that any changes observed in the absorbance spectrum would be due to changes in the secondary structure and not the tertiary structure.

Cisplatin binds preferentially to guanine and cytosine base pairs[15], thus it can be reasoned that if **T8a** displays similar behaviour to cisplatin, it might also display the same preferential binding character. The DNA migration studies are performed with pBluescript DNA, which consists of 50 % G + C base pairs, while salmon sperm DNA consists of 41 % G + C base pairs. Thus, should **T8a** display the same preferential binding character as cisplatin, it would thus bind more readily to the pBluescript DNA than to the salmon sperm DNA, allowing for greater DNA interaction in the migration study than in the titration study.

Additionally, the DNA migration study allows for the evaluation of high compound concentrations. The electronic absorption study does not, due to the absorbance limit on the instrument. The differences in concentration might also explain the increased DNA interaction observed for **T8a** in the DNA migration study.

Ligand **7a** showed hypochromism upon DNA addition, but unlike the other compounds investigated, it did not reach saturation within 10 additions of DNA, but only after 30 additions (Figure 4.13). It was interesting to observe that at high DNA concentrations the hypochromic shift trend reversed, as indicated by the red arrow and spectra, and a slight bathochromic shift (red shift) is observed from 252 nm to 258 nm, before the spectrum stabilizes. To the best of our knowledge, this has not been observed in the literature. This could potentially be attributed to DNA denaturation taking place in the sample cell. Denaturation is also observed in the DNA migration study for ligand **7a** (Figure 4.5A).

The absorbance at 252 nm was used for the kinetic investigations. Analysis according to the Wolfe-model did not yield a straight line and thus the binding constant could not be calculated. This is possibly an indication of multi-mode binding, but would require further investigation.

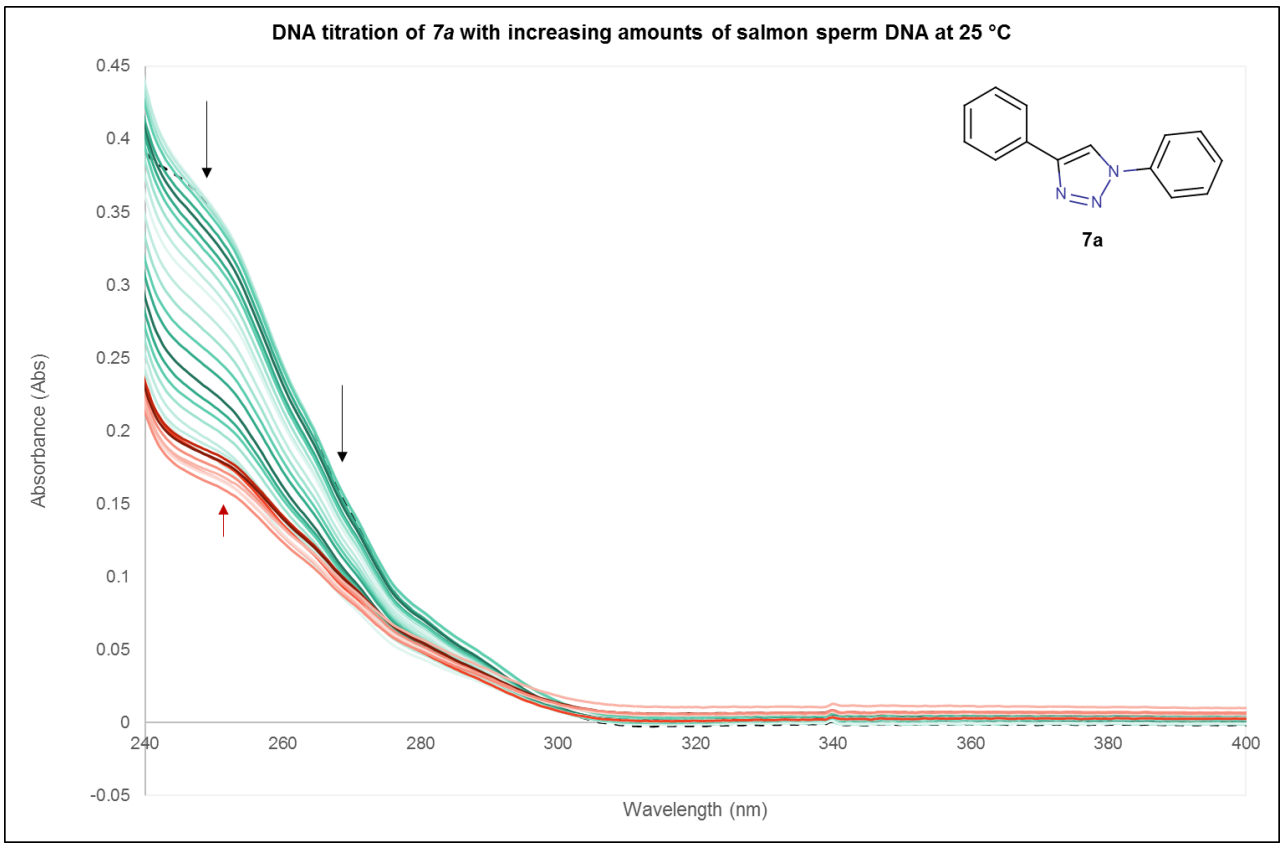

Figure 4.13: The spectra obtained for the titration of 20 µM *7a* with increasing amounts of 0.47 mM salmon sperm DNA. The arrow indicates the general change in die absorption upon DNA addition. The dotted line shows the spectrum of 7*a* in the absence for DNA.

Ligand **7a** was the most cytotoxic compound among those tested, displaying cytotoxicity against the MCF-7 cell line comparable to that of cisplatin. It was thus interesting to note that the DNA binding studies conducted on **7a** indicated that the ligand displayed a strong tendency towards multi-mode binding, while none of the other ligands displayed multi-mode binding character. Whether the increase in cytotoxicity can be attributed to the differences of the binding modes of the ligands investigated is unclear, but it may well be a contributing factor.

Without a binding constant it is difficult to evaluate the DNA binding abilities of **7a** and **3a**, but percentage hypochromism (%H) can give a qualitative indication as to the DNA interaction. Percentage hypochromism is calculated according to Equation 4.2.[47]

$$\%\,H = \left(\frac{A_{free} - A_{bound}}{A_{free}}\right) \times 100 \qquad (4.2)$$

Where A_{free} represents the absorbance of the ligand in the absence of DNA, and A_{bound} represents the absorbance of the fully bound ligand.

Table 4.5 shows the resulting binding constants and percentage hypochromism obtained for the compounds investigated.

Table 4.5: A summary of the kinetic information obtained as compared to the MTT Assay results.

	Functionality	λ (nm)	% H	$K_b \times 10^6$ (M^{-1})	IC_{50} (μM)[b]
1a	Octyl	250	65.0	6.39 (± 2.81)	80.0 (± 1.2)
2a	Cyclohexyl	327.5	55.8	0.06 (± 0.01)	33.3 (± 1.3)
3a	Ethanol	243	5.46	-[a]	24.5 (± 1.1)
4a	2-(2-ethoxy) ethanol	244	9.88	4.35 (± 1.28)	65.2 (± 2.5)
7a	Phenyl	252	50.5	-[a]	13.0 (± 1.2)

[a] Could not be determined with Wolfe-Model kinetics

[b] IC_{50} values evaluated against MCF-7 cancer cell lines.

As expected, the higher the percentage hypochromism, the greater the binding constant obtained, however, the cytotoxicity does not agree with the expected trend. The greater the binding constant, the larger the IC_{50} value obtained, which indicates that the affinity of the ligand towards the DNA does not affect the cytotoxicity of the compound. It is thus possible that the DNA might not be the primary pharmacological target of the ligands.

This is not unexpected as DNA is the main target for metal containing compounds, but organic compounds tend to interact more with proteins and other metabolites, as discussed in Chapter 1. Ligand **7a** displays a high percentage hypochromism but a low IC_{50} concentration, thus differing from the other ligands evaluated. This might indicate that the multi-mode binding character of the ligand enables it to influence the DNA to a greater extent than the other ligands, ultimately leading to a higher cytotoxicity.

4.3 Conclusion

The complexes synthesized were subjected to a turbidimetric assay in order to determine their kinetic solubility, and it was found that the majority of the palladium complexes investigated show moderate solubility in a 2 % DMSO/PBS buffer solution.

The cytotoxicity of the complexes was evaluated against two breast adenocarcinoma cell lines, MCF-7 and MDA-MB-231. Only one complex, **T8a**, displayed moderate anti-cancer activity. Subsequently, the ligands were evaluated against MCF-7 and **1a**, **2a**, **3a**, **4a** and **7a** displayed good to moderate anti-cancer activities. A structure-activity relationship was established in favour of the least flexible N-bound substituents.

The DNA binding modes of the active compounds were investigated with two methods, a DNA migration study utilizing horizontal gel electrophoresis and a UV-Vis absorbance DNA titration. Ligands **1a**, **2a**, **3a** and **4a** displayed intercalative character and **T8a** displayed covalent binding in the DNA migration study. Ligand **7a** could not be evaluated with the chosen kinetic model, but displayed some multi-mode binding character.

The affinity of the ligands to the DNA did not reflect the IC_{50} concentrations obtained, thus indicating that the main target of these ligands might not be DNA, and thus warrants further investigation.

It is also necessary to concede that the Wolfe-model is not suitable to describe the interaction of these ligands with DNA as evidenced by the ill-fitting R^2-values obtained. When combined with the data obtained from the DNA migration study, it would appear that ligands **1a** – **4a** are weak intercalators, but additional information is required. It is suggested that a competitive DNA-EtBr florescence study be conducted for additional kinetic data.

4.4 Experimental Procedures

4.4.1 General Methods and Materials

All starting materials used were obtained from Merck and Sigma-Aldrich and used without additional purification. Solvents used were obtained from Merck, Protea Chemicals, Kimix and Sigma-Aldrich and purified accordingly. THF, DCM, hexane, and diethyl ether were purified and degassed with PureSolv Micro purifiers. Acetonitrile, methanol and ethanol were distilled over the appropriate drying agents. Acetonitrile was distilled over phosphorous pentoxide and both methanol and ethanol were distilled over magnesium filings and iodine. The turbidimetric assay was performed in 96-well microplates and the absorbance measured on a Thermo Fisher Multiskan GO UV-Vis plate reader.

MTT Assays were performed at the Department of Human Biology, UCT Medical School. DMEM medium and RPMI 1640 was purchased from Highveld Biological, UK. The MTT assay was performed according to the manufacturer's instructions accompanying the MTT Assay Kit, obtained from Roche, USA. The IC_{50} values were calculated by fitting a variable slope curve to the data obtained, using GraphPad Prism 7 software.

Overnight cultures of pBluescript *E. coli* was obtained from the Department of Microbiology, Stellenbosch University. The plasmid was isolated with a Zippy Plasmid Isolation Miniprep kit obtained from Inqaba Biotech and the concentration determined with a Thermo Fisher Scientific Nanodrop spectrophotometer. The agarose gels were viewed with a UV lamp at 254 nm and the photos obtained with a Sony Xperia M4 aqua camera in ISO mode. Images were processed with Image J freeware.

UV-Vis DNA binding studies were performed with Invitrogen salmon sperm DNA solution (10 mg/mL) obtained from Life biotechnologies. All buffers used were prepared with a Metrohm 744 pH meter. UV-Vis investigations were performed on a Shimadzu UV-1800 UV spectrophotometer equipped with a CPS cell positioner and temperature control attachment. Binding constants were calculated with Origin Pro 8.5.

4.4.2 Turbidimetric Assay

The protocol for the turbidimetric assay has been published previously[48] and was adapted slightly by using duplicate plates for the assessment of solubility at different temperatures. A 0.01 M pH 7.4 Phosphate Buffered Saline (PBS) solution was prepared by dissolving one PBS tablet, obtained from Sigma-Aldrich, in 200 mL distilled water at 25 °C in order to yield a buffered solution containing 0.01 M phosphate buffer, 0.003 M KCl and 0.14 M NaCl. The solution was allowed to equilibrate at 25 °C for one hour upon which the pH was confirmed with a pH meter. The solution was then filtered through a 0.45 µM Nylon syringe filter in order to remove any undissolved particulates.

A 10 mM stock solution in DMSO of each test compound was prepared and filtered through a 0.45 µM PVDF syringe filter prior to use. A preparation plate (96-well flat bottomed) was prepared by serially diluting the compound in order to achieve the desired concentrations (5.0 µM to 200 µM). The test plate was prepared by pipetting 196 µL DMSO into wells 1 – 6 and 196 µL PBS into wells 7 – 12. Each compound was tested in triplicate thus a single plate could be used to evaluate two compounds. 4 µL of each compound concentration was pipetted from the preparation plate into the test plate in order to bring the total volume up to 200 µL and to ensure that a 2 % (v/v) DMSO/PBS solution is achieved.

Test plates were prepared in duplicate and one plate was incubated at room temperature (25 °C) and the second at physiological temperature (37 °C). Both test plates were incubated for 2 hours upon which the UV-Vis absorbance readings were measured at 620 nm. The corrected absorbance readings were obtained by subtracting the blank readings from each concentration absorbance.

4.4.3 MTT Assay

MDF-7 oestrogen positive breast cancer cells were maintained in RPMI 1640 medium, and MDA-MB-231 triple negative metastatic breast cancer cells were maintained in DMEM medium. Both media were supplemented with 10 % FBS, 100 U/mL penicillin and 100 µg/mL streptomycin. The cells were maintained at 37 °C in a 5 % CO_2/air humidified incubator.

Stock solutions of each compound were made by dissolving the compound in 100 % DMSO to yield a stock solution of 5 mM, and stored at room temperature for no more than seven days. Cells were seeded into 96-well microplates at 5000 cells/well for MCF-7 and 5500 cells/well for MDA-MB-231 and allowed to settle for 48 hours. The cells were treated for 48 hours with a range of compound concentrations (5, 10,15 and 20 µM) and a blank vehicle test.

Cytotoxicity was assessed with the addition of 10 µL MTT to each well followed by incubation at 37 °C for 4 hours. After incubation, 100 µL of solubilizer (10 % SDS, 0.01 HCl) was added followed by overnight incubation at 37 °C. Cell viability was monitored using UV-Vis spectroscopy at 585 nm and calculated as a percentage of the mean vehicle control.

4.4.4 DNA binding

4.4.4.1 Horizontal gel electrophoresis

Samples were prepared by combining pBluescript DNA (40 µg/mL, 10 µL) with compound stock solution in DMSO (34, 340 and 680 µM, 5 µl) in order to obtain samples with final concentrations of 10, 100 and 200 µM (total volume 15 µL). The samples were incubated at 25 °C for 24 hours.

An agarose gel was prepared by dissolving 0.8 g agarose in 100 mL 1× TBE (Tris/borate/EDTA) buffer with microwave radiation at 300 W in 30 second intervals until the agarose was completely dissolved. The agarose solution was then poured into the gel mould and allowed to set at room temperature for 30 minutes.

After 24 hours the samples were centrifuged at 6000 rpm for 1 minute in order to ensure that any condensation droplets settled in the bottom of the microtubes. Loading buffer (2 µL) was added to each sample before being loaded into a prepared agarose gel. The samples were loaded in 15 µL quantities into the gel. Electrophoresis took place at 80 V for three hours in 1× TBE buffer.

After three hours the gel was removed from the electrophoresis tank and stained in 100 mL 1× TBE buffer with ethidium bromide (10 mg/mL, 30 µL) for 15 minutes with constant linear agitation. After 15 minutes of staining the gel was placed in 100 mL distilled water and destained for 5 minutes in order to remove any excess staining solution from the outside of the gel.

The gel was viewed under a UV lamp at 254 nm.

4.4.4.2 UV-Vis DNA binding study: Electronic absorbance titration

A 200 µM stock solution of the test compound was prepared in DMSO and diluted with Tris-HCl buffer (pH = 7.2) to yield a final solution of 20 µM test compound in a 10 % DMSO/Tris-HCl solution. A 10 % DMSO/Tris-HCl reference sample was prepared and the UV-Vis spectrum collected from 230 – 630 nm. Aliquots (5 – 20 µL) of salmon sperm DNA (0.43 – 0.47 mM) were added to both the sample cell and the reference cell respectively. The samples were stirred manually and placed in the spectrophotometer to incubate for 5 minutes at 25 °C before the absorbance spectrum was acquired. This process was repeated until the same spectrum was obtained for three additions of DNA, indicating that saturation has been achieved. This method as an inherent dilution factor that occurs with each addition of DNA to the sample cell. In order to minimize the dilution, a high concentration of DNA stock solution was used and the data obtained adjusted accordingly.

4.5 References

1. J. A. Amott and S. L. Planeyt, *Expert Opin. Drug Discov.*, 2012, **7**, 863–875.

2. J. P. Hughes, S. S. Rees, S. B. Kalindjian, and K. L. Philpott, *Br. J. Pharmacol.*, 2011, **162**,

1239–1249.

3. E. H. Kerns and L. Di, *Drug-like Properties: Concepts, Structure Design and Methods from ADME to Toxicity Optimization*, 1st edn., 2008.

4. M. N. Alam and F. Huq, *Coord. Chem. Rev.*, 2016, **316**, 36–67.

5. A. Avdeef, *Adsoption and Drug Development: solubility, permeability and charge state*, John Wiley and Sons, Inc., Hoboken, USA, 2003.

6. M. Fanelli, M. Formica, V. Fusi, L. Giorgi, M. Micheloni, and P. Paoli, *Coord. Chem. Rev.*, 2016, **310**, 41–79.

7. J. Alsenz and M. Kansy, *Adv. Drug Deliv. Rev.*, 2007, **59**, 546–567.

8. D. Wishart, C. Knox, A. Guo, S. Shrivastava, M. Hassanali, P. Stothard, Z. Chang, and J. Woolsey, *Nucleic Acids Res*, 2006, **34**.

9. B. E. Rabinow, *Nat. Rev. Drug Discov.*, 2004, **3**, 785–796.

10. A. R. Kapdi and I. J. S. Fairlamb, *Chem. Soc. Rev.*, 2014, **43**, 4751–4777.

11. S. B. Deepthi, R. Trivedi, P. Sujitha, C. G. Kumar, B. Sridhar, and S. K. Bhargava, *J. Chem. Sci.*, 2012, **124**, 1405–1413.

12. R. Vrzal, P. Štarha, Z. Dvořák, and Z. Trávníček, *J. Inorg. Biochem.*, 2010, **104**, 1130–1132.

13. T. L. Fuller and R. G. Canada, *Cancer Chemother. Pharmacol.*, 1999, **44**, 249–252.

14. R. Palchaudhuri and P. J. Hergenrother, *Curr. Opin. Biotechnol.*, 2007, **18**, 497–503.

15. P. K. Ganguli and T. Theophanides, *Eur. J. Biochem.*, 1979, **101**, 377–383.

16. B. Rosenberg, *Platin. Met. Rev.*, 1971, **15**, 42–51.

17. M. Marques, *ISRN Spectrosc.*, 2013, **2013**, 1–29.

18. G. S. Khan, A. Shah, Zia-Ur-Rehman, and D. Barker, *J. Photochem. Photobiol. B Biol.*, 2012, **115**, 105–118.

19. Y.-G. Sun, D. Sun, W. Yu, M.-C. Zhu, F. Ding, Y.-N. Liu, E.-J. Gao, S.-J. Wang, G. Xiong, I. Dragutan, and V. Dragutan, *Dalton Trans.*, 2013, **42**, 3957–3967.

20. J. Zhao, S. Gou, F. Liu, Y. Sun, and C. Gao, *Inorg. Chem.*, 2013, **52**, 8163–8170.

21. M. Gay, Á. M. Montaña, C. Batalla, J. M. Mesas, and M. T. Alegre, *J. Inorg. Biochem.*, 2015, **142**, 15–27.

22. C. Icsel, V. T. Yilmaz, F. Ari, E. Ulukaya, and W. T. A. Harrison, *Eur. J. Med. Chem.*, 2013,

60, 386–394.

23. K. S. Prasad, L. S. Kumar, S. Chandan, R. M. Naveen Kumar, and H. D. Revanasiddappa, *Spectrochim. Acta - Part A Mol. Biomol. Spectrosc.*, 2013, **107**, 108–116.

24. J. Albert, R. Bosque, M. Crespo, G. García, J. Granell, C. López, M. V. Lovelle, R. Qadir, A. González, A. Jayaraman, E. Mila, R. Cortés, J. Quirante, C. Calvis, R. Messeguer, J. Badía, L. Baldomà, and M. Cascante, *Eur. J. Med. Chem.*, 2014, **84**, 530–536.

25. X. Qu and J. B. Chaires, *Methods Enzymol.*, 2000, **321**, 353–369.

26. J. Albert, R. Bosque, M. Crespo, J. Granell, C. López, R. Cortés, A. Gonzalez, J. Quirante, C. Calvis, R. Messeguer, L. Baldomà, J. Badia, and M. Cascante, *Bioorganic Med. Chem.*, 2013, **21**, 4210–4217.

27. M. Marques, *ISRN Spectrosc.*, 2013, **2013**, 1–29.

28. S. K. Kim and B. Norden, *FEBS Lett.*, 1993, **315**, 61–64.

29. P. O. Vardevanyan, A. P. Antonyan, M. A. Parsadanyan, M. A. Shahinyan, and L. A. Hambardzumyan, *J. Appl. Spectrosc.*, 2013, **80**, 595–599.

30. R. Rohs and H. Sklenar, *J. Biomol. Struct. Dyn.*, 2004, **21**, 699–711.

31. R. Rohs, I. Bloch, H. Sklenar, and Z. Shakked, *Nucleic Acid Res.*, 2005, **33**, 7048–7057.

32. A. G. Quiroga, J. M. Pérez, I. López-Solera, J. R. Masaguer, A. Luque, P. Román, A. Edwards, C. Alonso, and C. Navarro-Ranninger, *J. Med. Chem.*, 1998, **41**, 1399–1408.

33. A. A. Legin, M. A. Jakupec, N. A. Bokach, M. R. Tyan, V. Y. Kukushkin, and B. K. Keppler, *J. Inorg. Biochem.*, 2014, **133**, 33–39.

34. T. V. Serebryanskaya, T. Yung, A. A. Bogdanov, A. Shchebet, S. A. Johnsen, A. S. Lyakhov, L. S. Ivashkevich, Z. A. Ibrahimava, T. S. Garbuzenco, T. S. Kolesnikova, N. I. Melnova, P. N. Gaponik, and O. A. Ivashkevich, *J. Inorg. Biochem.*, 2013, **120**, 44–53.

35. E.-J. Gao, Hong Fu, M.-C. Zhu, C. Ma, S.-K. Liang, J. Zhang, L.-F. Li, L. Wang, Y.-Y. Li, and Wei Jiao, *Eur. J. Med. Chem.*, 2014, **82**, 172–80.

36. Z. C. Liu, B. D. Wang, B. Li, Q. Wang, Z. Y. Yang, T. R. Li, and Y. Li, *Eur. J. Med. Chem.*, 2010, **45**, 5353–5361.

37. N. Shahabadi, S. Mohammadi, and R. Alizadeh, *Bioinorg. Chem. Appl.*, 2011, **2011**.

38. T. Topală, A. Bodoki, L. Oprean, and R. Oprean, *Farmacia*, 2014, **62**, 1049–1061.

39. X. Yang, Y. Liu, S. Yao, Y. Xia, Q. Li, W. Zheng, L. Chen, and J. Liu, *J. Coord. Chem.*, 2011,

64, 1491–1502.

40. A. Wolfe, G. H. Shimer, and T. Meehan, *Biochemistry*, 1987, **26**, 6392–6396.

41. H. A. Benesi and J. H. Hildebrand, *J. Am. Chem. Soc.*, 1949, **71**, 2703–2707.

42. R. B. Martin, *J. Chem. Educ.*, 1997, **74**, 1238.

43. D. E. V Schmechel and D. M. Crothers, *Biopolymers*, 1971, **10**, 465–480.

44. P. Kalaivani, R. Prabhakaran, M. V. Kaveri, R. Huang, R. J. Staples, and K. Natarajan, *Inorganica Chim. Acta*, 2013, **405**, 415–426.

45. M. N. Patel, A. P. Patidar, P. S. Karia, and P. a. Vekariya, *Inorganica Chim. Acta*, 2014, **419**, 45–54.

46. K. M. Sovenyhazy, J. A. Bordelon, and J. T. Petty, *Nucleic Acids Res.*, 2003, **31**, 2561–2569.

47. M. A. Bork, C. G. Gianopoulos, H. Zhang, P. E. Fanwick, J. H. Choi, and D. R. McMillin, *Biochemistry*, 2014, **53**, 714–724.

48. P. Chellan, University of Cape Town, 2013.

49. C. A. Lipinski, F. Lombardo, B. W. Dominy, and P. J. Feeney, *Adv. Drug Deliv. Rev.*, 2012, **64**, 4–17.

50. E. H. Kerns and L. Di, *J. Assoc. Lab. Autom.*, 2005, **10**, 114–123.

Chapter 5: Conclusions and Future Prospects

5.1 General Conclusions

The aim of this study was to synthesize a number of *trans*-Pd(II)-phenyl-1,2,3-triazolyl and *N,N'*-bidentate Pd(II)-pyridyl-1,2,3-triazolyl complexes as potential anti-cancer agents.

A modified microwave 'click' reaction using a sterically hindered copper catalyst, $Cu(PPh_3)_3Br$, resulted in the best yield of a number of known and novel 1-substituted-4-phenyl-1,2,3-triazole and 1-substituted-4-pyridyl-1,2,3-triazole ligands.[1] The organoazide substituents were chosen in such a way as to allow us to investigate the influence of sterics, electronics and ligand hydrophilicity. All ligands were fully characterized with various analytical techniques.

Complexation of the 1-substituted-4-phenyl-1,2,3-triazole ligands to palladium, using $(MeCN)_2PdCl_2$ as a precursor, yielded the *trans*-Pd(II)-phenyl-1,2,3-triazolyl complexes in moderate to good yields. Full characterization with various analytical techniques confirmed the PdL_2Cl_2 nature of these complexes. It was noted that the *trans*-Pd(II) complexes dissociated in DMSO and that the extent of dissociation is dependent on the N-bound substituents of the 1,2,3-triazole ring, with aromatic substituents leading to a greater extent of dissociation than the aliphatic and hydrophilic substituents. Since the cytotoxicity evaluation of these complexes relies on the solvation of the complex in DMSO, stability of the complex is important to ascertain the active species of the complex. The dissociation of the complex in DMSO means that the cytotoxicity evaluations conducted were done with a mixture of species in solution, as discussed in Chapter 3.

Complexation of the 1-substituted-4-pyridyl-1,2,3-triazole ligands to palladium, using $(MeCN)_2PdCl_2$ as a precursor, yielded the *N,N'*-bidentate-Pd(II)-pyridyl-1,2,3-triazolyl complexes in moderate to good yields. Full characterization using a variety of analytical techniques confirmed the successful synthesis of the complexes.

The kinetic solubility of the palladium complexes synthesized was determined using a turbidimetric assay. It was found that all complexes were moderately soluble in a 2 % DMSO/PBS buffer solution except complexes **T2a**, **T7a**, **T9a** and **N1b**. Cytotoxicity of the insoluble complexes was thus evaluated as suspensions.

The complexes synthesized were investigated as anti-cancer agents against breast cancer cell lines, MCF-7 and MDA-MB-231, and the cytotoxicity evaluated with an MTT assay. Complex **T8a** displayed moderate anti-cancer activity, IC_{50} = 40.7 (± 1.1) µM, while the remainder of the *trans*-Pd(II)-1-substituted-4-phenyl-1,2,3-triazolyl complexes were inactive as anti-cancer agents. None of the *N,N'*-bidentate-Pd(II)-1-substituted-4-phenyl-1,2,3-triazolyl complexes displayed anti-cancer activity.

It is proposed that low solubility and lability in solution contributes to the lack of anti-cancer activity observed.

Subsequently, the cytotoxicity of the ligands was investigated against MCF-7 and **1a** - **4a** and **7a** displayed good to moderate anti-cancer activities. A trend was observed in which an increase in the flexibility of the N-bound substituent resulted in decreased cytotoxicity. It was interesting to observe that the phenyl ring in the 1-substituted-4-phenyl-1,2,3-triazole ligands appear to be crucial for the cytotoxicity of the ligands, as none of the 1-substituted-4-pyridyl-1,2,3-triazole ligands displayed any anti-cancer activity.

The DNA binding capabilities of the active compounds were investigated with two studies, a DNA migration study utilizing horizontal gel electrophoresis and a UV-Vis absorbance DNA titration. Ligands **1a** - **4a** displayed intercalative character in both studies and **T8a** displayed covalent binding in the DNA migration study. Ligand **7a** displayed potential intercalative character as ascertained from the DNA migration study. The DNA titration study, on the other hand, revealed possible multi-mode binding characteristics.

The affinity of the ligands towards DNA did not correlate with the results obtained for the MTT assays conducted. This would seem to indicate that the main target of these ligands might not be DNA, and this thus warrants further investigation.

In summary, the aims and objectives, as outlined in Chapter 1, were achieved. A small library of 1,4-disubstituted-1,2,3-triazole ligands were synthesized and complexed to a Pd-precursor to yield *trans*-Pd(II)-1-substituted-4-phenyl-1,2,3-triazolyl and *N,N'*-bidentate-Pd(II)-1-substituted-4-pyridyl-1,2,3-triazolyl complexes, respectively. The cytotoxicity of the complexes was evaluated against the MCF-7 and MDA-MB-231 cancer cell lines, and it was found that only one complex, **T8a**, displayed moderate anti-cancer activity. A number of ligands, **1a** - **4a** and **7a,** displayed moderate to good cytotoxicity against MCF-7 and their DNA interaction modes were investigated by utilizing UV-Vis spectrometry and horizontal gel electrophoresis. The active ligands displayed weak intercalation with the exception of **7a**, which seem to display a multi-mode binding character.

5.2 Future Prospects

Owing to the continuous flow of experimental research, there are always opportunities for expansion. When the work presented in this thesis is considered, there are two areas in which future endeavours can be focussed, 1) changes pertaining to the chemical structure of the complexes investigated and 2) the types of biological interaction studies pursued.

5.2.1 Structural investigations

In order to combat the ligand dissociation observed for the *trans*-Pd(II)-1-substituted-4-phenyl-1,2,3-triazolyl complexes, a stronger metal-ligand bond is required. As mentioned in Chapter 1, the strength provided by a Pd-C bond has proven to provide the solution stability required.

All the 1-substituted-4-phenyl-1,2,3-triazole ligands synthesized in this paper can be used to synthesize NHC-carbenes of the type published by Hong and co-workers[2] as shown in Figure 5.1. The complexes investigated by these authors were applied in Suzuki-Miyuara cross-couplings but their biological applications have not been investigated. This would afford the opportunity for the investigation of the 1,2,3-triazolyl ligands in a *trans*-Pd(II) complex.

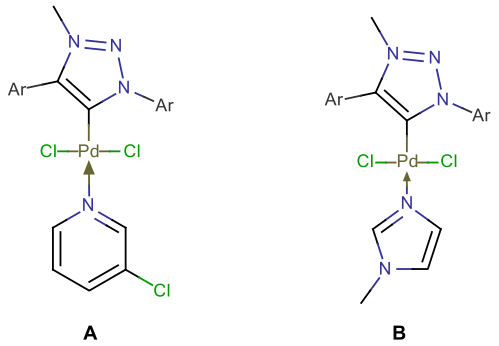

Figure 5.1: The PEPPSI (pyridine-enhanced precatalyst preparation stabilization and initiation) type NHC-carbenes synthesized by Hong and co-workers.[2]

Similarly, the 1-substituted-4-pyridyl-1,2,3-triazole ligands can be used to synthesize abnormal carbenes, as investigated by Albrecht and colleagues[3] (Figure 5.2).In this case the complex investigated was an efficient water oxidation catalyst, but the biological application has not been investigated. This would result in the investigation of the ligand in a chelated position.

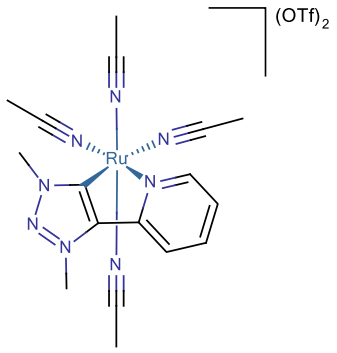

Figure 5.2: An abnormal carbene complex investigated by Albrecht and colleagues[3] as a water oxidation catalyst.

Alternatively, the N-bound substituent of the 1-substituted-4-pyridyl-1,2,3-triazole can be altered to include a bioactive molecule, such as a carbohydrate[4] or folic acid. This would result in the complex being more readily available to enter the cellular matrix through a Trojan horse mechanism[5].

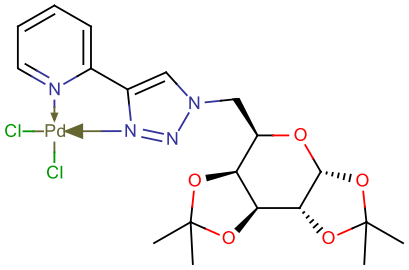

Figure 5.3: One of the carbohydrate containing 1,2,3-triazolyl Pd(II) complexes investigated by Trivedi and colleagues[4]

Owing to the simple nature of the ligands that displayed anti-cancer activity, there is a myriad of structural changes that can be applied in an effort to include the palladium and increase the cytotoxicity. However, investigating the mode of action of the active ligands, especially ligand **7a**, would also be prudent.

5.2.2 Biological interactions

The DNA binding observed in the DNA titration of **7a** was not quantitative, possibly due to multi-mode binding, as discussed in Chapter 4. In order to ascertain that DNA damage does occur, it is recommended that proteins from treated cells are extracted and a Western blot for PARP cleavage is performed.[6] This should indicate whether DNA damage does indeed occur, or whether the interaction observed in the DNA migration and DNA titration studies is merely an artefact of the assay conditions.

If PARP cleavage is observed, the DNA interaction of the ligand needs to be investigated with different methods. For quantitative purposes, it is advised to use a competitive ethidium bromide DNA fluorescence study, from which the binding constant can be calculated. During this assay the fluorescence spectrum of EtBr-DNA is recorded with the ligand being titrated into the sample.[7–9]

Should the Western blot indicate that DNA damage does not take place, the mode of action of the ligand can be evaluated against a number of biological macromolecules. There are many examples of alternative biologically abundant molecules with which the ligand could potentially interact.

The interaction of various heterocyclic ligands with bovine serum albumin (BSA) has been prevalent in literature recently.[8,10–14] BSA is an abundant protein in the circulatory system which is responsible for the transportation of steroids, metal ion and drugs among others.[8] This provides the opportunity to investigate the drug-protein interaction, rather than the drug-DNA interaction.

Alternatively, the interaction of the ligand with topoisomerase would also provide some insights into the mode of interaction of the ligand. Topoisomerase is an enzyme which controls the coiling of DNA. Owing to the fact that the DNA titration and migration studies for **7a** indicated that some form of DNA interaction is taking place, it might be worthwhile to investigate whether the change in DNA is due to an interaction with the topoisomerase.[11,13,15–17]

5.3 References

1. N. Moitra, J. J. E. Moreau, X. Cattoën, and M. Wong Chi Man, *Chem. Commun.*, 2010, **46**, 8416–8418.
2. J. Huang, J. T. Hong, and S. H. Hong, *European J. Org. Chem.*, 2012, **3**, 6630–6635.
3. L. Bernet, R. Lalrempuia, W. Ghattas, H. Mueller-Bunz, L. Vigara, A. Llobet, and M. Albrecht, *Chem. Commun. (Camb).*, 2011, **47**, 8058–60.
4. S. B. Deepthi, R. Trivedi, P. Sujitha, C. G. Kumar, B. Sridhar, and S. K. Bhargava, *J. Chem. Sci.*, 2012, **124**, 1405–1413.
5. M. Marques, *ISRN Spectrosc.*, 2013, **2013**, 1–29.
6. S. Aliwaini, A. J. Swarts, A. Blanckenberg, S. Mapolie, and S. Prince, *Biochem. Pharmacol.*, 2013, **86**, 1650–1663.
7. H. Mansouri-Torshizi, S. Shahraki, Z. S. Nezami, A. Ghahghaei, S. Najmedini, A. Divsalar, H. Ghaemi, and A.A. Saboury, *Complex Met.*, 2014, **1**, 23–31.
8. L. Tabrizi, H. Chiniforoshan, and H. Tavakol, *Spectrochim. Acta Part A Mol. Biomol. Spectrosc.*, 2015, **141**, 16–26.
9. D. Ajloo, M. Eslami Moghadam, K. Ghadimi, M. Ghadamgahi, A. A. Saboury, A. Divsalar, M. SheikhMohammadi, and K. Yousefi, *Inorganica Chim. Acta*, 2015, **430**, 144–160.
10. K. Karami, M. Hosseini-Kharat, H. Sadeghi-Aliabadi, J. Lipkowski, and M. Mirian, *Eur. J. Med. Chem.*, 2014, **73**, 8–17.

11. P. Thirumurugan, D. Matosiuk, and K. Jozwiak, *Chem. Rev.*, 2013, **113**, 4905–4979.

12. Q. P. Qin, Z. F. Chen, J. L. Qin, X. J. He, Y. L. Li, Y. C. Liu, K. Bin Huang, and H. Liang, *Eur. J. Med. Chem.*, 2015, **92**, 302–313.

13. A. P. Neves, M. X. G. Pereira, E. J. Peterson, R. Kipping, M. D. Vargas, F. P. Silva-Jr, J. W. M. Carneiro, and N. P. Farrell, *J. Inorg. Biochem.*, 2013, **119**, 54–64.

14. M. Saeidifar and H. Mansouri-Torshizi, *Nucleosides, Nucleotides and Nucleis Acids*, 2015, **34**, 16–32.

15. R. Cincinelli, L. Musso, S. Dallavalle, R. Artali, S. Tinelli, D. Colangelo, F. Zunino, M. De Cesare, G. L. Beretta, and N. Zaffaroni, *Eur. J. Med. Chem.*, 2013, **63**, 387–400.

16. R. D. Snyder, *Mutat. Res. - Fundam. Mol. Mech. Mutagen.*, 2007, **623**, 72–82.

17. L. R. Ferguson and W. A. Denny, *Mutat. Res. - Fundam. Mol. Mech. Mutagen.*, 2007, **623**, 14–23.